

AWARD NUMBER: W81XWH-18-1-0547

TITLE: Brigatinib and Its Combination with INK-128 as a Novel Treatment for NF2-Deficient Meningiomas

PRINCIPAL INVESTIGATOR: Long-Sheng Chang, Ph.D.

CONTRACTING ORGANIZATION: The Research Institute at Nationwide Children's Hospital,
Columbus, OH 43205-2696

REPORT DATE: October 2020

TYPE OF REPORT: Annual

PREPARED FOR: U.S. Army Medical Research and Development Command
Fort Detrick, Maryland 21702-5012

DISTRIBUTION STATEMENT: Approved for Public Release;
Distribution Unlimited

The views, opinions and/or findings contained in this report are those of the author(s) and should not be construed as an official Department of the Army position, policy or decision unless so designated by other documentation.

REPORT DOCUMENTATION PAGE

Form Approved
OMB No. 0704-0188

Public reporting burden for this collection of information is estimated to average 1 hour per response, including the time for reviewing instructions, searching existing data sources, gathering and maintaining the data needed, and completing and reviewing this collection of information. Send comments regarding this burden estimate or any other aspect of this collection of information, including suggestions for reducing this burden to Department of Defense, Washington Headquarters Services, Directorate for Information Operations and Reports (0704-0188), 1215 Jefferson Davis Highway, Suite 1204, Arlington, VA 22202-4302. Respondents should be aware that notwithstanding any other provision of law, no person shall be subject to any penalty for failing to comply with a collection of information if it does not display a currently valid OMB control number. **PLEASE DO NOT RETURN YOUR FORM TO THE ABOVE ADDRESS.**

1. REPORT DATE October 2020		2. REPORT TYPE Annual		3. DATES COVERED 15 Sept. 2019 – 14 Sept. 2020	
4. TITLE AND SUBTITLE Brigatinib and Its Combination with INK-128 as a Novel Treatment for NF2-Deficient Meningiomas				5a. CONTRACT NUMBER	
				5b. GRANT NUMBER W81XWH-18-1-0547	
				5c. PROGRAM ELEMENT NUMBER	
6. AUTHOR(S) Long-Sheng Chang, Ph.D. E-Mail: Long-Sheng.Chang@nationwidechildrens.org				5d. PROJECT NUMBER	
				5e. TASK NUMBER	
				5f. WORK UNIT NUMBER	
7. PERFORMING ORGANIZATION NAME(S) AND ADDRESS(ES) Research Institute at Nationwide Children's Hospital 700 Children's Drive Columbus, OH 43205-2696				8. PERFORMING ORGANIZATION REPORT NUMBER	
9. SPONSORING / MONITORING AGENCY NAME(S) AND ADDRESS(ES) U.S. Army Medical Research and Development Command Fort Detrick, Maryland 21702-5012				10. SPONSOR/MONITOR'S ACRONYM(S)	
				11. SPONSOR/MONITOR'S REPORT NUMBER(S)	
12. DISTRIBUTION / AVAILABILITY STATEMENT Approved for Public Release; Distribution Unlimited					
13. SUPPLEMENTARY NOTES					
14. ABSTRACT Presently, an FDA-approved medical therapy for the treatment of <i>NF2</i> -deficient meningiomas is not available. To identify novel targeted therapies for these tumors, we, as members of the Synodos for NF2 Consortium, in collaboration with the National Center for Advancing Translational Sciences (NCATS), identified Brigatinib, a potent inhibitor of anaplastic lymphoma kinase (ALK) and other receptor tyrosine kinases (RTKs), to be effective as a single agent in inhibiting proliferation of <i>NF2</i> -deficient meningioma cells and suppressing tumor growth in an orthotopic <i>NF2</i> -deficient meningioma animal model. Additionally, we showed that INK-128, a dual mTORC1/2 inhibitor, synergized with Brigatinib to potently suppress meningioma cell proliferation <i>in vitro</i> . Based on these data, we have proposed to evaluate the Brigatinib/INK-128 combination as an effective treatment for <i>NF2</i> -deficient meningiomas and investigate their mechanisms of action. We have found that <i>NF2</i> -deficient meningiomas did not express ALK and that Brigatinib potently suppressed the growth of <i>NF2</i> -deficient tumors via inhibition of multiple RTKs and non-RTKs, such as focal adhesion kinase (FAK). These findings have led to a phase II clinical trial to evaluate Brigatinib in patients with NF2 with associated progressive tumors of vestibular schwannomas, non-vestibular schwannomas, meningiomas, and ependymomas. Also, we showed that in addition to <i>NF2</i> -deficient meningioma, Brigatinib had anti-tumor efficacy against and <i>NF1</i> -deficient MPNST, suggest that Brigatinib may also be a viable treatment for MPNST. Intriguingly, combination of Brigatinib with the dual MTORC1/2 inhibitor INK128 only modestly enhances the anti-tumor effects. In addition, we have generated an NF2-associated meningioma cell line AG-NF2-Men-1. Luciferase-expressing AG-NF2-Men-1 cells are being used to establish an orthotopic NF2-associated meningioma model for drug evaluation.					
15. SUBJECT TERMS Neurofibromatosis type 2 (NF2), <i>NF2</i> gene, meningioma, Brigatinib, anaplastic lymphoma kinase (ALK), receptor tyrosine kinase (RTK), INK-128, mTOR1/2, inhibitor, imaging					
16. SECURITY CLASSIFICATION OF:			17. LIMITATION OF ABSTRACT Unclassified	18. NUMBER OF PAGES 177	19a. NAME OF RESPONSIBLE PERSON USAMRMC
a. REPORT Unclassified	b. ABSTRACT Unclassified	c. THIS PAGE Unclassified			19b. TELEPHONE NUMBER (include area code)

TABLE OF CONTENTS

	<u>Page</u>
1. Introduction	4
2. Keywords	4
3. Overall Project Summary	4
4. Key Research Accomplishments	5
5. Impact	14
6. Changes/Problems	15
7. Publications, Abstracts, and Presentations	15
8. Participants & Other Collaborating Organizations	18
9. Reportable Outcomes	18
10. Other Achievements	18
11. References	18
12. Appendices	19-

1. INTRODUCTION

Meningiomas, originating from the meningotheial cells of the arachnoid layer lining the brain, are the most common brain tumors (Ostrom et al., 2018). About 80% of these tumors are benign (WHO grade I), whereas the remaining are atypical (grade II) and anaplastic (grade III). Meningiomas can occur spontaneously in the general population or frequently found in patients with neurofibromatosis type 2 (NF2), an autosomal-dominant genetic disorder caused by mutations in the *NF2* tumor suppressor gene (Rouleau et al., 1993; Trofatter et al., 1993). Also, about 50-60% of sporadic meningiomas harbor *NF2* mutations. Surgery and radiation are the current treatment options for meningiomas; however, these treatments could cause severe complications, including seizure, intracranial bleeding, and stroke (Suppiah et al., 2019). As patients with NF2 often develop multiple meningiomas, surgery may not be possible due to too many tumors or the locations that are difficult to operate, such as in the skull base. Incomplete tumor resection is not uncommon and is a main cause of tumor recurrence. In addition, radiation therapy may induce malignant transformation of benign tumors and increase risk for secondary malignancies. Together, these factors underscore the importance of developing effective medical therapies that stop tumor growth or completely eradicate meningiomas. To accelerate drug development for NF2-associated tumors, the Children's Tumor Foundation previously sponsored the establishment of the multi-institutional Synodos for NF2 Consortium aiming to apply system biology to create tools and treatment paradigms for NF2-associated meningiomas and schwannomas (Synodos for NF2 Consortium, 2018). The Synodos for NF2 team, which included us, in collaboration with the NIH National Center for Advancing Translational Sciences (NCATS), previously conducted high-throughput drug screening of isogenic pairs of *NF2*-deficient and *NF2*-expressing disease-relevant cells to identify actionable drug targets for the treatment of NF2-related tumors. From this screening, several targeted drugs and drug combinations with potent growth-inhibitory activities in NF2 cell panels were identified. Using a noninvasive, quantifiable, orthotopic *NF2*-deficient meningioma animal model, we showed that the FDA-approved, multi-receptor tyrosine kinase (RTK) inhibitor, Brigatinib (ALUNBRIG®), caused tumor regression. In addition, together with Dr. Vijaya Ramesh, also a member of the Synodos for NF2 Consortium at Massachusetts General Hospital (MGH), we found that INK-128 (TAK228, Sapanisertib, MLN0128), an inhibitor of mTORC1 and mTORC2, previously shown to be aberrantly activated in *NF2*-deficient meningiomas, synergized with Brigatinib to suppress the growth of *NF2*-deficient meningioma cells *in vitro*. Based on these findings, we (Dr. Chang and Dr. Ramesh) have proposed to evaluate Brigatinib and INK-128 as a novel drug combination to treat *NF2*-deficient meningiomas and to investigate its molecular mechanisms of action. It is hoped that the results to be obtained from this study will potentially lead to an effective combination treatment approach for NF2.

2. KEYWORDS

Neurofibromatosis type 2 (NF2), *NF2* gene, meningioma, Brigatinib, anaplastic lymphoma kinase (ALK), receptor tyrosine kinase (RTK), INK-128, mTORC1/2, inhibitor, imaging

3. OVERALL PROJECT SUMMARY

Presently, an FDA-approved medical therapy is not available for the treatment of *NF2*-deficient meningiomas. To identify novel targeted therapies, either alone or in combination, for these tumors, we, as members of the Synodos for NF2 team, in collaboration with Dr. Marc Ferrer of the NCATS, previously identified Brigatinib, an inhibitor of anaplastic lymphoma kinase (ALK) and several other RTKs, to be effective as a single agent in suppressing the growth of *NF2*-deficient meningioma *in vitro* and *in vivo*. In addition, we found that INK-128, a dual mTORC1 and mTORC2 inhibitor, synergizes with Brigatinib to inhibit proliferation of *NF2*-deficient meningioma cells *in vitro*. Based on these findings, we have proposed to further evaluate the Brigatinib/INK-128 combination as an effective treatment for *NF2*-deficient meningiomas. The **objective** of this research is to investigate the mechanistic aspects of Brigatinib activity either alone or in combination with INK-128 in *NF2*-null *in vitro* and *in vivo* meningioma models. To achieve this goal, we propose:

Aim 1. To evaluate the mechanism by which Brigatinib inhibits proliferation of *NF2*-null meningioma cells and to understand the synergy between Brigatinib and INK-128 in growth inhibition. Brigatinib was originally designed as a highly selective and potent inhibitor of ALK. It also has activity against ROS1 and other

RTKs (Huang et al., 2016; Zhang et al., 2016). We hypothesize that mutation-independent activation of ALK/ROS1 is likely in *NF2*-null meningioma cells. To test this hypothesis, we have proposed to examine the expression and activation of ALK and ROS1 upon *NF2* loss and to address whether Brigatinib functions in an ALK/ROS1-dependent manner or as an inhibitor of other RTKs. Further, we plan to address how Brigatinib synergizes with INK-128 in growth inhibition by examining the bypass signaling after single and combination treatment with these two drugs.

Aim 2. To determine the anti-tumor activity of the Brigatinib and INK-128 combination in orthotopic *NF2*-deficient meningioma models. We have found that as a single agent, INK-128 also effectively suppresses intracranial Ben-Men-1 meningioma growth in mice (Angus et al., 2018). We hypothesize that combined Brigatinib and INK-128 treatment restrains activation of bypass signaling pathways, such as the AKT-mTOR pathway, resulting in efficient tumor inhibition. We plan to evaluate the antitumor effects of the Brigatinib/INK-128 combination in *NF2*-deficient sporadic as well as *NF2*-associated meningiomas. We will analyze treated tumors for inhibition of any bypass signaling pathways.

Brigatinib is an FDA-approved drug, and a recent Phase I clinical study of INK-128 has demonstrated tolerability and encouraging tumor responses (Ghobrial et al., 2016). Should the proposed Brigatinib/INK-128 combination demonstrate synergistic anti-tumor efficacy in *NF2*-deficient meningiomas, the results could be quickly translated to human evaluation. Identification of a medical therapy that effectively eradicates *NF2*-related tumors would significantly advance our current approach to *NF2* treatment and greatly improve the clinical care and long-term treatment outcomes for patients afflicted by *NF2*.

4. KEY RESEARCH ACCOMPLISHMENTS:

(i) What were the major goals of the project?

The major **goals** of this project are to evaluate Brigatinib and INK-128 as a novel drug combination to treat *NF2*-deficient meningiomas and to investigate its molecular mechanisms of action.

(ii) What was accomplished under these goals?

To investigate how Brigatinib suppressed the growth of *NF2*-deficient meningioma, we profiled the expression of 28 phosphorylated or activated RTKs (p-RTKs) and 11 downstream signaling nodes in *NF2*-deficient Ben-Men-1 meningioma cells treated with one- IC_{50} dose (50% inhibitory concentration) of Brigatinib or dimethyl sulfoxide (DMSO) as the vehicle control under active growth conditions in 10% fetal bovine serum (FBS) or in growth-arrested cells stimulated with 20% FBS using the PathScan[®] RTK Signaling Antibody Array (Cell Signaling Technology). Intriguingly, while Brigatinib has been described as a potent ALK inhibitor and is used clinically to treat ALK+ non-small cell lung carcinoma (Huang et al., 2016; Zhang et al., 2016), we did not detect any ALK signal in Ben-Men-1 cells with or without Brigatinib treatment under both growth conditions (Figure 1). Western blot analysis confirmed that ALK expression was not detected in Ben-Men-1 cells (Figure 2A) or normal meningeal cells, three *NF2*-deficient meningioma cell lines, and four primary meningioma cell cultures with or without *NF2* loss (Figure 3A). Similarly, we also did not detect ALK expression in primary vestibular schwannoma cells and cell lines as well as schwannoma tumors (Figure 3B).

In contrast, we observed a broad range of kinases that were active in Ben-Men-1 cells, with similar patterns of activity between logarithmically growing cells and growth-arrested cells stimulated with 20% serum (Figures 1A and 1C). Notably, strong expression of phosphorylated ErbB2, ErbB3, INSR, FGFR1, TRKA, c-Kit, VEGFR2, and several EPH receptors was observed. Importantly, Brigatinib treatment reduced the levels of most of these p-RTKs with the most significant reduction in EGFR, ErbB2, ErbB3, VEGFR2, and EPH receptors, particularly in cells treated for 2h. In addition, Brigatinib treatment led to attenuation of the downstream signals from these RTKs, including p-AKT(S473 and T308) and p-ERK1/2. The phosphorylation of most of the Brigatinib-inhibited RTKs showed some recovery to baseline levels after 24h, although some of their downstream signaling proteins, such as ERK1/2, AKT, and S6, remained markedly suppressed (compare Figures 1A and 1C with Figures 1B

and 1D).

Figure 1. Inhibition of multiple RTKs and non-RTKs in Brigatinib-treated Ben-Men-1 cells grown under various conditions. PathScan® RTK signaling antibody array analysis was conducted using cells grown in 10% FBS and treated with 1x IC₅₀ of brigatinib for 2h (A) and 24 h (B) or in growth-arrested cells stimulated with 20% FBS in the presence of 1x IC₅₀ of brigatinib for 2h (C) and 24 h (D). The numeric table below each pair of arrays displays the fold-change in fluorescence detected for each phospho-protein expressed in cells treated with brigatinib relative to DMSO control after subtraction of the fluorescence in the background control spots (indicated as "-"). Positive control spots are denoted as "+".

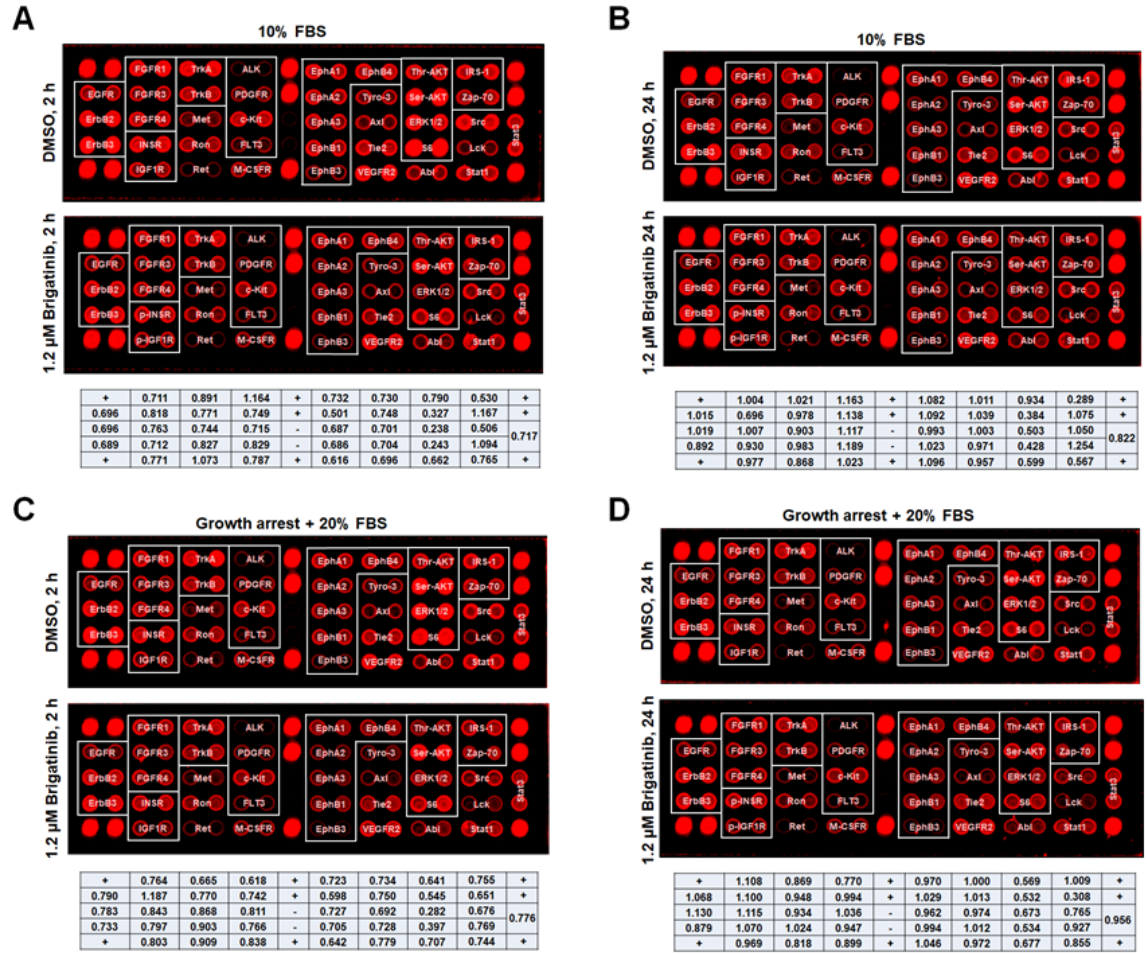


Figure 2. Brigatinib inhibits multiple RTKs, non-RTKs, and their downstream signals. (A) Western blot analysis was conducted to detect ALK expression in Ben-Men-1 cells grown under various growth conditions and with or without brigatinib treatment. (B) Brigatinib treatment greatly reduced phosphorylation of non-RTKs FER and FAK, RTKs EPHA2 and ErbB3, and their downstream signaling molecules AKT, ERK1/2, and S6 in active growing Ben-Men-1 cells or growth-arrested cells stimulated with 20% serum. (C) Brigatinib blocked phosphorylation of EGFR, ErbB3, and IGF1R in growth-arrested Ben-Men-1 cells stimulated with each cognate ligand.

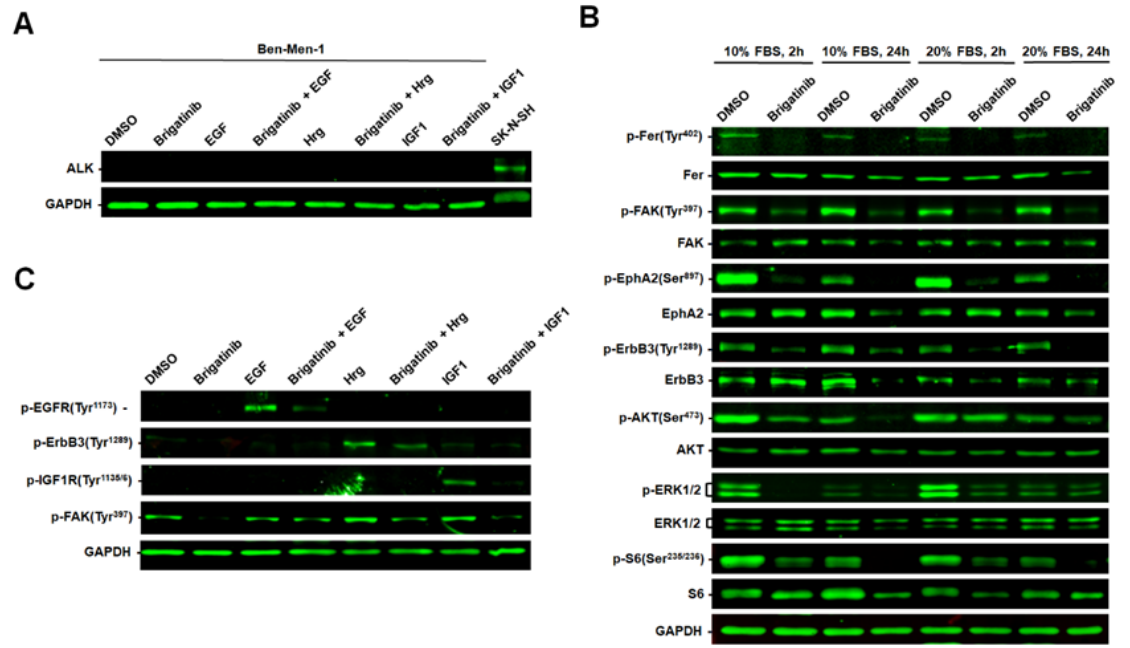
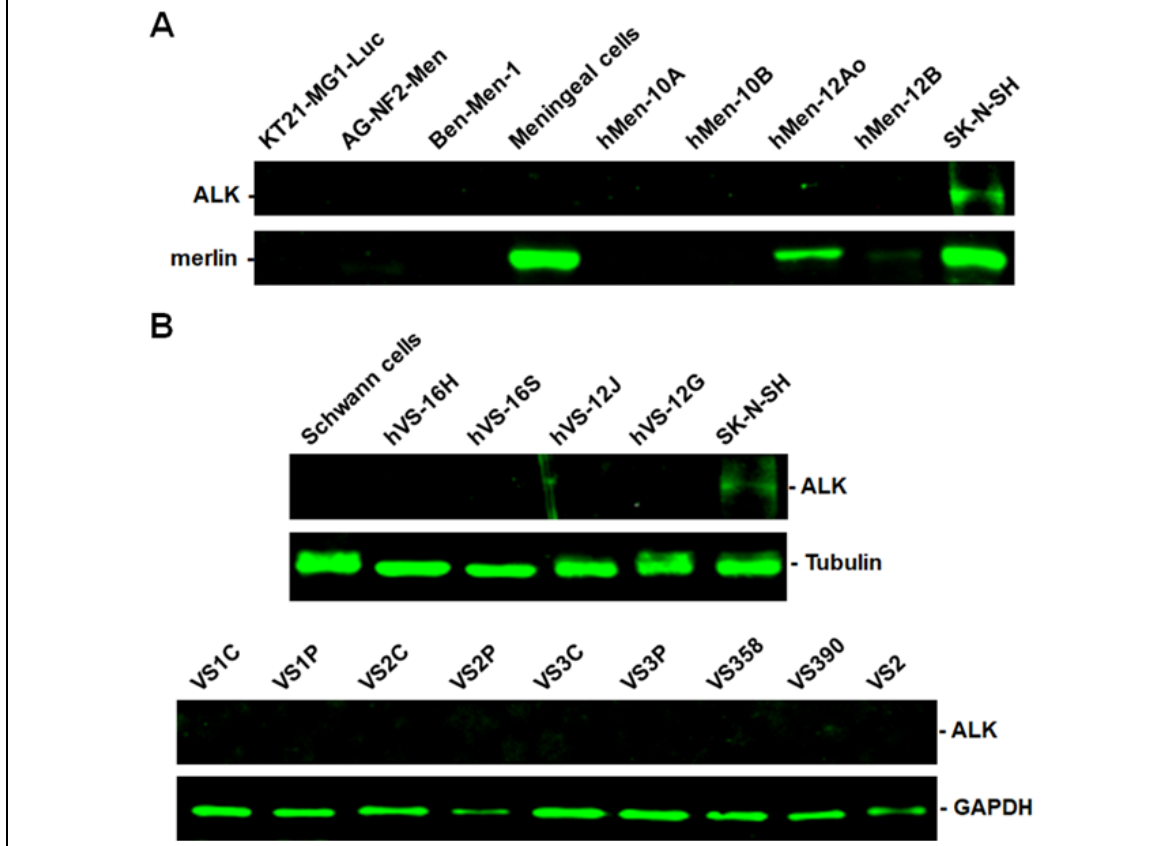
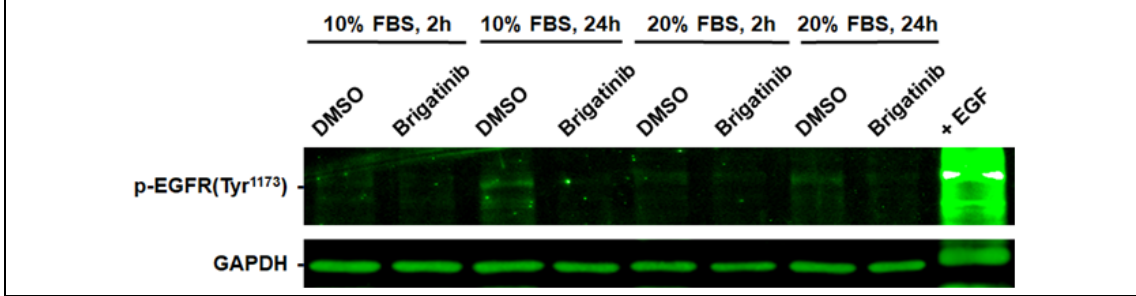


Figure 3. Meningioma and schwannoma cells do not express ALK. (A) ALK was not detected in meningeoma cells with or without NF2 expression as well schwannoma cells and tumors. Equal amounts of protein lysates from three human meningeoma cell lines (KT21-MG1-Luc, AG-NF2-Men, and Ben-Men-1), normal meningeal cells, and four primary meningeoma cultures (hMen-10A, hMen-10B, hMen-12Ao, hMen-12B) were used in Western blot analysis to probe ALK and merlin expression. SK-N-SH neuroblastoma cells, which express ALK, were used as a positive control. (B) **ALK expression was not detected in Schwann and schwannoma cells.** Western blotting was performed to detect ALK expression in human Schwann cells, four primary vestibular schwannoma cultures (hVS-16H, hVS-16S, hVS-12J, hVS-12Ga), SK-N-SH neuroblastoma cells and nine vestibular schwannomas (VS). Tubulin or GAPDH was used as a loading control.



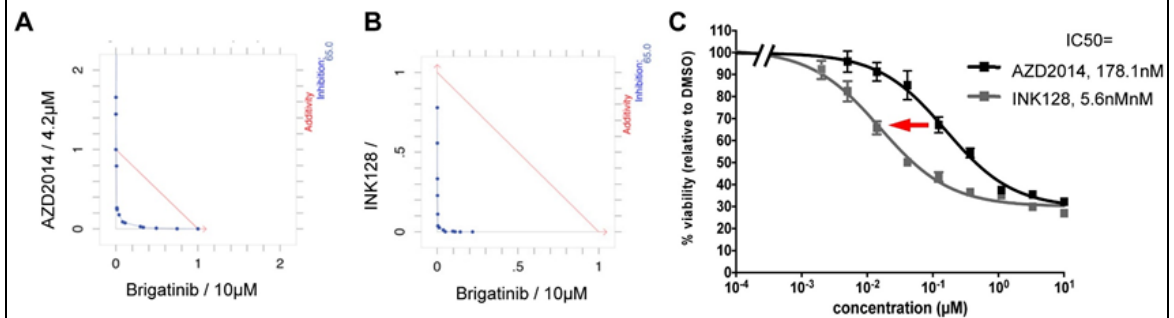
Further, Western blot analysis corroborated that phosphorylation of the non-RTKs focal adhesion kinase (FAK)/PTK2 and FER were noticeably reduced in Brigatinib-treated Ben-Men-1 cells under active growth conditions in 10% FBS or in growth-arrested cells stimulated with 20% serum (Figure 2B). Similar to p-RTK array analysis, we observed reduced phosphorylation of ErbB3 and EphA2 in Brigatinib-treated cells. Also, the downstream signaling nodes of these RTKs, including ERK1/2, AKT, and S6, were all markedly decreased. However, under the same growth conditions, the basal levels of p-EGFR were minimally detectable and were lost following Brigatinib treatment particularly after 24h (Figure 4). Additionally, we did not detect p-IGF1R under these growth conditions (data not shown). Therefore, we investigated the effects of Brigatinib in ligand-induced activation of IGF1R, EGFR, and ErbB3 in Ben-Men-1 cells. Upon each cognate ligand stimulation, p-EGFR, p-ErbB3, and p-IGF1R were readily detected in Ben-Men-1 cells, and Brigatinib treatment abrogated their phosphorylation (Figure 2C).

Figure 4. Ben-Men-1 cells expressed low levels of p-EGFR, which was abolished by brigatinib treatment. Western blot analysis revealed that while phosphorylated EGFR was robustly induced in EGF-stimulated Ben-Men-1 cells, only very low levels of p-EGFR were detected in actively-growing cells or growth-arrested cells stimulated with 20% serum for 24h. Brigatinib treatment diminished p-EGFR expression.



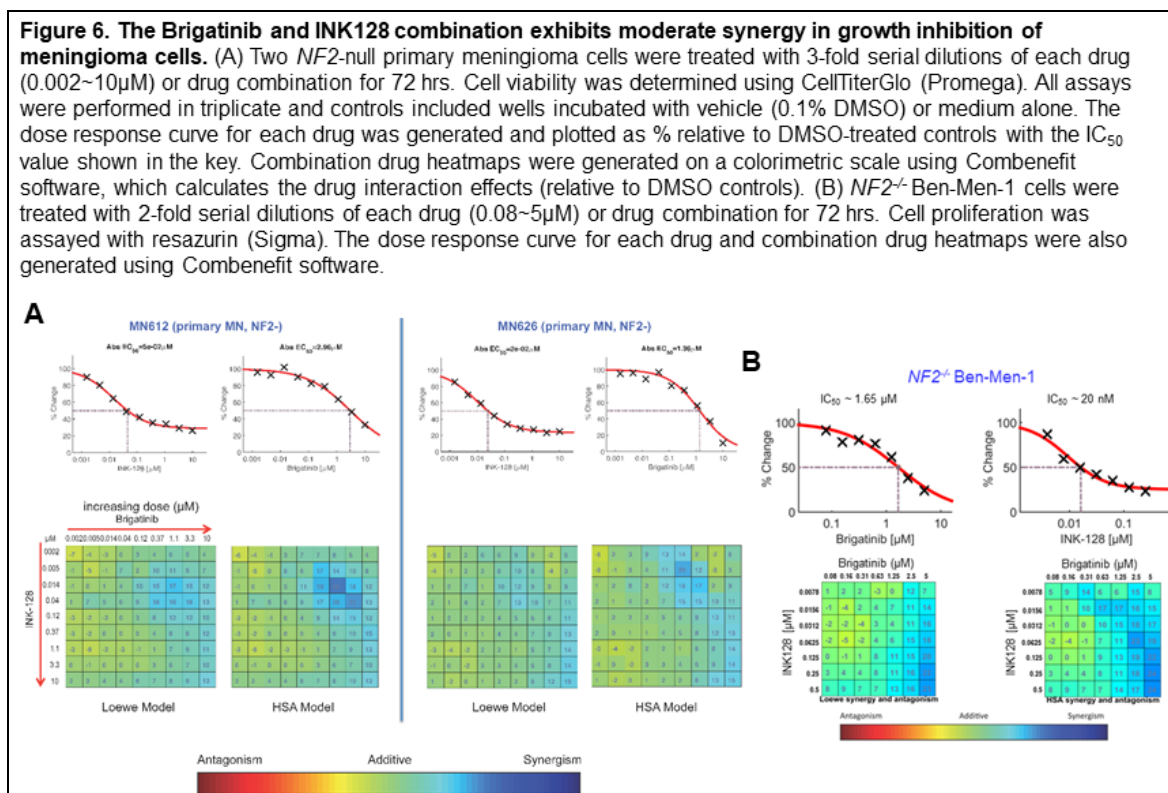
It should be mentioned that the Synodos for NF2 team also demonstrated anti-tumor activity of Brigatinib in a genetically-engineered mouse model for NF2-associated schwannoma. Collectively, these results indicate that Brigatinib possessed potent anti-tumor activity against *NF2*-deficient tumors via inhibition of multiple RTKs frequently activated in these tumors, but not ALK, as well as blockade of several non-RTKs, such as FAK, which has previously been recognized as an oncoprotein in NF2-related tumors (Ammoun and Hanemann, 2011; Blakeley and Plotkin, 2016). The results presented here together with the findings obtained previously by the Synodos for NF2 team have been combined and written into a manuscript currently under review (please see the attached manuscript [Chang et al., submitted] in Appendix). In addition, we have presented these findings to the 2018 and 2019 NF Conferences (also see Appendix). Based on these findings, the CTF in collaboration with Takeda Pharmaceutical Company has initiated a multi-site, phase II clinical trial to evaluate the efficacy of Brigatinib in patients with NF2 with associated progressive tumors of vestibular schwannomas, non-vestibular schwannomas, meningiomas, and ependymomas (Innovative Trial for Understanding the Impact of Targeted Therapies in NF2 [INTUITT-NF2]; ClinicalTrials.gov Identifier: NCT04374305; Principal Investigator: Scott R Plotkin, MD, PhD, Massachusetts General Hospital).

Figure 5. Combined treatment with Brigatinib and a dual mTORC1/2 inhibitor resulted in synergistic growth inhibition. Drug synergism experiments using the standard 6x6 dose matrix screen method were carried out for *NF2*-deficient primary meningioma cells treated with a combination of AZD2014 and Brigatinib (A) or INK128 and Brigatinib (B) for 72hr. Isobolograms were generated using Chalice Analyzer (Horizon CombinitorX; <http://chalice.horizondiscovery.com/analyzer-server/cwr/analyze.jsp>) and show synergism, defined as combination index (CI) <1 (blue plot), compared to Loewe Additivity model (CI=1, red plot). (C) As a representative, single drug dose response curves generated reveal increased sensitivity of meningioma cells to INK128 (decreased IC₅₀ dose) compared to AZD2014, defined by the shift of IC₅₀ curve to the left (red arrow). The IC₅₀ value for each drug is shown in the key.



Using Isobolograms (Horizon CombinitorX; <http://chalice.horizondiscovery.com/analyzer-server/cwr/analyze.jsp>), we showed that Brigatinib synergized with the dual mTORC1/2 inhibitor, AZD2014 or INK128 in inhibiting the growth of *NF2*-deficient primary meningioma cells (Figures 5A and 5B). In addition, we observed increased sensitivity of meningioma cells to INK128 treatment (>10-fold reduction in IC₅₀ dose), compared to AZD2014, indicating INK128 to be more potent (Figure 5C). The enhanced growth inhibition by the Brigatinib and INK128 combination was also observed in two *NF2*-null meningioma cell lines and the *NF2*-deficient Ben-Men-1 cell line. Using Combenefit software, we showed that the Brigatinib and INK128 combination exhibited moderate synergy in growth inhibition of both *NF2*-null meningioma (Figure 6A) and Ben-Men-1 cells (Figure 6B), particularly at higher

concentrations of Brigatinib.



Prior to initiation of the proposed animal studies, we worked with the Human Research Protection Office (HRPO) of the US Army Medical Research and Materiel Command (USAMRMC) Office of Research Protections (OPR) and received approval for our Institutional Review Board (IRB)-approved Human Subjects protocol using established human cell lines. In addition, we submitted ACURO Animal Use Appendix for Research Involving Animals to the Animal Care and Use Review Office (ACURO) and received approval for our Institutional Animal Care and Use Committee (IACUC)-approved animal protocol. With these approvals, we determined the maximal tolerable doses (MTDs) for the Brigatinib and INK-128 drug combination. We found immunodeficient NSG (*NOD.Cg-Prkdc^{scid} Il2rg^{tm1Wjl}/SzJ*) mice to tolerate Brigatinib at 50 mg/kg/day (formulated in 90% polyethylene glycol and 10% 1-methyl-2-pyrrolidinone) and INK-128 at 0.75 mg/mg/kg/day (prepared in 5% 1-methyl-2-pyrrolidinone, 15% polyvinylpyrrolidone, and 80% water), either alone or in combination.

To assess the *in vivo* efficacies of the Brigatinib and INK128, mice bearing established luciferase-expressing Ben-Men-1-LucB tumors, as defined by an increase in BL signal over at least two time points (Burns et al., 2013), were treated with Brigatinib, INK128, or their combination at the MTDs, or vehicle. BLI showed that vehicle-treated tumors grew steadily over time (an average of 440% after six weeks; Figure 7). Brigatinib alone effectively blocked meningioma growth with slight tumor shrinkage over the 6-week treatment period. INK128 alone also effectively blocked meningioma growth at the first two weeks, and treated tumors showed slight growth after four weeks. Nevertheless, treatment with INK128 for six weeks resulted in 85% reduction in tumor volume compared to the vehicle control. Combined treatment with Brigatinib and INK128 effectively shrank meningiomas over the entire six weeks. While there was a trend of more tumor shrinkage by the combination treatment than that that by Brigatinib alone; however, the differences in tumor shrinkage was not statistically significant.

Figure 7. Anti-tumor efficacy of Brigatinib and INK128, alone or in combination in the *NF2*-deficient Ben-Men-1-LucB meningioma mouse model. Mice with established meningioma xenografts were treated with vehicle, Brigatinib, INK128, or Brigatinib+INK128 by oral gavage and tumor growth was monitored by BLI as previously described (Burns et al., 2013). The relative tumor-emitted BL signals were quantified and denoted as % of total flux after treatment relative to the total flux prior to treatment designated as one (100%). The data are shown as mean \pm standard deviation.

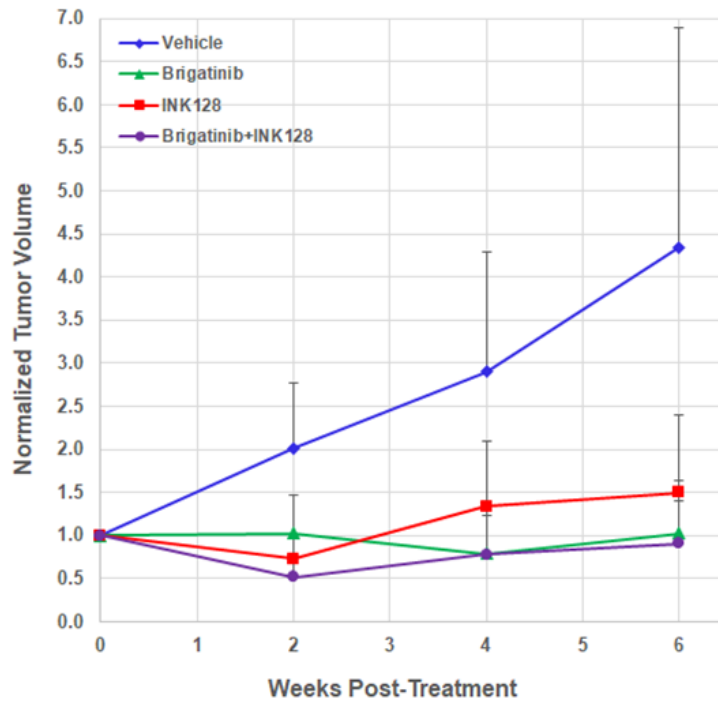
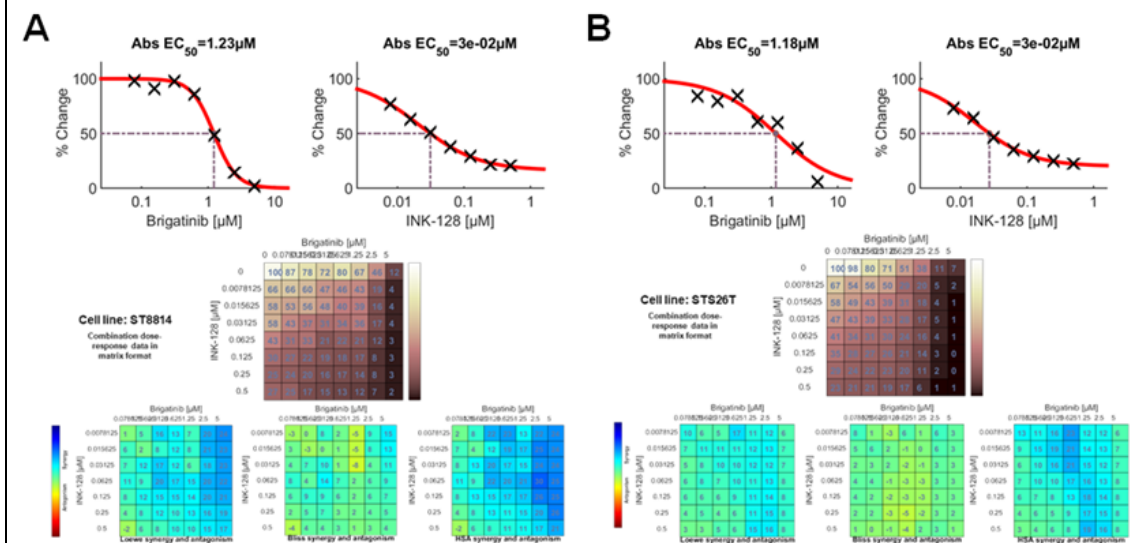
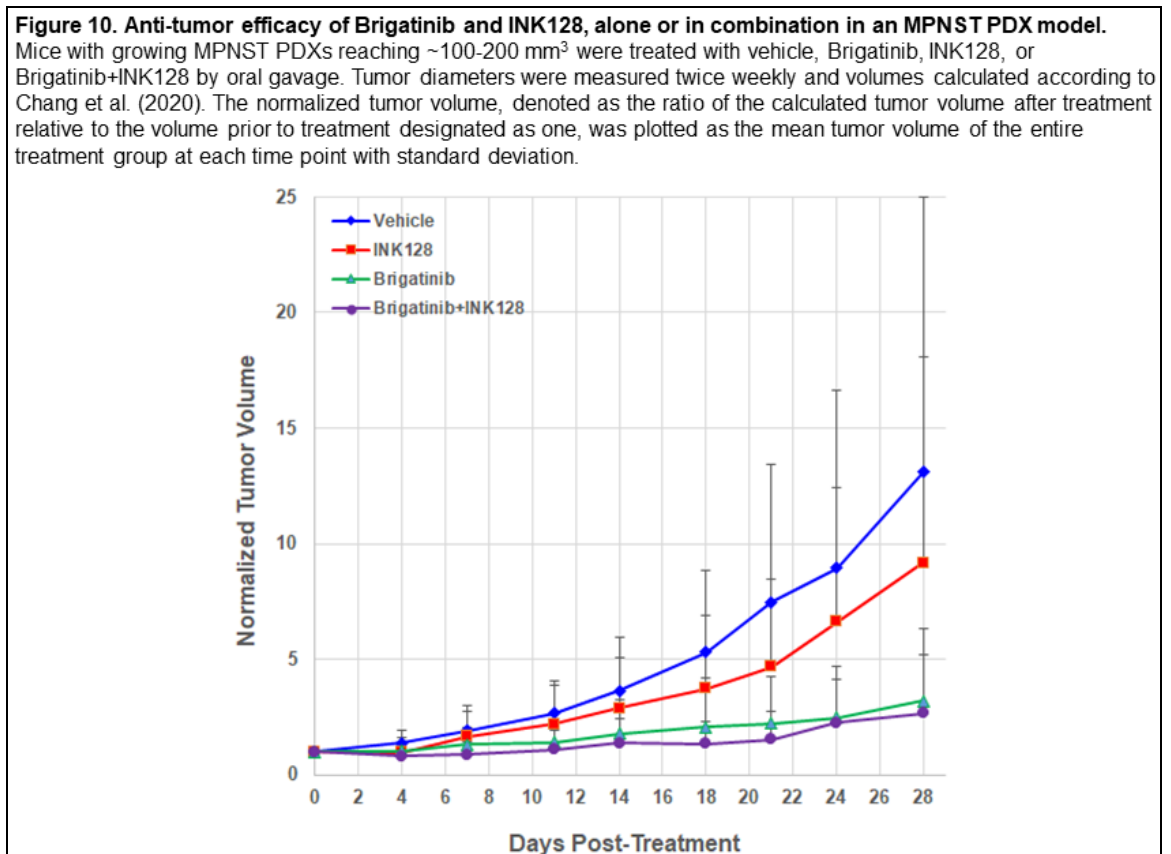
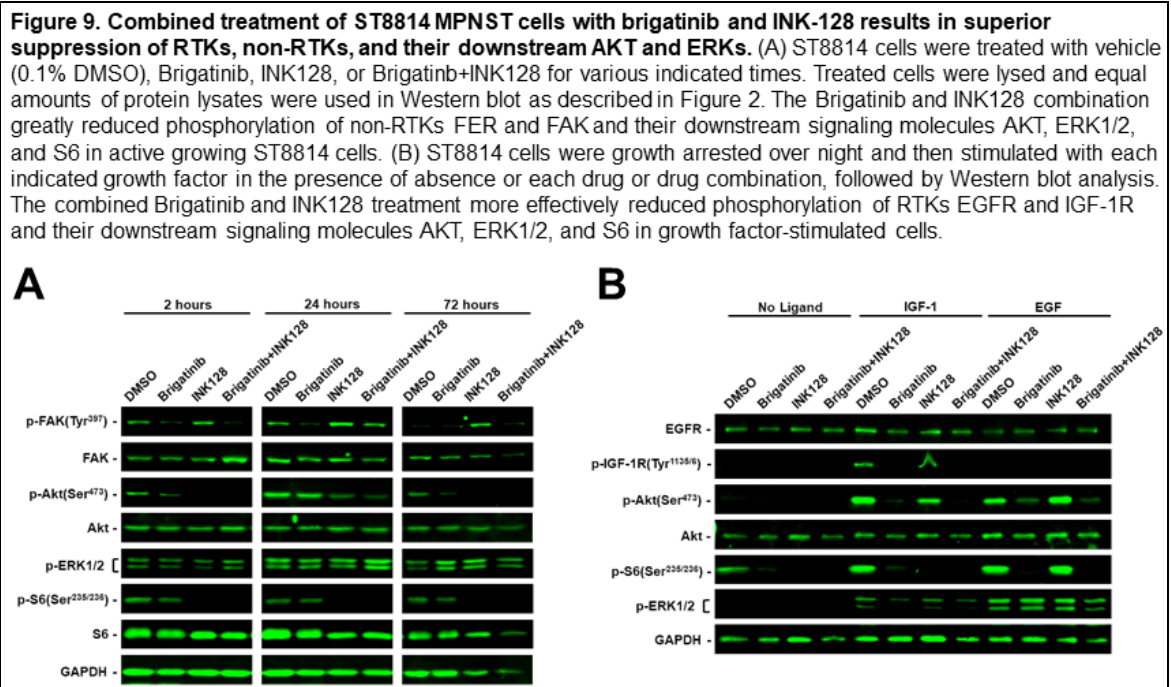


Figure 8. The Brigatinib and INK128 combination exhibits enhanced growth inhibition in MPNST cells. *NF1*-deficient ST8814 (A) and *NF1*-expressing STS26T (B) cells were treated with 2-fold serial dilutions of each drug or drug combination for 72 hrs. Cell proliferation was assessed with resazurin assays. All assays were performed in triplicate and controls included wells incubated with vehicle (0.1% DMSO) or medium alone. The dose response curve for each drug was generated and plotted as % relative to DMSO-treated controls with the IC_{50} value shown in the key. Combination drug heatmaps were generated on a colorimetric scale using Combenefit software, which calculates the drug interaction effects (relative to DMSO controls),



Previously, the Synodos for *NF2* team also demonstrated that Brigatinib alone significantly decreased the volume of schwannoma-bearing dorsal root ganglion in *Postn-Cre;Nf2^{flx/flx}* mice (see manuscript [Chang et al., submitted] in Appendix). Therefore, we examined whether the Brigatinib and INK128 combination exhibits anti-tumor effects in malignant schwannomas, such as malignant peripheral nerve sheath tumors (MPNSTs). We found that Brigatinib and INK128 had growth-inhibition activity in MPNST cells, and combination of Brigatinib with combination exhibits enhanced growth inhibition (Figure 8). Western blot analysis revealed that brigatinib, when combined with INK-128, in

MPNST cells resulted in superior suppression of RTKs, non-RTKs, and their downstream AKT and ERKs, compared with cells treated with each individual drug (Figure 9).

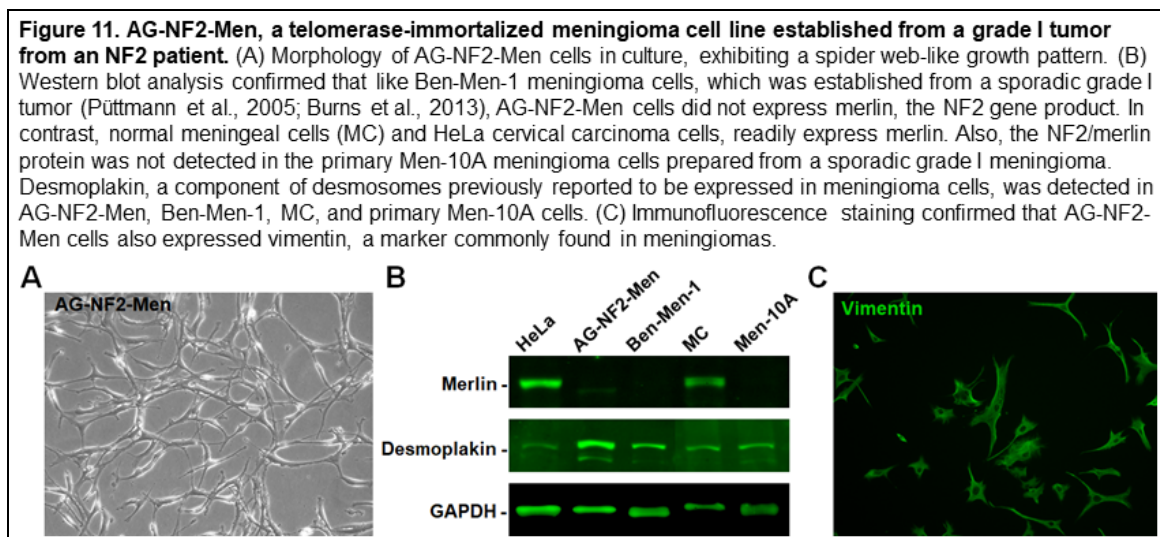


To examine the *in vivo* efficacy of the Brigatinib and INK128 combination in MPNSTs, we used an MPNST patient-derived xenograft (PDX) model. Mice bearing growing MPNST PDXs were treated them with Brigatinib, INK128, or their combination at the MTDs, or vehicle, and tumor volumes were measured twice a week. As expected, vehicle-treated tumors grew ~13-fold larger in tumor volume after 28 days (Figure 10). Brigatinib alone effectively suppressed the growth of MPNST PDXs by an average of 82% over four weeks of treatment, while INK-128 alone only modestly inhibited tumor

growth by ~32%, compared with the vehicle control group. Intriguingly, like in the Ben-Men-1 meningioma model, combined treatment with brigatinib and INK128 also effectively suppressed MPNST growth by an average 86% over four weeks; however, the anti-tumor effects were only slightly better than Brigatinib alone and their differences was not statistically significant.

Collectively, our results indicate that combination of Brigatinib with INK-128 modestly enhances the anti-tumor effects against meningioma and malignant schwannoma.

To compare the anti-tumor activity of Brigatinib, INK128, and their combination in an NF2-associated meningioma model, we have generated a meningioma cell line from a grade I tumor from an NF2 patient by telomerase immortalization. We named this NF2-associated meningioma cell line AG-NF2-Men-1, which retained many characteristics of the original tumor. It was slow growing and morphologically looked fibroblastic in culture (Figure 11A). Western blot analysis confirmed that AG-NF2-Men-1 cells did not express the *NF2* protein merlin, indicating that they are *NF2*-null (Figure 11B). Also, AG-NF2-Men-1 cells expressed several meningioma markers, including desmoplakin and vimentin (Figures 11B and 11C).



To generate a quantifiable, orthotopic animal model for NF2-associated meningioma, we transduced AG-NF2-Men-1 cells with Lenti-CMV-Luc lentiviruses, which carry a luciferase-expressing cassette and also express a puromycin-resistant marker, as we did to establish Ben-Men-1-LucB cells previously (Burns et al., 2013). Puromycin-resistant clones were isolated, and the clone that express the highest level of luciferase activity was identified. This clone AG-NF2-Men-Luc1 is currently being stereotactically injected into the skull base to generate tumor-bearing mice for further evaluation of the Brigatinib and INK128 combination.

(iii) What opportunities for training and professional development has the project provided?

This project was not intended to provide training and professional development opportunities; therefore, we have "Nothing to Report."

(iv) How were the results disseminated to communities of interest?

Our results indicate that Brigatinib possessed potent anti-tumor activity against *NF2*-deficient tumors via inhibition of multiple RTKs, but not ALK, as well as blockade of several non-RTKs, such as FAK, which has previously been recognized as an oncoprotein in *NF2*-related tumors. These findings have been combined with the data obtained previously by the Synodos for *NF2* team, in which I am a member, and written into a manuscript that has been submitted for publication (see [Chang et al., submitted] in Appendix). Also, we have presented these findings to various national/international meetings (see Appendix). Based on our and the Synodos for *NF2* team findings, the CTF has collaborated with Takeda Pharmaceutical Company, the developer of Brigatinib, to conduct a multi-site,

phase II clinical trial of Brigatinib to treat NF2-associated progressive tumors of vestibular schwannomas, non-vestibular schwannomas, meningiomas, and ependymomas (Innovative Trial for Understanding the Impact of Targeted Therapies in NF2 [INTUITT-NF2]; ClinicalTrials.gov Identifier: NCT04374305; Principal Investigator: Scott R Plotkin, MD, PhD, Massachusetts General Hospital). In addition, we have found that Brigatinib has anti-tumor efficacy against both *NF2*-deficient sporadic meningioma and *NF1*-deficient MPNST, its combination with the dual MTORC1/2 inhibitor INK128 modestly enhances the anti-tumor effects.

(v) What do you plan to do during the next reporting period to accomplish the goals?

We are in the process of generating a quantifiable, orthotopic animal model for NF2-associated meningioma. We have successfully transduced AG-NF2-Men-1 cells, established from a grade I meningioma from an NF2 patient by telomerase immortalization, with Lenti-CMV-Luc lentiviruses, which carry a luciferase-expressing cassette and express a puromycin-resistant marker. We have isolated several Puromycin-resistant clones and identified one of them that express the highest level of luciferase activity. This clone AG-NF2-Men-Luc1 is currently being stereotactically injected into the skull base to generate tumor-bearing mice for further evaluation of the Brigatinib and INK128 combination in this NF2-associated meningioma model.

5. IMPACT

(i) What was the impact on the development of the principal discipline(s) of the project?

Identification of a medical therapy that effectively eradicates NF2-related tumors would significantly advance our current approach to NF2 treatment and greatly improve the clinical care and long-term treatment outcomes for these patients. We have found that Brigatinib caused tumor shrinkage in *NF2*-deficient meningiomas by inhibiting multiple RTKs, but not ALK, as well as blocking several non-RTKs, such as FAK. As Brigatinib is an FDA-approved drug, a multi-center, phase II INTUITT-NF2 clinical trial has been initiated to evaluate Brigatinib in patients with NF2 with associated progressive tumors of vestibular schwannomas, non-vestibular schwannomas, meningiomas, and ependymomas (ClinicalTrials.gov Identifier: NCT04374305).

Our results further show that Brigatinib has anti-tumor efficacy against both *NF2*-deficient sporadic meningioma and *NF1*-deficient MPNST, its combination with the dual MTORC1/2 inhibitor INK128 modestly enhances the anti-tumor effects. These results suggest that Brigatinib should also be further evaluate as a potential treatment for MPNST. In addition, we have generated, for the first time, a telomerase-immortalized NF2-associated meningioma cell line AG-NF2-Men-1. Luciferase-expressing AG-NF2-Men-1 cells have been used to establish an orthotopic NF2-associated meningioma model for drug evaluation.

(ii) What was the impact on other disciplines?

As we have found that Brigatinib suppressed the growth *NF2*-deficient tumors via inhibition of multiple RTKs and non-RTKs, including FAK. Many of these kinases have also been found to be activated in other human cancers, including malignant peripheral nerve sheath tumors (MPNSTs) which are frequently found in patients with NF1. Indeed, Brigatinib also exhibited anti-tumor effects in MPNSTs, suggesting that it may also be a viable treatment for MPNSTs.

(iii) What was the impact on technology transfer?

Nothing to report.

(iv) What was the impact on society beyond science and technology?

Nothing to report.

6. CHANGES/PROBLEMS:

(i) Changes in approach and reasons for change

None

(ii) Actual or anticipated problems or delays and actions or plans to resolve them

None

(iii) Changes that had a significant impact on expenditures

None

(iv) Significant changes in use or care of human subjects

None

(v) Significant changes in use or care of vertebrate animals

None

(vi) Significant changes in use of biohazards and/or select agents

None

7. Publications, Abstracts, and Presentations

(1) Journal publications or manuscripts under review

The works described in the following publications or manuscripts were supported, in part, by this grant. We have acknowledged the DOD support in these papers (please see Appendices).

- (i) Fuse MA, Dinh CT, Vitte J, Kirkpatrick J, Mindos T, Plati SK, Young JI, Huang J, Carlstedt A, Franco MC, Brnjos K, Nagamoto J, Petrilli A, Copik AJ, Soulakova JN, Bracho O, Yan D, Mittal R, Shen R, Telischi FF, Morrison H, Giovannini M, Liu XZ, Chang LS, Fernandez-Valle C. Preclinical Assessment of MEK1/2 Inhibitors for Neurofibromatosis Type 2-Associated Schwannomas Reveals Differences in Efficacy and Drug Resistance Development. *Neuro-Oncol.* 2019;21:486-497. PMID: 30615146

To identify an effective treatment for NF2-associated schwannomas, we collaborated with Dr. Cristina Fenandez-Valle at the University of Central Florida to investigate repurposing drugs targeting MEK1/2 kinases as merlin, the *NF2* gene product, has been shown to modulate activity of the Ras/Raf/MEK/ERK pathway. Among six MEK inhibitors examined, trametinib, PD0325901, and cobimetinib were most effective in reducing the viability of merlin-deficient mouse and human Schwann cells. Also, the three inhibitors slowed the growth of schwannoma allografts. However, when we analyzed drug-treated tumors, we found decreased pERK1/2 levels only in the tumors treated with PD0325901 and cobimetinib but not trametinib. Similarly, tumor burden and average tumor size were reduced in trametinib-treated NF2 transgenic mice, and we also did not find reduced pERK1/2 in treated mouse tumors. The results show that MEK inhibitors exhibited differences in anti-tumor efficacy resistance in schwannoma models with possible emergence of trametinib resistance.

- (ii) Chang L-S, Oblinger JL, Burns SS, Huang J, Anderson LW, Hollingshead MG, Shen R, Pan L, Agarwal G, Ren Y, Roberts R, O'Keefe BR, Kinghorn AD, Collins JM. 2020. Targeting protein translation by rocaglamide and didesmethylrocaglamide to treat MPNST and other sarcomas. *Mol Cancer Ther.* 19:731-741.

Previously we showed that malignant schwannomas, such as malignant peripheral nerve sheath tumors (MPNSTs) which are frequently found in patients with NF1, and benign schwannoma including those commonly seen in patients with NF2, often overexpress eIF4F components, and the eIF4A inhibitor silvestrol potently suppresses MPNST growth (Oblinger JL et al. *Neuro-Oncol.* 2016;18:1265-1277). However, silvestrol has suboptimal drug-like properties, including a bulky structure, poor oral bioavailability, sensitivity to MDR1 efflux, and pulmonary toxicity in dogs. We compared 10 silvestrol-related rocaglates lacking the dioxanyl ring and found that didesmethylrocaglamide (DDR) and rocaglamide (Roc) had growth-inhibitory activity comparable to silvestrol. Both DDR and Roc arrested MPNST cells at G₂/M, increased the sub-G₁ population, induced cleavage of caspases and poly(ADP-ribose) polymerase, and elevated the levels of the DNA-damage response marker γ H2A.X, while decreasing the expression of AKT and ERK1/2, consistent with translation inhibition. Unlike silvestrol, DDR and Roc were not sensitive to MDR1 inhibition and pharmacokinetic analysis confirmed that Roc had 50% oral bioavailability. Importantly, Roc, when administered intraperitoneally or orally, showed potent anti-tumor effects in an orthotopic MPNST mouse model and did not induce pulmonary toxicity in dogs as found with silvestrol. Treated tumors displayed degenerative changes and had more cleaved caspase 3-positive cells, indicative of increased apoptosis. Furthermore, Roc effectively suppressed the growth of osteosarcoma, Ewing sarcoma, and rhabdomyosarcoma cells and patient-derived xenografts. Both Roc- and DDR-treated sarcoma cells showed decreased levels of multiple oncogenic kinases, including IGF-1R. The more favorable drug-like properties of DDR and Roc and the potent anti-tumor activity of Roc suggest that these rocaglamides could become viable treatments for MPNST and other sarcomas.

- (iii) Chang L-S, Oblinger JL, Smith A, Ferrer M, Angus S, Petrilli AM, Beauchamp RL, Riecken LB, Erdin S, Poi M, Huang J, Bessler W, Zhang X, Rajarshi G, Thomas C, Burns SS, Jiang L, Li X, Lu Q, Yuan J, He Y, Masters A, Jones DR, Yates CW, Haggarty Stephen J, La Rosa S, Welling DB, Stemmer-Rachamimov AO, Plotkin SR, Blakeley JO, Gusella JF, Morrison H, Ramesh V, Fernandez-Valle C, Johnson GL, Clapp DW, on behalf of the Synodos for NF2 Consortium. 2020. Brigatinib causes tumor shrinkage in both *NF2*-deficient meningioma and schwannoma through inhibition of multiple tyrosine kinases but not ALK. Submitted to PLoS ONE.

We, as members of the Synodos for NF2 Consortium in collaboration with the NIH-NCATS, conducted high-throughput drug screening of isogenic pairs of *NF2*-deficient and *NF2*-expressing disease-relevant cells and identified several actionable drug targets for the treatment of both *NF2*-related schwannomas and meningiomas. We further showed that Brigatinib, developed for inhibition of ALK, potently suppressed the growth of *NF2*-deficient meningioma and schwannoma cells *in vitro* and of established xenograft and spontaneous *NF2*-deficient meningiomas and schwannomas *in vivo*. With this support, we found that Brigatinib specifically inhibited multiple RTKs and non-RTKs, such as focal adhesion kinase, but not ALK, in *NF2*-deficient tumor cells. These findings represent a major advance for the development of a treatment of *NF2*-related malignancies and demonstrate the power of a *de novo* unbiased approach to drug development.

- (iv) Amaravathi A, Oblinger JL, Welling DB, Kinghorn AD, Chang L-S. Neurofibromatosis: Molecular Pathogenesis and Natural Compounds as Potential Treatments. Submitted to Neuro-Oncology.

In this paper, we review the neurofibromatosis tumor suppressor syndromes, including NF1, NF2, and schwannomatosis, which are characterized by multiple nervous system tumors, particularly Schwann cell neoplasms. NF-related tumors are mainly treated by surgery and often refractory to conventional chemotherapy. Recent advances in molecular genetics and genomics alongside the development of multiple animal models have provided a better understanding of NF tumor biology and facilitated target identification and therapeutic evaluation. Many targeted therapies have been evaluated in preclinical models and patients, including the MEK inhibitor selumetinib recently approved by the FDA for treating NF1-associated plexiform neurofibroma. Due to their anti-neoplastic, antioxidant, and anti-inflammatory properties, selected natural compounds

could be useful as adjuvant therapy for patients with tumor predisposition syndromes as patients often take them as dietary supplements and for health enhancement purposes. Several natural compounds have been tested in NF models. Some have demonstrated potent anti-tumor effects and may become viable treatments in the future.

(2) Abstracts presented at national/international conferences

We presented the following ten abstracts at the national/international meetings over the last two years and have acknowledged the DOD support in these abstracts (please see Appendices).

- (i) Chang L-S, SS Burns, JL Oblinger, M Ferrer, J Huang, M Poi, V Ramesh, On behalf of the Synodos for NF2 Consortium. 2018. Novel drug discovery for NF2-deficient meningiomas: Brigatinib causes tumor shrinkage in NF2-deficient meningiomas. The 2018 Joint Global NF Conference, Paris, France. (Platform presentation)
- (ii) Chang L-S, JL Oblinger, SS Burns, J Huang, L Anderson, R Shen, L Pan, Y Ren, BR O'Keefe, AD Kinghorn, JM Collins. 2018. Identification of silvestrol-related rocaglates with better bioavailability and high potency against malignant peripheral nerve sheath tumors. The 2018 Joint Global NF Conference, Paris, France. (Poster presentation)
- (iii) Fernandez-Valle C, M Fuse, C Dinh, J Vitte, J Kirkpatrick, T Mindos, S Champion, K Brnjos, MC Franco, J Huang, J Young, A Petrilli, D Yan, R Mittal, R Shen, F Telischi, L-S Chang, H Morrison, M Giovannini, X-Z Liu. 2018. Preclinical Assessment of MEK1/2 Inhibitors for Neurofibromatosis Type 2-Associated Schwannomas Reveals Differences in Efficacy and Drug Resistance Development. The 2018 Joint Global NF Conference, Paris, France. (Platform presentation)
- (iv) Welling DB, SS Burns, JL Oblinger, B Miles-Markley, A Quinkert, J Blakeley, BA Neff, RK Jackler, L-S Chang. 2018. Phase 1 and Phase 0 studies of AR-42, a pan histone deacetylase inhibitor, in subjects with neurofibromatosis type 2 (NF2)-associated vestibular schwannomas and meningiomas. The 2018 Joint Global NF Conference, Paris, France. (Poster presentation)
- (v) Beauchamp RL, S Erdin, SP Angus, TJ Stuhlmiller, JL Oblinger, JT Jordan, SJ Haggarty, SR Plotkin, L-S Chang, GL Johnson, JF Gusella, V Ramesh. 2018. High throughput kinome and transcriptome analyses reveal novel therapeutic targets in *NF2*-deficient meningioma. The 2018 Society for Neuro-Oncology Meeting, New Orleans, LA. (Poster presentation)
- (vi) Oblinger J, L-S Chang. 2019. Brigatinib as a potential therapy for malignant peripheral nerve sheath tumors. The 2019 NF Conference, San Francisco, CA. (Poster presentation)
- (vii) Chang L-S, JL Oblinger, SS Burns, J Huang, L Anderson, R Shen, L Pan, Y Ren, R Roberts, BR O'Keefe, AD Kinghorn, JM Collins. Targeting protein translation with rocaglamide and didesmethylrocaglamide to treat NF1 and NF2 tumors. The 2019 NF Conference, San Francisco, CA. (Platform presentation)
- (viii) Chang L-S. 2019. Drug Discoveries from Synodos for NF2 and Identification of Natural Compounds to Treat NF1 and NF2 Tumors. NF Symposium and iNFo Fair 2019 - Annual NF Midwest Neurofibromatosis Family Symposium, Northern Illinois University, Hoffman Estates, IL. (Platform presentation)
- (ix) Chang L-S. 2020. Targeting protein translation via eIF4A inhibition with didesmethylrocaglamide (DDR) and rocaglamide (Roc) to treat pediatric osteosarcoma. Keats Beating Cancer – Science Is the Cure Symposium, Orlando, FL. (Platform presentation)
- (x) Chang L-S, JL Oblinger, G Agarwal, TA Wilson, R Roberts, J Fuchs, BR O'Keefe, AD Kinghorn, JM Collins. 2020. The eIF4A inhibitors didesmethylrocaglamide and rocaglamide as effective treatments for pediatric bone and soft-tissue sarcomas. AACR Annual Meeting 2020, San Diego,

CA. (Poster presentation)

8. PARTICIPANTS & OTHER COLLABORATING ORGANIZATIONS

(i) What individuals who have worked on the project

The Research Institute at Nationwide Children's Hospital
Long-Sheng Chang, Ph.D., Professor, Principal Investigator - 15% effort
Janet Oblinger, Ph.D., Research Associate - 50% effort
Michael Hsu, M.S., Research Assistant – 75% effort
Massachusetts General Hospital
Vijaya Ramesh, Ph.D., Professor, Site Principal Investigator - 10% effort
Roberta Beauchamp, M.S., Research Associate - 25% effort

(ii) Has there been a change in the active other support of the PD/PI(s) or senior/key personnel since the last reporting period?

Nothing to report.

(iii) What other organizations were involved as partners

Massachusetts General Hospital - Vijaya Ramesh, Ph.D., Site Principal Investigator

9. Reportable Outcome

Two peer-reviewed publication, two manuscripts under review, and ten abstracts at national/international conferences.

10. Other Achievements

Nothing to report.

11. References

- Ammoun S, Hanemann CO. 2011. Emerging therapeutic targets in schwannomas and other merlin-deficient tumors. *Nat Rev Neurol*. 2011;7:392-399. <https://www.ncbi.nlm.nih.gov/pubmed/21647202>
- Angus SP, Oblinger JL, Stuhlmiller TJ, DeSouza PA, Beauchamp RL, Witt L, Chen X, Jordan JT, Gilbert TSK, Stemmer-Rachamimov A, Gusella JF, Plotkin SR, Haggarty SJ, Chang LS, Johnson GL, Ramesh V; Children's Tumor Foundation Synodos for NF2 Consortium. EPH receptor signaling as a novel therapeutic target in NF2-deficient meningioma. *Neuro Oncol*. 2018;20:1185-1196. <https://www.ncbi.nlm.nih.gov/pubmed/29982664>
- Blakeley JO, Plotkin SR. Therapeutic advances for the tumors associated with neurofibromatosis type 1, type 2, and schwannomatosis. *Neuro Oncol*. 2016;18:624-638. <https://www.ncbi.nlm.nih.gov/pubmed/26851632>
- Burns SS, Akhmametyeva EM, Oblinger JL, Bush ML, Huang J, Senner V, Chen C-S, Jacob A, Welling DB, Chang L-S. 2013. AR-42, a Histone Deacetylase Inhibitor, Differentially Affects Cell-Cycle Progression of Meningeal and Meningioma Cells and Potently Inhibits NF2- Meningioma Growth. *Cancer Res*. 73:792-804. <http://www.ncbi.nlm.nih.gov/pubmed/23151902>
- Ghobrial IM, Siegel DS, Vij R, Berdeja JG, Richardson PG, Neuwirth R, Patel CG, Zohren F, Wolf JL. TAK-228 (formerly MLN0128), an investigational oral dual TORC1/2 inhibitor: A phase I dose escalation study in patients with relapsed or refractory multiple myeloma, non-Hodgkin lymphoma, or Waldenström's macroglobulinemia. *Am J Hematol*. 2016;91:400-405. <https://www.ncbi.nlm.nih.gov/pubmed/26800393>

- Huang WS, Liu S, Zou D, Thomas M, Wang Y, Zhou T, Romero J, Kohlmann A, Li F, Qi J, Cai L, Dwight TA, Xu Y, Xu R, Dodd R, Toms A, Parillon L, Lu X, Anjum R, Zhang S, Wang F, Keats J, Wardwell SD, Ning Y, Xu Q, Moran Le, Mohemmad QK, Jang HG, Clackson T, Narasimhan NI, Rivera VM, Zhu X, Dalgarno D, Shakespeare WC. Discovery of brigatinib (ap26113), a phosphine oxide-containing, potent, orally active inhibitor of anaplastic lymphoma kinase. *J Med Chem.* 2016; 59:4948-4964.
<https://www.ncbi.nlm.nih.gov/pubmed/27144831>
- Ostrom Qt, Gittleman H, Truitt G, Boscia A, Kruchko C, Barnholtz-Sloan Js. CBTRUS statistical report: primary brain and other central nervous system tumors diagnosed in the united states in 2011-2015. *Neuro Oncol.* 2018;20(SUPPL_4):IV1-IV86. <https://www.ncbi.nlm.nih.gov/pubmed/30445539>
- Püttmann S, Senner V, Braune S, Hillmann B, Exeler R, Rickert C, Paulus W. 2005. Establishment of a benign meningioma cell line by hTERT-mediated immortalization. *Lab Invest.* 85:1163-1171.
<http://www.ncbi.nlm.nih.gov/pubmed/15965488>
- Rouleau GA, Merel P, Lutchman M, Sanson M, Zucman J, Marineau C, Hoang-Xuan K, Demczuk S, Desmaze C, Plougastel B, et al. Alteration in a new gene encoding a putative membrane-organising protein causes neurofibromatosis type 2. *Nature* 1993;363:515-521.
<http://www.ncbi.nlm.nih.gov/pubmed/8379998>
- Suppiah S, Nassiri F, Bi WL, Dunn IF, Hanemann CO, Horbinski CM, Hashizume R, James CD, Mawrin C, Noushmehr H, Perry A, Sahm F, Sloan A, Von Deimling A, Wen PY, Aldape K, Zadeh G; International Consortium on Meningiomas. Molecular and translational advances in meningiomas. *Neuro Oncol.* 2019;21(Supplement_1):i4-i17. <https://www.ncbi.nlm.nih.gov/pubmed/30649490>
- Synodos for NF2 Consortium, Allaway R, Angus SP, Beauchamp RL, Blakeley JO, Bott M, Burns SS, Carlstedt A, Chang LS, Chen X, Clapp DW, Desouza PA, Erdin S, Fernandez-Valle C, Guinney J, Gusella JF, Haggarty SJ, Johnson GL, La Rosa S, Morrison H, Petrilli AM, Plotkin SR, Pratap A, Ramesh V, Sciaky N, Stemmer-Rachamimov A, Stuhlmiller TJ, Talkowski ME, Welling DB, Yates CW, Zawistowski JS, Zhao WN. Traditional and systems biology based drug discovery for the rare tumor syndrome neurofibromatosis type 2. *PLoS One.* 2018;13:e0197350.
<https://www.ncbi.nlm.nih.gov/pubmed/29897904>
- Trofatter JA, MacCollin MM, Rutter JL, Murrell JR, Duyao MP, Parry DM, Eldridge R, Kley N, Menon AG, Pulaski K, Haase VH, Ambrose CM, Munroe D, Bove C, Haines JL, Martuza RL, MacDonald ME, Seizinger BR, Short MP, Buckler AJ, Gusella JF. A novel moesin-, ezrin-, radixin-like gene is a candidate for the neurofibromatosis 2 tumor-suppressor. *Cell* 1993;72:791-800.
<http://www.ncbi.nlm.nih.gov/pubmed/8453669>
- Zhang S, Anjum R, Squillace R, Nadworny S, Zhou T, Keats J, Ning Y, Wardwell SD, Miller D, Song Y, Eichinger L, Moran L, Huang WS, Liu S, Zou D, Wang Y, Mohemmad Q, Jang HG, Ye E, Narasimhan N, Wang F, Miret J, Zhu X, Clackson T, Dalgarno D, Shakespeare WC, Rivera VM. The Potent ALK Inhibitor Brigatinib (AP26113) Overcomes Mechanisms of Resistance to First- and Second-Generation ALK Inhibitors in Preclinical Models. *Clin Cancer Res.* 2016;22:5527-5538.
<https://www.ncbi.nlm.nih.gov/pubmed/27780853>

12. Appendices

The attachment includes two publication, two manuscripts, and ten abstracts.

Preclinical assessment of MEK1/2 inhibitors for neurofibromatosis type 2–associated schwannomas reveals differences in efficacy and drug resistance development

Marisa A. Fuse, Christine T. Dinh, Jeremie Vitte, Joanna Kirkpatrick, Thomas Mindos, Stephani Klingeman Plati, Juan I. Young, Jie Huang, Annemarie Carlstedt, Maria Clara Franco, Konstantin Brnjos, Jackson Nagamoto, Alejandra M. Petrilli, Alicja J. Copik, Julia N. Soulakova, Olena Bracho, Denise Yan, Rahul Mittal, Rulong Shen, Fred F. Telischi, Helen Morrison, Marco Giovannini, Xue-Zhong Liu, Long-Sheng Chang, and Cristina Fernandez-Valle

Burnett School of Biomedical Sciences, College of Medicine, University of Central Florida (UCF), Orlando, Florida, USA (M.A.F., S.K.P., M.C.F., K.B., J.N., A.P., A.J.C., J.N.S., C.F.V.); Department of Otolaryngology, University of Miami Miller School of Medicine, Miami, Florida, USA (C.T.D., O.B., D.Y., R.M., F.F.T., X.Z.-L.); Department of Head and Neck Surgery, David Geffen School of Medicine at UCLA and Jonsson Comprehensive Cancer Center, University of California at Los Angeles (UCLA), Los Angeles, California, USA (J.V., M.G.); Leibniz Institute on Aging, Fritz Lipmann Institute, Jena, Germany (J.K., T.M., A.C., H.M.); Department of Human Genetics, University of Miami Miller School of Medicine, Miami, Florida, USA (J.I.Y., X.-Z.L.); Center for Childhood Cancer and Blood Diseases, Nationwide Children's Hospital (J.H., L.-S.C.) and Departments of Pediatrics (J.H., L.-S.C.) and Pathology, The Ohio State University (R.S.), Columbus, Ohio, USA

Corresponding Author: Cristina Fernandez-Valle, Ph.D., Burnett School of Biomedical Sciences, College of Medicine, University of Central Florida, 6900 Lake Nona Blvd, Orlando, FL 32827 (cfv@ucf.edu).

Abstract

Background. Neurofibromatosis type 2 (NF2) is a genetic tumor-predisposition disorder caused by *NF2*/merlin tumor suppressor gene inactivation. The hallmark of NF2 is formation of bilateral vestibular schwannomas (VS). Because merlin modulates activity of the Ras/Raf/mitogen-activated protein kinase kinase (MEK)/extracellular signal-regulated kinase (ERK) pathway, we investigated repurposing drugs targeting MEK1 and/or MEK2 as a treatment for NF2-associated schwannomas.

Methods. Mouse and human merlin-deficient Schwann cell lines (MD-MSCHSC) were screened against 6 MEK1/2 inhibitors. Efficacious drugs were tested in orthotopic allograft and *NF2* transgenic mouse models. Pathway and proteome analyses were conducted. Drug efficacy was examined in primary human VS cells with *NF2* mutations and correlated with DNA methylation patterns.

Results. Trametinib, PD0325901, and cobimetinib were most effective in reducing MD-MSCHSC viability. Each decreased phosphorylated pERK1/2 and cyclin D1, increased p27, and induced caspase-3 cleavage in MD-MSCHSCs. Proteomic analysis confirmed cell cycle arrest and activation of pro-apoptotic pathways in trametinib-treated MD-MSCHSCs. The 3 inhibitors slowed allograft growth; however, decreased pERK1/2, cyclin D1, and Ki-67 levels were observed only in PD0325901 and cobimetinib-treated grafts. Tumor burden and average tumor size were reduced in trametinib-treated *NF2* transgenic mice; however, tumors did not exhibit reduced pERK1/2 levels. Trametinib and PD0325901 modestly reduced viability of several primary human VS cell cultures with *NF2* mutations. DNA methylation analysis of PD0325901-resistant versus -susceptible VS identified genes that could contribute to drug resistance.

Conclusion. MEK inhibitors exhibited differences in antitumor efficacy resistance in schwannoma models with possible emergence of trametinib resistance. The results support further investigation of MEK inhibitors in combination with other targeted drugs for NF2 schwannomas.

Key Points

1. Cobimetinib and trametinib reduced NF2 schwannoma model cell proliferation in vitro and in vivo.
2. Biochemical/proteome analyses reveal cell cycle arrest and apoptosis of trametinib-treated cells.
3. Human vestibular schwannoma cell viability is modestly inhibited by PD0325901 and trametinib.

Importance of the Study

There are currently no FDA-approved drug therapies for the treatment of NF2-associated schwannomas. Clinical trials for selumetinib and cobimetinib are ongoing for assessment of efficacy for NF2-associated tumors and hearing loss; however, little preclinical data have been published. Here, we evaluated 6 MEK1/2 inhibitors for efficacy in mouse and human cell and animal models as well as

patient-derived vestibular schwannoma cells with *NF2* mutations. We observed differences in efficacy among the inhibitors as well as the possibility of drug resistance development. Our work highlights the importance of comprehensive drug screening in multiple model systems and supports further investigation of MEK inhibitors alone and in combination with other targeted therapies.

Neurofibromatosis type 2 (NF2) is caused by mutations in the *NF2* gene encoding the merlin tumor suppressor.^{1,2} NF2 patients classically present with bilateral vestibular schwannomas (VS) involving the cochleovestibular nerves important for hearing and balance, and can develop additional peripheral schwannomas, meningiomas, and ependymomas.³ Management of NF2 requires a complex, multidisciplinary approach focused on balancing tumor control and nerve function preservation to improve quality of life and maximize survival.⁴ Whereas microsurgical resection of tumors risks permanent nerve injury, radiation therapy increases the chance of malignant transformation of benign tumors and secondary malignancies.⁵⁻¹⁰ Therefore, there is an ongoing search for effective drug therapies for NF2.

Schwann cells with loss of merlin tumor suppressor function have elevated levels of Ras/Raf/mitogen-activated protein kinase kinase (MEK)/extracellular signal-regulated kinase (ERK) signaling that promotes cell proliferation.¹¹⁻¹³ Sixteen small molecule MEK inhibitors have entered clinical trials for various cancers.¹⁴ Among these MEK inhibitors, selumetinib (AZD6244) was recently granted Orphan Drug Designation by the FDA for treatment of inoperable plexiform neurofibromas in children with NF1.¹⁵ Additionally, selumetinib reduced growth of an in vitro human schwannoma model.^{16,17} This success has prompted additional trials of selumetinib for NF1 and NF2 (NCT numbers: 01089101, 01362803, 02839720, 03259633, 03095248).

Trametinib (Mekinist, GSK1120212, JTP-74057, GlaxoSmithKline) is an allosteric, second-generation, adenosine triphosphate non-competitive reversible MEK1/2 inhibitor that also blocks Raf-dependent phosphorylation

of MEK Ser218.¹⁴ Trametinib promotes cell cycle arrest and caspase cleavage in cultured colorectal cells, and demonstrates more potent antitumor activity than other second-generation MEK inhibitors, PD0325901 and selumetinib. It is FDA approved for metastatic melanoma and is in phase I clinical trial for NF1-associated plexiform neurofibromas (NCT02124772).¹⁸

PD0325901 (Pfizer) is also an allosteric MEK1/2 inhibitor and is a synthetic analog of the first-generation MEK1/2 inhibitor, CI-1040.^{14,19} In an *Nf1* genetically engineered mouse model, PD0325901 prolonged survival of mice with malignant peripheral nerve sheath tumors and decreased neurofibroma size in over 80% of mice.²⁰ Tumor regrowth was observed when treatment was suspended.²¹ A phase II open-label study is ongoing for PD0325901 in NF1 (NCT02096471).¹⁴

Cobimetinib (XL518, GDC-0973, Cotellic, Exelixis/Genentech) is derived from methanone and was FDA approved in 2015 for use in combination with vemurafenib, a BRAF inhibitor, for advanced melanoma with *BRAF* mutations.^{22,23} Cobimetinib inhibited growth of tumors with *BRAF* and *KRAS* mutations in xenograft models.²⁴⁻²⁶ Phase I studies of cobimetinib for solid tumors reported a manageable toxicity profile with signs of efficacy in tumors with *BRAF*^{V600E} mutations.²⁷ Cobimetinib is in clinical trial for pediatric and young adult patients with rasopathies, including NF2 (NCT02639546), treated previously for solid tumors.

Here, we used mouse and human merlin-deficient Schwann cell lines (MD-MSCHSC) and animal models to evaluate the growth-inhibitory and antitumor activities of a panel of MEK inhibitors. Also, we assessed their efficacy in primary human VS with NF2 mutations.

Materials and Methods

Cell Culture

Wild-type (WT)-MSCs and MD-MSCs were generated and characterized in 2010.²⁸ MD-MSCs were transduced with lentiviral luciferase as previously reported.²⁹ MD-schwannoma (MD-SCN) cells were derived from paraspinal schwannomas of *Periostin-Cre:Nf2^{flox2/flox2}* mice with *Nf2* inactivation (provided by Dr Wade Clapp, Indiana University). Human Schwann cells (HSCs) were purchased from ScienCell Research Laboratories (catalog #1700, lot #7228), and the generation of a merlin-deficient HSC (MD-HSC) line using lentiviral short hairpin (sh)RNA targeting *NF2* (Sigma Mission, SHCLNV-TRCN0000237845) was previously described.³⁰ Cells were tested monthly for *Mycoplasma* contamination (Lookout *Mycoplasma* PCR Detection Kit, Sigma).

Mouse Model Systems

NSG (*NOD.Cg-Prkdcscid Il2rgtm1Wjl/SzJ*) mice were used at 6–10 weeks of age. *P0-SCH-Δ(39–121)-27* transgenic mice³¹ in the BALB/c background were used as a genetically engineered mouse (GEM) model of NF2 schwannomas. Animal use was approved by the Institutional Animal Care and Usage Committees of UCF and UCLA, and the Animal Care and Use Review Office of the United States Army Medical Research and Materiel Command.

Human VS Samples

Through an institutional review board (IRB) approved protocol, the University of Miami Tissue Bank Core Facility (UM-TBCF) consented patients undergoing surgery for brain tumors to harvest samples for research purposes. De-identified fresh human VS were obtained from UM-TBCF through an IRB-exempt protocol. Primary VS cells were prepared and cultured as previously reported.^{29,30}

Drug Formulations

MEK inhibitors were purchased from MedChemExpress. Drugs were prepared in dimethyl sulfoxide (DMSO) (stock 10 mM) and diluted to final concentrations in cell culture medium for in vitro work. For animal studies, drugs were solubilized in DMSO at 50–100 mg/mL and diluted in 0.1 M citrate buffer (pH 3) for oral dosing.

Cell Viability Assays

Cells were seeded in 384-well CellBind plates (Corning) at 2000–2500 cells/well in phenol red-free growth medium. WT-MSCs were seeded at 15000 cells/well in 96-well plates coated with poly-L-lysine (200 μg/mL) and laminin (25 μg/mL). Attached cells were treated with drug or DMSO for 48 h (mouse) or 72 h (human); viability was measured with the CellTiter-Fluor Assay (Promega). Primary human VS

cells were seeded (passage 1 or 2) in 96-well plates at 10000 cells/well. After 24 hours, cells were treated with drug or DMSO for 72 h. Crystal violet assay was performed using a SpectraMax 190 microplate reader (Molecular Devices) to assess cell number, as previously described.^{29,30}

Membrane Asymmetry Assay

MD-MSCs were grown at 200000 cells/well in 12-well CellBind plates (Corning). When at ~80% confluency, cells were treated with drug for 18–24 h, then harvested with 0.05% trypsin and resuspended in Hanks Balanced Salt Solution. The Violet Ratiometric Membrane Asymmetry Assay (Invitrogen) was used to detect apoptosis per the manufacturer's instructions. Cell populations were measured by flow cytometry (Cytotflex, Beckman Coulter) and analyzed with CytExpert software (Beckman Coulter).

Mouse Studies

For pharmacokinetic analysis, at each timepoint 3 mice received drug (1 mg/kg trametinib, 1.5 mg/kg PD0325901, or 20 mg/kg cobimetinib); one mouse received vehicle alone (0.1 M citrate, pH 3, 2% DMSO). Mice were sacrificed after 0.5–32 h; blood and sciatic nerve samples were collected and analyzed by mass spectrometry at Sanford Burnham Prebys Medical Discovery Institute (Lake Nona, Florida).

The orthotopic allograft model using luciferase-expressing MD-MSCs was generated as previously described.²⁹ Upon confirmation of successful grafting, mice were randomized into treatment groups and received drug or vehicle at the above concentrations daily by oral gavage. Mice were imaged weekly for bioluminescence using the In Vivo Imaging System (IVIS, Caliper) or Bruker MI Imaging System. After 13–14 days of treatment, mice were sacrificed; grafts and contralateral sciatic nerves were removed, weighed, and photographed. Grafts were fixed overnight in 4% paraformaldehyde and stored in 30% sucrose (0.02% azide in phosphate buffered saline) at 4°C. List of antibodies used is provided in Supplementary Methods.

Four-week-old *P0-SCH-Δ(39–121)-27* transgenic mice³¹ were treated daily with trametinib (1 mg/kg) or vehicle (0.1 M citrate buffer pH 3, 0.2% DMSO) by oral gavage for 8 weeks. Spinal nerve roots were histopathologically scored at the endpoint as previously described.³² Following a blind procedure, measurements of tumors and nerve root areas were performed using Zeiss Axiovision software on hematoxylin and eosin stained parasagittal sections of cervical, thoracic, lumbar, and sacral spinal cord segments. The total area of nerve root analyzed was comparable between the trametinib and vehicle-treated groups ($P = 0.1541$).

Western Blotting

Western blots were performed as previously described.²⁹ Protein was extracted from human VS tumors using radioimmunoprecipitation buffer with protease and phosphatase inhibitors (ThermoFisher). Human VS blots were blocked in 3% bovine serum albumin and incubated

overnight in primary antibody solution at 4°C, followed by incubation with Alexa Fluor 488 and 647 conjugated secondary antibodies (1:200; ThermoFisher) for 2 hours at room temperature and imaged using the ImageQuant LAS 4000 Imager (GE Healthcare).

NF2 Mutation Analysis

Total DNA was extracted from fresh tumor tissues using the QIAamp DNA Mini Kit (Qiagen) and purified using the QIAquick PCR Purification Kit (Qiagen). All VS were tested for mutations within the NF2 gene with multiplex ligation-dependent probe amplification using the Salsa MLPA NF2 Kit (MRC-Holland) per the manufacturer's instructions. Copy number alterations in all 17 exons of the NF2 gene (NM_000268.3) were analyzed with Coffalyser. Additional details are provided in the [Supplementary Methods](#).

DNA Methylation Analysis

High-throughput DNA methylation analysis was performed for 7 human VS tumors using the Infinium MethylationEPIC Kit (Illumina) according to the manufacturer's instructions. Methylation patterns were compared between VS that had a statistically significant decrease in cell number following a 72 hour incubation with 3 μ M PD0325901 and those with no response. Additional details are provided in [Supplementary Methods](#).

Proteome

Protein from cell pellets of MD-MSCs treated with trametinib or vehicle was extracted, denatured and prepared for liquid chromatography–tandem mass spectrometry (LC-MS/MS) as described in the [Supplementary Methods](#). MS/MS spectra were searched against the *Mus Musculus* Swiss-Prot entries of the Uniprot KB (database release 2016_01, 16755 entries) using the Andromeda search engine.³³ The specific search criteria and analytics used are provided in [Supplementary Methods](#). Protein differential expression between the trametinib and vehicle control samples was evaluated using the Limma package.³⁴

Statistics

Using GraphPad Prism 6, ANOVA with Bonferroni posttest, or Kruskal–Wallis test with Dunn's comparison was applied to all in vitro data. For in vivo allograft studies, we used SAS version 9.4 to test the overall differences in median tumor weight and median fold change in flux after 14 days treatment among the 4 cohorts (vehicle treatment served as the control). Nonparametric ANOVA with Bonferroni adjustments were used to adjust for small group sample sizes and non-normal distributions. The ANOVA for the median tumor weight and median fold change in flux indicated the overall significance differences. We tested 1-tailed hypothesis of improvements. For the *P0-SCH- Δ (39–121)-27* NF2 mouse model, 2-tailed unpaired Student's *t*-test was used to compare tumor burden and sizes in the trametinib- and vehicle-treated groups.

Results

We screened selumetinib, trametinib, PD0325901, MEK162, cobimetinib, and refametinib for effectiveness in reducing viability of 9 WT and MD-MSC/HSC lines after 48-hour (mouse) and 72-hour (human) treatments. Based upon 50% inhibitory concentration (IC_{50}) values, the inhibitors were overall more effective in MSCs compared with HSCs. Maximum loss of cell viability at 10 μ M observed for all inhibitors tested was ~90–95% in MD-MSCs, compared with ~60% in MD-HSCs ([Fig. 1A–B](#)). The lowest inhibitor concentration tested produced a 20–40% reduction in MD-MSC viability. MEK inhibitors promoted a dose-dependent decrease in incorporation of 5-ethynyl-2'-deoxyuridine in both MD-MSC and MD-HSC ([Supplementary Fig. 1](#)). All 6 MEK inhibitors also exhibited less selectivity between WT- and MD-HSCs compared with MSC lines (2–5 fold compared with 6–15 fold; [Fig. 1A–B](#) and [Supplementary Fig. 2](#)).

Trametinib, PD0325901, and cobimetinib were further evaluated in vitro and in an allograft mouse model because each reduced viability of both MD-MSCs and MD-HSCs with submicromolar IC_{50} values and had some selectivity in HSCs. Each drug decreased phosphorylated pERK levels in MD-MSCs at 5 and 24 hours of treatment ([Fig. 2A–B](#), [Supplementary Fig. 3](#)). Trametinib was the most potent, as pERK was not detected in the 0.001 μ M sample. Among these 3 MEK1/2 inhibitors, cobimetinib was the least effective, based on sustained reduction of pERK levels over 24 hours. Higher cobimetinib concentrations (0.3–1 μ M) were required to achieve an equivalent pERK reduction observed with 0.001 μ M trametinib and PD0325901. As reported in other cell types, MEK inhibition is associated with a compensatory increase in pMEK levels ([Fig. 2A–B](#), [Supplementary Fig. 3](#)).³⁵ In MD-MSCs, a more robust increase in pMEK levels was observed in cells treated with cobimetinib at 5 hours and PD0325901 at 24 hours. Because trametinib uniquely blocks Raf-dependent MEK phosphorylation,¹⁴ the lowest increase in pMEK was observed in trametinib-treated cells. MD-HSCs also exhibited decreased pERK and increased pMEK following MEK inhibition, but at higher drug concentrations compared with MD-MSCs ([Supplementary Fig. 4](#)).

An examination of downstream MEK/ERK effectors in MD-MSCs treated with these inhibitors revealed decreased levels of cyclin D1, and increased p27^{kip1} and cleaved caspase 3 levels ([Fig. 2C–D](#)). Membrane asymmetry assays confirmed an increase in apoptotic cell populations from ~2% in DMSO-treated to 20% and 45% in trametinib- and cobimetinib-treated MD-MSCs, respectively ([Fig. 2E](#), [Supplementary Fig. 4](#)).

A proteomic analysis of trametinib-treated MD-MSCs was conducted to assess global changes in protein expression. The results were consistent with effective inhibition of MEK1/2 and downstream effectors and induction of apoptotic pathways. Trametinib-treated MD-MSCs had reduced expression of Ras/Raf/MEK/ERK pathway effectors including cyclin D1 and c-Myc and increased expression of pro-apoptotic proteins such as Bcl-2 interacting protein 3 like (BNIP3L) at 24 hours, compared with DMSO control ([Fig. 3A](#)). Ingenuity Pathway Analysis identified upstream regulators whose

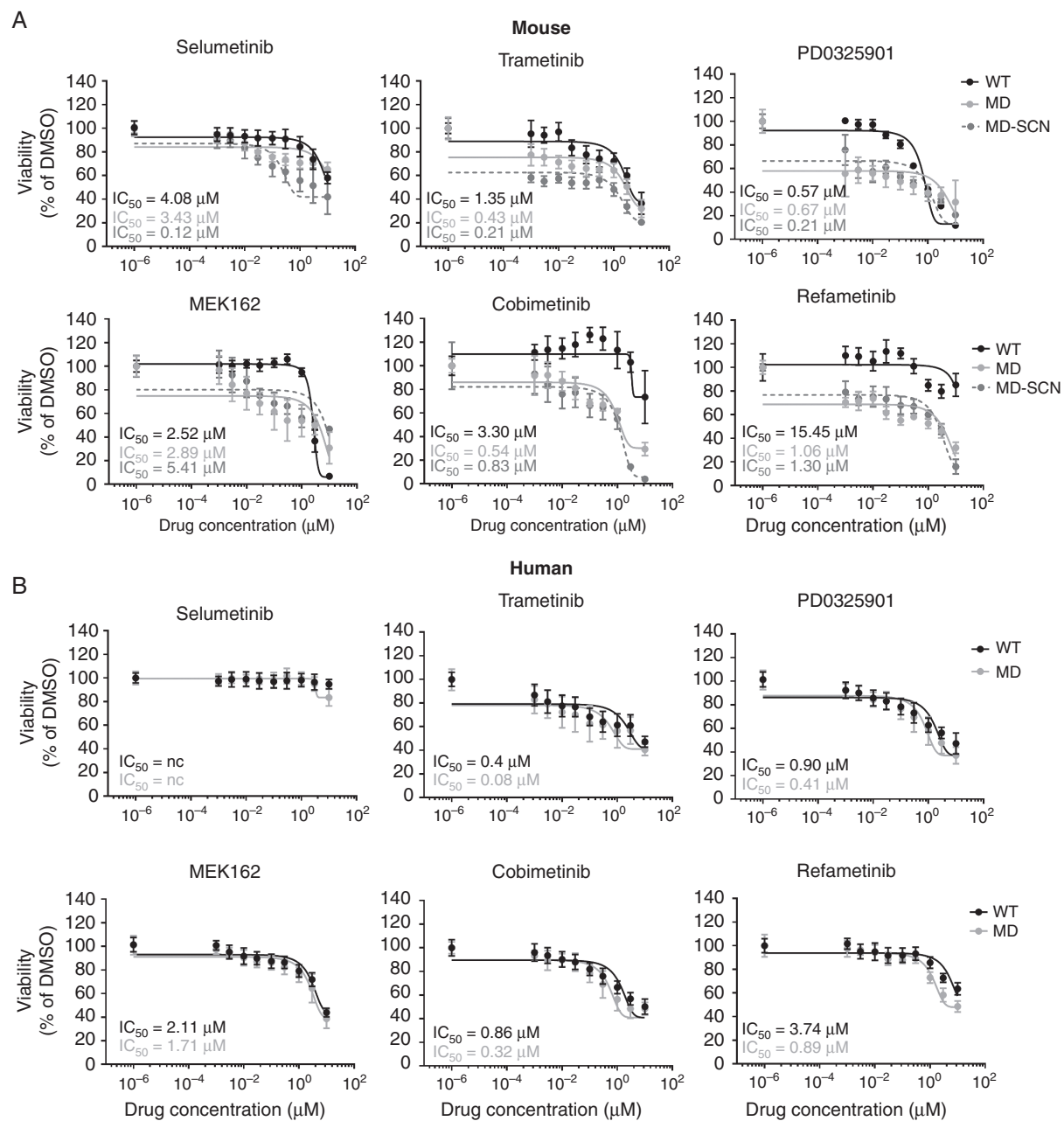


Fig. 1 MEK inhibitors reduce MD-MSC and MD-HSC viability. Screen of 6 MEK inhibitors against (A) mouse and (B) human WT and MD-SC lines treated for 48–72 h. Mean viability is plotted with IC_{50} values ($n = 1–3$ independent experiments; 8 replicates each).

modulation is consistent with the observed changes in protein levels. These included transforming growth factor beta (TGF β), specificity protein 1, and p53 levels, whose levels were higher in trametinib-treated MD-MSCs compared with DMSO-treated controls (Fig. 3B–D).

To assess in vivo efficacy, we employed an orthotopic allograft model by grafting luciferase-expressing MD-MSCs into the sciatic nerves of NSG mice.

Pharmacokinetic studies revealed that trametinib and cobimetinib had long $t_{1/2}$ values (~ 8 h and 4.8 h, respectively) and their nerve/plasma ratios increased with time (Fig. 4A). Upon confirmation of successful grafting (Supplementary Fig. 5), mice were gavaged daily for 14 days with trametinib (1 mg/kg), PD0325901 (1.5 mg/kg), or cobimetinib (20 mg/kg). All 3 MEK inhibitors significantly reduced the median tumor weight by 60–70% and the median fold change in flux from 0 to 14 days

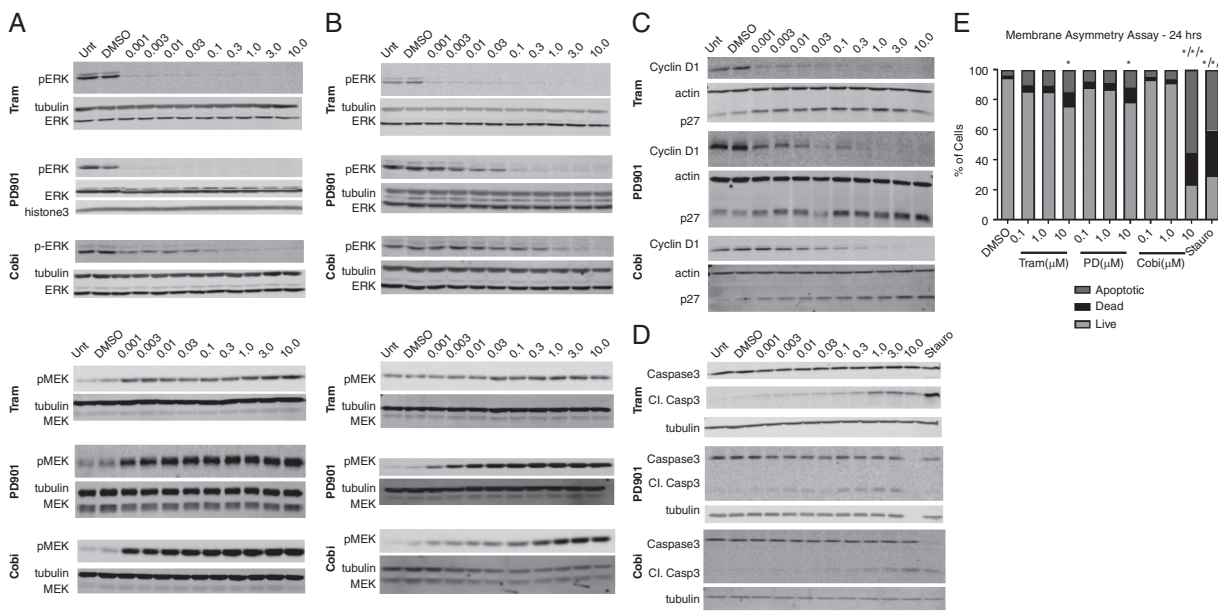


Fig. 2 MEK inhibitors promote G1 arrest and caspase-dependent apoptosis of MD-MSc in vitro. pERK1/2, pMEK1/2, cyclin D1, p27, and caspase-3 western blots of MD-MSc treated as indicated for (A) 5 h and (B-D) 24 h. All western blots are representative of 3–5 independent experiments. (E) Quantitation of membrane asymmetry assay of MD-MSc treated for 20 h with MEK inhibitors. Staurosporine (0.1 μ M) served as a positive control for apoptosis ($n = 3$ independent experiments, 2-way ANOVA, $*P < 0.05$).

by at least 80% compared with controls (Fig. 4B–D, Supplementary Fig. 6). Immunohistochemical analysis revealed that PD0325901 and cobimetinib were superior to trametinib in reducing pERK levels compared with the vehicle-treated group (Fig. 4E). Additionally, both inhibitors caused a more robust decrease in Ki-67 and cyclin D1 than trametinib, suggesting they were more potent inhibitors of graft growth in vivo. None of the inhibitors produced detectable caspase 3 cleavage nor did they affect vascularity as evidenced by CD31 staining (Fig. 4E).

Because trametinib is a well-tolerated FDA-approved drug and outperformed cobimetinib in cell assays, we assessed its efficacy in an 8-week study using the *PO-SCH-Δ(39–121)-27 NF2* schwannoma mouse model.^{31,32} In this GEM model, trametinib efficacy was assessed by comparing the tumor burden, as defined by the percentage of tumor area versus total spinal nerve root area. Overall, trametinib promoted a 25% reduction in tumor burden ($P < 0.0001$) and a 37% decrease of average tumor size ($P = 0.0023$) (Fig. 5). Phosphorylated ERK immunohistochemistry of tumor samples revealed equivalent staining in trametinib- and vehicle-treated mice (data not shown), consistent with the allograft findings.

To examine the effect of MEK inhibition on human VS cells, primary cultures from 7 VS tumors were prepared and treated with PD0325901 or trametinib. All 7 VS tumors demonstrated ≥ 1 mutation in the *NF2* gene (Supplementary Table 1) and varying degrees of MEK1/2, pMEK, and pERK expression (Fig. 6A–B). Compared with DMSO-treated cells, trametinib (3 μ M) moderately

reduced cell viability of 2 of 7 VS, whereas PD0325901 (3 μ M) reduced cell viability of 5 of the 7 VS tested (Fig. 6C–D). No significant correlations between viabilities and MEK1/2 and pMEK protein expression levels were identified, suggesting that drug response was independent of MEK expression.

To assess whether aberrant DNA methylation of the genome was associated with a lack of drug response, we compared methylation profiles of 2 VS with no response to PD0325901 tumors (VS27 and VS32) to the remaining 5 PD0325901-responsive tumors. In an unbiased evaluation, we identified 17 299 single cytosine-phosphate-guanine (CpG) sites with significantly different methylation levels ($P < 0.05$) between the drug responsive and nonresponsive VS. Among significant CpG sites, 4773 were hypermethylated (covering 3090 genes) and 12526 were hypomethylated (covering 8051 genes) in the PD0325901-resistant compared with drug-sensitive VS. Supplementary Table 2 displays the top 20 hypermethylated and hypomethylated genes between the 2 groups. However, when false discovery rate (FDR) < 0.05 was applied, *ELMOD1* (NM_001130037; Engulfment and cell motility domain 1) was the only gene that contained a CpG site (cg22355889) in the promoter region that was significantly hypermethylated in the PD0325901 nonresponsive VS.

Neighboring CpG sites often display closely related methylation patterns. To account for spatial correlations, we identified 34 differentially methylated regions (DMRs) with at least 5 consecutive

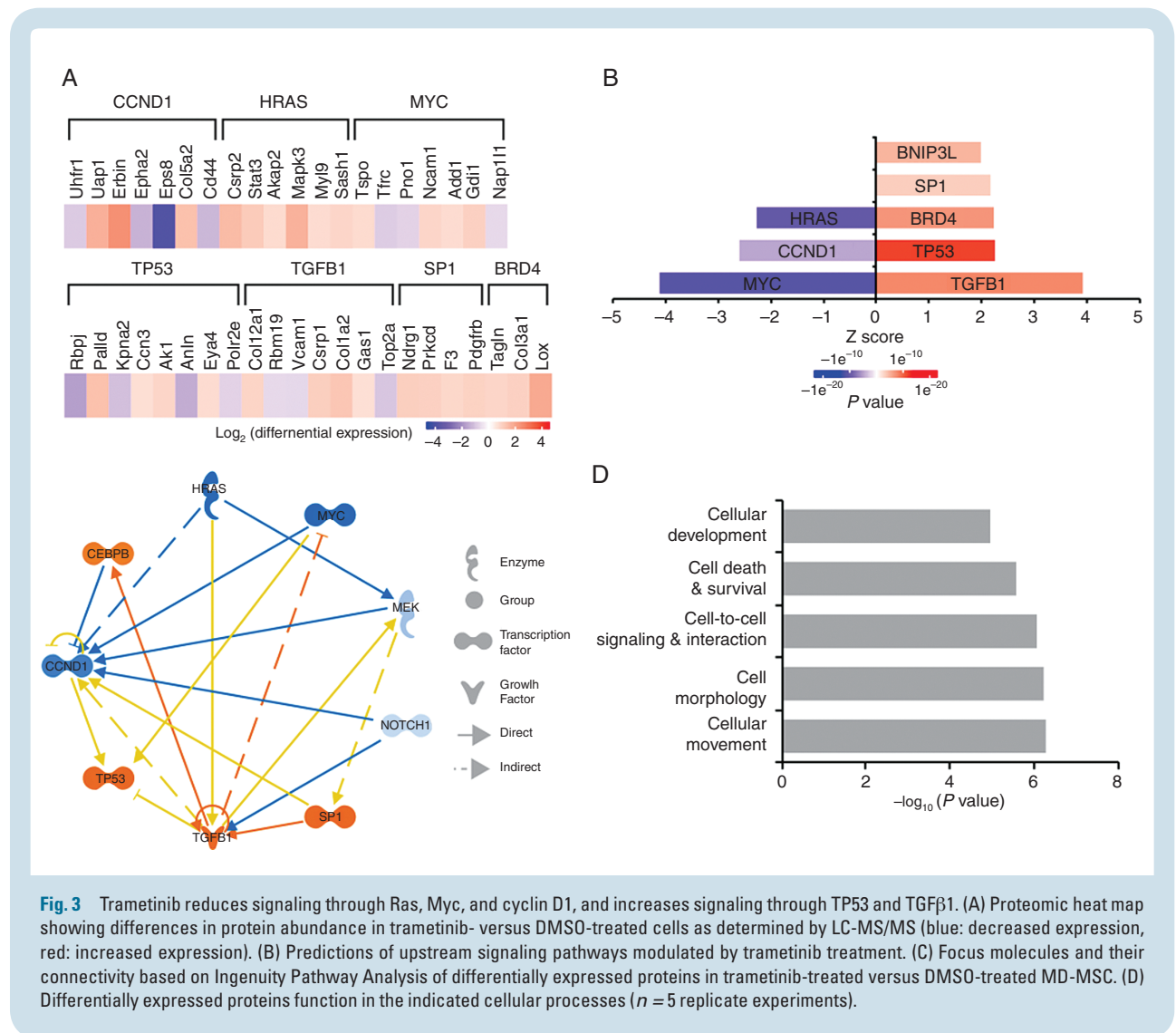


Fig. 3 Trametinib reduces signaling through Ras, Myc, and cyclin D1, and increases signaling through TP53 and TGFβ1. (A) Proteomic heat map showing differences in protein abundance in trametinib- versus DMSO-treated cells as determined by LC-MS/MS (blue: decreased expression, red: increased expression). (B) Predictions of upstream signaling pathways modulated by trametinib treatment. (C) Focus molecules and their connectivity based on Ingenuity Pathway Analysis of differentially expressed proteins in trametinib-treated versus DMSO-treated MD-MSC. (D) Differentially expressed proteins function in the indicated cellular processes ($n = 5$ replicate experiments).

hypermethylated or hypomethylated CpG loci in the PD0325901-nonresponsive compared with responsive VS (Supplementary Table 3). When examining individual DMRs, PD0325901 nonresponsive VS had DMRs in genes involved in non-MEK merlin signaling, including the *ATF6B* (activating transcription factor 6) and *RXR* (retinoid x receptor) genes associated with the phosphoinositide 3-kinase (PI3K/Akt) pathway and *ATP6V1C1* (V-type proton ATPase subunit C1) of the mammalian target of rapamycin pathway. Gene ontology pathway analysis revealed no significant enrichment pathways for DMRs. However, when using a targeted approach assessing genes associated with merlin signaling, cancer, drug resistance, cell death, and survival, additional DMRs were identified. ARCHS4 pathway analysis revealed significant enrichment in epidermal growth factor receptor and tumor suppressor RPS6KA2 (ribosomal protein S6 kinase A2) human kinase pathways (<http://amp.pharm.mssm.edu/Enrichr/>. Accessed January 20, 2019).

Discussion

NF2 is a genetic disorder involving the development of multiple nervous system tumors that each impact neurological functions. Individuals affected by NF2 develop bilateral VS that cause severe hearing loss, disabling imbalance, and even life-threatening hydrocephalus from brainstem and cerebellar compression. Observation of tumor growth rate and hearing is standard as enthusiasm for microsurgical resection in NF2 is low due to consequential and irreversible limitations on nerve function and quality of life.⁸ In the same respect, the long-term sequelae of utilizing radiotherapy is not so uncommon to disregard the risk of developing malignant transformation of benign tumors.^{5-7,9,10} Off-label use of select FDA-approved chemotherapeutic agents for NF2 in clinical trials show moderate tumor control at best and hearing stabilization in only some NF2 patients.³⁶⁻⁴¹ However, even small effects

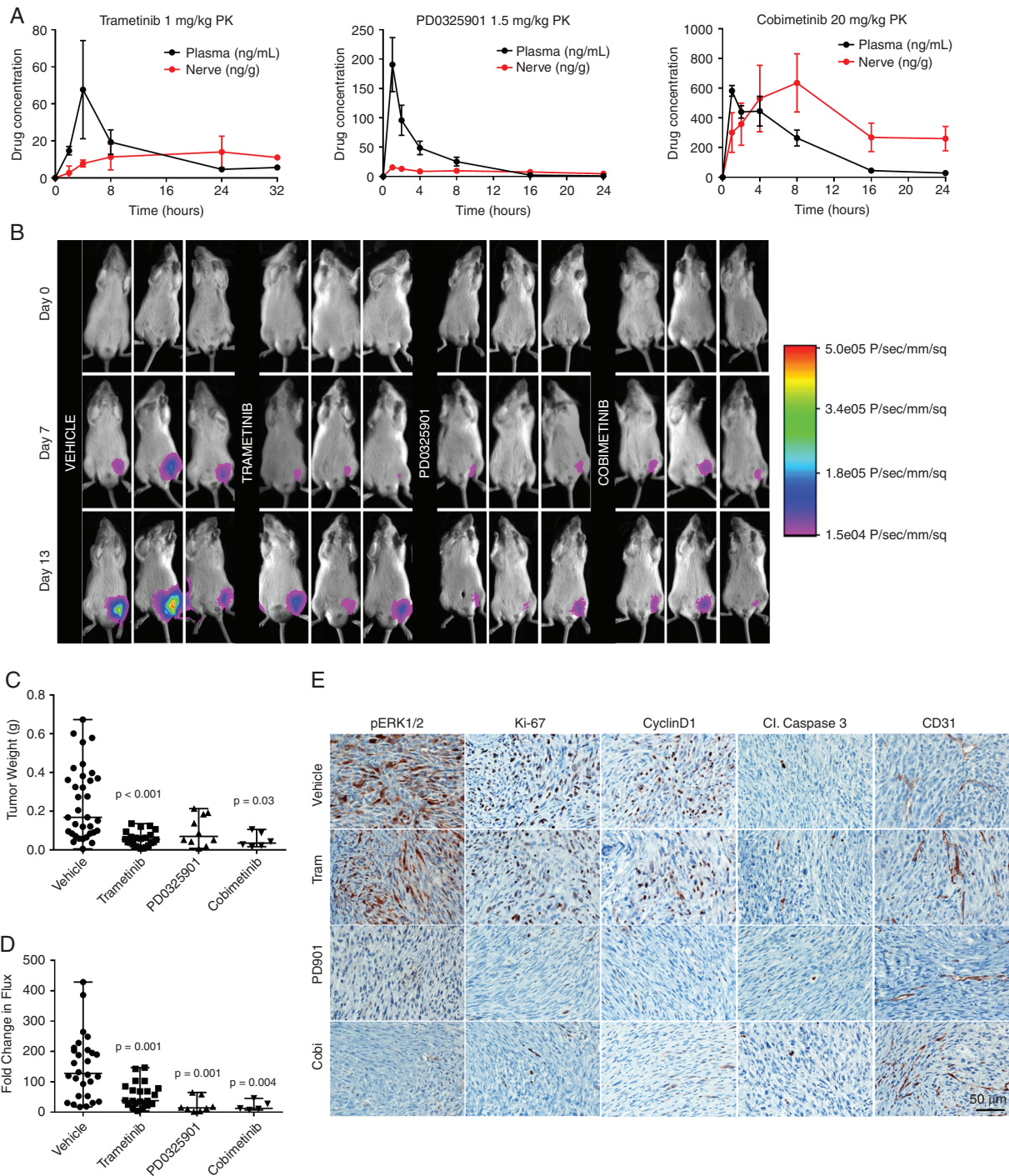


Fig. 4 MEK inhibitors slow MD-MSC growth in NSG mice. (A) Pharmacokinetic analysis for plasma and nerve following a single drug dose. (B) Representative bioluminescent (BL) images for indicated times. (C) Median tumor weights after 14 days of drug treatment compared with vehicle ($n = 6-35$ mice, nonparametric ANOVA). (D) BL signals were normalized to day 0 for each mouse and fold change in flux (photons/sec) after 14 days of treatment is shown (nonparametric ANOVA, median values shown). (E) Representative graft immunohistochemistry images for pERK1/2, Ki-67, cyclin D1, cleaved caspase 3, and CD31.

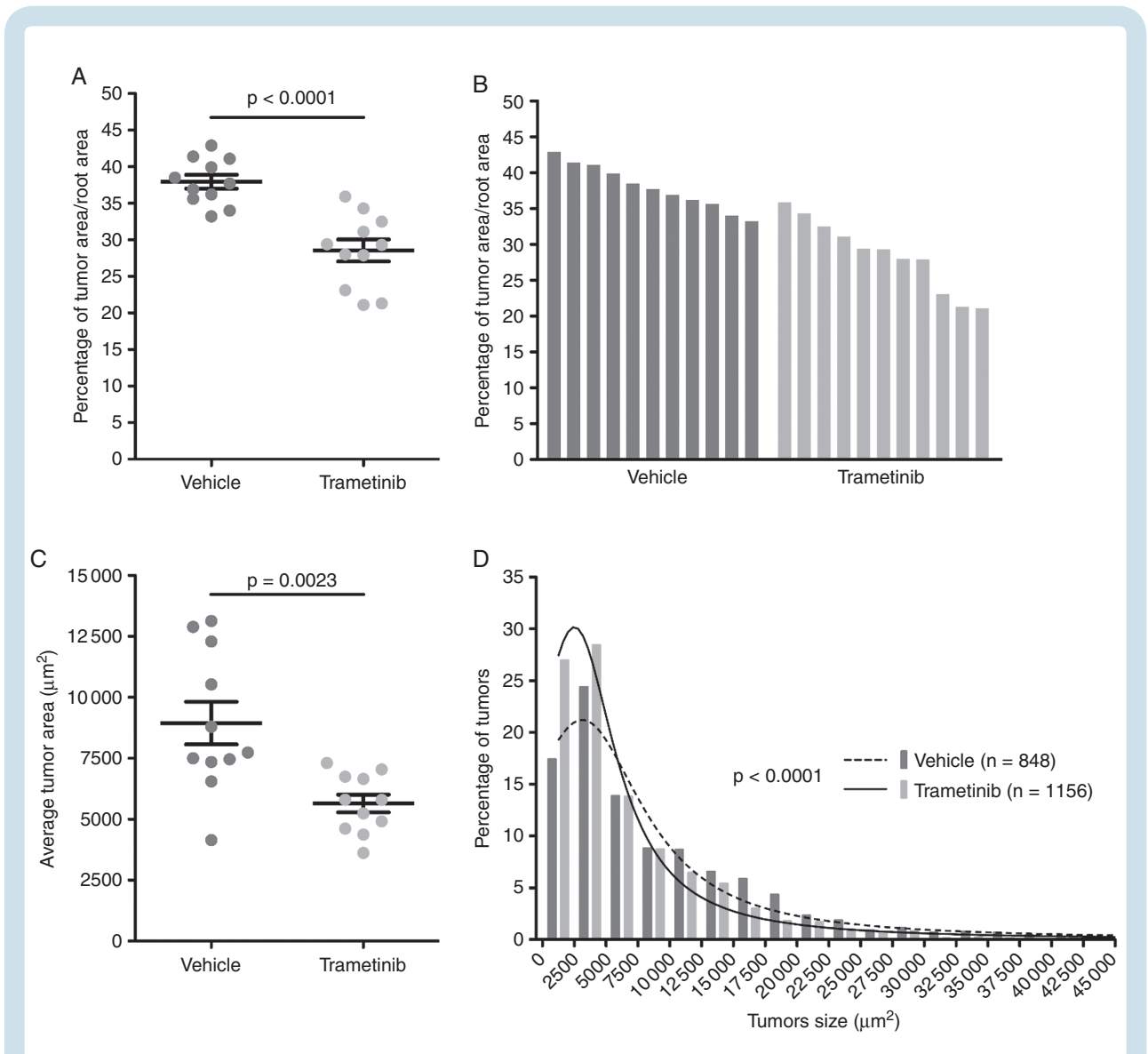


Fig. 5 Trametinib reduces schwannoma growth in the *P0-SCH-Δ(39–121)-27NF2* mouse model. *P0-SCH-Δ(39–121)-27NF2* mice were treated daily with trametinib (1 mg/kg, p.o., 7 d/wk) for 8 weeks starting at 4 weeks of age. (A) Reduction by 25% of the average tumor burden, calculated as percentage of tumor area versus total spinal nerve root area for trametinib-treated mice ($n = 11$) compared with vehicle-treated mice ($n = 11$). (B) Waterfall plot showing tumor burden for each vehicle- and trametinib-treated mouse. (C) Treatment with trametinib reduced average tumor size by 37% in trametinib-treated compared with vehicle-treated mice. (D) Histogram of tumor size distribution demonstrated a significantly higher percentage of smaller tumors in trametinib-treated ($n = 1156$ tumors) compared with vehicle-treated ($n = 848$ tumors) mice.

can impact survival and quality of life in individual NF2 patients. Therefore, the discovery of effective NF2 drug therapies is critical.

Currently, 2 clinical trials are enrolling pediatric NF2 patients to test effectiveness of selumetinib and cobimetinib in reducing tumor volume and preserving hearing (NCT03095248 and NCT02639546). However, the preclinical efficacies for selumetinib and cobimetinib have not been established. These trials are supported by knowledge that merlin loss is associated with increased mitogen-activated protein kinase signaling, and⁴² success of selumetinib in shrinking plexiform neurofibromas in NF1 children.¹⁵ Our study is the first to evaluate

a panel of MEK inhibitors in mouse and human NF2 schwannoma models.

Of the 6 inhibitors screened against multiple mouse and human SC lines, trametinib, PD0325901, and cobimetinib reduced MD-SC viability at submicromolar IC_{50} values and were the most effective in non-immortalized human MD-SCs (Fig. 1A). Notably, selumetinib was the least effective in MD-HSCs and was not a top performer in MD-MSCs (based on maximum effect and IC_{50} values). In vitro, trametinib, PD0325901, and cobimetinib reduced pERK levels, modulated cyclin D1 and p27 levels in a manner consistent with a G_1/S cell cycle arrest, and induced caspase-dependent apoptosis in MD-MSCs. The proteomic study conducted in

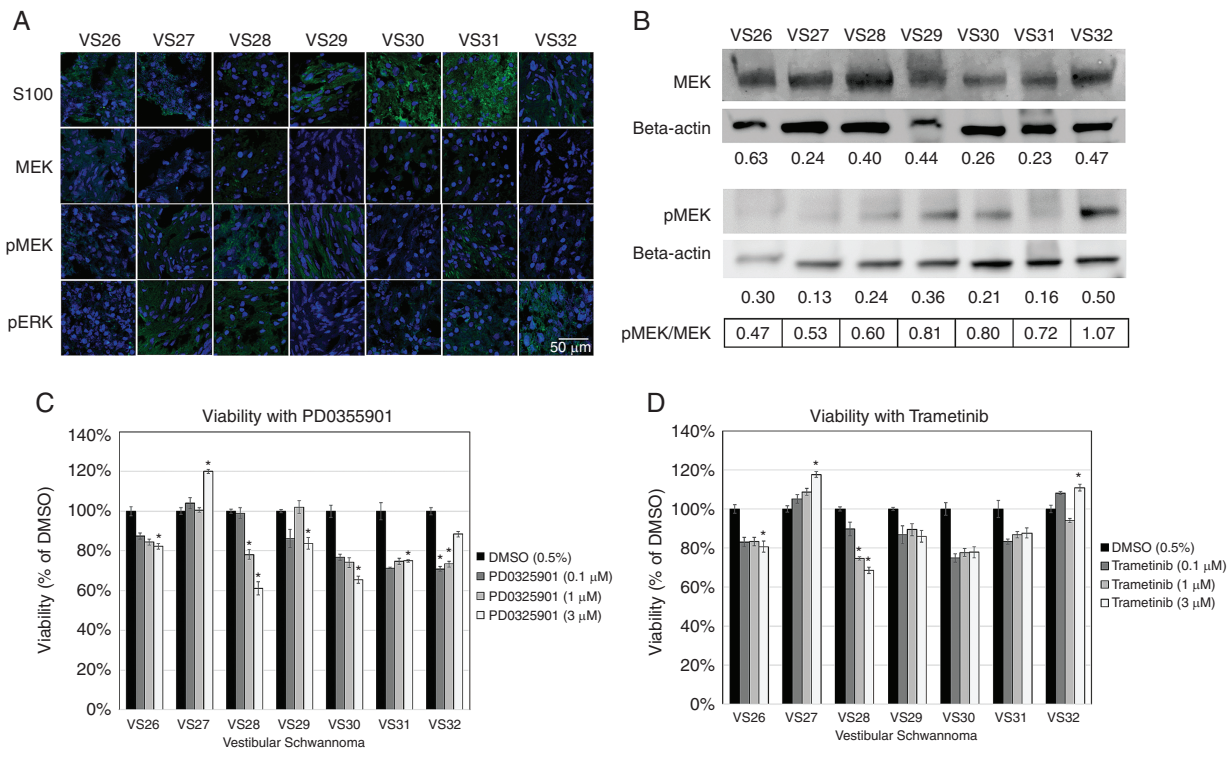


Fig. 6 MEK inhibitors reduce viability of a subset of primary human VS cells. (A) Immunohistochemistry shows S100 positivity and variable expression levels of MEK, pMEK, and pERK (green) in VS tumors (4',6'-diamidino-2-phenylindole nuclear stain, blue). (B) Western blots demonstrate expression of MEK and pMEK for VS with beta-actin as the standard. Relative expression levels of MEK and pMEK were displayed and expressed as a ratio of pMEK/MEK. (C–D) Cell viability assays for PD0325901 and trametinib were performed and viability was normalized to 0.5% DMSO controls.

trametinib-treated MD-MSC further corroborated this conclusion by revealing decreased signaling in the Ras-ERK-cyclin D1 pathway and increased signaling from BNIP3L, a pro-apoptotic subfamily in the Bcl-2 family of proteins.

We used 2 *in vivo* models to evaluate drug efficacy: a 2-week treatment protocol aimed at slowing growth of established MD-MSCs nerve grafts in NSG mice, and an 8-week chemoprevention protocol aimed at preventing appearance of schwannomas in a GEM model. In the nerve grafts, PD0325901 and cobimetinib produced a stronger reduction in MD-MSC growth compared with trametinib, likely from persistent inhibition of pERK, cyclin D1, and Ki-67 levels. Trametinib did not significantly decrease pERK, cyclin D1 and Ki-67 levels in allografts at the study endpoint when compared with vehicle-treated controls, supporting the conclusion that cells in the allografts were developing resistance to trametinib. Similar responses to trametinib were obtained with the GEM model. Although the number and size of schwannomas were reduced in the GEM model following 8 weeks of trametinib treatment, immunohistochemically, pERK levels in trametinib-treated schwannomas were equivalent to controls. An adaptive response to trametinib has been reported in triple-negative breast cancer.⁴³ Trametinib treatment resulted in degradation of c-Myc and in assembly of bromodomain containing 4 (BRD4)-containing transcriptional enhancers on promoters

of adaptive response genes, resulting in activation of compensatory pathways associated with drug resistance.⁴³ Our proteomic analysis similarly revealed decreased c-Myc levels and increased BRD4 levels in MD-MSCs treated with trametinib (Fig. 3). BRD4 in trametinib-induced adaptive response promoter complexes can be displaced by treatment with bromodomain and extraterminal domain family (BET) bromodomain inhibitors.⁴⁴ A study of BET bromodomain inhibitors in ovarian cancer revealed reduced activation of ERK, Akt, and Src kinase following treatment, suggesting that these pathways may be activated by bromodomain-containing transcriptional enhancers.⁴⁵ Additionally, BET family bromodomains were involved in reactivation of the Src/focal adhesion kinase pathway in breast cancer cells following inhibition of ErbB2 with lapatinib.⁴⁶ Collectively, these studies suggest that trametinib treatment may promote assembly of BRD-containing transcriptional enhancers that can activate compensatory proliferative pathways. Future studies examining the effects of bromodomain and Src inhibitors in combination with MEK inhibitors are warranted.

Of the 7 primary human VS cultures tested, only a subset responded to either PD0325901 or trametinib by reducing cell viability by 15–40% of controls. Although the trend of response to both drugs was similar within individual VS cultures, the differing response rate to the drugs was

71% versus 29%, respectively, and did not correlate with baseline MEK or pMEK expression (Fig. 6A–D). The differing response rate can be attributed to the 10-fold higher potency of cobimetinib compared with PD0325901 (Fig. 6C–D).^{18,19} VS cells also demonstrated a large variety of NF2 mutations, which can have differential effects on merlin-dependent cell proliferation and survival pathways. Methylome exploration identified *ELMOD1* as the single gene with a hypermethylated promoter and an FDR <0.05 in nonresponsive VS compared with responsive VS. *ELMOD1* is a GTPase activator for small GTPases in the ADP ribosylation factor (Arf) and Arf-like families (Arl2). In PD0325901 nonresponsive VS, a hypermethylated promoter in *ELMOD1* is expected to reduce *ELMOD1* expression, increase Arl2 activity, and alter normal microtubule dynamics.⁴⁷ This may allow VS cells to circumvent traditional mechanisms of cell cycle arrest and cell death.⁴⁷ Further investigation into how tumor heterogeneity in NF2 contributes to drug resistance and disease progression is imperative for identifying treatment modalities to overcome resistance to MEK inhibition.

We present a comprehensive preclinical analysis of MEK inhibitors in mouse and human NF2 schwannoma models and primary human VS. Although differences in response were observed between drugs, species, and models, our cumulative results support MEK inhibitors for the treatment of a subset of NF2 schwannomas. We demonstrate that differences in treatment response to MEK inhibitors depends on genetic and epigenetic differences between tumors that can impact downstream merlin signaling, drug resistance mechanisms, and adaptive pathways to evade cell death or arrest. By understanding the mechanisms of drug response and resistance to MEK inhibitors in individual tumors, we can identify optimal combination therapies to maximize tumor control, determine important genetic and molecular biomarkers to predict patient outcomes, and develop precision medicine algorithms for NF2 treatment.

Supplementary Material

Supplementary data are available at *Neuro-Oncology* online.

Keywords

merlin tumor suppressor | methylome | NF2 transgenic mice | MEK inhibitors | patient-derived vestibular schwannomas

Funding

This work was supported by Department of Defense Congressionally Directed Medical Research Program (W81XWH-15-1-0446 to CFV and W81XWH-16-1-0104 to LSC), National Institutes of Health/National Institute on Deafness and Other Communication Disorders (R0-DC005575 and R01-DC012115 to XZL), and the Children's Tumor Foundation with contracts to CFV and MAF.

Acknowledgments

We thank Drs Jacques Morcos and Michael Ivan for their efforts harvesting human VS tumors and patients for donated tumor samples. We acknowledge Anthony Griswold, PhD, Division Head of the Center for Genetic Epidemiology and Statistical Genetics at the University of Miami Miller School of Medicine, for bioinformatics and statistical analysis of DNA methylation experiments.

Conflict of interest statement. CFV is a named inventor on unrelated patents. MG and JV receive research funding from Recursion Pharmaceuticals. Other authors report that no conflicts of interest exist.

Authorship statement. *Designed experiments:* CFV, MCF, MAF, JV, MG, JK and CTD. *Supervised work:* CFV, CTD, MG, HM, and LSC. *Cell and allograft studies:* MAF, SKP, JN, KB, AP, MCF. *Human VS work:* CTD, OB, RM, DY, XL, FT, JIY. *GEM model:* MG, JV. *Proteome analysis:* AC, JK, TM, HM. *Histology:* LSC, RS, JH. *Flow cytometry analysis:* AJC. *Statistical analysis:* JNS. CFV, MAF and LSC wrote the initial draft and all authors edited the manuscript.

Portions of Figs. 1, 3, and 5 were presented at the annual Neurofibromatosis Conference in Washington DC in June 2017.

References

- Rouleau GA, Merel P, Lutchman M, et al. Alteration in a new gene encoding a putative membrane-organizing protein causes neuro-fibromatosis type 2. *Nature*. 1993;363(6429):515–521.
- Trofatter JA, MacCollin MM, Rutter JL, et al. A novel moesin-, ezrin-, radixin-like gene is a candidate for the neurofibromatosis 2 tumor suppressor. *Cell*. 1993;72(5):791–800.
- Evans DG. Neurofibromatosis type 2 (NF2): a clinical and molecular review. *Orphanet J Rare Dis*. 2009;4:16.
- Blakeley JO, Evans DG, Adler J, et al. Consensus recommendations for current treatments and accelerating clinical trials for patients with neurofibromatosis type 2. *Am J Med Genet A*. 2012;158A(1):24–41.
- Chung LK, Nguyen TP, Sheppard JP, et al. A systematic review of radio-surgery versus surgery for neurofibromatosis type 2 vestibular schwannomas. *World Neurosurg*. 2018;109:47–58.
- Evans DG, Birch JM, Ramsden RT, Sharif S, Baser ME. Malignant transformation and new primary tumours after therapeutic radiation for benign disease: substantial risks in certain tumour prone syndromes. *J Med Genet*. 2006;43(4):289–294.
- Kim BS, Seol HJ, Lee JI, et al. Clinical outcome of neurofibromatosis type 2-related vestibular schwannoma: treatment strategies and challenges. *Neurosurg Rev*. 2016;39(4):643–653.

8. Nowak A, Dziedzic T, Czernicki T, et al. Strategy for the surgical treatment of vestibular schwannomas in patients with neurofibromatosis type 2. *Neurol Neurochir Pol.* 2015;49(5):295–301.
9. Seferis C, Torrens M, Paraskevopoulou C, Psychidis G. Malignant transformation in vestibular schwannoma: report of a single case, literature search, and debate. *J Neurosurg.* 2014;121(Suppl):160–166.
10. Sun S, Liu A. Long-term follow-up studies of Gamma Knife surgery for patients with neurofibromatosis type 2. *J Neurosurg.* 2014;121(Suppl):143–149.
11. Hilton DA, Ristic N, Hanemann CO. Activation of ERK, AKT and JNK signalling pathways in human schwannomas in situ. *Histopathology.* 2009;55(6):744–749.
12. Morrison H, Sperka T, Manent J, Giovannini M, Ponta H, Herrlich P. Merlin/neurofibromatosis type 2 suppresses growth by inhibiting the activation of Ras and Rac. *Cancer Res.* 2007;67(2):520–527.
13. Petrilli AM, Fernández-Valle C. Role of merlin/NF2 inactivation in tumor biology. *Oncogene.* 2016;35(5):537–548.
14. McDermott L, Qin C. Allosteric MEK1/2 inhibitors for the treatment of cancer: an overview. *J Drug Res Dev.* 2015;1:1–9. doi: 10.16966/jdrd.101.
15. Dombi E, Baldwin A, Marcus LJ, et al. Activity of selumetinib in neurofibromatosis type 1–related plexiform neurofibromas. *N Engl J Med.* 2016;375(26):2550–2560.
16. Ammoun S, Schmid MC, Ristic N, et al. The role of insulin-like growth factors signaling in merlin-deficient human schwannomas. *Glia.* 2012;60(11):1721–1733.
17. Ammoun S, Schmid MC, Triner J, Manley P, Hanemann CO. Nilotinib alone or in combination with selumetinib is a drug candidate for neurofibromatosis type 2. *Neuro Oncol.* 2011;13(7):759–766.
18. Yamaguchi T, Kakefuda R, Tajima N, Sowa Y, Sakai T. Antitumor activities of JTP-74057 (GSK1120212), a novel MEK1/2 inhibitor, on colorectal cancer cell lines in vitro and in vivo. *Int J Oncol.* 2011;39(1):23–31.
19. Barrett SD, Bridges AJ, Dudley DT, et al. The discovery of the benzhydroxamate MEK inhibitors CI-1040 and PD 0325901. *Bioorg Med Chem Lett.* 2008;18(24):6501–6504.
20. Jessen WJ, Miller SJ, Jousma E, et al. MEK inhibition exhibits efficacy in human and mouse neurofibromatosis tumors. *J Clin Invest.* 2013;123(1):340–347.
21. Jousma E, Rizvi TA, Wu J, et al. Preclinical assessments of the MEK inhibitor PD-0325901 in a mouse model of Neurofibromatosis type 1. *Pediatr Blood Cancer.* 2015;62(10):1709–1716.
22. Signorelli J, Shah Gandhi A. Cobimetinib. *Ann Pharmacother.* 2017;51(2):146–153.
23. Wong H, Vernillet L, Peterson A, et al. Bridging the gap between preclinical and clinical studies using pharmacokinetic-pharmacodynamic modeling: an analysis of GDC-0973, a MEK inhibitor. *Clin Cancer Res.* 2012;18(11):3090–3099.
24. Choo EF, Ng CM, Berry L, et al. PK-PD modeling of combination efficacy effect from administration of the MEK inhibitor GDC-0973 and PI3K inhibitor GDC-0941 in A2058 xenografts. *Cancer Chemother Pharmacol.* 2013;71(1):133–143.
25. Hoefflich KP, Merchant M, Orr C, et al. Intermittent administration of MEK inhibitor GDC-0973 plus PI3K inhibitor GDC-0941 triggers robust apoptosis and tumor growth inhibition. *Cancer Res.* 2012;72(1):210–219.
26. Rice KD, Aay N, Anand NK, et al. Novel carboxamide-based allosteric MEK inhibitors: discovery and optimization efforts toward XL518 (GDC-0973). *ACS Med Chem Lett.* 2012;3(5):416–421.
27. Rosen LS, LoRusso P, Ma WW, et al. A first-in-human phase I study to evaluate the MEK1/2 inhibitor, cobimetinib, administered daily in patients with advanced solid tumors. *Invest New Drugs.* 2016;34(5):604–613.
28. Petrilli AM, Fuse MA, Donnan MS, et al. A chemical biology approach identified PI3K as a potential therapeutic target for neurofibromatosis type 2. *Am J Transl Res.* 2014;6(5):471–493.
29. Fuse MA, Plati SK, Burns SS, et al. Combination therapy with c-Met and Src inhibitors induces caspase-dependent apoptosis of merlin-deficient schwann cells and suppresses growth of schwannoma cells. *Mol Cancer Ther.* 2017;16(11):2387–2398.
30. Petrilli AM, Garcia J, Bott M, et al. Ponatinib promotes a G1 cell-cycle arrest of merlin/NF2-deficient human schwann cells. *Oncotarget.* 2017;8(19):31666–31681.
31. Giovannini M, Robanus-Maandag E, Niwa-Kawakita M, et al. Schwann cell hyperplasia and tumors in transgenic mice expressing a naturally occurring mutant NF2 protein. *Genes Dev.* 1999;13(8):978–986.
32. Giovannini M, Bonne NX, Vitte J, et al. mTORC1 inhibition delays growth of neurofibromatosis type 2 schwannoma. *Neuro Oncol.* 2014;16(4):493–504.
33. Cox J, Neuhauser N, Michalski A, Scheltema RA, Olsen JV, Mann M. Andromeda: a peptide search engine integrated into the MaxQuant environment. *J Proteome Res.* 2011;10(4):1794–1805.
34. Smyth GK, Michaud J, Scott HS. Use of within-array replicate spots for assessing differential expression in microarray experiments. *Bioinformatics.* 2005;21(9):2067–2075.
35. Gilmartin AG, Bleam MR, Groy A, et al. GSK1120212 (JTP-74057) is an inhibitor of MEK activity and activation with favorable pharmacokinetic properties for sustained in vivo pathway inhibition. *Clin Cancer Res.* 2011;17(5):989–1000.
36. Blakeley JO, Plotkin SR. Therapeutic advances for the tumors associated with neurofibromatosis type 1, type 2, and schwannomatosis. *Neuro Oncol.* 2016;18(5):624–638.
37. Goutagny S, Raymond E, Esposito-Farese M, et al. Phase II study of mTORC1 inhibition by everolimus in neurofibromatosis type 2 patients with growing vestibular schwannomas. *J Neurooncol.* 2015;122(2):313–320.
38. Karajannis MA, Legault G, Hagiwara M, et al. Phase II trial of lapatinib in adult and pediatric patients with neurofibromatosis type 2 and progressive vestibular schwannomas. *Neuro Oncol.* 2012;14(9):1163–1170.
39. Karajannis MA, Legault G, Hagiwara M, et al. Phase II study of everolimus in children and adults with neurofibromatosis type 2 and progressive vestibular schwannomas. *Neuro Oncol.* 2014;16(2):292–297.
40. Plotkin SR, Halpin C, McKenna MJ, Loeffler JS, Batchelor TT, Barker FG 2nd. Erlotinib for progressive vestibular schwannoma in neurofibromatosis 2 patients. *Otol Neurotol.* 2010;31(7):1135–1143.
41. Plotkin SR, Merker VL, Halpin C, et al. Bevacizumab for progressive vestibular schwannoma in neurofibromatosis type 2: a retrospective review of 31 patients. *Otol Neurotol.* 2012;33(6):1046–1052.
42. Yi C, Troutman S, Fera D, et al. A tight junction-associated merlin-angiotensin complex mediates merlin's regulation of mitogenic signaling and tumor suppressive functions. *Cancer Cell.* 2011;19(4):527–540.
43. Bevill SM, Zawistowski JS, Johnson GL. Enhancer remodeling regulates epigenetic adaptation and resistance to MEK1/2 inhibition in triple-negative breast cancer. *Mol Cell Oncol.* 2017;4(6):e1300622.
44. Zawistowski JS, Bevill SM, Goulet DR, et al. Enhancer remodeling during adaptive bypass to MEK inhibition is attenuated by pharmacologic targeting of the P-TEFb complex. *Cancer Discov.* 2017;7(3):302–321.
45. Kurimchak AM, Shelton C, Duncan KE, et al. Resistance to BET bromodomain inhibitors is mediated by kinome reprogramming in ovarian cancer. *Cell Rep.* 2016;16(5):1273–1286.
46. Stuhlmiller TJ, Miller SM, Zawistowski JS, et al. Inhibition of lapatinib-induced kinome reprogramming in ERBB2-positive breast cancer by targeting BET family bromodomains. *Cell Rep.* 2015;11(3):390–404.
47. Zhou C, Cunningham L, Marcus AI, Li Y, Kahn RA. Arl2 and Arl3 regulate different microtubule-dependent processes. *Mol Biol Cell.* 2006;17(5):2476–2487.

Targeting Protein Translation by Rocaglamide and Didesmethylocaglamide to Treat MPNST and Other Sarcomas



Long-Sheng Chang^{1,2,3,4}, Janet L. Oblinger^{1,2}, Sarah S. Burns^{1,2}, Jie Huang^{1,2}, Larry W. Anderson⁵, Melinda G. Hollingshead⁵, Rulong Shen⁴, Li Pan⁶, Garima Agarwal⁶, Yulin Ren⁶, Ryan D. Roberts^{1,2}, Barry R. O'Keefe^{5,7}, A. Douglas Kinghorn⁶, and Jerry M. Collins⁵

ABSTRACT

Malignant peripheral nerve sheath tumors (MPNST) frequently overexpress eukaryotic initiation factor 4F components, and the eIF4A inhibitor silvestrol potently suppresses MPNST growth. However, silvestrol has suboptimal drug-like properties, including a bulky structure, poor oral bioavailability (<2%), sensitivity to MDR1 efflux, and pulmonary toxicity in dogs. We compared ten silvestrol-related rocaglates lacking the dioxanyl ring and found that didesmethylrocaglamide (DDR) and rocaglamide (Roc) had growth-inhibitory activity comparable with silvestrol. Structure-activity relationship analysis revealed that the dioxanyl ring present in silvestrol was dispensable for, but may enhance, cytotoxicity. Both DDR and Roc arrested MPNST cells at G₂-M, increased the sub-G₁ population, induced cleavage of caspases and PARP, and elevated the levels of the DNA-damage response marker γ H2A.X, while decreasing the expression of AKT and ERK1/2, consistent with translation inhibition. Unlike silvestrol,

DDR and Roc were not sensitive to MDR1 inhibition. Pharmacokinetic analysis confirmed that Roc had 50% oral bioavailability. Importantly, Roc, when administered intraperitoneally or orally, showed potent antitumor effects in an orthotopic MPNST mouse model and did not induce pulmonary toxicity in dogs as found with silvestrol. Treated tumors displayed degenerative changes and had more cleaved caspase-3-positive cells, indicative of increased apoptosis. Furthermore, Roc effectively suppressed the growth of osteosarcoma, Ewing sarcoma, and rhabdomyosarcoma cells and patient-derived xenografts. Both Roc- and DDR-treated sarcoma cells showed decreased levels of multiple oncogenic kinases, including insulin-like growth factor-1 receptor. The more favorable drug-like properties of DDR and Roc and the potent antitumor activity of Roc suggest that these rocaglamides could become viable treatments for MPNST and other sarcomas.

Introduction

Malignant peripheral nerve sheath tumors (MPNST) are characterized as aggressive soft-tissue sarcomas with a high risk of recurrence and metastasis. Often refractory to current treatment, patients with these tumors have a poor 5-year survival rate of only about 20% to 50% (1). Therefore, development of a more effective medical therapy

that eradicates MPNSTs is of significant clinical need. MPNSTs can occur sporadically or arise from preexisting plexiform neurofibromas in patients with neurofibromatosis type 1 (NF1), a tumor predisposition syndrome caused by mutations in the *NF1* gene which encodes the Ras-GTPase-activating protein neurofibromin. Importantly, even sporadic tumors frequently harbor mutations in the *NF1* gene or the Ras pathway. Consequently, both sporadic and NF1-associated MPNSTs exhibit upregulation of Ras downstream kinase signaling, including the PI3K-AKT-mTOR and Raf-MEK-ERK mitogen-activated protein kinases. MPNSTs also exhibit overexpression or aberrant activation of epidermal growth factor receptor (EGFR), platelet-derived growth factor receptor (PDGFR), and insulin-like growth factor-1 receptor (IGF-1R; refs. 2, 3). These reports suggest that these Ras downstream kinases and deregulated receptor tyrosine kinases (RTKs) may be therapeutic targets. In addition, recurrent mutations in the tumor-suppressor genes *CDKN2A* and *TP53* and the subunits of the chromatin-modifying polycomb repressor complex-2 (PRC2), *SUZ12* and *EED*, have been identified and are important for MPNST progression (4). Inactivation of *CDKN2A* and *TP53* disables the G₁-S checkpoint. The loss of PRC2 function can lead to enhanced Ras-driven gene transcription (5).

As MPNSTs often exhibit hyperactive Ras activity, statins and farnesyl transferase inhibitors, which prevent localization of Ras to the membrane and inhibit MPNST cell growth (6, 7), have been evaluated but do not improve survival in patients with advanced cancer (8-10). Drugs that target the deregulated RTKs and mitogenic kinases have also been investigated in patients with MPNSTs; however, the results have so far been disappointing. The EGFR inhibitor erlotinib elicited poor response rates in MPNSTs with only 1 of 20 patients exhibiting stable disease (11). The IGF-1R-blocking

¹Center for Childhood Cancer and Blood Diseases, Abigail Wexner Research Institute, Nationwide Children's Hospital, Columbus, Ohio. ²Department of Pediatrics, The Ohio State University College of Medicine, Columbus, Ohio. ³Department of Otolaryngology-Head and Neck Surgery, The Ohio State University College of Medicine, Columbus, Ohio. ⁴Department of Pathology, The Ohio State University College of Medicine, Columbus, Ohio. ⁵Division of Cancer Treatment and Diagnosis, Center for Cancer Research, National Cancer Institute, NIH, Frederick, Maryland. ⁶Division of Medicinal Chemistry and Pharmacognosy, The Ohio State University College of Pharmacy, Columbus, Ohio. ⁷Molecular Targets Program, Center for Cancer Research, National Cancer Institute, NIH, Frederick, Maryland.

Note: Supplementary data for this article are available at Molecular Cancer Therapeutics Online (<http://mct.aacrjournals.org/>).

Corresponding Author: Long-Sheng Chang, Center for Childhood Cancer and Blood Diseases, Abigail Wexner Research Institute at Nationwide Children's Hospital and The Ohio State University College of Medicine, 700 Children's Drive, Columbus, OH 43205. Phone: 614-355-2658; Fax: 614-722-5895; E-mail: lchang@chi.osu.edu

Mol Cancer Ther 2020;19:731-41

doi: 10.1158/1535-7163.MCT-19-0809

©2019 American Association for Cancer Research.

antibodies, such as ganitumab, show limited objective single-agent activity (12). Sorafenib, which inhibits Raf and several RTKs, has only minimal activity in patients with sarcomas (13). The mTOR inhibitor rapamycin and its derivatives, such as everolimus, cause cytostatic responses and are being evaluated in combination with other targeted drugs. However, a recent trial showed that combination of everolimus with bevacizumab, a monoclonal antibody that binds VEGF and prevents activation of the RTK VEGF receptor, was not effective in patients with refractory MPNSTs (14). A phase II study is ongoing to evaluate the dual mTOR complexes 1 and 2 inhibitor TAK-228 in soft-tissue sarcomas (<https://clinicaltrials.gov> Identifier: NCT02987959). Collectively, the modest and transient patient responses from the completed trials indicate that targeting more than one critical pathway is likely needed to achieve a cure.

To sustain uncontrolled growth, cancer cells commonly exhibit enhanced protein translation by upregulation of the translation machinery (15). The most highly regulated step in the protein biosynthetic pathway occurs during translation initiation, in which the eukaryotic initiation factor 4F (eIF4F) complex is recruited to the 5' untranslated region (5'-UTR) of mRNA. This complex is composed of three subunits: eIF4G, a scaffolding protein; eIF4E, a cap-binding protein; and eIF4A, an RNA helicase which unwinds the secondary structure of the 5'-UTR. We have shown overexpression of the three eIF4F components in multiple types of human cancer, including MPNST (16, 17). Genetic inhibition of eIF4A and eIF4E using short-hairpin RNAs reduces MPNST cell proliferation. In addition, the prosurvival and progrowth activities of several signaling pathways, such as PI3K-AKT-mTOR and Raf-MEK-ERK frequently activated in human cancer, occur in part by facilitating eIF4F-mediated translation initiation. The mTOR kinase phosphorylates and inactivates the eIF4E-binding protein translational repressors (18). Both AKT and ERKs phosphorylate eIF4B, which then associates with and increases the helicase activity of eIF4A (19). Moreover, AKT, mTOR, and the downstream ERK1/2 kinase, p90 ribosomal S6 kinase, can phosphorylate and inactivate an endogenous repressor of eIF4A activity, the programmed cell death 4 protein. Further, the mRNAs that depend upon eIF4A for efficient translation usually contain long 5'-UTRs with guanine-rich sequences termed G-quadruplexes which can form four-stranded structures with G-tetrads stacked on one another (15). These eIF4A-dependent transcripts are often found in genes encoding oncoproteins, transcription factors associated with super enhancers, epigenetic regulators, and kinases (20). Interestingly, we found that the eIF4A inhibitor silvestrol suppresses MPNST cell growth at low nanomolar of IC₅₀, decreases the levels of multiple mitogenic kinases including AKT and ERKs, and profoundly impairs the growth of MPNST xenografts (16). These results suggest that direct targeting of the translation initiation components, particularly eIF4A, might be an effective treatment strategy for these tumors.

Silvestrol is part of a large family of compounds termed flavaglines or rocaglates, which share a cyclopenta[*b*]benzofuran structure (21, 22). It possesses potent antitumor activity in multiple other cancer models (23–25). However, silvestrol has some suboptimal drug-like properties. It is relatively large with a bulky dioxanyl ring, making the total synthesis of silvestrol laborious (26–28). It is a substrate for the multidrug resistance 1 (MDR1) transporter (29) and has very limited oral bioavailability of <2% (30).

To search for compounds with better drug-like properties, we analyzed ten rocaglates that lack the dioxanyl moiety and examined the structure-activity relationships for this compound class. We showed that two of these compounds, rocaglamide (Roc) and didesmethylrocaglamide (DDR), exhibited potent growth inhibitory activ-

ity with IC₅₀ values comparable to silvestrol. Importantly, these rocaglamides were not sensitive to MDR1 inhibition, and Roc exhibited oral bioavailability and potent antitumor effects against multiple types of sarcomas.

Materials and Methods

Natural compounds

Ten silvestrol-related rocaglates, inclusive of (–)-didesmethylrocaglamide, were isolated from the tropical plant *Aglaia perviridis*, collected in Vietnam as part of a multi-institutional collaborative project on the discovery of new antineoplastic natural compounds. The full structures and absolute configurations of these rocaglates were determined (31). For *in vitro* studies, purified silvestrol and related rocaglates were dissolved as a 10 mmol/L stock in DMSO (Sigma-Aldrich). A 60-mg sample of (–)-rocaglamide (NSC326408) was prepared at the U.S. National Cancer Institute for *in vivo* studies.

Cell lines, cell proliferation assays, and flow cytometry

Various MPNST, Ewing sarcoma, osteosarcoma, rhabdomyosarcoma, schwannoma, meningioma, and leukemia cell lines used in this study are described in Supplementary Methods. All cell lines were authenticated by short tandem repeat genotyping and tested to be mycoplasma-free. Cell proliferation was assessed using resazurin assays, and cell-cycle analysis was performed as previously described (32).

Western blots

Subconfluent cells were treated with the indicated doses of Roc or DDR for 1 to 3 days and lysed. Equal amounts of protein lysates were analyzed by immunoblotting. Detailed procedures and the antibodies used are described in Supplementary Methods.

Pharmacokinetic analysis

Mice were administered with a 5 mg/kg dose of Roc by i.v. or i.p. injection or by oral gavage (p.o.). Blood samples were collected before and at multiple time-points after dosing ($n = 3$). Plasma concentrations of Roc were analyzed using a sensitive LC/MS-MS (Supplementary Methods).

Cell line-derived xenograft and patient-derived xenograft models and *in vivo* efficacy

All animal work was performed according to the protocols approved by the Institutional Animal Care and Use Committee at Nationwide Children's Hospital. For animal dosing, Roc was formulated in 30% hydroxypropyl-β-cyclodextrin (HPβCD). The quantifiable, orthotopic MPNST cell line-derived xenograft (CDX) model was generated as described previously (33). Mice bearing established ST8814-Luc tumors (16) were randomized into three groups ($n = 10$ /group) and treated with the predetermined MTD of Roc at 4 mg/kg by i.p. or 1.2 mg/kg by oral gavage, or the vehicle HPβCD every other day. Tumor growth was measured weekly by bioluminescence imaging (BLI).

To generate patient-derived xenograft (PDX) models, the Nationwide Children's Hospital Institutional Review Board approved the Human Subjects Protocol. After obtaining informed written consents from the subjects, tumor specimens were used to establish PDX models. Mice with actively growing PDX tumors for a Ewing sarcoma (NCH-EWS-2), an osteosarcoma (NCH-OS-7), and an alveolar rhabdomyosarcoma (NCH-ARMS-2) reaching approximately 100 to 200 mm³ were randomized into two treatment groups ($n = 10$ /group) for each PDX model and treated with 3 mg/kg of Roc or HPβCD by i.p.

every other day, followed by tumor measurement twice weekly (Supplementary Methods).

Immunohistochemistry

Sections from Roc or vehicle-treated MPNST tumors were prepared and stained with hematoxylin and eosin (H&E) or immunostained for p-histone H3(Ser¹⁰) (pH3; ab32107, Abcam) or CC3 (#9664, Cell Signaling Technology) as previously described (32).

Results

DDR and Roc possess potent growth-inhibitory activity comparable with silvestrol

To search for compounds with better drug-like properties, we side-by-side compared ten rocaglates lacking the dioxanyl ring (31) with silvestrol for growth-inhibitory activity in a panel of MPNST, schwannoma, and meningioma cell lines, which we previously showed to be sensitive to the antiproliferative action of silvestrol (16, 17). We found that several of these rocaglates maintained potent growth inhibition comparable with silvestrol. In particular, the IC₅₀ values of Roc were

slightly higher than silvestrol, whereas DDR reliably demonstrated approximately 2-fold more potent than silvestrol in all cell lines tested (Fig. 1; Table 1; and Supplementary Fig. S1), indicating that the dioxanyl moiety is dispensable for cytotoxicity. Further structure-activity comparison discerned some positions on the cyclopenta[*b*]benzofuran scaffold that affected the antiproliferative activity of rocaglates. Similar to previous observations, the substitution of a methoxy group at position 8b, as in 8b-*O*-methylrocaglaol versus rocaglaol, abolished the activity (Fig. 1). This methoxy substitution at 8b could be partly mitigated by the addition of a methylenedioxy ring to phenyl ring B. In addition, the presence of amide or ester groups at position C-2 of the benzofuran scaffold appeared to enhance the activity, as compounds such as DDR, Roc, and methyl rocaglate were more potent than rocaglaol. Because the amide group at the C-2 position confers superior growth inhibition, we further evaluated DDR and Roc for their mechanisms of action.

Rocaglamides induce G₂-M arrest and cell death

Flow cytometry analysis revealed that human *NFI*-expressing STS26T and *NFI*-null ST8814 MPNST cells treated with one- or

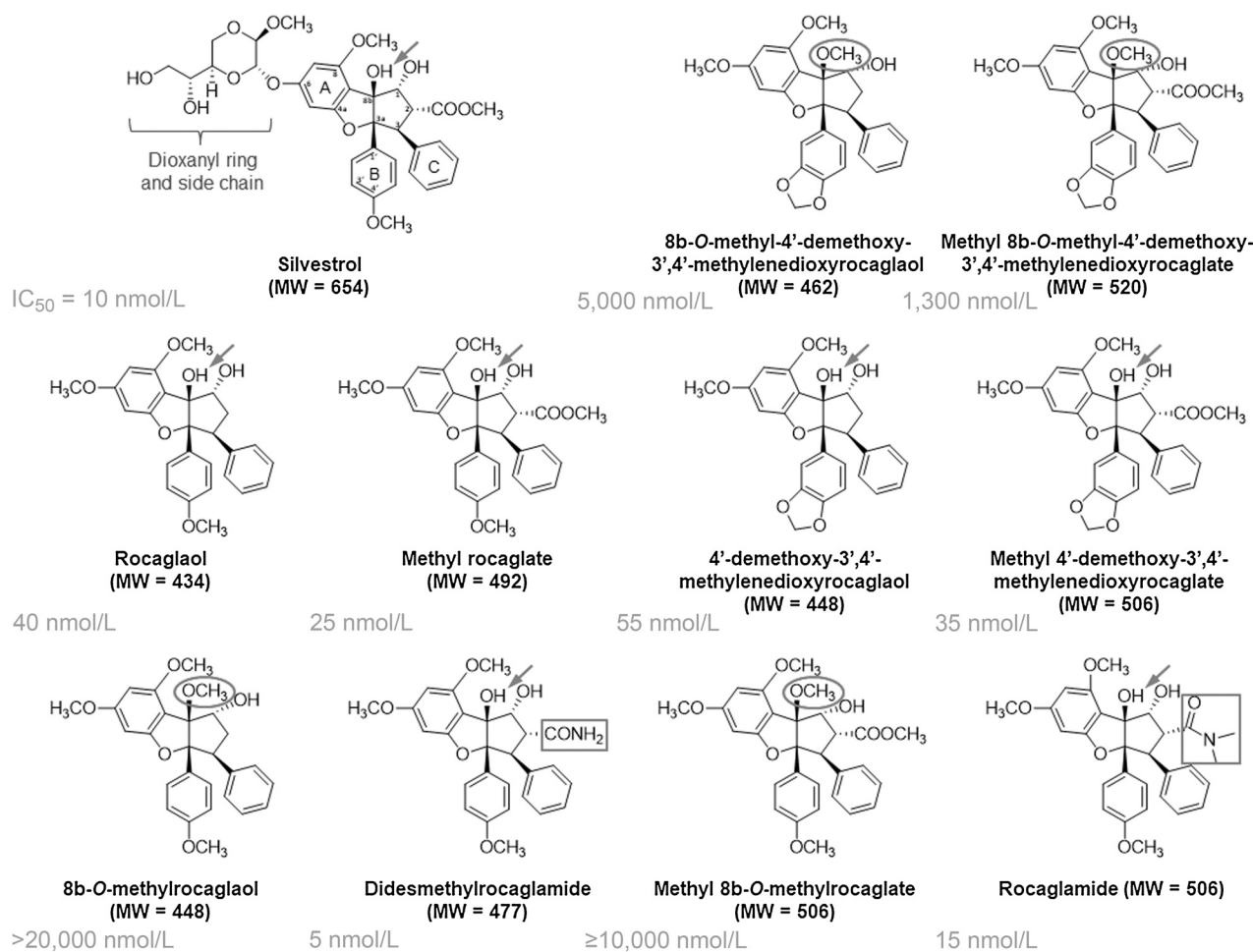


Figure 1.

Identification of DDR and Roc with potent growth-inhibitory activity comparable with silvestrol. The structure of each rocaglate is shown along with its IC₅₀ value in STS26T MPNST cells as determined in Table 1. Structure-activity comparison revealed that the dioxanyl (dioxanyloxy) ring is dispensable but may enhance the cytotoxicity of rocaglates. An unmethylated C-8b hydroxyl group (arrow) and the amide functionality (rectangle) of DDR and Roc are important for optimum antiproliferative activity, whereas methylation of the C-8b hydroxyl group (oval) substantially impaired the activity.

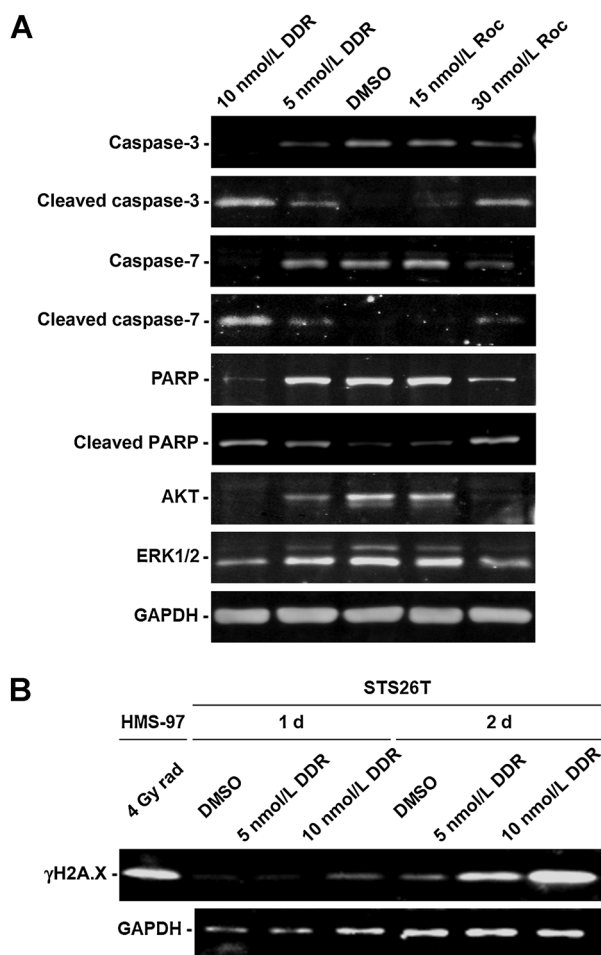
Chang et al.

Table 1. The growth-inhibitory activity of silvestrol and 10 related rocaglates lacking the dioxanyl ring in *NF1*^{+/+} STS26T and *NF1*^{-/-} ST8814 MPNST, *Nf2*^{-/-} schwannoma, and *NF2*^{-/-} meningioma cells.

Compound	MW (Da)	IC ₅₀ (nmol/L)			
		Sch10545 <i>Nf2</i> ^{-/-} schwannoma cells	Ben-Men-1 <i>NF2</i> ^{-/-} meningioma cells	STS26T <i>NF1</i> ^{+/+} MPNST cells	ST8814 <i>NF1</i> ^{-/-} MPNST cells
Silvestrol	654	70	10	10	40
8b-O-methyl-4'-demethoxy-3',4'-methyleneoxyrocaglaol	462	>2,500	>2,500	5,000	10,000
Methyl 8b-O-methyl-4'-demethoxy-3',4'-methyleneoxyrocaglate	520	1,900	3,800	1,300	2,000
Rocaglaol	434	60	100	40	90
Methyl rocaglate	492	50	55	25	35
4'-demethoxy-3',4'-methyleneoxyrocaglaol	448	65	85	55	120
Methyl 4'-demethoxy-3',4'-methyleneoxyrocaglate	506	60	80	35	70
8b-O-methylrocaglaol	448	>20,000	>20,000	>20,000	>20,000
Didesmethylrocaglamide	477	10	5	5	5
Methyl 8b-O-methylrocaglate	506	9,300	>10,000	>10,000	>20,000
Rocaglamide	506	ND	15	15	20

Note: The average IC₅₀ value of each rocaglate was determined by 3-day resazurin proliferation assays as described in Materials and Methods. Didesmethylrocaglamide and rocaglamide were found to possess growth-inhibitory activity similar to or more potent than silvestrol.

Abbreviation: ND, not determined.



two-IC₅₀ doses of DDR or Roc for 3 days exhibited a marked increase in the G₂-M fraction (Supplementary Fig. S2A and S2B). The sub-G₁ fraction, suggestive of apoptosis, was noticeably prominent in treated STS26T cells, especially at the two-IC₅₀ dose (Supplementary Fig. S2A). Phase contrast micrographs taken of cells prior to cell-cycle analysis showed increased floating dead cells and debris in DDR- or Roc-treated dishes. Although ST8814 cells treated for 3 days did not show obvious signs of cell death (Supplementary Fig. S2B), a 6-day incubation resulted in increased numbers of floating dead cells with a commensurate expansion of the sub-G₁ fraction (Supplementary Fig. S2C). Collectively, these results indicate that, like silvestrol (16), DDR and Roc inhibit MPNST cell proliferation by inducing cell-cycle arrest at G₂-M and subsequently, cell death.

DDR and Roc increase caspase and PARP cleavage and activate the DNA damage response, while suppressing mitogenic signaling pathways

To confirm induction of apoptosis in Roc-treated MPNST cells, we analyzed protein expression of several markers important for this process. STS26T cells treated for 3 days with either DDR or Roc exhibited increased cleavage of the executioner caspases-3 and 7 and their downstream substrate PARP (Fig. 2A). A concomitant decrease in the amounts of intact

Figure 2. DDR and Roc increase caspase and PARP cleavage and elevate the levels of γH2A.X while decreasing AKT and ERK expression in MPNST cells. **A**, Protein lysates prepared from STS26T cells treated for 3 days with 1- or 2-IC₅₀ of DDR or Roc were analyzed by Western blots for full-length and cleaved caspase-3/7 and PARP, as well as AKT and ERK1/2. GAPDH served as a loading control. **B**, Protein lysates from STS26T cells treated for 1 and 2 days with 1- or 2-IC₅₀ of DDR were probed for the expression of phosphorylated H2A.X (γH2A.X). As a positive control, lysates from HMS-97 human malignant schwannoma cells irradiated with 4 grays (Gy) of X-ray (rad) were used.

Rocaglamide and Didesmethyrocaglamide for Sarcoma Treatment

caspsases 3 and 7 and PARP was observed, consistent with the enhanced cleavage of these apoptotic markers and possibly due to direct effects of these rocaglamides on protein translation. Likewise, the levels of the prosurvival kinases AKT and ERK1/2 were diminished in Roc- and DDR-treated MPNST cells. Importantly, treatment with rocaglamides also resulted in higher levels of the DNA damage response marker γ H2A.X. This increase occurred as early as one day after DDR treatment before the occurrence of cell death (Fig. 2B). Similarly, cleavage of caspase-3 and PARP and induction of γ H2A.X were also detected in *NF1*-null ST8814 cells treated with DDR and Roc (Supplementary Fig. S3). These results demonstrate that DDR and Roc induce apoptosis in both *NF1*-expressing and *NF1*-deficient MPNST cells, possibly subsequent to the activation of the DNA damage response.

Rocaglamides are not sensitive to MDR1 inhibition, and Roc is orally bioavailable

The MDR1/P-glycoprotein (Pgp) encoded by the *ABCB1* (ATP-binding cassette subfamily B member 1) gene is implicated in limiting the bioavailability of several chemotherapeutics and confers drug resistance in tumors that overexpress this protein. Silvestrol is a substrate of MDR1/Pgp, which may be related to its poor oral bioavailability (29, 30). To determine whether there are any differences in the sensitivity to MDR1/Pgp between rocaglamides and silvestrol, we treated silvestrol-resistant 697-R leukemic cells, which overexpress MDR1/Pgp (Supplementary Fig. S4), and the parental silvestrol-sensitive 697 cells with various concentrations of each compound. Similar to previous findings (29), we found that 697-R cells were less sensitive to silvestrol inhibition than 697 cells (26 vs. 3.5 nmol/L of IC_{50} , respectively; Fig. 3A). Surprisingly, DDR- and Roc-treated 697-R

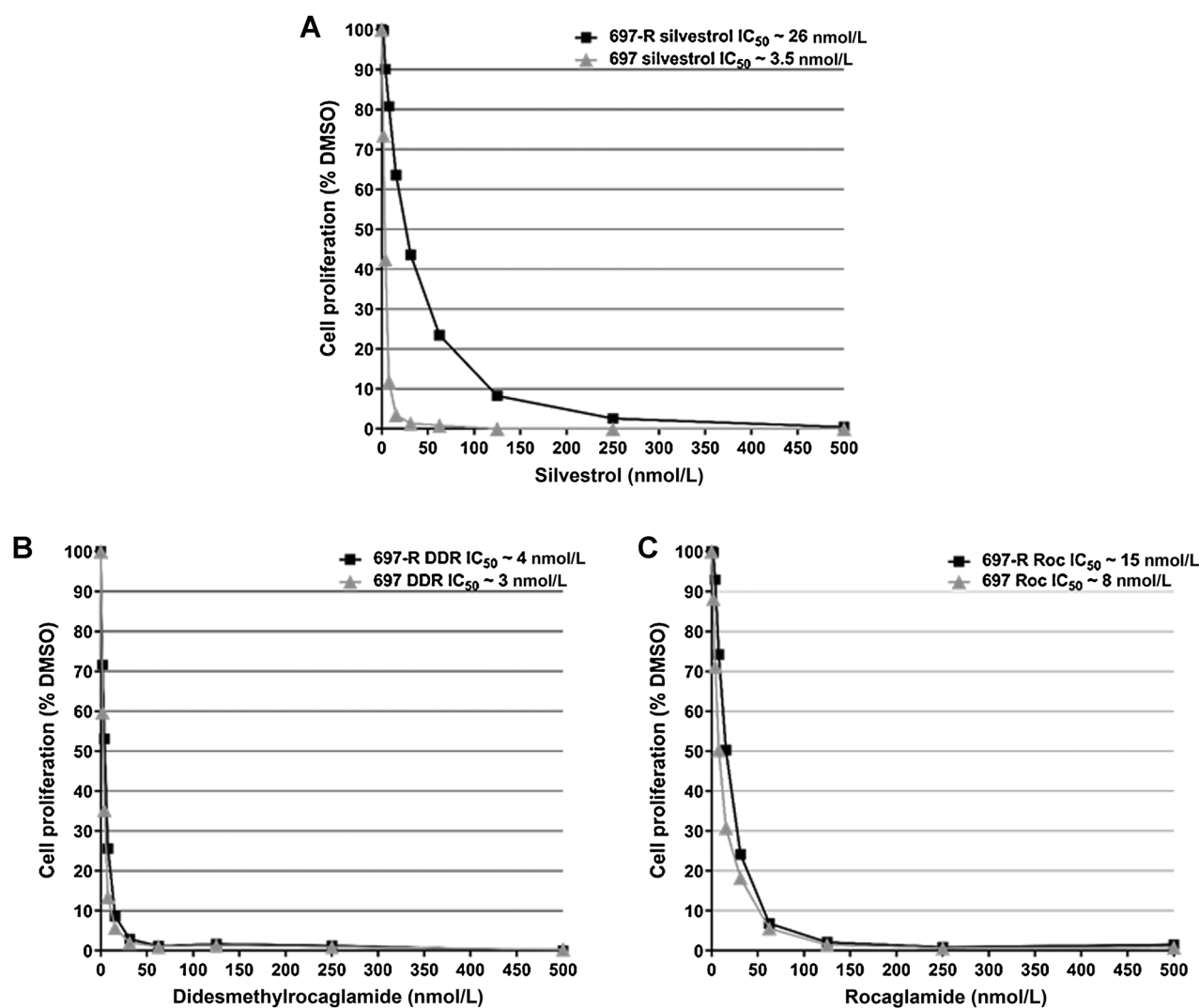


Figure 3.

Unlike silvestrol, DDR and Roc inhibit proliferation of MDR1-overexpressing 697-R leukemic cells at IC_{50} values similar to parental 697 cells. Cell proliferation was measured on 697-R and 697 cells treated for 3 days with various concentrations of silvestrol (A), DDR (B), and Roc (C). Each treatment was performed in six replicates, and each experiment was repeated twice. Shown are representative dose-response growth inhibition curves for all three drugs from experiments run in parallel. The insets show the IC_{50} values for each compound.

Chang et al.

cells exhibited IC_{50} values very similar to those of parental 697 cells (4 vs. 3 nmol/L of IC_{50} , respectively, for DDR and 15 vs. 8 nmol/L of IC_{50} , respectively, for Roc; **Fig. 3B** and **C**). Also, we observed that various MPNST cell lines expressed different levels of MDR1 protein (Supplementary Fig. S4). For example, ST8814 cells expressed a higher level of MDR1 than STS26T cells. Curiously, both cell lines showed similar sensitivity to growth inhibition by DDR and Roc (**Table 1**; Supplementary Fig. S1). Together, these results indicate that these rocaglamides are no longer sensitive to MDR1 inhibition.

To examine the oral bioavailability, we conducted pharmacokinetic (PK) studies to compare mice that had been dosed with Roc at 5 mg/kg via the i.v., i.p., or p.o. route, followed by measuring Roc concentrations in blood samples collected at various times post dosing. Two separate studies with 3 mice at each time point for each dosing route were conducted. The maximum mean observed concentration (C_{max})

reached approximately 11 $\mu\text{mol/L}$ for the i.v. route, approximately 4 $\mu\text{mol/L}$ for the i.p. route, and approximately 0.8 $\mu\text{mol/L}$ for the p.o. route (**Fig. 4A**). Areas under the plasma concentration-time curves (AUC_{0-7h}) produced 245 $\mu\text{mol/L}\cdot\text{min}$ of exposure in the i.v. route and 142 $\mu\text{mol/L}\cdot\text{min}$ of exposure in the p.o. route. The concentrations of Roc appeared to decline more slowly in the plasma over 24 hours ($T_{1/2} = 2.4\text{h}$) with the p.o. route compared with those dosed by the i.v. route ($T_{1/2} = 1.5\text{h}$). Based on the estimation from AUC_{0-7h} , Roc exhibited approximately 50% oral bioavailability, confirming improved bioavailability of Roc over silvestrol.

Roc, when administered intraperitoneally or orally, exhibits potent antitumor effects in an orthotopic MPNST model

To evaluate the *in vivo* activity of Roc, we treated NSG mice bearing luciferase-expressing ST8814-Luc tumors implanted in the sciatic

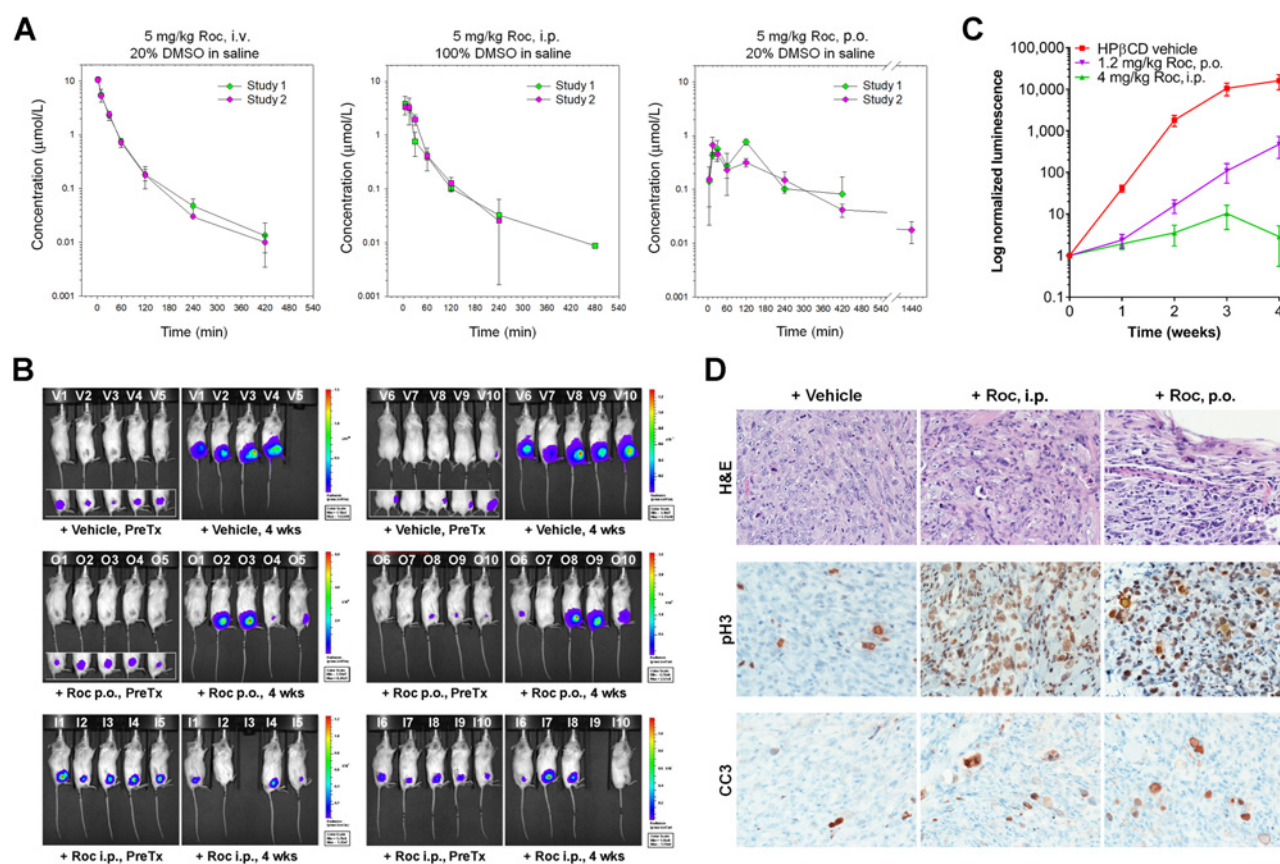


Figure 4.

Roc has 50% oral bioavailability and potently suppresses the growth of orthotopic MPNST xenografts. **A**, Plasma concentration-time profiles of Roc were obtained by PK analysis according to Materials and Methods. The mean concentration of Roc with SD in mouse plasma for each time point after i.v., i.p., and p.o. administration was plotted. For each dosing route, two independent studies were performed. **B**, Shown are representative BL images of ST8814-Luc MPNST-bearing mice prior to (PreTx) and 4 weeks (wks) after treatment with Roc at 4 mg/kg by i.p., 1.2 mg/kg by p.o., or HP β CD vehicle every other day. **C**, The relative tumor-emitted BL signals were denoted as percentage of total flux after treatment relative to the total flux prior to treatment designated as one (100%). The data are shown as mean \pm SD. For each treatment group, at least 7 mice completed the full treatment schedule. Note that tumor bioluminescence from vehicle-treated mice rapidly increased by an average of approximately 17,000-fold over 4 weeks. However, tumor bioluminescence from the Roc i.p. group grew only by approximately 3-fold and from the Roc p.o. group increased approximately 470-fold on average. **D**, H&E staining shows that although vehicle-treated xenografts contained large vesicular nuclei with prominent nucleoli and mitotic activity, tumors treated with Roc by i.p. had pleomorphic nuclei, and many enlarged tumor cells had abundant foamy cytoplasm resembling histiocytoid degenerative changes along with scattered apoptosis (top panels). Degenerative tumor cells were also present in tumors treated with orally delivered Roc. Tumor necrosis with necrotic debris separating mostly degenerative tumor cells with viable vasculature was also observed. Immunostaining revealed abundant phospho-histone H3 (pH3)-labeled cells in Roc-treated tumors compared with vehicle-treated tumors (middle panels). Increased numbers of cleaved caspase-3 (CC3)-positive cells were detected in Roc-treated tumors (bottom panels).

Rocaglamide and Didesmethylocaglamide for Sarcoma Treatment

nerve with Roc at the predetermined MTD (4 mg/kg by i.p. or 1.2 mg/kg orally), or HP β CD vehicle every other day. As shown in Fig. 4B and C, tumor bioluminescence from vehicle-treated mice steadily and rapidly increased by >10,000-fold over 4-week treatment. In contrast, tumor bioluminescence from mice treated with Roc by i.p. only increased by an average of <10-fold, showing >99% reduction in tumor luminescence compared with controls. Similarly, Roc, when administered orally, also exhibited potent tumor inhibition with bioluminescence decreasing by >95%. In addition, we did not observe any significant changes in body weight of animals treated with the indicated doses of Roc, compared with vehicle-treated controls (Supplementary Fig. S5).

Histologic analysis revealed that although MPNSTs treated with HP β CD vehicle for 4 weeks had large nuclei with prominent nucleoli and displayed active mitotic figures (Fig. 4D, top left panel), tumors treated with Roc by i.p. had pleomorphic nuclei with abundant foamy cytoplasm resembling histiocytoid degenerative changes (top middle panel). A few enlarged tumor cells with multinucleated appearance and scattered apoptosis were present. Degenerative changes and cell death were also observed in tumors treated with orally delivered Roc (top right panel). Consistent with G₂-M arrest, tumor cells treated with i.p. or orally delivered Roc exhibited much higher prevalence of phospho-histone H3 labeling compared with vehicle-treated tumors (middle panel). In addition, Roc-treated tumors displayed increased numbers of cleaved caspase-3-positive cells which often coincided with those with multinucleated-like appearance (bottom panel). Taken together, these

results indicate that Roc has oral bioavailability and possesses potent *in vivo* efficacy against MPNSTs.

Roc and DDR have broad antitumor activity against common types of pediatric sarcoma

Because MPNSTs comprise only approximately 2% of all sarcomas (34), we expanded our testing of Roc and DDR to three other types of sarcomas more prevalently seen in children and young adults: Ewing sarcoma, osteosarcoma, and rhabdomyosarcoma. Using a series of commonly used cell lines, including two Ewing sarcoma cell lines (A673 and TC32), four osteosarcoma cell lines (143B, MG-63, Saos2, and OS17), and one rhabdomyosarcoma cell line (RD), we showed that, as in MPNST cells, both rocaglamides were highly active against all of these sarcoma cell lines (Supplementary Fig. S6A–S6C). Also, we observed that DDR consistently exhibited lower IC₅₀ values than Roc in every sarcoma cell line tested.

Subsequently, we evaluated the *in vivo* activity of Roc using PDX models for a Ewing sarcoma, an osteosarcoma, and an alveolar rhabdomyosarcoma. We discovered that Roc was highly potent in suppressing the growth of Ewing sarcoma PDXs and inhibited tumor growth by an average of approximately 90% over 4-week treatment (Fig. 5A). Similarly, the average size of Roc-treated osteosarcoma PDX tumors was reduced by approximately 80% compared with those of vehicle-treated tumors (Fig. 5B). Also, Roc inhibited the growth of rhabdomyosarcoma PDXs by approximately 70% (Fig. 5C). Notably, the volumes of tumors in individual Roc-treated mice showed very little overlap with those in

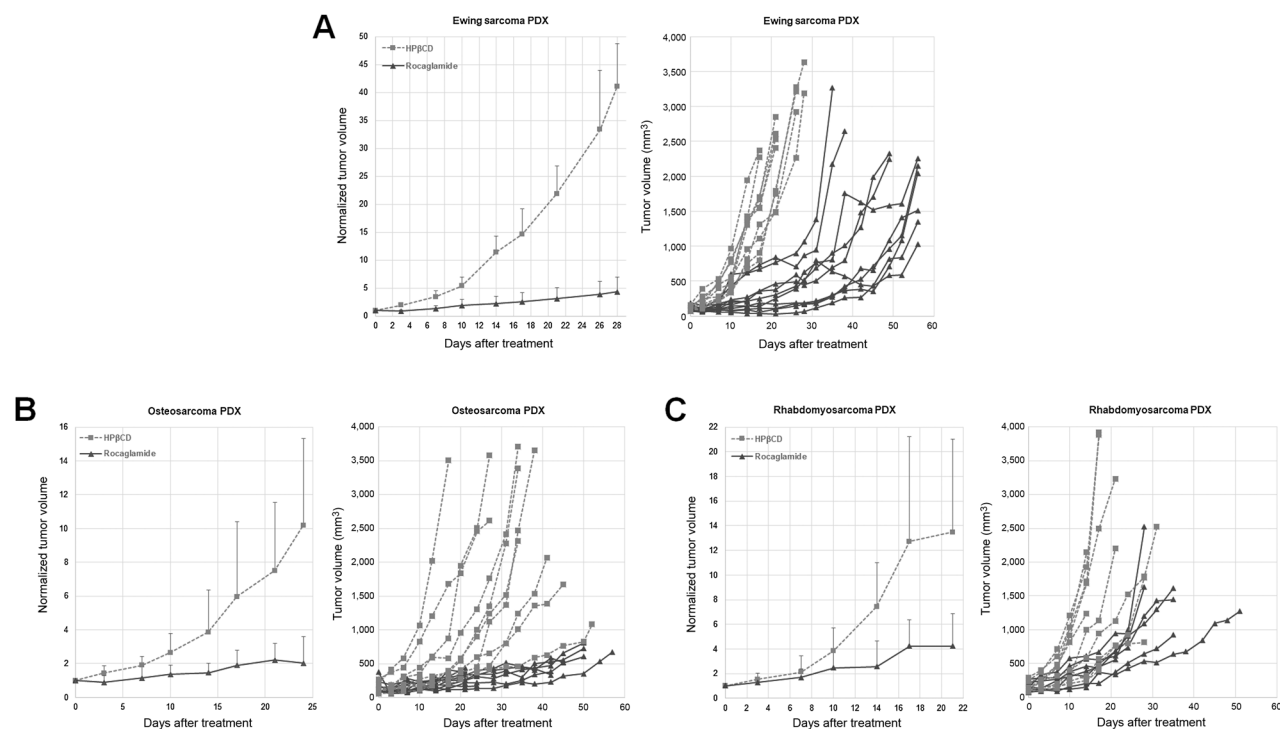


Figure 5.

Roc exhibits potent antitumor effects in multiple sarcoma PDX models. Mice with growing Ewing sarcoma (A), osteosarcoma (B), and rhabdomyosarcoma (C) PDXs were treated with 3 mg/kg of Roc or HP β CD vehicle by i.p. every other day. Tumor diameters were measured twice weekly, and volumes calculated according to Materials and Methods. The normalized tumor volume, denoted as the ratio of the calculated tumor volume after treatment relative to the volume prior to treatment designated as one, was plotted as the mean tumor volume of the entire treatment group at each time point with SD (left panels). The calculated tumor volume for each individual mouse over time was also plotted (right panels).

Chang et al.

vehicle-treated mice, particularly for the Ewing sarcoma and osteosarcoma PDX models (Fig. 5). Together with the findings from the MPNST model, these results demonstrate that Roc displays significant antitumor effects against multiple types of sarcoma.

Rocaglamides decrease multiple signaling kinases and transcription factors important for sarcoma cell growth

To further examine the molecular mechanisms underlying the antiproliferative effects of rocaglamides, we treated TC32 Ewing sarcoma, 143B osteosarcoma, and RD rhabdomyosarcoma cells with one- or two- IC_{50} dose of DDR or Roc for 1 to 2 days followed by Western blotting for several known drivers of cell survival and proliferation. Interestingly, we found that these rocaglamides reliably reduced the levels of the β subunit of IGF-1R, an upstream activator of PI3K-AKT signaling, in all three sarcoma cell lines (Fig. 6A-C). We also observed reduction of the IGF-1R β levels in Roc-treated MPNST cells (Supplementary Fig. S7). In addition, both rocaglamides decreased the levels of AKT, ERKs, cyclin D1 and survivin in treated TC32, 143B, and RD cells (Fig. 6). Intriguingly, the oncogenic fusion protein EWS-FLI1, which acts as an aberrant transcription factor in Ewing sarcoma (35), was not affected in Roc- and DDR-treated TC32 Ewing sarcoma cells (Fig. 6A). Consistent with this observation, these rocaglamides did not inhibit EWS expression in 143B osteosarcoma and RD rhabdomyosarcoma cells (Fig. 6B and C). However, the levels of lysine demethylase 1 (LSD1), which modulates EWS-FLI1 transcriptional activity (36), and NKX2.2, an EWS-FLI1-regulated gene necessary for oncogenic transformation (37), were diminished by these rocaglamides in TC32 cells (Fig. 6A). Collectively, these results suggest that rocaglamides potently suppress sarcoma growth by decreasing multiple key signaling proteins important for tumor growth and survival.

Comparative toxicology studies in canines show that Roc does not induce pulmonary toxicity found with silvestrol

As the next part of the standard process for developing compounds as candidates for human evaluation, a toxicology study in dogs was conducted through a contractor of the NCI Experimental Therapeutics program. Unexpectedly, silvestrol was found to cause massive lung damage, whereas Roc did not produce adverse pulmonary findings when tested on the same protocol at the same lab. Further details are contained in the online summary reports for both silvestrol and Roc at https://dtp.cancer.gov/publications/silvestrol_rocaglamide_studies.pdf.

Discussion

For decades, treatments for MPNSTs and other sarcomas have remained largely unchanged with current standard of care combining surgical resection with intensive multiagent chemotherapy (1, 34, 38, 39). Radiation may be used depending upon the tumor type and clinical presentation. Although this multidisciplinary treatment strategy may help local control, it is not effective for metastatic and recurrent disease. Also, these multimodal regimens are associated with considerable acute and long-term toxicities that affect patients' quality of life. Despite recent advances in understanding tumor biology and targeted therapy development, an FDA-approved medical therapy for the treatment of these malignancies is still not available. We previously showed that eIF4A is a vulnerable point of disruption in MPNSTs and that the eIF4A inhibitor silvestrol potently suppresses MPNST growth (16). Regrettably, silvestrol exhibited an unexpected

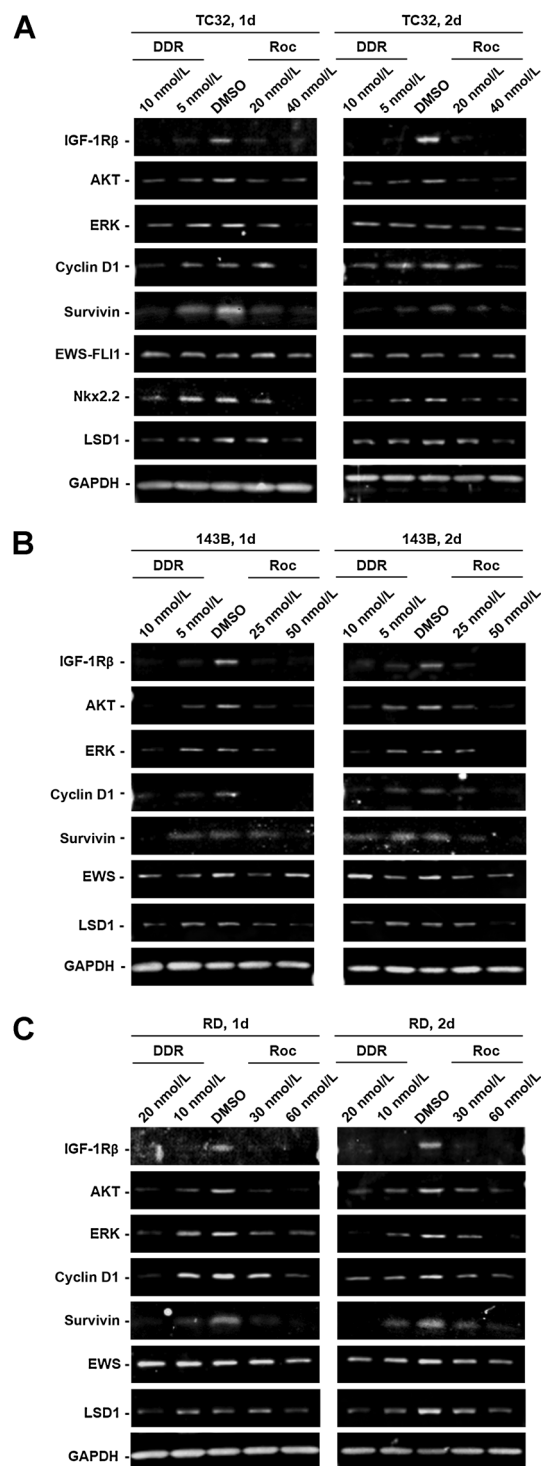


Figure 6.

DDR and Roc reduce multiple signaling proteins important for sarcoma cell growth and survival. Protein lysates from TC32 Ewing sarcoma (A), 143B osteosarcoma (B), and RD rhabdomyosarcoma (C) cells treated for 1 and 2 days with the indicated concentrations of DDR or Roc were analyzed by Western blotting for various oncogenic driver proteins. GAPDH was used as a loading control.

Rocaglamide and Didesmethylocaglamide for Sarcoma Treatment

pulmonary toxicity in dogs, and its further development as a cancer therapy was suspended (D.M. Lucas, M.A. Phelps, A.D. Kinghorn, M. Grever; in preparation). We have identified two rocaglates lacking the dioxanyl ring, Roc and DDR, with better drug-like properties than silvestrol and possessing antitumor efficacy in multiple sarcoma models, including MPNST. Most critically, Roc did not induce the toxicity found in dogs with silvestrol under the same conditions.

Our side-by-side comparison of ten rocaglates lacking the bulky dioxanyl ring present in silvestrol has allowed us to discern certain structure-activity relationships, particularly the C-8b, C-2, and C-6 positions along the cyclopenta[*b*]benzofuran core. Consistent with previous reports (22, 40), the hydroxy group at the C-8b position is essential for antiproliferative activity. This finding is consistent with the crystal structure of Roc complexed with eIF4A and polypurine RNA, which reveals hydrogen bonding between the 8b-OH of Roc and a guanine base in the RNA (41). Also, the phenyl rings A and B of Roc parallel stack with RNA bases, which may explain our finding that adding a methylenedioxy group to ring B modestly improved the growth-inhibitory activity of rocaglates with methylated 8b-OH (Fig. 1). It is possible that this methylenedioxy ring may enhance the affinity of the rocaglates to the eIF4A-RNA complex, partially compensating for the loss of 8b hydrogen bonding.

Among the rocaglates lacking the dioxanyl ring that we evaluated, DDR was the most potent, suggestive of the importance of having a simple primary amide group at the C-2 position. Although the presence of a dioxanyl ring instead of a methoxy group at the C-6 position enhances the potency of silvestrol compared with methyl rocaglate (22, 42), our data indicated that this ring is not required for cytotoxicity. However, it appears to play an important role in MDR1-induced resistance as Roc and DDR are no longer susceptible to this inhibitory effect. Consistent with this notion, we detected a higher level of MDR1 in ST8814 MPNST cells than that in STS26T cells (Supplementary Fig. S4), whereas the IC₅₀ values of Roc and DDR in ST8814 cells were similar to those in STS26T cells (Table 1; Supplementary Fig. S1). The MDR1 transporter binds to silvestrol and is thought to limit its oral bioavailability (29). Our PK analysis demonstrating 50% oral bioavailability of Roc, a >25-fold improvement over silvestrol, confirms this prediction and strongly suggests a possible interaction of MDR1 with the dioxanyl moiety. The observed oral bioavailability of Roc allows a greater flexibility for dosing. More importantly, we found that Roc, when administered i.p. or p.o., showed potent antitumor effects in an orthotopic MPNST CDX mouse model and effectively suppressed the growth of PDX models for Ewing sarcoma, osteosarcoma, and rhabdomyosarcoma.

Like silvestrol, rocaglamides exert their potent growth-inhibitory and antitumor activities mainly through inhibition of eIF4A and protein translation (43, 44). Consistently, we observed that Roc and DDR decreased the levels of multiple signaling proteins important for tumor growth and survival, leading to G₂-M cell-cycle arrest and activation of executioner caspases. In addition to AKT and ERKs, rocaglamides reduced the levels of IGF-1R in all sarcoma cell lines tested. This decrease in IGF-1R expression, coupled with the simultaneous inhibition of AKT and ERKs, likely results in superior inhibition of IGF-1 signaling compared with the simple blockade at the receptor level. Our results further suggest that IGF-1R may serve as a biomarker for responsiveness to rocaglamides in sarcomas.

It should be noted that the effects of translation inhibition mediated by eIF4A are different from those by eIF4E, which can be activated by

the AKT/mTOR pathway, a commonly deregulated event in sarcomas (18). The mTOR inhibitor, rapamycin and its analogs, and mTOR kinase inhibitors only cause cytostatic effects and tumor stabilization (45). Also, blocking mTOR signaling is associated with activation of bypass signaling pathways that can restore critical survival signals, enabling tumor regrowth. Inhibition of eIF4E tends to decrease translation of the mRNAs with 5' terminal oligopyrimidine tracts, which encode ribosomal proteins, elongation factors, lysosomal-related and metabolic-related proteins. However, the eIF4A activity is more critical in unwinding the mRNAs with long 5'-UTRs that can form G-quadruplexes, such as *AKT* and *IGF-1R* (15, 20). In addition, some transcripts, e.g., *c-MYC*, are translated from internal ribosomal entry sites that do not require the cap binder eIF4E and are insensitive to eIF4E inhibition (46). Thus, blocking eIF4A may have a stronger effect on tumor growth and survival.

Ewing sarcoma is frequently driven by the chimeric fusion oncogene *EWS-FLI1* due to a chromosomal translocation that fuses an RNA-binding protein, EWSR1, with the FLI1 transcription factor (35). Surprisingly, we found that the levels of *EWS-FLI1* remained unchanged in Roc-treated Ewing sarcoma cells (Fig. 6A). As a ubiquitously expressed protein, the EWSR1 levels were also not affected in other types of sarcoma cells treated with rocaglamides (Fig. 6B and C). In contrast, the levels of the epigenetic modulator LSD1, a protein needed for optimal activity of the *EWS-FLI1* transcriptional complex (36), and a key *EWS-FLI1* downstream target *NKX2.2*, a homeobox transcription factor implicated in development (37), were diminished by DDR and Roc treatment (Fig. 6). Upon inspection of these genes, we noted that the *EWSR1* transcript has a very short 5'-UTR, whereas the mRNAs for *NKX2.2* and *LSD1/KDM1A* contain longer G+C-rich 5'-UTRs. Therefore, we hypothesize that the *NKX2.2* and *LSD1/KDM1A* transcripts are eIF4A-dependent.

Intriguingly, prior to caspase activation, Roc-treated MPNST cells exhibited increased γ H2A.X, suggesting that DNA damage may be a key underlying cause of the apoptosis seen at later time points. Rocaglamides may affect prohibitin-mediated ERK activation, cause the disruption of mitochondrial integrity, and/or promote the generation of reactive oxygen species (47, 48). Alternatively, they may affect translation of the proteins responsible for DNA replication and repair, resulting in stalled replication forks or inadequate repair of DNA damage. We are presently examining these possibilities.

Roc was the first member of the cyclopenta[*b*]benzofuran class identified as a novel antileukemic agent from *Aglaia elliptifolia* by King and colleagues (49). It is worth mentioning that the structures of Roc and DDR are simpler than silvestrol; therefore, they should be more amenable to chemical synthesis (50). As DDR exhibited higher *in vitro* potency against various types of sarcoma cells than Roc, we anticipate that DDR will have superior antitumor efficacy. Experiments are in progress to compare these rocaglamides in various sarcoma animal models.

In summary, we have demonstrated that Roc and DDR, as eIF4A inhibitors, simultaneously suppressed multiple growth-promoting signaling pathways and induced apoptosis in tumor cells. Roc was no longer sensitive to MDR1 inhibition. It was orally bioavailable and exhibited potent antitumor effects in multiple sarcoma models with no overt toxicity. These promising results indicate that these rocaglamides merit further investigation as treatments for patients with MPNSTs and other sarcomas.

Disclosure of Potential Conflicts of Interest

No potential conflicts of interest were disclosed.

Chang et al.

Authors' Contributions

Conception and design: L.-S. Chang, J.L. Oblinger, S.S. Burns, J.M. Collins

Development of methodology: L.-S. Chang, J.L. Oblinger, S.S. Burns, J. Huang, L.W. Anderson, R.D. Roberts

Acquisition of data (provided animals, acquired and managed patients, provided facilities, etc.): L.-S. Chang, J.L. Oblinger, S.S. Burns, J. Huang, L.W. Anderson, M.G. Hollingshead, R. Shen, G. Agarwal, R.D. Roberts

Analysis and interpretation of data (e.g., statistical analysis, biostatistics, computational analysis): L.-S. Chang, J.L. Oblinger, S.S. Burns, L.W. Anderson, M.G. Hollingshead, R. Shen, R.D. Roberts, J.M. Collins

Writing, review, and/or revision of the manuscript: L.-S. Chang, J.L. Oblinger, L.W. Anderson, M.G. Hollingshead, Y. Ren, R.D. Roberts, B.R. O'Keefe, A.D. Kinghorn

Administrative, technical, or material support (i.e., reporting or organizing data, constructing databases): L.-S. Chang, J.L. Oblinger, S.S. Burns, L. Pan, J.M. Collins

Study supervision: L.-S. Chang, B.R. O'Keefe, A.D. Kinghorn, J.M. Collins

Other (isolated and identified the test compounds, rocaglamide, and didesmethylrocaglamide): L. Pan

Acknowledgments

We thank Melissa Sammons of NCH Tumor Core for assistance with PDX models, Eva Majerova for technical help with plasma analysis, John Byrd for 697 and 697-R cells, Stephen Lessnick for Ewing sarcoma cells, and Ruoning Wang for rhabdomyosarcoma cells.

This study was supported by grants from CancerFree KIDS, Sunbeam Foundation, and Department of Defense (W81XWH-16-1-0104 and W81XWH-18-1-0547 to L.-S. Chang), National Cancer Institute (P01CA125066 to A.D. Kinghorn and P30CA16058 to The OSU Comprehensive Cancer Center), and NCI Experimental Therapeutics program (NCI Contract HHSN261200800001 to Leidos Biomedical Research).

The costs of publication of this article were defrayed in part by the payment of page charges. This article must therefore be hereby marked *advertisement* in accordance with 18 U.S.C. Section 1734 solely to indicate this fact.

Received August 19, 2019; revised December 2, 2019; accepted December 13, 2019; published first December 17, 2019.

References

- Kim A, Stewart DR, Reilly KM, Viskochil D, Miettinen MM, Widemann BC. Malignant peripheral nerve sheath tumors state of the science: leveraging clinical and biological insights into effective therapies. *Sarcoma* 2017;2017:7429697.
- Perrone F, Da Riva L, Orsenigo M, Losa M, Jocolle G, Millefanti C, et al. PDGFRA, PDGFRB, EGFR, and downstream signaling activation in malignant peripheral nerve sheath tumor. *Neuro Oncol* 2009;11:725–36.
- Yang J, Ylipää A, Sun Y, Zheng H, Chen K, Nykter M, et al. Genomic and molecular characterization of malignant peripheral nerve sheath tumor identifies the IGF1R pathway as a primary target for treatment. *Clin Cancer Res* 2011;17:7563–73.
- Kim A, Pratilas CA. The promise of signal transduction in genetically driven sarcomas of the nerve. *Exp Neurol* 2018;299(Pt B):317–25.
- De Raedt T, Beert E, Pasmant E, Luscan A, Brems H, Ortonne N, et al. PRC2 loss amplifies Ras-driven transcription and confers sensitivity to BRD4-based therapies. *Nature* 2014;514:247–51.
- Sebti SM, Tkalecic GT, Jani JP. Lovastatin, a cholesterol biosynthesis inhibitor, inhibits the growth of human H-ras oncogene transformed cells in nude mice. *Cancer Commun* 1991;3:141–7.
- Barkan B, Starinsky S, Friedman E, Stein R, Kloog Y. The Ras inhibitor farnesylthiosalicylic acid as a potential therapy for neurofibromatosis type 1. *Clin Cancer Res* 2006;12:5533–42.
- Rao S, Cunningham D, de Gramont A, Scheithauer W, Smakal M, Humblet Y, et al. Phase III double-blind placebo-controlled study of farnesyl transferase inhibitor R115777 in patients with refractory advanced colorectal cancer. *J Clin Oncol* 2004;22:3950–7.
- Cloughesy TF, Wen PY, Robins HI, Chang SM, Groves MD, Fink KL, et al. Phase II trial of tipifarnib in patients with recurrent malignant glioma either receiving or not receiving enzyme-inducing antiepileptic drugs: a North American Brain Tumor Consortium Study. *J Clin Oncol* 2006;24:3651–6.
- Hanrahan EO, Kies MS, Glisson BS, Khuri FR, Feng L, Tran HT, et al. A phase II study of lonafarnib (SCH66336) in patients with chemorefractory, advanced squamous cell carcinoma of the head and neck. *Am J Clin Oncol* 2009;3:274–9.
- Albritton KH, Rankin C, Coffin CM, Ratner N, Budd GT, Schuetz SM, et al. Phase II study of erlotinib in metastatic or unresectable malignant peripheral nerve sheath tumors (MPNST). *J Clin Oncol* 2006;24 Suppl 18:9518.
- Tap WD, Demetri G, Barnette P, Desai J, Kavan P, Tozer R, et al. Phase II study of ganitumab, a fully human anti-type-1 insulin-like growth factor receptor antibody, in patients with metastatic Ewing family tumors or desmoplastic small round cell tumors. *J Clin Oncol* 2012;30:1849–56.
- Maki RG, D'Adamo DR, Keohan ML, Saule M, Schuetz SM, Undevia SD, et al. Phase II study of sorafenib in patients with metastatic or recurrent sarcomas. *J Clin Oncol* 2009;27:3133–40.
- Widemann BC, Meyer CF, Cote GM, Chugh R, Milhem MM, Van Tine BA, et al. SARC016: phase II study of everolimus in combination with bevacizumab in sporadic and neurofibromatosis type 1 (NF1) related refractory malignant peripheral nerve sheath tumors (MPNST). *J Clin Oncol* 2016;34 Suppl 15:11053.
- Malka-Mahieu H, Newman M, Désaubry L, Robert C, Vagner S. Molecular pathways: the eIF4F translation initiation complex—new opportunities for cancer treatment. *Clin Cancer Res* 2017;23:21–5.
- Oblinger JL, Burns SS, Akhmametyeva EM, Huang J, Pan L, Ren Y, et al. Components of the eIF4F complex are potential therapeutic targets for malignant peripheral nerve sheath tumors and vestibular schwannomas. *Neuro-Oncol* 2016;18:1265–77.
- Oblinger JL, Burns SS, Huang J, Pan L, Ren Y, Shen R, et al. Overexpression of eIF4F components in meningiomas and suppression of meningioma cell growth by inhibiting translation initiation. *Exp Neurol* 2018;299(Pt B):299–307.
- Mamane Y, Petroulakis E, LeBacquer O, Sonenberg N. mTOR, translation initiation and cancer. *Oncogene* 2006;25:6416–22.
- Chu J, Cargnello M, Topisirovic I, Pelletier J. Translation initiation factors: reprogramming protein synthesis in cancer. *Trends Cell Biol* 2016;26:918–33.
- Wolfe AL, Singh K, Zhong Y, Drewe P, Rajasekhar VK, Sanghvi VR, et al. RNA G-quadruplexes cause eIF4A-dependent oncogene translation in cancer. *Nature* 2014;513:65–70.
- Pan L, Woodard JL, Lucas DM, Fuchs JR, Kinghorn AD. Rocaglamide, silvestrol, and related bioactive compounds from *Aglaia* species. *Nat Prod Rep* 2014;31:924–31.
- Kinghorn AD, DE Blanco EJ, Lucas DM, Rakotondraibe HL, Orjala J, Soejarto DD, et al. Discovery of anticancer agents of diverse natural origin. *Anticancer Res* 2016;36:5623–37.
- Lucas DM, Edwards RB, Lozanski G, West DA, Shin JD, Vargo MA, et al. The novel plant-derived agent silvestrol has B-cell selective activity in chronic lymphocytic leukemia and acute lymphoblastic leukemia in vitro and in vivo. *Blood* 2009;113:4656–66.
- Kogure T, Kinghorn AD, Yan I, Bolon B, Lucas DM, Grever MR, et al. Therapeutic potential of the translation inhibitor silvestrol in hepatocellular cancer. *PLoS One* 2013;8:e76136.
- Boussemaert L, Malka-Mahieu H, Girault I, Allard D, Hemmingsson O, Tomasic G, et al. eIF4F is a nexus of resistance to anti-BRAF and anti-MEK cancer therapies. *Nature* 2014;513:105–9.
- El Sous M, Khoo ML, Holloway G, Owen D, Scammells PJ, Rizzacasa MA. Total synthesis of (–)-episilvestrol and (–)-silvestrol. *Angew Chem Int Ed Engl* 2007;46:7835–8.
- Gerard B, Cencic R, Pelletier J, Porco JA Jr. Enantioselective synthesis of the complex rocaglate (–)-silvestrol. *Angew Chem Int Ed Engl* 2007;46:7831–4.
- Adams TE, El Sous M, Hawkins BC, Hirner S, Holloway G, Khoo ML, et al. Total synthesis of the potent anticancer *Aglaia* metabolites (–)-silvestrol and (–)-episilvestrol and the active analogue (–)-4'-desmethoxyepisilvestrol. *J Am Chem Soc* 2009;131:1607–16.
- Gupta SV, Sass EJ, Davis ME, Edwards RB, Lozanski G, Heerema NA, et al. Resistance to the translation initiation inhibitor silvestrol is mediated by ABCB1/P-glycoprotein overexpression in acute lymphoblastic leukemia cells. *AAPS J* 2011;13:357–64.
- Saradhi UV, Gupta SV, Chiu M, Wang J, Ling Y, Liu Z, et al. Characterization of silvestrol pharmacokinetics in mice using liquid chromatography-tandem mass spectrometry. *AAPS J* 2011;13:347–56.

Rocaglamide and Didesmethylocaglamide for Sarcoma Treatment

31. Pan L, Acuña UM, Li J, Jena N, Ninh TN, Pannell CM, et al. Bioactive flavaglines and other constituents isolated from *Aglaia perviridis*. *J Nat Prod* 2013;76:394–404.
32. Burns SS, Akhmametyeva EM, Oblinger JL, Bush ML, Huang J, Senner V, et al. Histone deacetylase inhibitor AR-42 differentially affects cell-cycle transit in meningeal and meningioma cells, potently inhibiting NF2-deficient meningioma growth. *Cancer Res* 2013;73:792–803.
33. Burns SS, Chang LS. Generation of noninvasive, quantifiable, orthotopic animal models for NF2-associated schwannoma and meningioma. *Methods Mol Biol* 2016;1427:59–72.
34. Farid M, Demicco EG, Garcia R, Ahn L, Merola PR, Cioffi A, et al. Malignant peripheral nerve sheath tumors. *Oncologist* 2014;19:193–201.
35. Delattre O, Zucman J, Plougastel B, Desmaze C, Melot T, Peter M, et al. Gene fusion with an ETS DNA-binding domain caused by chromosome translocation in human tumours. *Nature* 1992;359:162–5.
36. Sankar S, Bell R, Stephens B, Zhuo R, Sharma S, Bearss DJ, et al. Mechanism and relevance of EWS/FLI-mediated transcriptional repression in Ewing sarcoma. *Oncogene* 2013;32:5089–100.
37. Smith R, Owen LA, Trem DJ, Wong JS, Whangbo JS, Golub TR, et al. Expression profiling of EWS/FLI identifies NKX2.2 as a critical target gene in Ewing's sarcoma. *Cancer Cell* 2006;9:405–16.
38. Brown HK, Schiavone K, Gouin F, Heymann MF, Heymann D. Biology of bone sarcomas and new therapeutic developments. *Calcif Tissue Int* 2018; 102:174–95.
39. Skapek SX, Ferrari A, Gupta AA, Lupo PJ, Butler E, Shipley J, et al. Rhabdomyosarcoma. *Nat Rev Dis Primers* 2019;5:1.
40. Ebada SS, Lajkiewicz N, Porco JA Jr, Li-Weber M, Proksch P. Chemistry and biology of rocaglamides (= flavaglines) and related derivatives from *Aglaia* species (Meliaceae). *Prog Chem Org Nat Prod* 2011;94:1–58.
41. Iwasaki S, Iwasaki W, Takahashi M, Sakamoto A, Watanabe C, Shichino Y, et al. The translation inhibitor rocaglamide targets a bimolecular cavity between eIF4A and polypurine RNA. *Mol Cell* 2019;73:738–48.
42. Kim S, Salim AA, Swanson SM, Kinghorn AD. Potential of cyclopenta[b]benzofurans from *Aglaia* species in cancer chemotherapy. *Anticancer Agents Med Chem* 2006;6:319–45.
43. Cencic R, Carrier M, Galicia-Vázquez G, Bordeleau ME, Sukarieh R, Bourdeau A, et al. Antitumor activity and mechanism of action of the cyclopenta[b]benzofuran, silvestrol. *PLoS One* 2009;4:e5223.
44. Sadlish H, Galicia-Vazquez G, Paris CG, Aust T, Bhullar B, Chang L, et al. Evidence for a functionally relevant rocaglamide binding site on the eIF4A-RNA complex. *ACS Chem Biol* 2013;8:1519–27.
45. D'Abronzio LS, Ghosh PM. eIF4E phosphorylation in prostate cancer. *Neoplasia* 2018;20:563–73.
46. Wiegner A, Uthe FW, Jamieson T, Ruoss Y, Hüttenrauch M, Küspert M, et al. Targeting translation initiation bypasses signaling crosstalk mechanisms that maintain high MYC levels in colorectal cancer. *Cancer Discov* 2015;5:768–81.
47. Polier G, Neumann J, Thuaud F, Ribeiro N, Gelhaus C, Schmidt H, et al. The natural anticancer compounds rocaglamides inhibit the Raf-MEK-ERK pathway by targeting prohibitin 1 and 2. *Chem Biol* 2012;19:1093–104.
48. Callahan KP, Minhajuddin M, Corbett C, Lagadinou ED, Rossi RM, Grose V, et al. Flavaglines target primitive leukemia cells and enhance anti-leukemia drug activity. *Leukemia* 2014;28:1960–8.
49. King ML, Chiang CC, Ling HC, Fujita E, Ochiai M, McPhail AT. X-ray crystal structure of rocaglamide, a novel antileukemic 1H-cyclopenta[b]benzofuran from *Aglaia elliptifolia*. *J Chem Soc, Chem Commun* 1982;20:1150–1.
50. Liu T, Nair SJ, Lescarbeau A, Belani J, Peluso S, Conley J, et al. Synthetic silvestrol analogues as potent and selective protein synthesis inhibitors. *J Med Chem* 2012; 55:8859–78.

Molecular Cancer Therapeutics

Targeting Protein Translation by Rocaglamide and Didesmethylocaglamide to Treat MPNST and Other Sarcomas

Long-Sheng Chang, Janet L. Oblinger, Sarah S. Burns, et al.

Mol Cancer Ther 2020;19:731-741. Published OnlineFirst December 17, 2019.

Updated version Access the most recent version of this article at:
doi:[10.1158/1535-7163.MCT-19-0809](https://doi.org/10.1158/1535-7163.MCT-19-0809)

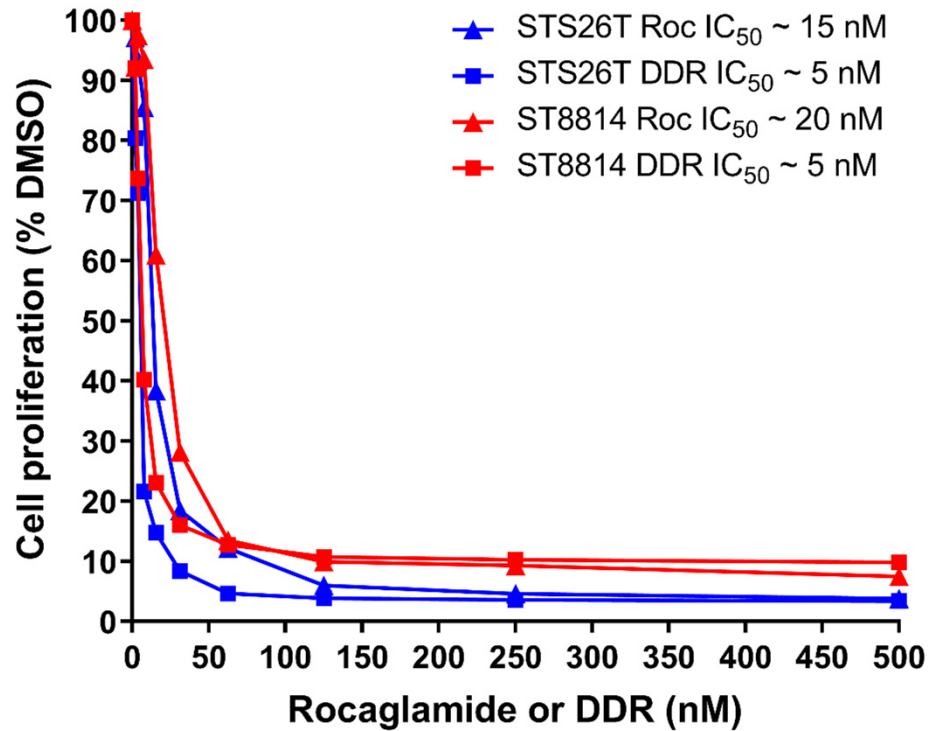
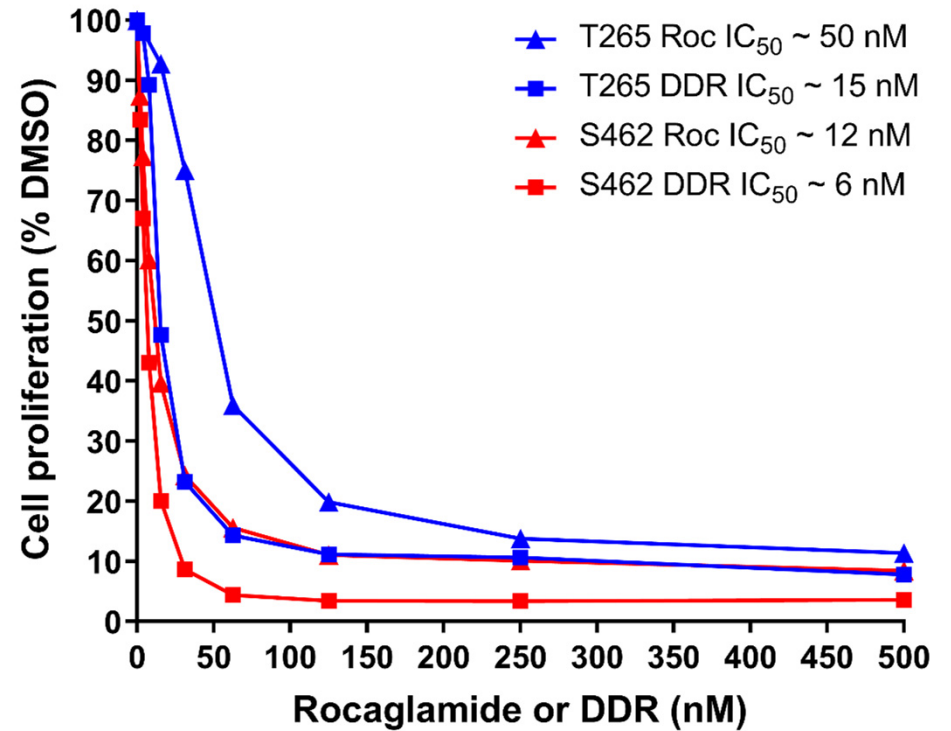
Supplementary Material Access the most recent supplemental material at:
<http://mct.aacrjournals.org/content/suppl/2019/12/17/1535-7163.MCT-19-0809.DC1>

Cited articles This article cites 49 articles, 12 of which you can access for free at:
<http://mct.aacrjournals.org/content/19/3/731.full#ref-list-1>

E-mail alerts [Sign up to receive free email-alerts](#) related to this article or journal.

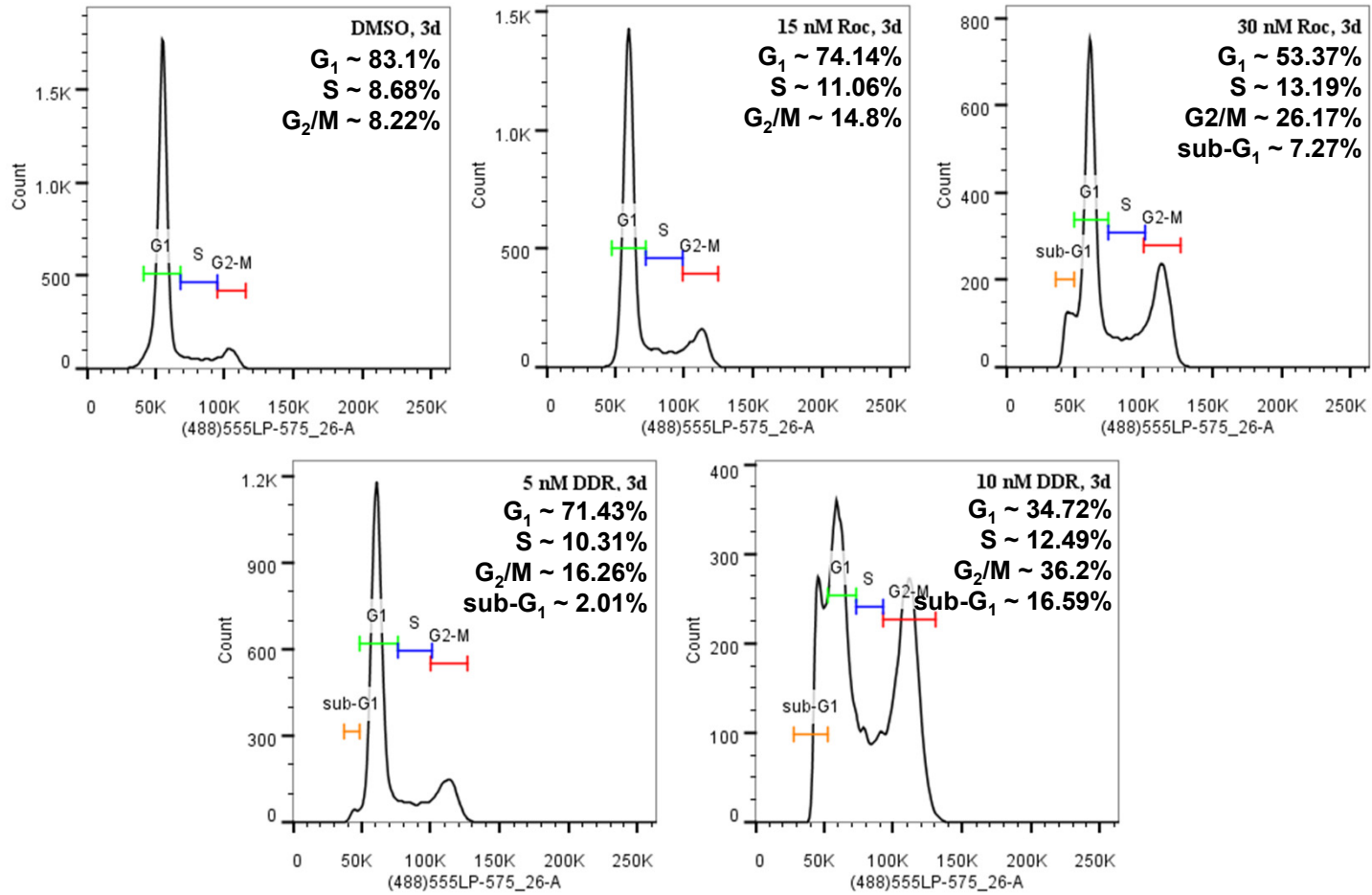
Reprints and Subscriptions To order reprints of this article or to subscribe to the journal, contact the AACR Publications Department at pubs@aacr.org.

Permissions To request permission to re-use all or part of this article, use this link
<http://mct.aacrjournals.org/content/19/3/731>.
Click on "Request Permissions" which will take you to the Copyright Clearance Center's (CCC) Rightslink site.

A**B**

Supplementary Figure S1. Dose-response growth inhibition curves of DDR and Roc in MPNST cells. *NF1*-expressing STS26T (A) and T265 (B) (blue lines) and *NF1*-deficient ST8814 (A) and S462 (B) (red lines) MPNST cells were treated with various concentrations of DDR or Roc, followed by determination of cell proliferation as described in Methods. Experiments were performed in six replicates and were repeated three times. Data shown are the mean of replicates from one representative experiment for each cell line and compound. The graph inset shows the mean IC₅₀ values derived from three independent experiments.

Supplementary Fig. S2A



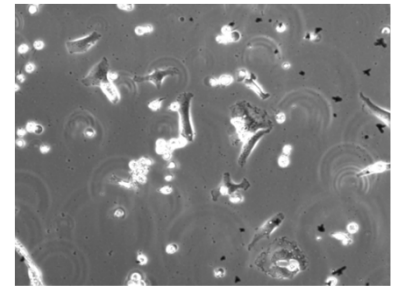
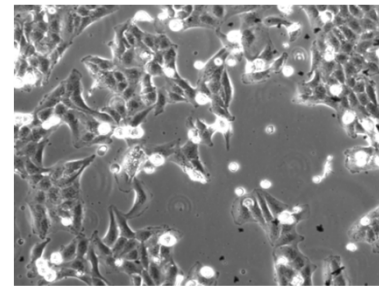
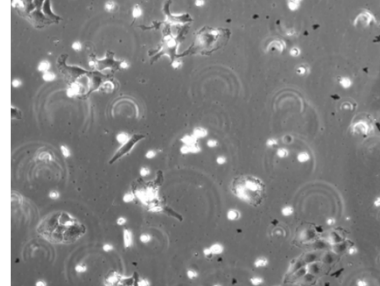
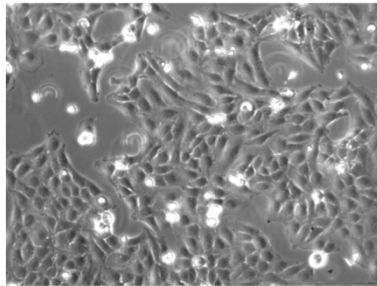
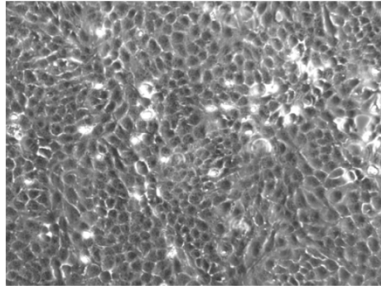
DMSO

15 nM Roc

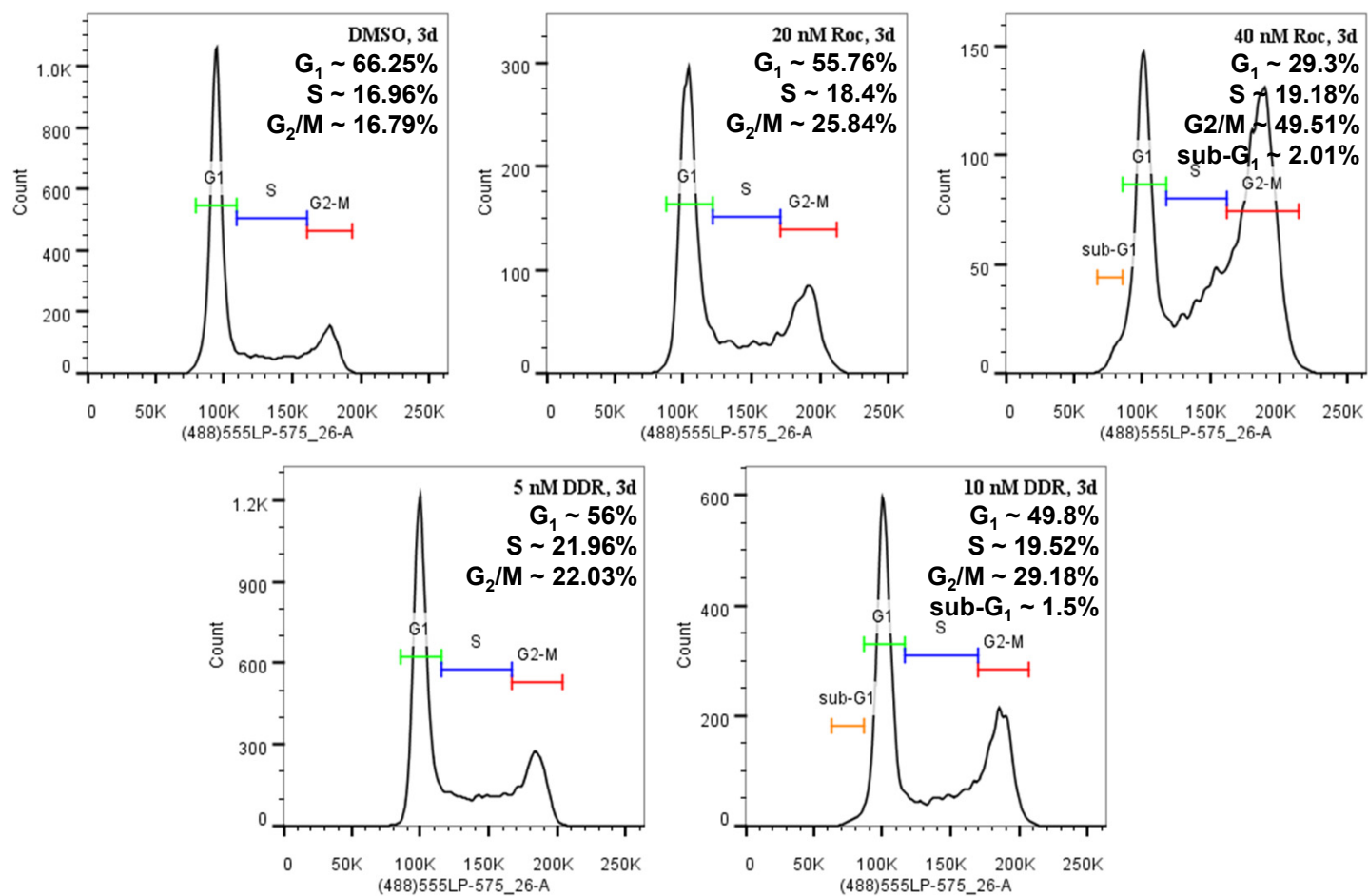
30 nM Roc

5 nM DDR

10 nM DDR



Supplementary Fig. S2B



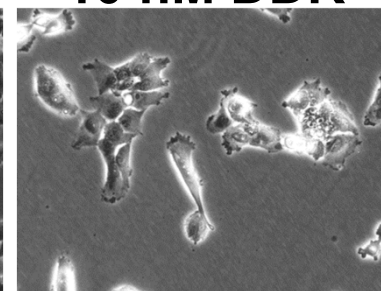
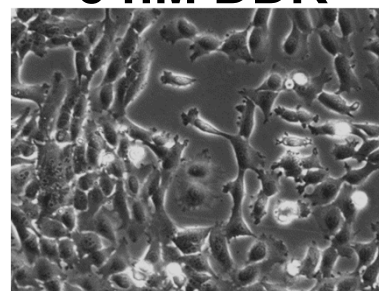
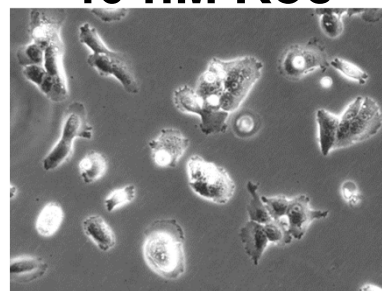
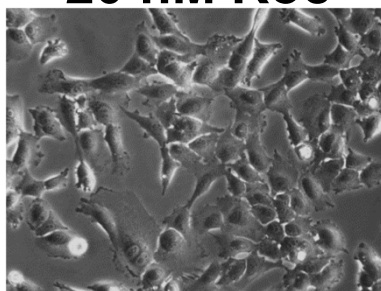
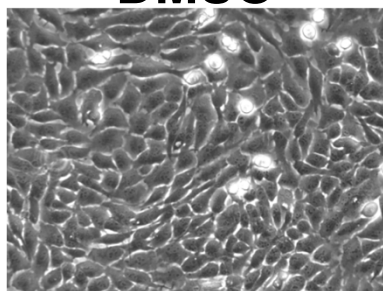
DMSO

20 nM Roc

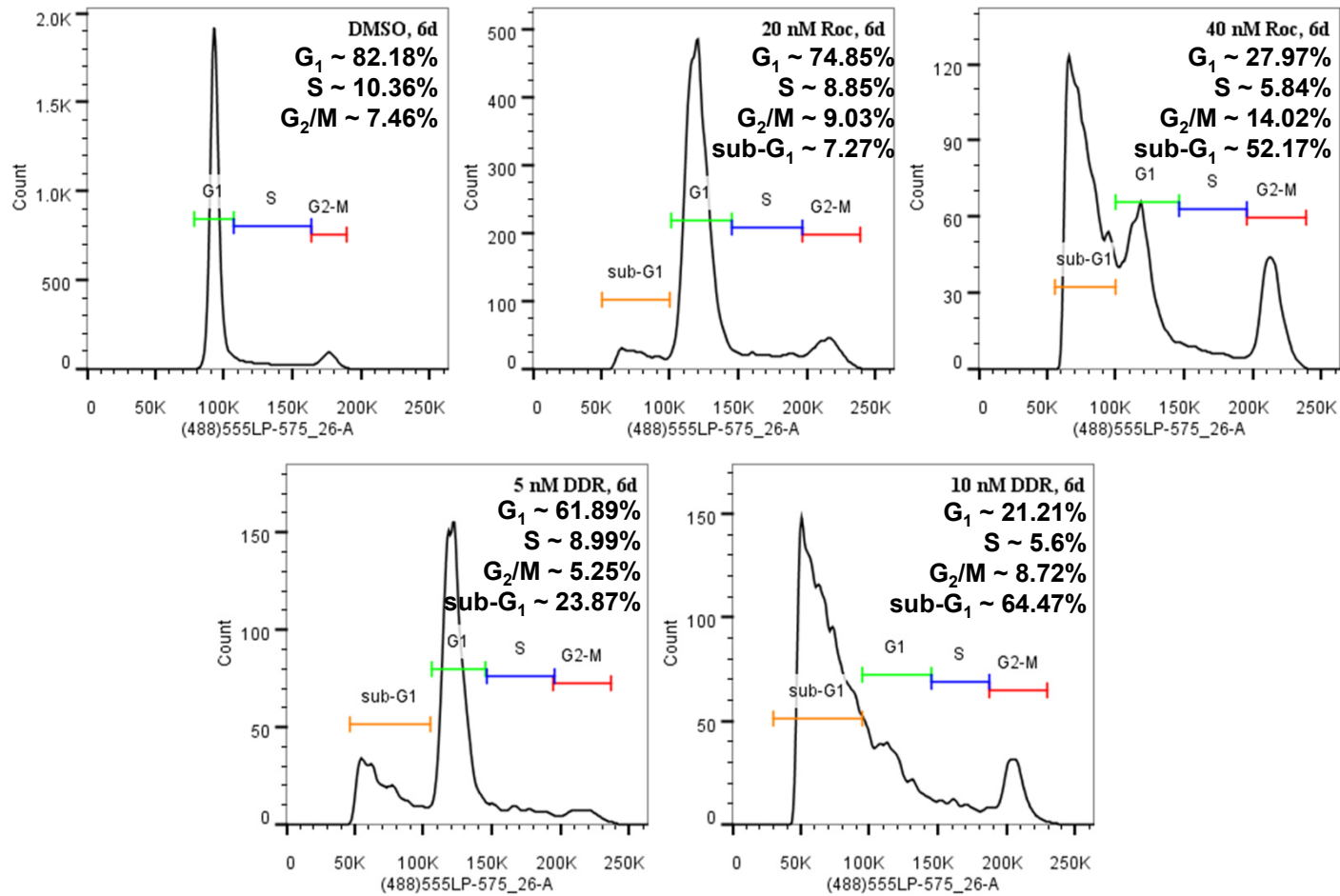
40 nM Roc

5 nM DDR

10 nM DDR



Supplementary Fig. S2C



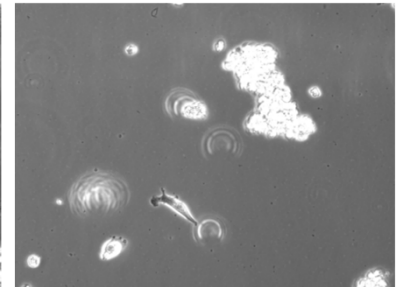
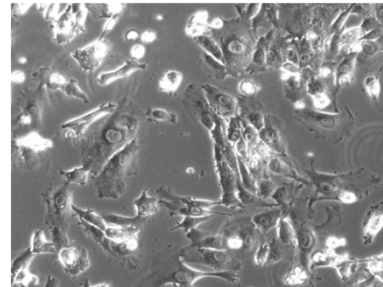
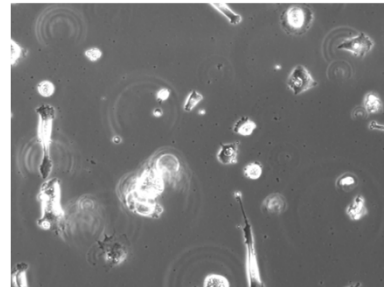
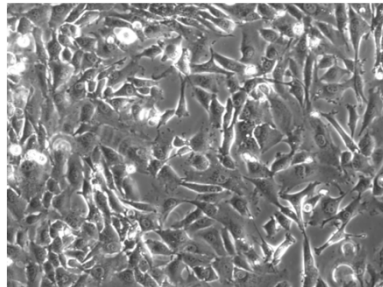
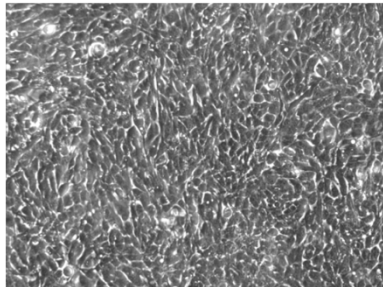
DMSO

20 nM Roc

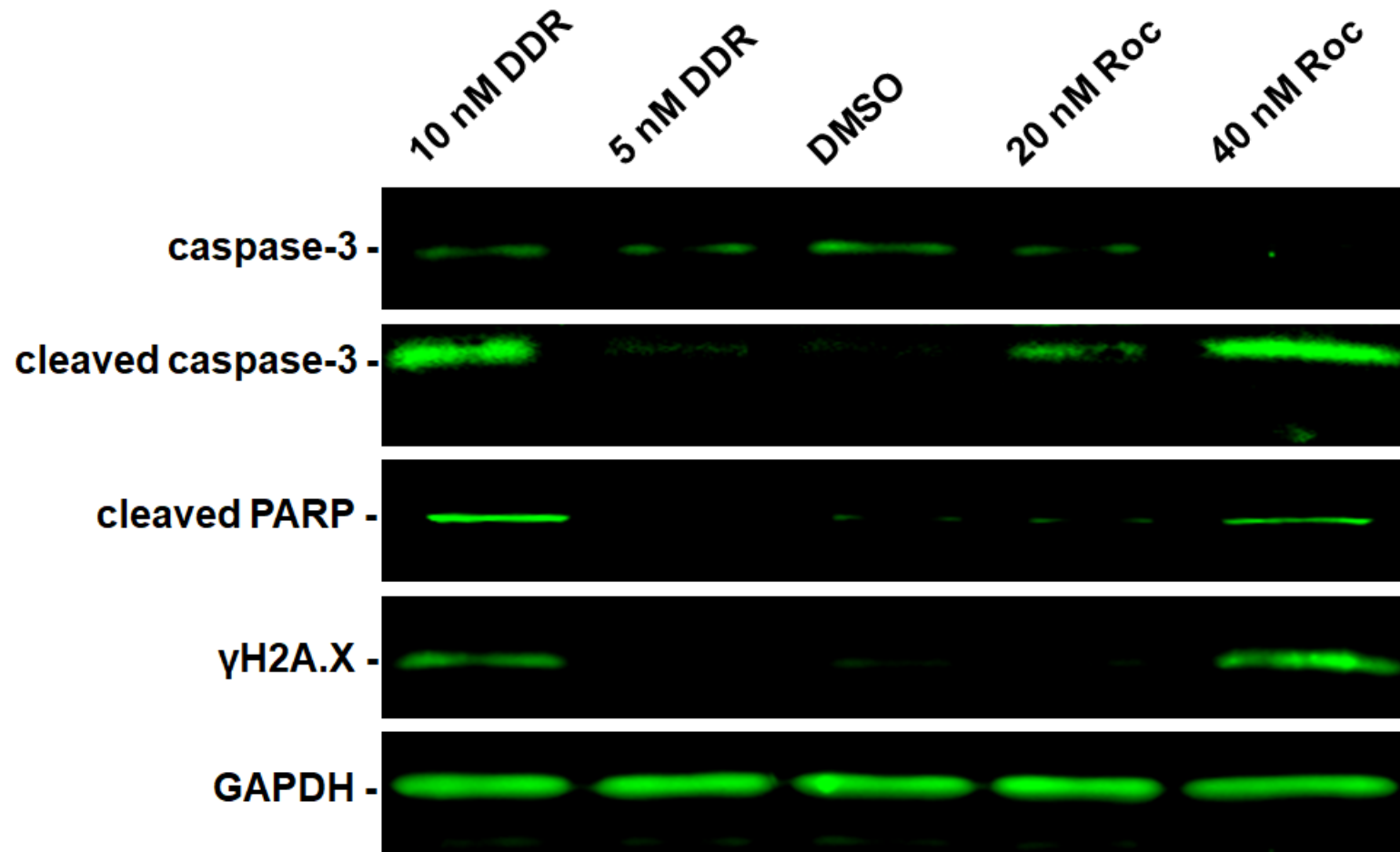
40 nM Roc

5 nM DDR

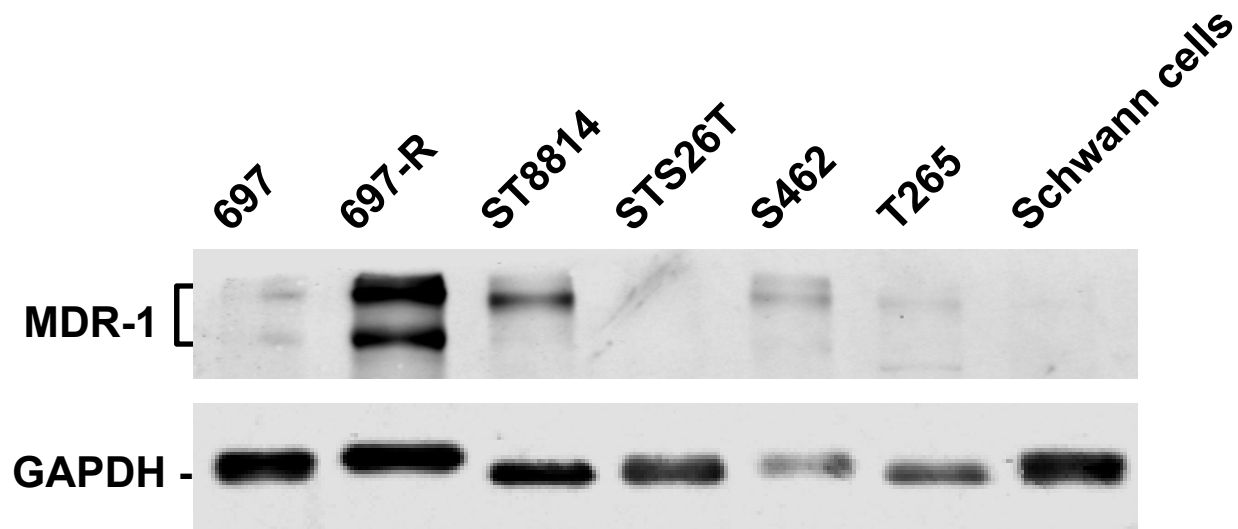
10 nM DDR



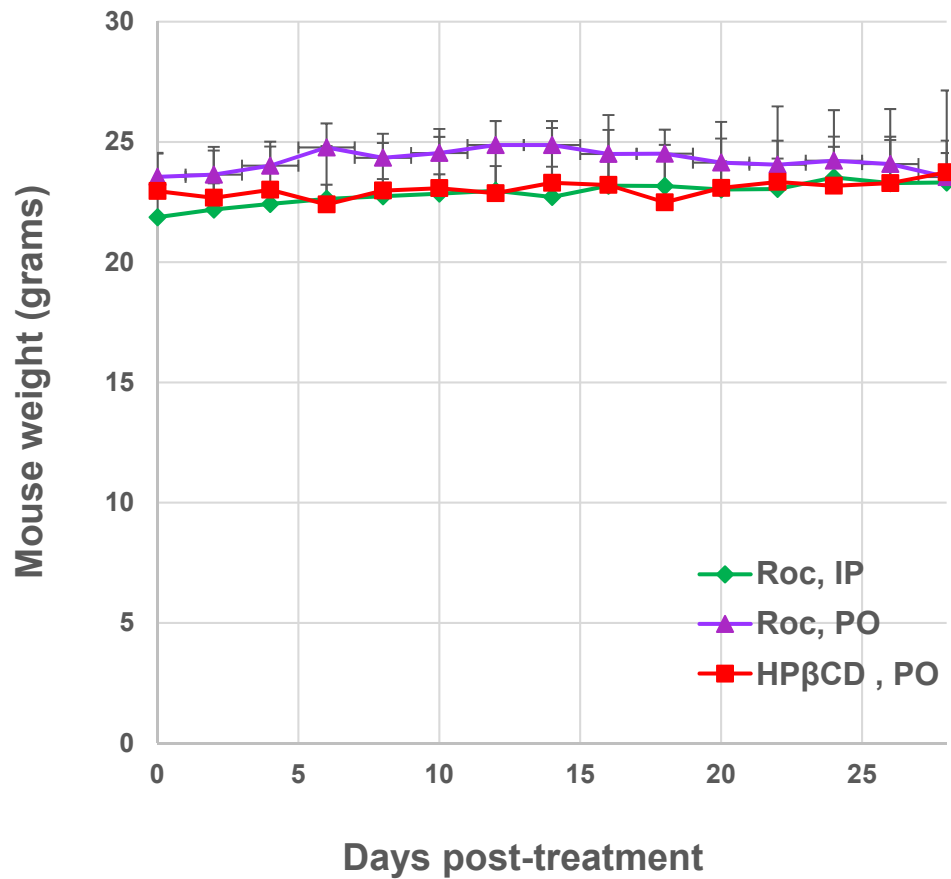
Supplementary Figure S2. DDR and Roc induce G₂/M arrest and increase sub-G₁ fraction in MPNST cells.
(A) STS26T cells were treated with the indicated concentrations of DDR and Roc for three days, and phase-contrast images of treated cells were taken, followed by cell harvesting for flow cytometry analysis as described in Methods. Cell-cycle histograms of propidium iodide-labeled cells revealed a prominent increase in the G₂/M and sub-G₁ peaks after treatment. (B-C) Flow cytometry analysis and phase-contrast images of ST8814 cells treated with DDR or Roc for three (B) or six days (C) were conducted and showed an increased G₂/M fraction in treated cells. Also, a large increase in the sub-G₁ fraction was observed in cells treated for six days.



Supplementary Figure S3. DDR and Roc increase caspase-3 and PARP cleavage and elevate the levels of γH2A.X in *NF1*-deficient ST8814 cells. Protein lysates from ST8814 cells treated for 4 days with 1- or 2-IC₅₀ of DDR or Roc were analyzed by Western blots for full-length and cleaved caspase-3, cleaved PARP, γH2A.X, and GAPDH as a loading control.

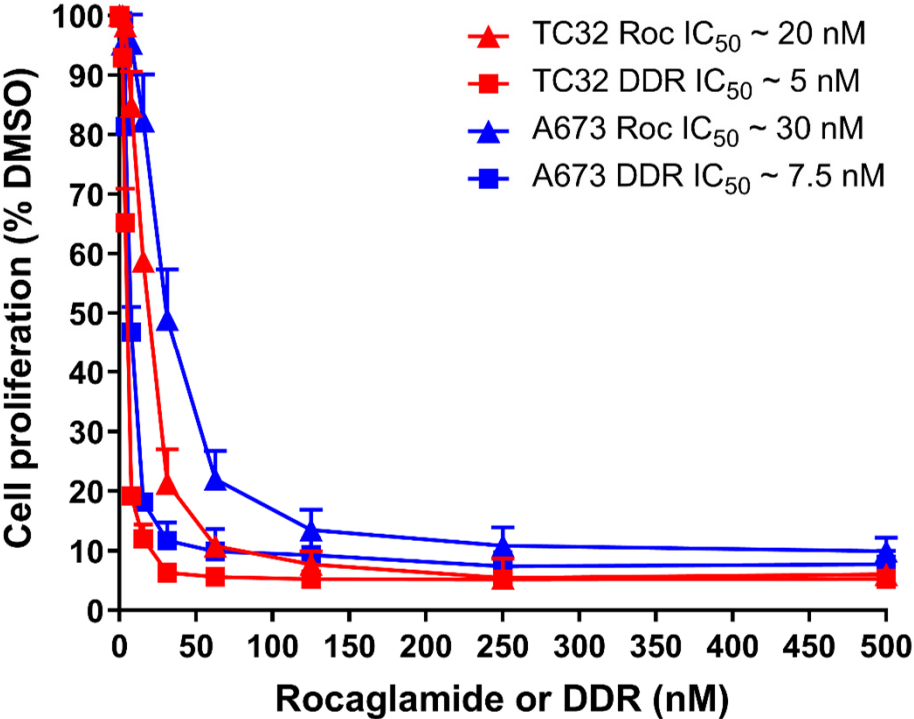


Supplementary Figure S4. Expression of the MDR1/Pgp protein in 697 and 697-R leukemic cells, various MPNST cell lines (ST8814, STS26T, S462, and T265), and primary human Schwann cells. Western blot analysis was conducted as described in Methods. GAPDH was used as a loading control.

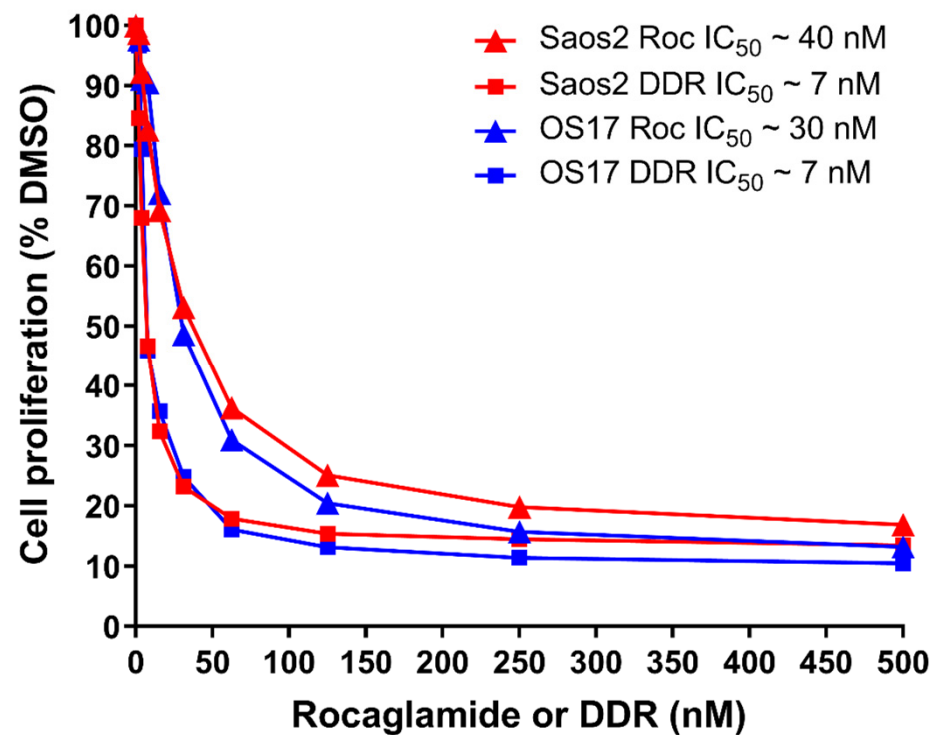
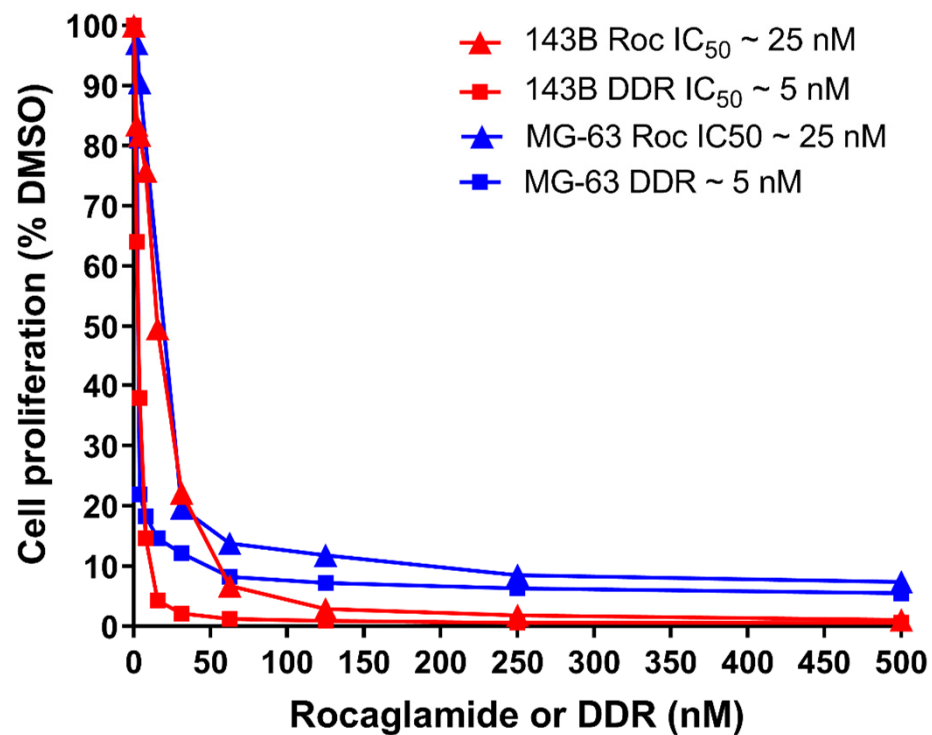


Supplementary Figure S5. Treatment with Roc did not significantly affect body weight, compared with vehicle-treated mice. ST8814-Luc MPNST-bearing NSG mice (n=10/group) were treated with Roc at 4mg/kg by IP, 1.2mg/kg by PO, or HPβCD vehicle every other day for four weeks. Mouse weights were measured every other day. Shown are the mean + standard deviation for each group of mice.

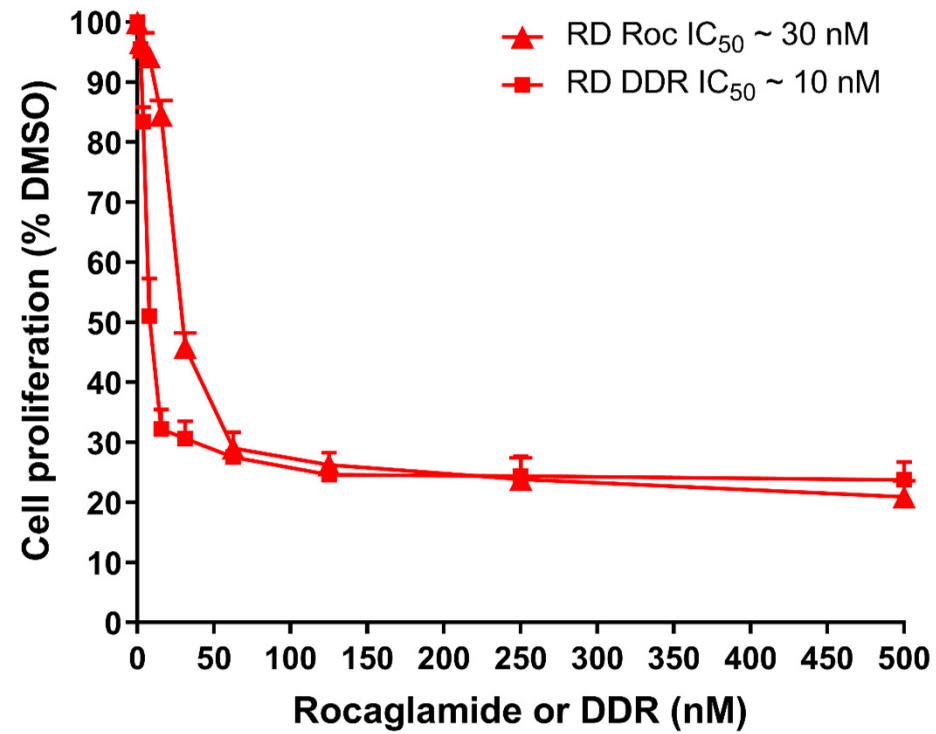
Supplementary Fig. S6A



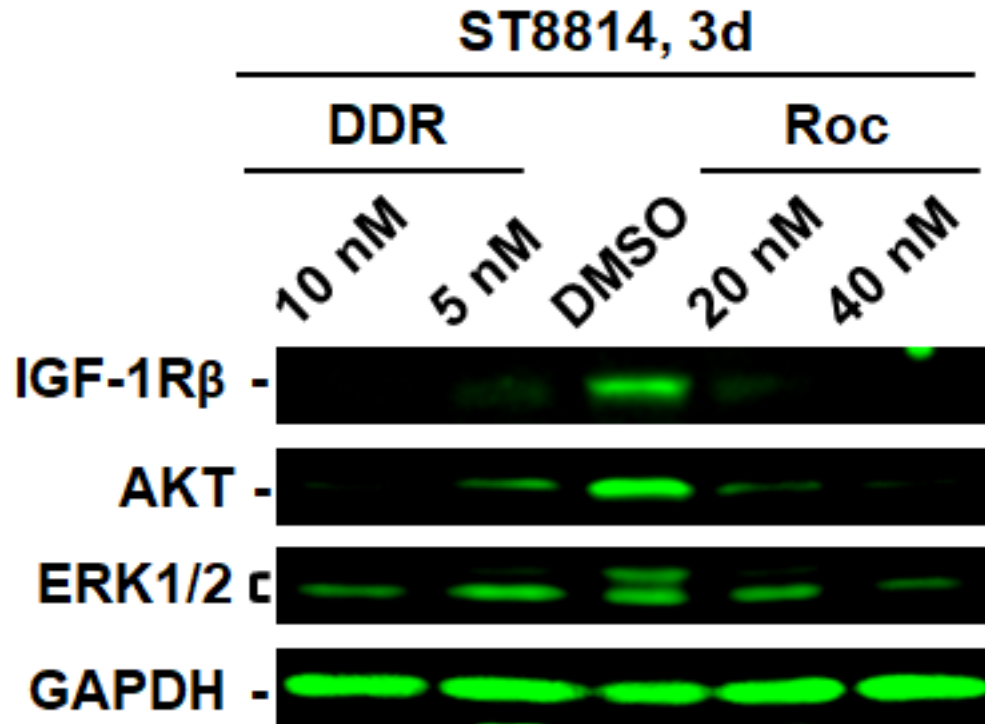
Supplementary Fig. S6B



Supplementary Fig. S6C



Supplementary Figure S6. DDR and Roc possess potent growth inhibitory activities against various Ewing sarcoma, osteosarcoma, and rhabdomyosarcoma cell lines. Cell proliferation assays were performed on the Ewing sarcoma cell lines A673 and TC32 (A), the osteosarcoma cell lines 143B, MG-63, Saos2, and OS17 (B), and the rhabdomyosarcoma cell line RD (C) treated with various concentrations of DDR (squares) or Roc (triangles) according to Methods. Each treatment was conducted in six replicates and the mean of replicates was calculated and used to generate the dose-response growth inhibition curve. Shown are representative curves for each cell line and treatment. The graph insets show the mean IC₅₀ values derived from two independent experiments.



Supplementary Figure S7. DDR and Roc decrease the expression of IGF-1R, AKT and ERKs in MPNST cells. Protein lysates prepared from ST8814 cells treated for 3 days with 1- or 2-IC₅₀ of DDR or Roc were analyzed by Western blots as described in Methods. GAPDH served as a loading control.

Brigatinib causes tumor shrinkage in both *NF2*-deficient meningioma and schwannoma through inhibition of multiple tyrosine kinases but not ALK

Chang, Long-Sheng^{1,*} (Long-Sheng.Chang@nationwidechildrens.org),
Oblinger, Janet L.^{1†} (Janet.Oblinger@nationwidechildrens.org),
Smith, Abbi^{2†} (abbismit@iu.edu),
Ferrer, Marc³ (marc.ferrer@nih.gov),
Angus, Steven P.⁴ (sangus@iu.edu),
Hawley, Eric² (ehawley@iupui.edu)
Petrilli, Alejandra M.⁵ (Alejandra.Petrilli@ucf.edu),
Beauchamp, Roberta L.⁶ (beauch@helix.mgh.harvard.edu),
Riecken, Lars Björn⁷ (lars.riecken@leibniz-fli.de),
Erdin, Serkan⁶ (SERDIN@mgh.harvard.edu),
Poi, Ming⁸ (Ming.Poi@osumc.edu),
Huang, Jie¹ (Jie.Huang@nationwidechildrens.org),
Bessler, Waylan K.² (wbessler@iu.edu),
Xiaohu Zhang³ (xiaohu.zhang@nih.gov),
Rajarshi Guha³ (rajarshi.guha@gmail.com),
Craig Thomas³ (craigt@mail.nih.gov),
Burns, Sarah S.¹ (Sarah.Burns@nationwidechildrens.org),
Gilbert, Thomas S. K.⁴ (tskqilbe@email.unc.edu)
Jiang, Li² (ljiang@iu.edu),
Li, Xiaohong² (xli@iu.edu),
Lu, Qingbo² (qlu@iu.edu),
Yuan, Jin² (jyuan@iu.edu),
He, Yongzheng² (yhe@iu.edu),
Masters, Andrea² (amasters@iu.edu),
Jones, David R.² (drjones1@iupui.edu),
Yates, Charles W.⁹ (cyates3@iuhealth.org),
Haggarty, Stephen J.⁶ (shaggarty@mgh.harvard.edu)
La Rosa, Salvatore¹⁰ (slarosa@ctf.org),
Welling, D. Bradley¹¹ (Brad.Welling@meei.harvard.edu),
Stemmer-Rachamimov, Anat O.¹² (ASTEMMERRACHAMIMOV@mgh.harvard.edu),
Plotkin, Scott R.⁶ (SPLITKIN@partners.org),
Gusella, James F.¹⁴ (gusella@helix.mgh.harvard.edu),
Morrison, Helen⁷ (Helen.Morrison@leibniz-fli.de),
Ramesh, Vijaya⁶ (ramesh@chgr.mgh.harvard.edu),
Fernandez-Valle, Cristina⁵ (cfv@ucf.edu),
Johnson, Gary L.⁴ (gary_johnson@med.unc.edu),
Blakeley, Jaishri O.¹³ (jblakel3@jhmi.edu),
Clapp, D. Wade^{2,*} (dclapp@iu.edu),
on behalf of the Synodos for NF2 Consortium (<http://dx.doi.org/10.7303/syn2343195>)

¹Center for Childhood Cancer & Blood Diseases, The Research Institute at Nationwide Children's Hospital and Department of Pediatrics, The Ohio State University College of Medicine, Columbus, OH 43205, USA;

²Department of Pediatrics, Indiana University, School of Medicine, Indianapolis, IN 46202, USA;

³Division of Preclinical Innovation, National Center for Advancing Translational Sciences, NIH, Bethesda, MD;

⁴University of North Carolina School of Medicine, Chapel Hill, NC 27599, USA;

⁵Burnett School of Biomedical Sciences, College of Medicine, University of Central Florida, Lake Nona-Orlando, FL 32827, USA;

⁶Center for Genomic Medicine, Massachusetts General Hospital and Department of Neurology, Harvard Medical School, Boston, MA 02114, USA;

⁷Leibniz Institute on Aging – Fritz-Lipmann Institute (FLI), Jena 07745, Germany;

⁸Division of Pharmacy Practice and Science, The Ohio State University College of Pharmacy

⁹Department of Otolaryngology & Head/Neck Surgery, Indiana University School of Medicine, Indianapolis, IN 46202;

¹⁰Children’s Tumor Foundation, New York, NY 10017, USA;

¹¹Department of Otolaryngology, Massachusetts Eye and Ear Infirmary, Massachusetts General Hospital and Harvard University, Boston, MA 02114, USA;

¹²Department of Pathology, Massachusetts General Hospital and Harvard Medical School, Boston, MA 02114;

¹³Departments of Neurology, Neurosurgery and Oncology, Johns Hopkins University School of Medicine, Baltimore, MD 21287, USA;

¹⁴Center for Genomic Medicine, Massachusetts General Hospital and Department of Genetics, Blavatnik Institute, Harvard Medical School, Boston, MA 02114;

¶ J. Oblinger, and A. Smith contributed equal effort in this study.

Precis: An unbiased, systems-based approach identified brigatinib as a novel therapy for the treatment of NF2-associated schwannomas and meningiomas.

Running title: Brigatinib for NF2 associated schwannoma and meningioma

Key words: Neurofibromatosis type 2 (NF2), schwannoma, meningioma, brigatinib, receptor tyrosine kinase (RTK), anaplastic lymphoma kinase (1), focal adhesion kinase (FAK)

*Corresponding authors:

Long-Sheng Chang, Center for Childhood Cancer & Blood Diseases, The Research Institute at Nationwide Children’s Hospital, 700 Children’s Drive, Columbus, OH 43205; Phone: 614-355-2658; e-mail: Long-Sheng.Chang@nationwidechildrens.org) and D. Wade Clapp, Department of Pediatrics, Indiana University, School of Medicine, 705 Riley Hospital Drive, Indianapolis, IN 46202; Phone: 317-944-7810; e-mail: dclapp@iu.edu

Disclosure of Potential Conflicts of Interest: No potential conflicts of interest were disclosed.

Word Counts: Abstract (171 words); Statement of Significance (47 words); Text including Abstract, Statement of Significance, Methods, Results, Discussion, and Acknowledgements (4949 words)

Abstract

Neurofibromatosis Type 2 (NF2) is an autosomal dominant genetic syndrome caused by mutations in the *NF2* tumor suppressor gene resulting in multiple schwannomas and meningiomas. There are no FDA approved therapies for these tumors and their relentless progression results in high rates of morbidity and mortality. Through a combination of high throughput screens, preclinical *in vivo* modeling, and evaluation of the kinome *en masse*, we identified actionable drug targets and efficacious experimental therapeutics for the treatment of NF2 related schwannomas and meningiomas. These efforts identified brigatinib (ALUNBRIG®), an FDA-approved inhibitor of multiple tyrosine kinases including ALK, to be a potent inhibitor of tumor growth in established *NF2* deficient xenograft meningiomas and a genetically engineered murine model of spontaneous NF2 schwannomas. Surprisingly, neither meningioma nor schwannoma cells express ALK. Instead, we demonstrate that brigatinib inhibited multiple tyrosine kinases, including EphA2, Fer and focal adhesion kinase 1 (FAK1). These data demonstrate the power of the *de novo* unbiased approach for drug discovery and represents a major step forward in the advancement of therapeutics for the treatment of NF2 related malignancies.

Statement of significance

An unbiased, systems-based approach including high-throughput drug screening of isogenic *NF2*-deficient and -expressing disease-relevant cells showed that the anaplastic lymphoma kinase inhibitor brigatinib shrinks *NF2*-related schwannomas and meningiomas. Surprisingly, ALK was not detected in *NF2* related tumors. Rather,

brigatinib was active through suppression of multiple tyrosine kinases.

Introduction

Neurofibromatosis Type 2 (NF2) is a rare disease in which biallelic loss of the *NF2* gene leads to the development of tumors of neural crest derived origin (2,3). *NF2* encodes the tumor suppressor Merlin, whose biochemical function is incompletely understood (4). Bilateral vestibular schwannomas are pathognomonic for NF2 and the condition is also commonly associated with the development of multiple meningiomas. Further, approximately 90% of sporadic schwannomas and 60% of sporadic meningiomas, the most common intracranial tumor in humans, have inactivation of *NF2* (5,6). There are no approved drug therapies for these common and relentlessly progressive tumors.

In this study, we applied a systems biology approach to: (1) utilize high throughput drug screens to identify FDA approved or late stage development compounds active against Merlin deficient schwannoma and meningioma cells, (2) integrate data from kinome profiling and transcriptome analysis to prioritize targets for future development and (3) utilize a genetically engineered mouse model and tumor xenograft model to establish preliminary preclinical efficacy data for a subset of compounds identified via the *in vitro* drug screening approaches with the goal of identifying at least one drug to move forward to a clinical trial. Using this approach we have identified for the first time, single and combinatorial agents that positively impact the treatment of both schwannomas and meningiomas associated with *NF2*. Importantly, we established the FDA approved, multi-tyrosine kinase inhibitor (TKI), brigatinib, as a potent inhibitor of Merlin-deficient

schwannoma and meningioma growth, both *in vitro* and in preclinical animals models. Interestingly, neither Merlin-deficient schwannoma nor meningioma cells express the primary published target of brigatinib, anaplastic lymphoma kinase (ALK) (1). Rather, we demonstrate that mechanistically, this compound inhibits multiple kinases, including focal adhesion kinase (FAK) previously recognized as an oncoprotein in *NF2* related tumors (7-9). These data demonstrate an effective systems biology approach for preclinical therapeutic discovery applicable to rare tumors and support the advancement of brigatinib, as a multi-TKI into clinical trials for the treatment of *NF2* associated meningiomas and schwannomas.

Results

Discovery of novel drug combinations for *NF2*-associated meningiomas and schwannomas.

To identify novel chemotherapeutic agents for *NF2*-associated tumors, we screened the NCATS MIPE library 4.0 of 1,932 compounds in a high-throughput dose-response format (9) using the isogenic pairs of *NF2*-expressing HS11 and *NF2*-deficient HS01 Schwann cells and *NF2*-expressing Syn1 and *NF2*-null Syn5 arachnoidal cells, as well as *Nf2*^{-/-} mouse MS02 schwannoma cells and human Ben-Men-1 meningioma cells (Syn6). This panel of cell lines was used to assess selectivity of pharmacological responses based on *NF2* status and to distinguish the differences in compound responses between human and mouse *NF2*-related tumor cells to better predict the drug activity in animal models. The MIPE library was initially screened as single agents in dose-response mode, to determine the potency (IC₅₀), efficacy (maximum % inhibition), and area under the curve (AUC) for each compound in each cell line. Active

compounds were selected using dose-response curve analysis algorithms, which assigns each tested compound a Curve Response Class (CRC) number (10). This method classified primary hits into different categories according to their IC_{50} , magnitude of response, quality of curve fitting (r^2), and number of asymptotes. A CRC of -1.1 represents a compound with a complete curve and with high efficacy; a CRC of -1.2 represents a compound with a complete curve but with partial efficacy. Compounds with CRC 4 are inactive. Compounds with CRCs of -1.1, -1.2, and a maximum response of <30% cell viability were considered for further testing in a combination screen. The heat map of the maximal % activity using the hierarchical clustering function in Spotfire Tibco is shown in Figure 1A. The results of this single-agent screen demonstrated that the pharmacological responses clustered cells by tumor type (meningioma versus schwannoma) rather than *NF2*-expressing versus *NF2*-deficient cells. Figure S1 provides a view of the pharmacological responses according to different relevant targets, cellular pathways and mechanisms, based on the AUC parameters which include both potency and efficacy of the compounds. This high-level biological analysis of pharmacological responses confirms that all cell lines tested, independent of Merlin status or tumor type, behaved very similarly and that compounds targeting proteasome, chaperone, topoisomerase, RTK, serine-threonine kinase (STK), phosphatidylinositol 3-kinase (PI3K), and tubulin are the most active (Fig. S1). 62 and 82 compounds were active in all cells by a maximum response criteria of <30% cell viability and CRC of -1.1 and -1.2, respectively. Compounds with CRC -1.1 were hypothesized to be cytotoxic, while compounds that were -1.2 could either be cytostatic or induce senescence and slow cell growth. Targets that were enriched for these active compounds included

inhibitors of histone deacetylase (HDAC), proteasome, Janus kinase 2 (JAK2), tubulin, mammalian target of rapamycin (mTOR), and cyclin-dependent kinase 1 (CDK1), PI3K, and topoisomerase (Fig. 1B and S1).

We then selected 45 compounds to be tested in combination based on: (1) the potency and efficacy in each cell line, (2) the targets in key pathways regulated by Merlin, and (3) mechanisms of interest identified by genome and kinome analyses. These compounds were first tested using the CellTiterGlo assay at 72-h, in 6x6, all versus all dose-response matrices, for a total of 990-pairwise combinations (Fig. 1C), with concentrations customized to include a range > 4 -fold and < 4 -fold the IC_{50} , to better determine possible synergies in both the meningioma (Syn1 vs Syn5) and the schwannoma cell (HSO1 vs HS11) models. Synergistic combinations were ranked based on the Delta Bliss Sum Negative (DBSumNeg) values (11) for each pairwise combination matrix. We detected 33 combinations that had a DBSumNeg value of < -2 in *Nf2*-deficient Syn5 cells, and 69 combinations, which had a DBSumNeg of < -2 in HSO1 cells. A heat map of hierarchical clustering of DBSumNeg for each pairwise compound combination in each cell line showed that meningioma and schwannoma cells each clustered separately by DBSumNeg synergy scores, regardless of *NF2* status as seen in the single agent screen (Fig. 1D).

Next we selected 176 pairwise compound combinations based on DBSumNeg values, synergy selectivity for *NF2*-deficient cells, mechanisms of interest, and clinical interest and tested them in 10x10 dose-response matrix format with the same set of

meningioma and schwannoma cell models using both a cell proliferation readout (CellTiterGlo at 72h) and an apoptosis readout (CaspaseGlo, 20h). Based on differential drug synergy in *NF2*-deficient versus *NF2*-expressing cells, the stage of drug development, and compound performance in prior preclinical and clinical evaluations including pharmacology, response rate, toxicity, and availability, we selected and ranked the top three drug combinations for each *NF2* tumor type. These combinations in meningioma cells included: cabozantinib (an inhibitor of RTKs, including vascular endothelial growth factor receptor 2 [VEGFR2] and hepatocyte growth factor receptor MET)/danusertib (an Aurora kinase inhibitor), dasatinib (an inhibitor of BCR-ABL and SRC-family TKs)/GSK2126458 (a dual PI3K/mTOR inhibitor), and MK-2206 (an AKT inhibitor)/ALK-IN-1 (an inhibitor of ALK and multiple other TKs) (Fig. 2A). The most effective combinations in Schwann cells were slightly different and included: ALK-IN-1/dasatinib, TAE226 (a dual FAK/IGF-1R inhibitor)/dasatinib, and dasatinib/simvastatin (an HMG-CoA reductase inhibitor) for schwannoma (Fig. 2E, S3 and S4).

ALK-IN-1 and its derivative brigatinib synergized with MK-2206 or dasatinib to inhibit *NF2*-deficient meningioma and schwannoma cell proliferation, respectively.

ALK-IN-1 is a chemical analogue of the FDA-approved ALK inhibitor brigatinib (AP26113. ALUNBRIG®) (12). As ALK-IN-1 is no longer in clinical development, we compared brigatinib with ALK-IN-1 for their ability to synergize with MK-2206 or dasatinib to inhibit proliferation of *NF2*-deficient cells. Similar to ALK-IN-1, brigatinib inhibited proliferation of *NF2*-deficient Syn5 arachnoidal and Ben-Men-1 meningioma

cells and two independent primary meningioma cell lines with *NF2* loss (MN612 and MN621). MK-2206 alone showed little growth-inhibitory activity (Fig. 2B and C), however, when combined with brigatinib, MK-2206 exhibited mild synergy in growth inhibition of Ben-Men-1 (Fig. 2D) and Syn5, MN612, and MN621 cells (Fig. S2).

Similarly, as a single agent, brigatinib inhibited proliferation of mouse *Nf2*^{-/-} schwannoma MS02 and human *NF2*-deficient HS01 Schwann cells (Fig. 2G). Mouse MS02 cells appeared more sensitive to brigatinib inhibition than human HS01 cells. As with ALK-IN-1 in the broad screen, brigatinib demonstrated significant synergy with dasatinib in reducing proliferation of both HS01 and MS02 cells (Fig. 2H and S3). Based on these results, we further evaluated brigatinib monotherapy and in combination with either MK-2206 or dasatinib by transcriptome analysis of treated cells and for effects on tumor growth *in vivo*.

Transcriptome analysis of drug-treated *NF2*-expressing and *NF2*-deficient cells

Baseline transcriptome analysis revealed that ALK is not expressed in Syn1/Syn5 arachnoidal and HS01/HS11 Schwann cells, suggesting that brigatinib acts through another target. Consistent with its effect on their growth, brigatinib treatment, with or without MK-2206, elicited an exaggerated response of Syn5 compared to Syn1 cells (Fig. S5A; Table S1), with the shared differentially expressed genes (DEGs) being enriched in DNA replication and cell cycle pathways, but the additional Syn5-specific DEGs being enriched in pathways related to RNA (Table S2A). MK-2206 treatment alone did not result in any DEGs. The number of DEGs elicited by brigatinib or brigatinib + MK-2206 in Syn5 was comparable to the number due to *NF2* inactivation (comparing

untreated Syn5 versus Syn1 cells). The DEGs among the *NF2* expressing Syn1 cells that also responded to drug treatment moved overwhelmingly toward wild-type Syn1 expression (Fig. S6B). Treatment of HS01 and HS11 cells with brigatinib did not significantly disrupt the transcriptome, while treatment with either dasatinib or simvastatin had modest effects (Table S1, Fig. S5C). The combination of brigatinib + dasatinib showed more robust effects, with DEGs in HS01 Schwann cells being enriched most significantly in cytoplasmic pathways, in contrast to the arachnoidal cells (Table S2B).

Kinome profiling in brigatinib- treated cells

Brigatinib is used clinically for the treatment of ALK-positive non small cell lung carcinoma. However, it has multiple additional kinase targets (13). To investigate the protein targets of brigatinib in schwannoma and meningioma cells, we conducted multiplexed kinase inhibitor bead (MIB) kinome profiling experiments. MIBs are a mixture of Type I kinase inhibitors designed to bind kinases when they are in the “Asp-Phe-Gly DFG-in” (active) conformation (14,15). A spectrum of MIBs capable of binding almost all expressed kinases is employed and binding is influenced not only by kinase expression but kinase activity as well. Kinases bound to the MIBs are subsequently identified and quantified via mass spectrometry (15,16). In *NF2*-expressing (Syn1) or *NF2*-deficient (Syn5) arachnoidal cells treated for 24 hours, brigatinib reduced MIB binding of multiple tyrosine kinases including FER, TNK2, and FAK(PTK2) (Fig. 3A and B). Similar target effects were observed with the addition of MK-2206, an allosteric AKT inhibitor, though unique peptides were only detected for AKT3 and in insufficient samples to quantitate (Fig. 3C and D). By adding kinase inhibitors to lysate or briefly

treating cells, the direct target spectrum can be assessed by kinome profiling. This approach has informed our knowledge of polypharmacology for numerous inhibitors in clinical use (17). To address this question, 2 hour incubation of 10 and 100nM brigatinib was performed prior to kinome profiling in an *NF2*-deficient meningioma cell line Ben-Men-1 (Fig. 3E). Brigatinib significantly reduced MIB binding of FER, TNK2, and FAK. In a compatible experiment using lysate prepared from schwannomas from a genetically engineered murine model (GEMM), *Nf2^{flox/flox};Postn-Cre* mice, a MIB competition assay demonstrated FAK and GAK as the primary targets of brigatinib (Fig. 3F and G). Further, kinome profiling from dorsal root ganglia in *Nf2^{flox/flox};Postn-Cre* mice treated for either 3 or 7 days with 50 mg/kg/qd brigatinib monotherapy demonstrated a significant reduction in activated FAK and GAK (Fig. 3G). The target specificity of brigatinib was distinct from dasatinib, which primarily inhibited Src family kinase and Ephrin receptors in HS01 and HS11 cells (Fig. S6B and C). Consistent with the transcriptome analysis, ALK was not detected using MIB kinome profiling methodology in either schwannomas or meningiomas. Collectively, these data identify brigatinib as a direct and potent inhibitor of multiple kinases including FAK in both arachnoid and schwannoma cells.

For validation of the targets identified in the kinome assay and to further probe known targets of brigatinib which were not altered in the kinome data set, a series of immunoblots were conducted on the Ben-Men-1 cell line. ALK expression was not observed in the Ben-Men-1 cells under any growth conditions (Fig. 4A, S7 and S8). When EGF, HRG, or IGF-1 were added to the culture media to stimulate EGFR, ErbB3, and IGF-1R respectively, brigatinib potently inhibited the activation of these receptors (Fig. 4B). It is possible that modulation of these known targets of brigatinib was not

observed in the MIB experiments because appropriate stimulatory ligands were not present in those cell culture conditions. At 2 hours and 24 hours post stimulation with 10% or 20% FBS, treatment with brigatinib resulted in a significant reduction in FAK activation (Fig. 4B). Treatment with brigatinib also reduced proliferative signaling as measured by p-ERK, p-AKT, p-S6 (Fig. 4B and S8). Similarly, in Merlin-deficient (*NF2*-deficient) Schwann cells, ALK expression was not detected at baseline and treatment with brigatinib resulted in a reduction in FAK phosphorylation as well as reductions p-ERK, p-AKT, and p-S6 (Fig. 4D and S10). In human Schwann cells treated with shRNA to knockdown expression of Merlin, brigatinib treatment reduced phosphorylation of FAK, ERK, AKT, and S6RP (Fig. 4E). These data validate and recapitulate the mass spectroscopy based findings that brigatinib is a potent inhibitor of FAK in both Merlin-deficient schwannoma and meningioma cell lines *in vitro*.

Brigatinib treatment of meningiomas and schwannomas in murine models of NF2

Patients with NF2 will often suffer from both meningiomas and schwannomas. Given the *in vitro* efficacy and the -omics supported mechanism of action in both tumor cell models, we chose to test brigatinib both alone and in combination with MK-2206 in a tumor xenograft model of meningioma. Mice were first injected with the human *NF2*-deficient Ben-Men-1 meningioma cells and then treated with either 120 mg/kg/qd MK-2206, 50 mg/kg/qd brigatinib, or the combination. Combination therapy increased concentrations of brigatinib in the serum but not in the CNS compared with treatment of brigatinib alone (Fig. 5A and S11). As measured by luminescence engineered into the meningioma cells, brigatinib, both alone and in combination with MK-2206 blocked outgrowth of the xenograft (Fig. 5B, 5C and S12).

To assess whether brigatinib and/or MK-2206 were tumoristatic or tumoricidal, treatment was halted after 14 weeks of therapy. Cessation of treatment was associated with rapid xenograft expansion (Fig. 5D). However, treatment re-initiation resulted in rapid loss of luminescence, indicating that the xenograft was still drug sensitive (Fig. 5D). Immunohistochemistry showed a significant reduction in tumor cell proliferation consistent with luminescence signal and proliferative signaling in treated xenografts. (Fig. 5E).

In parallel *in vivo* studies in schwannomas, *Postn-Cre;Nf2^{flox/flox}* mice were treated for 12 weeks with brigatinib and dasatinib, as single agents and in combination as well as dasatinib in combination with simvastatin, another FDA approved therapeutic which demonstrated synergy with dasatinib in the drug screens (Fig. S4). Mice treated with brigatinib alone received the maximum tolerated dose of 50 mg/kg/qd. Due to *in vivo* toxicity in the preclinical model, the dose of brigatinib in the brigatinib and dasatinib combination was reduced to 15 mg/kg/qd. The combination of the lower dosing and decreased half life of brigatinib in the combination therapy group significantly reduced total drug exposure as measured by AUC (Fig. 6A). Brigatinib alone (50 mg/kg), but not in combination (at 15 mg/kg) with dasatinib protected mice from development of sensorineural hearing loss as assessed by Auditory Brainstem Response (ABR) threshold over the 12 week treatment (Fig. 6B). Brigatinib alone significantly reduced the volume of tumor-bearing dorsal root ganglion (DRG) tissue (Fig. 6C). Finally, tissues from mice treated with brigatinib had some Schwann cell hypercellularity at the end of 12 weeks of treatment, but had far fewer areas of discrete schwannoma when

compared to the other treatment conditions (Fig. 6D). The brigatinib and dasatinib combination therapy also reduced the DRG volume, but by a smaller magnitude.

Discussion

In these studies, we undertook an unbiased, systems based approach to ultimately identify brigatinib as a novel monotherapy for the treatment of *NF2* related schwannomas and meningiomas. This work began with a series of cell based drug screens and utilized the ~2000 compounds contained in the MIPE 4.0 oncology collection. ALK-IN-1 was identified as a potent and selective inhibitor of *NF2*-deficient arachnoid and Schwann cell lines compared with otherwise isogenically matched *NF2/Nf2*-expressing cells. We chose not to pursue ALK-IN-1 directly as a therapeutic because ALK-IN-1 was originally generated as a part of a series of structural analogs which could inhibit ALK. Ultimately therapeutic development of that series of molecules favored a different analog, AP26113, now known as brigatinib. We confirmed that brigatinib had efficacy comparable to ALK-IN-1 in slowing the growth of schwannoma and meningioma cells lines and also exhibited modest *in vitro* synergy in growth inhibition of meningioma cells when combined with MK-2206 (Fig. 2B-D and S2). Hence, brigatinib replaced ALK-IN-1 for the *in vivo* studies.

The reasoning behind relying on an unbiased, systems based screen to identify novel therapeutics for *NF2* was driven in part by our incomplete understanding of the biochemical functions of Merlin which has hampered prior efforts to advance therapeutics for this disease. Indeed, we would not have anticipated a drug known for its ability to inhibit ALK demonstrating preclinical efficacy in either *NF2* associated schwannoma or meningioma. Given this observation, we were surprised that ALK is

not expressed in either tumorigenic cell type (Fig. 4A, S7, S8 and S10). Following up on this unexpected finding, we demonstrated that in our particular cell culture conditions and in the primary tumors *in vivo*, the kinases most inhibited by brigatinib were non-RTKs (FER, PTK2B/FAK2, and PTK2/FAK) and serine/threonine kinases (TNK2, STK33, and GAK). Similarly, the non-RTK PTK2/FAK and the serine-threonine kinases GAK, RPS6KA3/RSK2, and MARK3 were also found to be greatly suppressed in brigatinib-treated schwannoma cells (Fig. 3). Our findings underscore the importance of kinome profiling in disease models of interest to identify potentially relevant but unanticipated drug targets (17).

From the New Drug Application (18) information of ALUNBRIG™ submitted to the FDA, we learned that while brigatinib has an IC₅₀ of ~1 nM against ALK, it potently inhibits at relatively low IC₅₀ values (≤ 10 nM) other RTKs, like ROS1 and FLT3, several non-RTKs, including FER, FES/FPS, FAK/PTK2, and breast tumor kinase/protein tyrosine kinase 6 (BRK/PTK6), as well as the serine/threonine kinases STK22D and checkpoint kinase 2 (CHK2). Brigatinib is also active at IC₅₀ ≤ 100 nM against several RTKs, including the various EGFR-family members, vascular endothelial growth factor receptor 3 (VEGFR3), RET, and IGF-1R, non-RTKs, such as YES and PTK2B/FAK2, and a number of serine/threonine kinases. In addition, it inhibits at >100 nM but at concentrations (e.g., low micromolar) that have been achieved clinically by many other RTKs, including various fibroblast growth factor receptors (FGFRs), several EPH receptors, and non-RTKs. Using a proteome-wide drug screening approach, it was confirmed that brigatinib strongly interacts with ALK, PTK2/FAK, and PTK2B/FAK2 and has a medium affinity to IGF-1R and EGFR (19). These results suggest that the non-

RTKs FAK/PTK2 and FER, which are strongly inhibited by brigatinib in *NF2*-deficient meningioma and schwannoma cells, are important for the growth and survival of these tumors. However, the multiple other targets of brigatinib in signaling pathways linked to Merlin may also impact the therapeutic efficacy of this drug.

It should be emphasized that even though we did not detect changes in the RTKs that are frequently activated in *NF2*-related tumors by MIB/MS, we were able to demonstrate suppression of phosphorylated EGFR, ErbB3, and IGF-1R in cells treated with 1x IC₅₀ concentration of brigatinib under ligand-induced growth conditions (Fig. 3B). At this brigatinib concentration, we also detected inhibition of EphA2, which we previously showed increased expression and activation of this RTK in *NF2*-deficient cells (18). Consequently, activation of all these RTKs and non-RTKs leads to downstream activation of both PI3K-AKT and MEK-ERK signaling (Fig. 3). Collectively, our results suggest that the anti-tumor activity of brigatinib in *NF2* associated schwannoma and meningioma is mediated through blockade of multiple RTKs and non-RTKs.

Consistent with previous reports (13,20), brigatinib and MK-2206 exhibited an overall favorable PK profiles. In the plasma, brigatinib reached an average of 2.2 μ M when given orally (1,311 ng/ml of C_{max} in Fig. S11), which is above the IC₅₀ in Ben-Men-1 cells. Our PK data also showed effective blood-brain penetration and further indicates no drug-drug interaction between brigatinib and MK-2206 (Fig. 5A). These results should guide the dosing regimen for these drugs in a future clinical trial. Importantly, brigatinib monotherapy induced tumor regression in meningioma and its combination with MK-2206 resulted in further tumor shrinkage (Fig. 5B and C). Although meningiomas regrew upon cessation of treatment, these tumors remained responsive to

brigatinib, either alone or in combination with MK-2206 (Fig. 5D). These results suggest that it is possible to have short breaks from treatment while maintaining therapeutic responses to retreatment, particularly after treatment with the brigatinib/MK-2206 combination.

Brigatinib as a single agent was well-tolerated and showed efficacy in the *NF2* GEMM animals. We observed a nearly 40% reduction in average DRG volume after 12 weeks of daily brigatinib treatment, and those mice did not develop detectable sensorineural hearing loss over the course of the study (Fig. 6B). The two combinatorial therapeutics of brigatinib/dasatinib and dasatinib/simvastatin which were identified in the drug screen and tested *in vivo* were also efficacious in reducing schwannoma growth albeit to a lesser extent than what was observed with brigatinib alone at a higher concentration. Of note, significant toxicity was observed in the brigatinib/dasatinib treatment group. Due to toxicity, the dose of brigatinib in the brigatinib/dasatinib combination had to be reduced from 50 mg/kg to 15 mg/kg. The lower dose of brigatinib in the combination therapy group significantly reduced total drug exposure as measured by AUC (Fig. 6A).

Therefore we believe the reduction in efficacy of the brigatinib/dasatinib combination therapy over the brigatinib single agent treatment may be a result of the greater than three fold reduction in brigatinib dosing given to the combination treated mice. The magnitude of the reduction in average DRG volume observed in the Brigatinib treated mice is the largest we have seen for any treatment in the *Postn-Cre;Nf2^{flox/flox}* animals.

Based on the data presented here, brigatinib possesses potent anti-tumor activity against *NF2*-deficient tumors via inhibition of multiple RTKs frequently activated in these tumors as well as blockade of several non-RTKs and serine-threonine kinases, but not

ALK. Given the fact that brigatinib caused tumor shrinkage in both *NF2* associated schwannoma and meningioma, a clinical trial is being planned to evaluate it as a new treatment for patients with *NF2*.

ACKNOWLEDGMENTS

This study was supported by grants from the Children's Tumor Foundation for the Synodos for *NF2* consortium (grants 2014-18-001A to GLJ; 2014-18-001B to JFG; 2014-18-001C to JOB; 2014-18-001D to DWC; 2014-18-001E to DWB; 2014-18-001F to CFV; 2014-18-001G to HM; 2014-18-001H to LSC; 2014-04-008 to JG) and the US Department of Defense (W81XWH-17-NFRP-IIRA to LSC and VR). We sincerely thank Tracy Galloway, mother of a person with *NF2* and acting patient representative on the project, and the management team of the Children's Tumor Foundation for their contribution and support.

Materials and Methods

Compounds and library

The MIPE (Mechanism Interrogation Plates) oncology compound library 4.0 consisting of 745 FDA-approved drugs, 420 Phase I-III investigational agents, and 767 preclinical molecules was screened at the National Center for Advancing Translational Sciences (NCATS), National Institutes of Health. All compounds in the library have been annotated for their known nominal target, representing diverse and redundant

mechanisms of action. Also, the library contains several compounds per target, allowing target-based enrichment analysis of responses; however, most compounds have polypharmacology. See Supplemental Methods for additional details.

Cells and compound screening

A panel of NF2 tumor-relevant cells (Schwann cells for schwannoma and arachnoidal cells for meningioma with *NF2*-expressing or *NF2*-deficient) was previously assembled for systematic drug evaluation (1). In this study, we used the isogenic pairs of *NF2*-expressing HS11 and *NF2*-deficient HS01 Schwann cells and *NF2*-expressing Syn1 and *NF2*-null Syn5 arachnoidal cells (21,22). Also, human *NF2*-deficient meningioma Ben-Men-1, mouse *Postn-Cre; Nf2^{flox/flox}* schwannoma MS02, and primary human meningioma and schwannoma cells were used (23-25). All cells were grown and tested for mycoplasma contamination as previously described (1).

For compound screening, actively-growing HS11 and HS01 Schwann cells and Syn1 and Syn5 arachnoidal cells as well as Ben-Men-1 cells were seeded in white 1536-well plates (Corning, NY) at a density of 750 cells/well using a Multidrop Combi Reagent dispenser with a small pin cassette (ThermoFisher, Fair Lawn, NJ). The next day, cells were treated for 72 hours with 11 two-fold serial dilutions of each compound in the MIPE 4.0 library. Cell viability was measured using CellTiter-Glo (Promega, Madison, WI). The potency (IC₅₀) and efficacy (maximum % inhibition) of each compound in each cell line were calculated as described (10).

In vitro confirmation of compound efficacy and synergism

Meningioma-relevant cells, including Syn1, Syn5, Ben-Men-1, and primary cultures of *NF2*-null meningioma cells, were seeded in 384-well plates and treated the next day with serial dilutions of brigatinib, MK-2206, or the combination of MK-2206 with brigatinib in a 10x10 matrix format. Cells were treated with 0.1% DMSO as the vehicle control. Cell viability was measured after 72 h of treatment using CellTiter-Glo. DRCs were generated using GraphPad Prism 7.0 (www.graphpad.com).

For the schwannoma-relevant cell panel, HS01, HS11, and MS02 cells were seeded in 384-well plates overnight and incubated with various dilutions of ALK-IN-1, brigatinib, dasatinib, or the combination of dasatinib with ALK-IN-1 or brigatinib in the 10x10 matrix format. Cell viability was measured after 60 or 72 h of treatment for mouse MS02 or human HS01 and HS11 cells, respectively, using CellTiter-Fluor (Promega). A similar study to validate the efficacy of dasatinib, simvastatin, and their combination was also conducted.

For both cell types, dose-response measurements were normalized to vehicle controls and dose-response curves were generated. Drug combination synergy was analyzed using the Loewe, Bliss, and HSA models as previously described using the Combenefit software (26).

RNA isolation and transcriptome analysis

RNA was isolated from all meningioma- and schwannoma-relevant cell lines treated in triplicate with single and combination drugs and used to prepare RNA libraries for RNAseq using Illumina HiSeq2000 and 2500 platforms (1). Pairwise-compared, differentially-expressed genes were identified and gene ontology enrichment analysis

for each comparison was conducted as described in Supplementary Methods.

Kinome profiling

Multiplexed kinase inhibitor bead affinity chromatography and mass spectrometry (MIB/MS) was conducted to identify and quantitate the activity of the expressed kinome and their responses to drug treatment as previously described (1,16,27). Lysates prepared from cells treated with the indicated concentrations of each drug or drug combination for various times or from tissues from animals treated with the indicated drugs were prepared and loaded onto the column containing multiple inhibitor-conjugated beads (27). Kinase-bound inhibitor beads were stringently washed, followed by protein purification and trypsin digestion. Liquid chromatography, mass spectrometry, and analysis was essentially as previously described (27). Peptide suspension was separated using an EASY nLC-1000 System with an Easy-Spray C-18 column (Thermo Fisher). Raw files were processed for label-free quantification using MaxQuant LFQ and default parameters with the following modifications—razor plus unique peptides were used, matching between runs, fixed modifications [carbamidomethy (C)] and dynamic modifications [phospho(STY)] (28). Kinase LFQ intensities were used if two or more unique peptides were detected, and missing values were imputed in Perseus if observed in all replicates of another condition prior to log₂ transformation for comparison. Data for each treated sample was plotted as a mean of fold change (log₂) relative to DMSO- or vehicle-treated control or untreated animals. When at least three replicates were available, unpaired Student's t-tests were performed in Perseus with Benjamini-Hochberg correction.

Quantifiable orthotopic meningioma model

The Institutional Animal Care and Use Committee at Nationwide Children's Hospital approved this animal study. Ben-Men-1-LucB cells into the skull base of NSG mice as previously described (23) and monitored for tumor growth by bioluminescence imaging (BLI) every two weeks using a Xenogen IVIS[®] Spectrum imaging system (Perkin Elmer, Bradford, CT). Mice with were randomized into treatment groups, treated by oral gavage, and continued to be assessed by BLI biweekly. See Supplemental Methods for implantation details, drug treatment groups, and BLI quantification.

Schwannoma model and hearing tests

The methodologies of tumor and hearing assessment for the *PostnCre; Nf2^{flox/flox}* mice were used as previously described (29). Drugs were formulated as follows and administered by oral gavage: 50 mg/kg brigatinib dissolved in 90% PEG400 with 10% 1-methyl-2-pyrrolidinone; 20mg/kg dasatinib in pH3.0 citrate buffer; and 100 mg/kg simvastatin in 1% carboxymethylcellulosein water with 0.25% Tween80 and 0.05% antifoam 204 (Sigma).

Figure Legends

Figure 1. Single-agent dose response and matrix HTS of the oncology MIPE 4.0 collection in meningioma and schwannoma cells. (A) Heat map of pharmacological responses (as % cell viability at the maximum dose tested, 46 μ M, also called maximum response) of the MIPE 4.0 library in *NF2*-expressing Syn1 and *NF2*-null Syn5 human

arachnoidal cells, *NF2*-deficient Ben-Men-1 (Syn6) meningioma cells, *NF2*-expressing HS11 and *NF2*-knockdown HS01 human Schwann cells, and *Nf2^{-/-}* MS02 mouse schwannoma cells. Responses were clustered using a Hierarchical Clustering in Spotfire TIBCO. Red indicates low % cell viability and blue is high viability. (B) Target enrichment plots for pan active hits selected by % viability at the maximum concentration of compound tested (MAXR) <30% for both cell lines and all assay modes (top panel) and for pan active hits selected by CRCs -1.1 or -1.2 for both cell lines and all assay modes (bottom). The -log p-values were calculated as follows: given a selection of compounds, the annotated targets for these compounds were identified and the enrichment for each target computed, compared to background, using the Fishers exact test. For this test, the background was defined as all the targets annotated in the MIPE collection. The p-value from the test was adjusted for multiple hypothesis testing using the Benjamini-Hochberg method. A -log p-value >1 was used as a cut-off to consider a target or processed being overrepresented. (C) Number of combinations tested and assays used for the 6x6 and 10x10 matrix combination HTS. Delta bliss 6x6 and 10x10 matrix plots for the combination of MK-2206 and ALK-IN-1 in Syn5 cells, using the CellTiterGlo viability assay. Darker color indicates higher DeltaBliss scores for synergy. (D) Heat map of DeltaBliss Sum Negative for the 990 6x6 all vs. all pairwise combinations of the 45 drugs selected from the single-agent testing. The IC₅₀ and maximum % inhibition of each compound in each indicated cell line were calculated. Responses were clustered using a Hierarchical Clustering in Spotfire TIBCO. Red indicates low % cell viability and blue is high viability.

Figure 2. Like ALK-IN-1, brigatinib exhibited growth-inhibitory synergy with MK-2206 or dasatinib in meningioma and schwannoma cells, respectively. (A) The top synergistic drug combinations identified for *NF2*-deficient meningioma cells. (B) 10x10 dose-viability response matrix of ALK-IN-1 vs MK-2206 in Syn1 and Syn5 cells, assessed at 72h. (C) Single-drug dose-response curves (DRCs) for MK-2206 (left) or brigatinib (27) were generated for human *NF2*-null cell lines, including Syn5, Ben-Men-1, and two primary meningiomas (MN612, MN621). Drug concentrations are outlined under Supplementary Methods. n.d., not determined. Data is expressed as +/- SEM. (D) Combination treatment of Ben-Men-1 cells was carried out in a 10x10 dose-matrix format using the same increasing concentration range of MK-2206 and brigatinib as with single DRCs. Heatmaps were generated on a colorimetric scale using Combenefit software, which calculates the drug interaction effects (relative to vehicle/DMSO control). (E) The top synergistic drug combinations identified for *NF2*-related schwannoma cells. (F) 10x10 dose-viability response matrix of ALK-IN-1 vs dasatinib in HS11 and HS01 cells, assessed at 72h. (G) Brigatinib dose-response in mouse MS02 and human HS01 cells at 60 and 72h, respectively. (H) Loewe and highest single agent (HSA) synergy matrix analysis of brigatinib vs dasatinib in HS01 cells treated for 72h.

Figure 3. MIB/MS kinome profiling reveals brigatinib target specificity in multiple *NF2*-deficient cell models. (A-D) MIB/MS kinome profiling was performed following treatment of Syn1 and Syn5 cells with vehicle (DMSO), brigatinib (1 μ M) or the combination of MK-2206 (0.5 μ M) and brigatinib (1 μ M) for 24h in biological triplicate. MIB binding (log₂LFQ intensities) were used for comparisons and the volcano plots

indicate log₂ difference and significance (5% FDR, indicated by dashed line). (E) MIB/MS kinome profiling was performed following treatment of Ben-Men-1 cells with vehicle (DMSO) or brigatinib (10nM, blue or 100nM, red) for 2h in biological duplicate. The log₂ difference in MIB binding (LFQ intensity) was calculated and plotted relative to vehicle for each replicate. (F) Tumor lysates from the *Postn-Cre;Nf2^{flox/flox}* mouse model were prepared and equal amounts of total protein were incubated for 2h with vehicle (0.001% ethanol) or brigatinib (10nM, blue; 100nM, red; 1000nM, green) in biological duplicate prior to MIB/MS kinome profiling. The log₂ difference in MIB binding (LFQ intensity) was calculated and plotted relative to vehicle for each replicate. (G) *Postn-Cre;Nf2^{flox/flox}* mice were treated with vehicle or brigatinib for 3 or 7 days (gold and blue, respectively, for indicated kinases). Tumors were harvested and subjected to MIB/MS kinome profiling. MIB binding (log₂LFQ intensities) was determined and used for comparisons of brigatinib to vehicle treatment. The volcano plot indicates log₂ difference and significance (5% FDR, indicated by dashed line). (H) HS11 and HS01 cells were treated with vehicle (DMSO) or brigatinib (1μM) for 24h prior to MIB/MS kinome profiling. MIB binding (log₂LFQ intensities) was determined and the top 20 kinases with decreased MIB binding compared to vehicle are shown as a stacked bar plot for the two cell lines.

Figure 4. Brigatinib inhibits multiple RTKs, non-RTKs, and their downstream signals. (A) Western blot analysis was conducted to detect ALK expression in Ben-Men-1 cells grown under various growth conditions and with or without brigatinib treatment. (B) Brigatinib treatment greatly reduced phosphorylation of non-RTKs FER

and FAK, RTKs EPHA2 and ErbB3, and their downstream signaling molecules AKT, ERK1/2, and S6 in active growing Ben-Men-1 cells or growth-arrested cells stimulated with 20% serum. (C) Brigatinib blocked phosphorylation of EGFR, ErbB3, and IGF1R in growth-arrested Ben-Men-1 cells stimulated with each cognate ligand. (D) Brigatinib reduced the levels of p-FAK, p-ERK1/2, p-AKT, p-S6, and p-Gsk in *Nf2* deficient murine Schwann Cells. (E) Brigatinib blocked phosphorylation of FAK, ERK1/2, MEK, AKT, S6RP, and IGR in *NF2* deficient HS01 human Schwann cells.

Figure 5. Brigatinib and its combination with MK-2206 effectively shrank intracranial meningioma xenografts. (A) PK analysis was conducted to determine the concentrations of brigatinib and MK-2206 in mouse plasma and brain. Mice were treated with a single MTD of brigatinib or MK-2206. Prior to and at various times after dosing (n=3 per time point), blood and brain from each dosed mouse were collected for UHPLC-MS/MS analysis according to Supplementary Methods. The mean concentration of each drug at each indicated time point with standard deviation was plotted. Also, mice were treated with a combined dose of brigatinib and MK-2206 at their MTD (n=3), and the drug concentration in the plasma and brain determined (indicated with arrows). (B-C) Mice with established meningioma xenografts were treated with vehicle, brigatinib, MK-2206, or brigatinib+MK-2206 by oral gavage (n=10 each) and tumor growth was monitored by BLI. (B) Shown are representative BL images of tumor-bearing mice acquired prior to (PreTx) and 12 weeks (wks) after treatment. (C) The relative tumor-emitted BL signals were quantified and denoted as % of total flux after treatment relative to the total flux prior to treatment designated as one

(100%). The data are shown as mean \pm standard deviation. At least seven mice from each group completed the entire 12-week treatment. (D) Upon cessation of treatment, tumors in mice that had been treated with brigatinib or brigatinib+MK-2206 for 14 weeks (n=4 each) regrew. However, tumor shrinkage was observed when the treatment was re-initiated. Data shown for mice treated with brigatinib or brigatinib+MK-2206 are only from the cage of mice that had undergone cessation of treatment and retreatment. (E) Representative images of immunostained sections of the heads of tumor-bearing mice after 12-week treatment with vehicle, MK-2206, brigatinib, or MK-2206+brigatinib for Ki67, p-S6, p-ERKs, and cleaved caspase 3 (CC3) expression.

Figure 6. Brigatinib, Dasatinib, Simvastatin and combination treatments in the Schwannoma mouse model. (A) Single-dose pharmacokinetics of compounds in *PostnCre; Nf2^{flox/flox}* mice. Plasma compound concentrations were measured at baseline, 1, 2, 4, 8 and 24 hours after administering a single oral dose to n=3 *PostnCre; Nf2^{flox/flox}* mice. Parameters were calculated using a noncompartmental NCA-xls using PK add ins. (B) Auditory Brainstem Response (ABR) thresholds were measured pre-(baseline) and post-treatment with indicated drugs for 12 weeks. Brigatinib alone showed no significant increase in ABR threshold, indicating hearing was maintained at pre-treatment threshold. One-Way ANOVA with Dunnett's multiple comparison's test; p=0.0001(****), p=0.0004(***) , p<0.005(**). (C) Volume of dorsal root ganglia (DRG) was measured post-mortem. All treatment groups had significantly smaller DRG volume when compared to vehicle, and brigatinib-treated DRGs showed the greatest reduction. One-Way ANOVA with Dunnett's multiple comparison's test; p=0.0001(****),

$p=0.0007(***)$, $p<0.05(*)$. (D) Representative hematoxylin and eosin stained DRGs following 12 weeks of continuous treatment with the indicated drugs.

Supplemental Tables

Supplemental Table S1. Fold-change and significance of differential expression in treated and untreated cells.

Supplemental Table S2. Pathways enriched for differentially expressed genes

Supplemental Figure Legends

Supplemental Figure S1. Cell survival responses to all MIPE 4.0 library agents (as judged by relative AUCs) binned per mechanistic classes with mechanistic superclasses listed in order from top to bottom: transcriptional regulation, physiological homeostasis, other, metabolism, DNA repair, cell surface protein, cell signaling, cell growth, antimicrobial. Solid dots represent the median response for all the compounds, in each mechanistic class, and for each cell line.

Supplemental Figure S2. Single and combination drug treatment of meningioma-related cell lines. Drug treatment of the *NF2*-expressing Syn1(+) and *NF2*-null Syn5(-) cells (A), Ben-Men-1 cells (B), and two primary meningioma cultures MN612 and MN621 (C) was performed using the same drug doses as for Figs. 2C/D. Single drug DRCs and combination drug heatmaps were generated using Combenefit software. Note that heatmap data for Ben-Men-1 (B) is the same as shown in Fig. 2D.

Supplemental Figure S3. Brigatinib and dasatinib synergized to reduce *NF2*-

deficient Schwann cell viability. (A) *Nf2*^{-/-} mouse MS02 schwannoma and *NF2*-deficient human HS01 Schwann cells were plated and tested in dose-response 10x10 matrix format as described in Methods. Shown are single-agent dose response curves for ALK-IN-1 and brigatinib. (B) Brigatinib/dasatinib combination matrix analyses were conducted with HS01 cells. Shown are the brown-scale viability and synergy matrix plots with modeled surface synergy distributions in Loewe, Bliss, and HSA models. (C) Brigatinib/dasatinib combination matrix were analyzed with MS02 cells as described in Supplemental Fig. S3B.

Supplemental Figure S4. Dasatinib and simvastatin synergized to reduce the viability of Schwann and schwannoma cells. 10x10 matrix dose-response analysis was performed for *NF2*-deficient HS01 (A) and *NF2*-expressing HS11 (B) human Schwann cells and *Nf2*^{-/-} mouse schwannoma MS02 cells (C) treated with the brigatinib/simvastatin combination. Shown are the viability (brown scale) and synergy matrix (blue to red scale) plots with modeled surface synergy distributions in Loewe, Bliss, and HSA models.

Supplemental Figure S5. Gene expression changes caused by drug treatments. (A) Significant (Bonferroni-adjusted $p < 0.05$) changes in gene expression in Syn5 and Syn1 arachnoidal cells, which show extensive overlap with an overall greater response in the Syn5 merlin-null cells, are caused by brigatinib or brigatinib/MK-2206 treatment, but not by MK-2206 alone. (B) Genes whose expression is altered both by lack of merlin in Syn5 and by treatment of Syn5 with either brigatinib or brigatinib/MK-2206 treatment

overwhelmingly show the expression change in opposite directions. (C) Significant changes in gene expression in HS01 and HS11 Schwann cells are limited in single drug treatments and most pronounced with the brigatinib/dasatinib combination. (D) The small number of genes differentially expressed in HS01 as a result of merlin expression do not overlap extensively with those altered in HS01 by the brigatinib/dasatinib treatment, and those overlaps that do occur are concordant in direction, contrasting with the arachnoidal cells.

Supplemental Figure S6. MIB/MS kinome profiling reveals dasatinib and brigatinib target specificity. (A) Control sciatic nerve tissues from *Postn-Cre; Nf2^{flox/flox}* mice were used to prepare lysates. Equal amount of protein lysates (1mg) was incubated with vehicle (0.001% ethanol) or brigatinib (10nM, blue; 100nM, red; 1000nM, green) for 2h in biological duplicate. The log₂ difference in MIB binding (LFQ intensity) was calculated and plotted relative to vehicle for each replicate. (B) HS11 and HS01 cells were treated with vehicle or brigatinib (1μM) for 24h prior to MIB/MS kinome profiling. MIB binding (log₂LFQ intensities) was determined and PCA performed in Perseus. (C) HS11 and HS01 cells were treated with vehicle or dasatinib (0.6μM) for 24h prior to MIB/MS kinome profiling. MIB binding (log₂LFQ intensities) was determined and the top 20 kinases with decreased MIB binding compared to vehicle are shown as a stacked bar plot for the two cell lines.

Supplemental Figure S7. ALK was not detected in normal meningeal and meningioma cells with or without *NF2* expression. Equal amounts of protein lysates

from three human meningioma cell lines (KT21-MG1-Luc, NF2-Men-1, and Ben-Men-1), normal meningeal cells, and four primary meningioma cell cultures (hMen-10A, hMen-10B, hMen-12Ao, hMen-12B) were used in Western blot analysis to probe ALK and merlin expression. SK-N-SH neuroblastoma cells, which express ALK, were used as a positive control.

Supplemental Figure S8. Inhibition of multiple RTKs and non-RTKs in Ben-Men-1 cells treated with 1x IC₅₀ of brigatinib under various growth conditions.

PathScan® RTK signaling antibody array analysis was conducted according to Supplementary Methods using cells grown in 10% FBS and treated with 1x IC₅₀ of brigatinib for 2h (A) and 24 h (B) or in growth-arrested cells stimulated with 20% FBS in the presence of 1x IC₅₀ of brigatinib for 2h (C) and 24 h (D). The numeric table below each pair of arrays displays the fold-change in fluorescence detected for each phospho-protein expressed in cells treated with brigatinib relative to DMSO control after subtraction of the fluorescence in the background control spots (indicated as “-”). Positive control spots are denoted as “+”.

Supplemental Figure S9. Ben-Men-1 cells expressed low levels of p-EGFR, which was abolished by brigatinib treatment. Western blot analysis revealed that while phosphorylated EGFR was robustly induced in EGF-stimulated Ben-Men-1 cells, only very low levels of p-EGFR were detected in actively-growing cells or growth-arrested cells stimulated with 20% serum for 24h. Brigatinib treatment diminished p-EGFR expression.

Supplemental Figure S10. ALK expression was not detected in Schwann and schwannoma cells. (A) Western blotting was performed to detect ALK expression in human Schwann cells, four primary vestibular schwannoma cultures (hVS-16H, hVS-16S, hVS-12J, hVS-12Ga), and SK-N-SH neuroblastoma cells. Tubulin was used as a loading control. (B) Western blotting for ALK was also performed using extracts from nine vestibular schwannoma tumors. GAPDH was used as a loading control.

Supplemental Figure S11. Mouse PK parameters following a single oral dose of brigatinib or MK-2206 at the MTD. Mice were orally fed 50 mg/kg of brigatinib or 120 mg/kg of MK-2206. PK analysis was performed according to Supplementary Methods.

Supplemental Figure S12. Relative tumor sizes in meningioma-bearing mice prior to or after treatment with MK-2206 and brigatinib, either alone or in combination, for 12 weeks. Detailed drug treatment and tumor measurement were as described in Figs. 5B/C and Supplementary Methods.

Supplemental Figure S13. Brigatinib inhibited p-FAK, p-AKT, and p-S6 target pathways in *Postn-Cre;Nf2^{flox/flox}* mice. DRGs from *Postn-Cre;Nf2^{flox/flox}* mice treated with the indicated drug or drug combination were used in Western blotting as described in Supplementary Methods.

References

1. Synodos for NFC, Allaway R, Angus SP, Beauchamp RL, Blakeley JO, Bott M, *et al.* Traditional and systems biology based drug discovery for the rare tumor syndrome neurofibromatosis type 2. PLoS One **2018**;13:e0197350

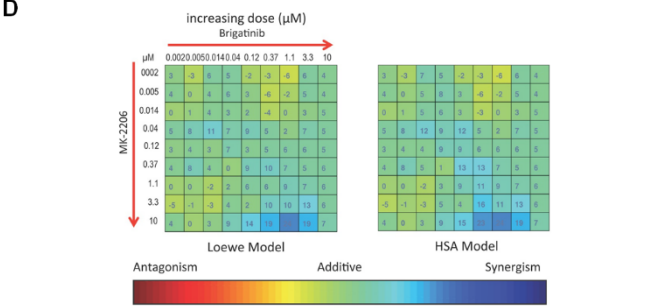
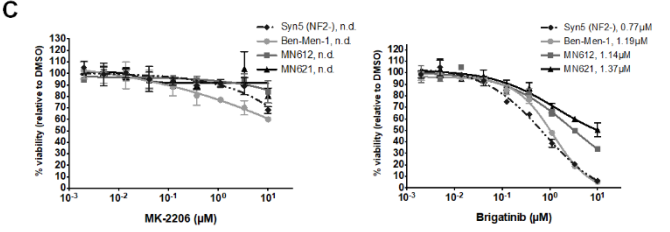
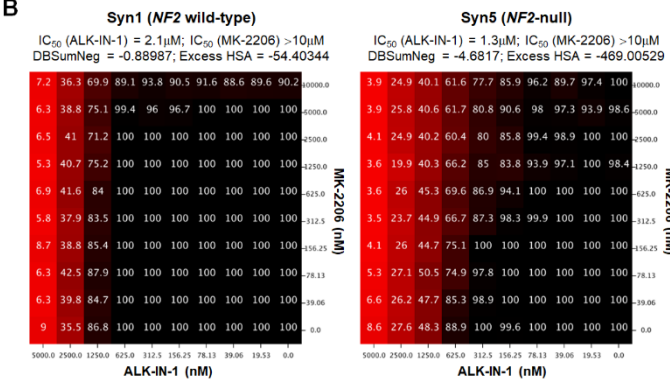
2. Blakeley JO, Evans DG, Adler J, Brackmann D, Chen R, Ferner RE, *et al.* Consensus recommendations for current treatments and accelerating clinical trials for patients with neurofibromatosis type 2. *Am J Med Genet A* **2012**;158A:24-41
3. Evans DG, Kalamarides M, Hunter-Schaedle K, Blakeley J, Allen J, Babovic-Vuskanovic D, *et al.* Consensus recommendations to accelerate clinical trials for neurofibromatosis type 2. *Clin Cancer Res* **2009**;15:5032-9
4. Cui Y, Groth S, Troutman S, Carlstedt A, Sperka T, Riecken LB, *et al.* The NF2 tumor suppressor merlin interacts with Ras and RasGAP, which may modulate Ras signaling. *Oncogene* **2019**;38:6370-81
5. Hadfield KD, Smith MJ, Urquhart JE, Wallace AJ, Bowers NL, King AT, *et al.* Rates of loss of heterozygosity and mitotic recombination in NF2 schwannomas, sporadic vestibular schwannomas and schwannomatosis schwannomas. *Oncogene* **2010**;29:6216-21
6. Rutledge MH, Sarrazin J, Rangaratnam S, Phelan CM, Twist E, Merel P, *et al.* Evidence for the complete inactivation of the NF2 gene in the majority of sporadic meningiomas. *Nat Genet* **1994**;6:180-4
7. Ammoun S, Hanemann CO. Emerging therapeutic targets in schwannomas and other merlin-deficient tumors. *Nat Rev Neurol* **2011**;7:392-9
8. Blakeley JO, Plotkin SR. Therapeutic advances for the tumors associated with neurofibromatosis type 1, type 2, and schwannomatosis. *Neuro Oncol* **2016**;18:624-38
9. Troutman S, Moleirinho S, Kota S, Nettles K, Fallahi M, Johnson GL, *et al.* Crizotinib inhibits NF2-associated schwannoma through inhibition of focal adhesion kinase 1. *Oncotarget* **2016**;7:54515-25
10. Ferrer M, Gosline SJC, Stathis M, Zhang X, Guo X, Guha R, *et al.* Pharmacological and genomic profiling of neurofibromatosis type 1 plexiform neurofibroma-derived schwann cells. *Sci Data* **2018**;5:180106
11. Borisy AA, Elliott PJ, Hurst NW, Lee MS, Lehar J, Price ER, *et al.* Systematic discovery of multicomponent therapeutics. *Proc Natl Acad Sci U S A* **2003**;100:7977-82
12. Markham A. Brigatinib: First Global Approval. *Drugs* **2017**;77:1131-5
13. Huang WS, Liu S, Zou D, Thomas M, Wang Y, Zhou T, *et al.* Discovery of Brigatinib (AP26113), a Phosphine Oxide-Containing, Potent, Orally Active Inhibitor of Anaplastic Lymphoma Kinase. *J Med Chem* **2016**;59:4948-64
14. Daub H, Olsen JV, Bairlein M, Gnad F, Oppermann FS, Korner R, *et al.* Kinase-selective enrichment enables quantitative phosphoproteomics of the kinome across the cell cycle. *Mol Cell* **2008**;31:438-48
15. Duncan JS, Whittle MC, Nakamura K, Abell AN, Midland AA, Zawistowski JS, *et al.* Dynamic reprogramming of the kinome in response to targeted MEK inhibition in triple-negative breast cancer. *Cell* **2012**;149:307-21
16. Stuhlmiller TJ, Miller SM, Zawistowski JS, Nakamura K, Beltran AS, Duncan JS, *et al.* Inhibition of Lapatinib-Induced Kinome Reprogramming in ERBB2-Positive Breast Cancer by Targeting BET Family Bromodomains. *Cell Rep* **2015**;11:390-404
17. Klaeger S, Heinzlmeir S, Wilhelm M, Polzer H, Vick B, Koenig PA, *et al.* The target landscape of clinical kinase drugs. *Science* **2017**;358
18. Angus SP, Oblinger JL, Stuhlmiller TJ, DeSouza PA, Beauchamp RL, Witt L, *et al.* EPH receptor signaling as a novel therapeutic target in NF2-deficient meningioma. *Neuro Oncol* **2018**;20:1185-96
19. Zhou Y, Liu Z, Rothschild KJ, Lim MJ. Proteome-wide drug screening using mass spectrometric imaging of bead-arrays. *Sci Rep* **2016**;6:26125

20. Yap TA, Yan L, Patnaik A, Fearon I, Olmos D, Papadopoulos K, *et al.* First-in-man clinical trial of the oral pan-AKT inhibitor MK-2206 in patients with advanced solid tumors. *J Clin Oncol* **2011**;29:4688-95
21. Beauchamp RL, James MF, DeSouza PA, Wagh V, Zhao WN, Jordan JT, *et al.* A high-throughput kinome screen reveals serum/glucocorticoid-regulated kinase 1 as a therapeutic target for NF2-deficient meningiomas. *Oncotarget* **2015**;6:16981-97
22. Petrilli AM, Garcia J, Bott M, Klingeman Plati S, Dinh CT, Bracho OR, *et al.* Ponatinib promotes a G1 cell-cycle arrest of merlin/NF2-deficient human schwann cells. *Oncotarget* **2017**;8:31666-81
23. Burns SS, Akhmametyeva EM, Oblinger JL, Bush ML, Huang J, Senner V, *et al.* Histone deacetylase inhibitor AR-42 differentially affects cell-cycle transit in meningeal and meningioma cells, potently inhibiting NF2-deficient meningioma growth. *Cancer Res* **2013**;73:792-803
24. Gehlhausen JR, Park SJ, Hickox AE, Shew M, Staser K, Rhodes SD, *et al.* A murine model of neurofibromatosis type 2 that accurately phenocopies human schwannoma formation. *Hum Mol Genet* **2015**;24:1-8
25. Puttmann S, Senner V, Braune S, Hillmann B, Exeler R, Rickert CH, *et al.* Establishment of a benign meningioma cell line by hTERT-mediated immortalization. *Lab Invest* **2005**;85:1163-71
26. Di Veroli GY, Fornari C, Wang D, Mollard S, Bramhall JL, Richards FM, *et al.* Combenefit: an interactive platform for the analysis and visualization of drug combinations. *Bioinformatics* **2016**;32:2866-8
27. Brighton HE, Angus SP, Bo T, Roques J, Tagliatela AC, Darr DB, *et al.* New Mechanisms of Resistance to MEK Inhibitors in Melanoma Revealed by Intravital Imaging. *Cancer Res* **2018**;78:542-57
28. Cox J, Hein MY, Luber CA, Paron I, Nagaraj N, Mann M. Accurate proteome-wide label-free quantification by delayed normalization and maximal peptide ratio extraction, termed MaxLFQ. *Mol Cell Proteomics* **2014**;13:2513-26

Fig. 2

A

Ranking	Drug combination	Targets	DBSumNeg in Syn1 (NF2 ⁺) cells	DBSumNeg in Syn5 (NF2 ⁻) cells
1	Cabozantinib/Danuseritib	VEGFR2/AURKa,b,c	-4.55567	-9.56327
2	Dasatinib/GSK2126458	BCR-ABL/Pi3K	-0.3212	-4.90171
3	MK-2206/ALK-IN-1	AKT/ALK	-0.88987	-4.68107



E

Ranking	Drug combination	Targets	DBSumNeg in HS11 (NF2 ⁺) cells	DBSumNeg in HS01 (NF2 ⁻) cells
1	ALK-IN-1/Dasatinib	ALK/BCR-ABL	-3.89768	-14.90194
2	TAE226/Dasatinib	FAK/BCR-ABL	-3.16579	-8.93415
3	Dasatinib/Simvastatin	BCR-ABL/HMG CoA Reductase	-2.79717	-7.11969

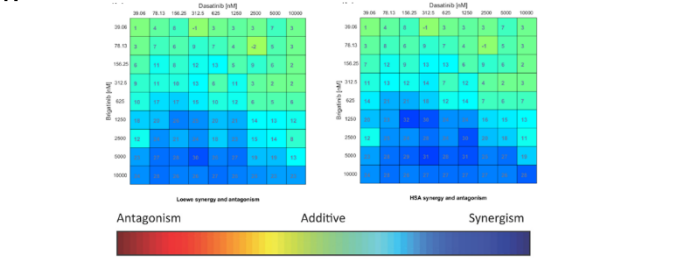
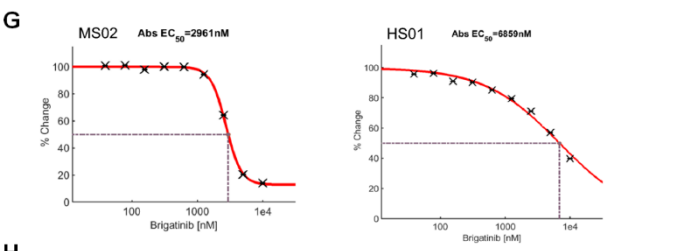
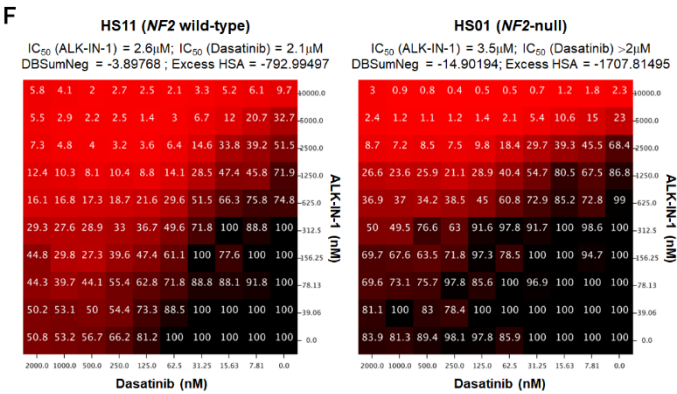


Fig. 3

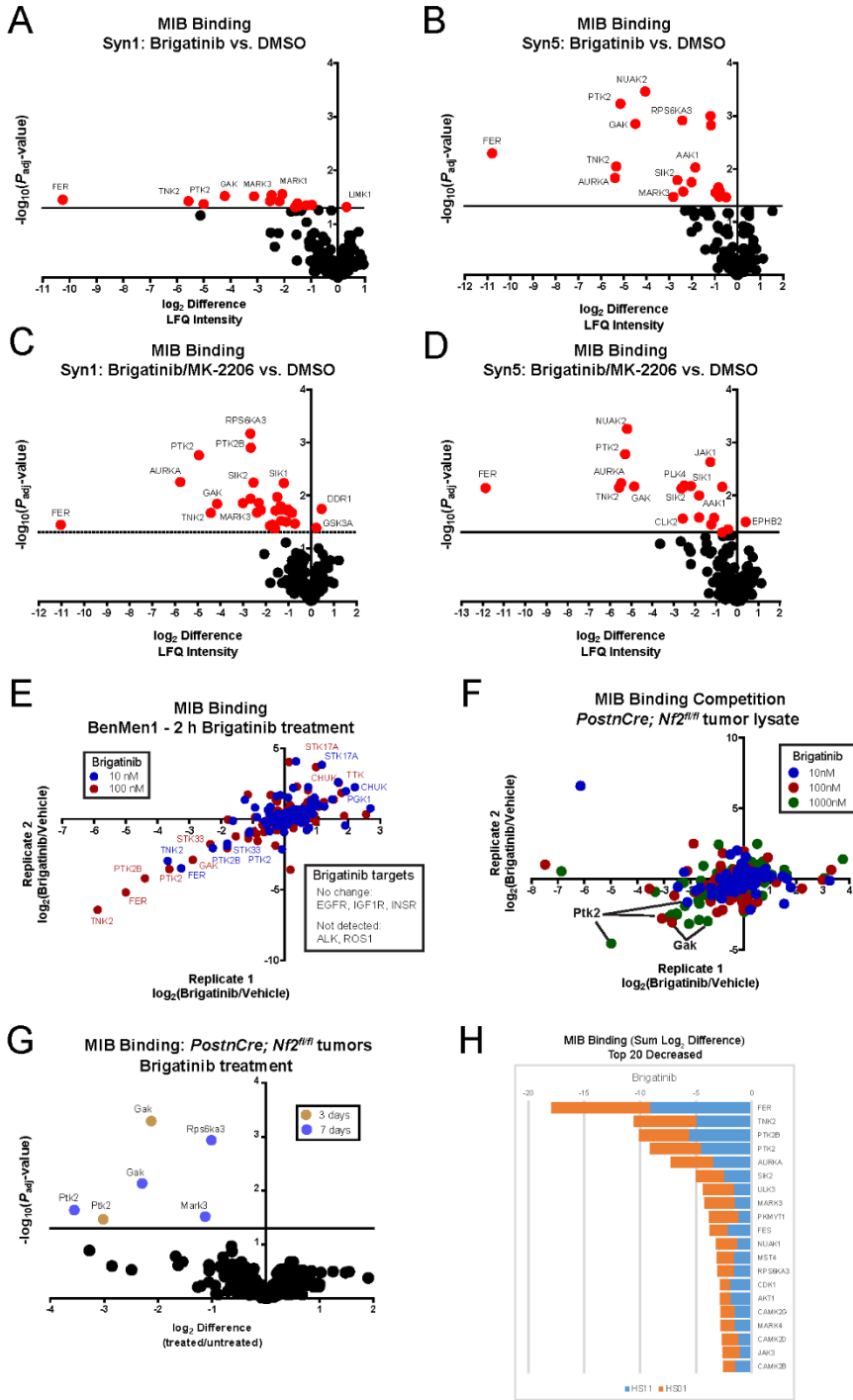


Fig. 4

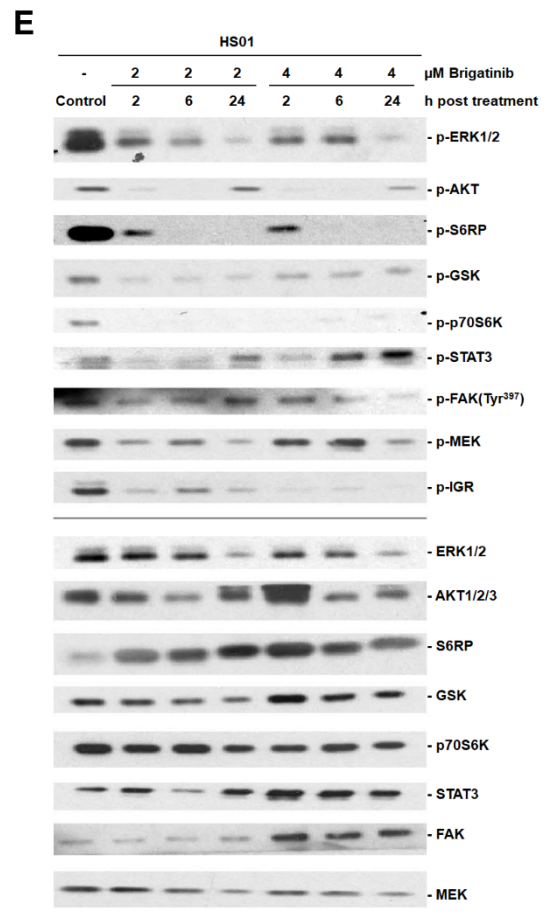
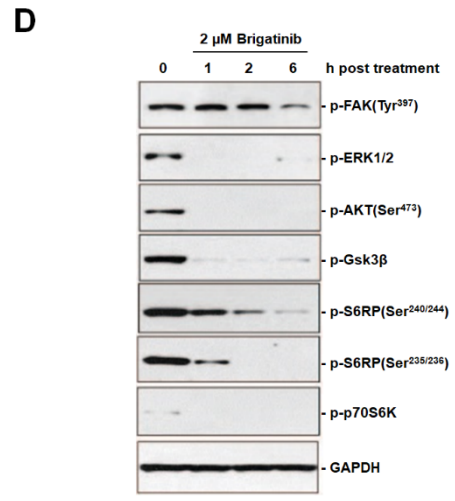
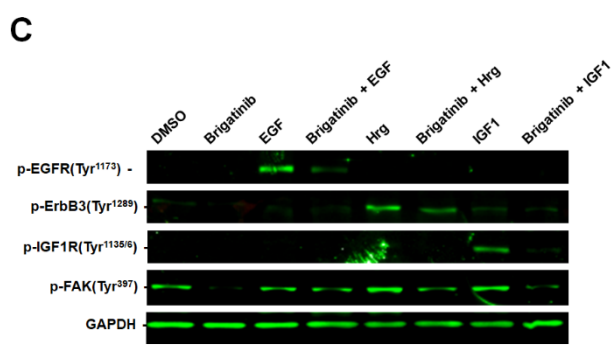
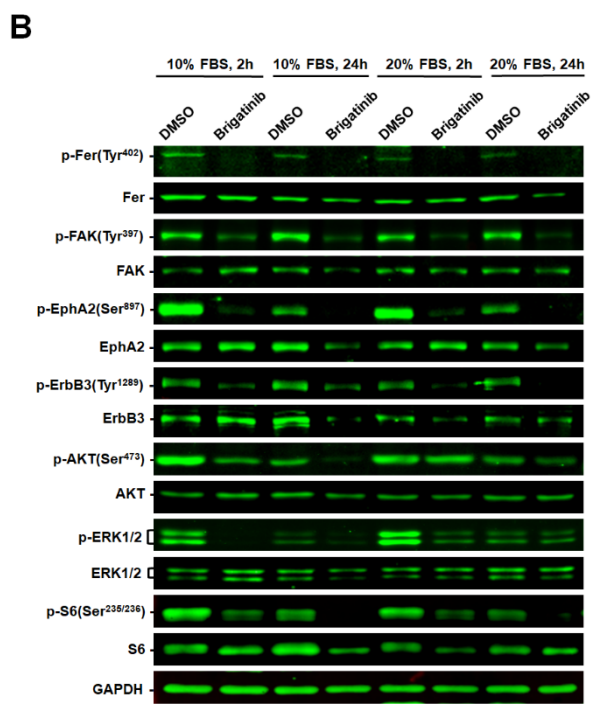
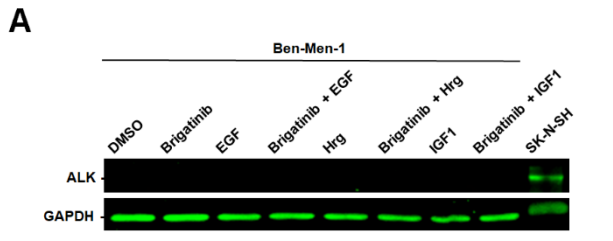
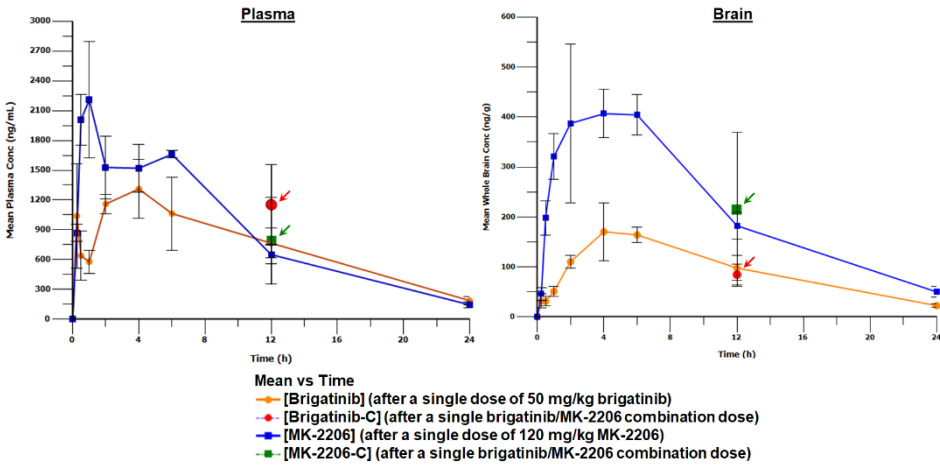
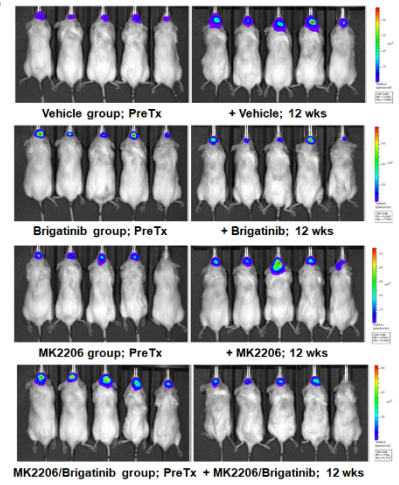


Fig. 5

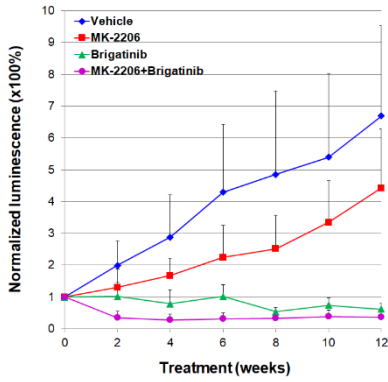
A



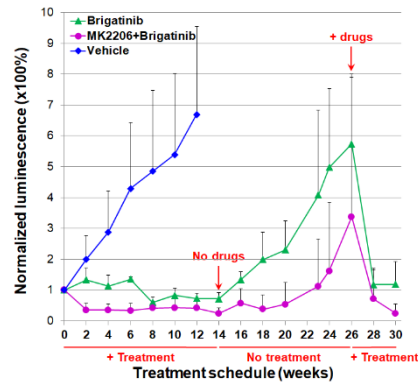
B



C



D



E

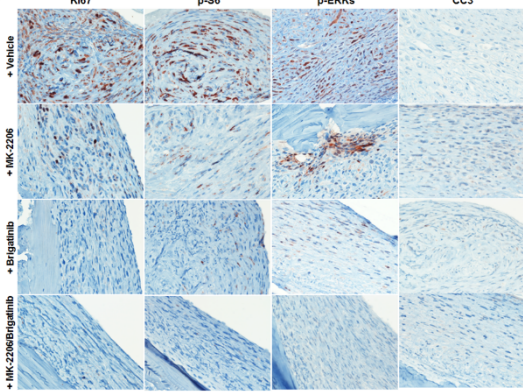
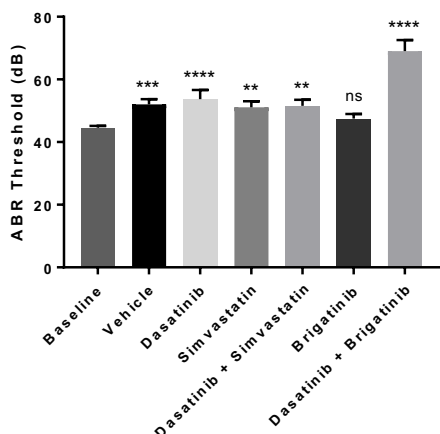


Fig. 6

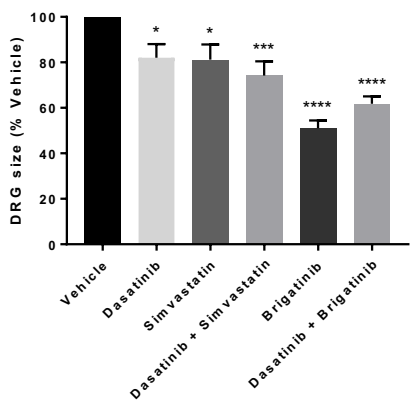
A

Compound	Dosage (mg/kg)	C _{max} (ng/mL)	t _{max} (hours)	AUC _{0-∞} (ng·mL ⁻¹ ·hr)	t _{1/2} (hours)	Cl/F (L/hr)	Vd _{ss} /F (L)
Brigatinib (alone)	50	2819	4	54907	8.8	0.019	0.26
Brigatinib (+Dasatinib)	15	818	1	9529	6.3	0.034	0.32
Dasatinib (alone)	20	115	1	537	0.94	0.82	2.32
Dasatinib (+Brigatinib)	20	507	1	2406	4.3	0.18	1.09

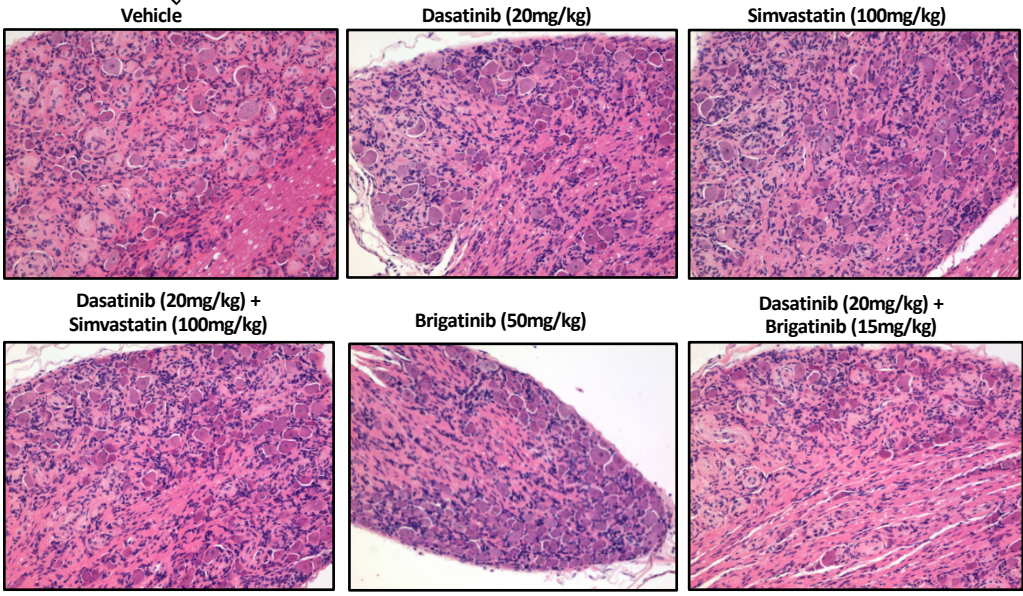
B



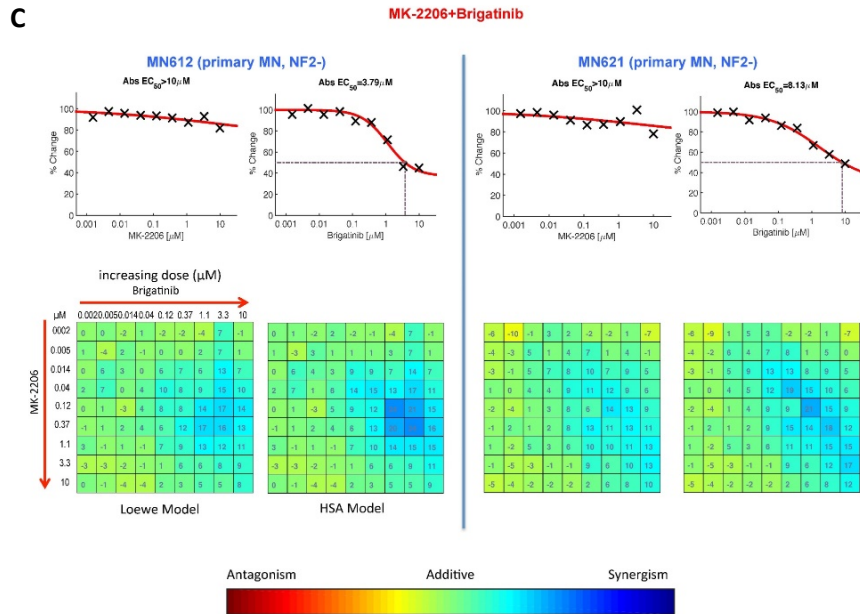
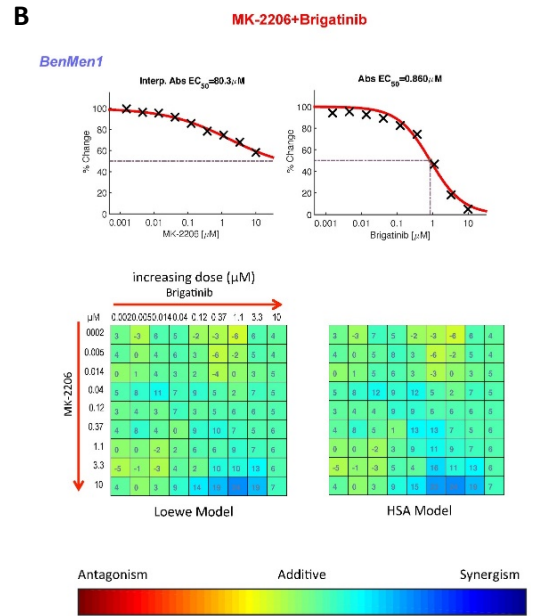
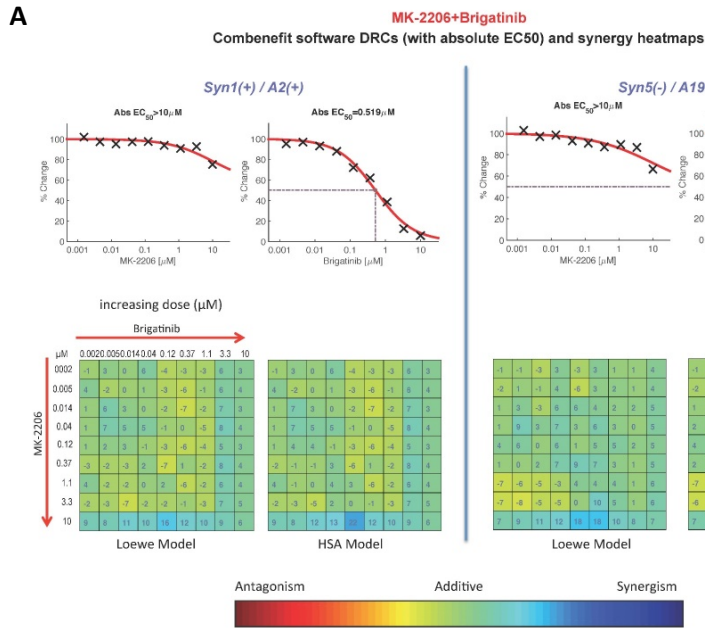
C



D



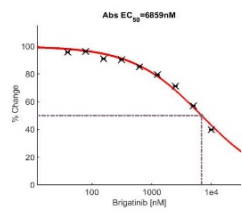
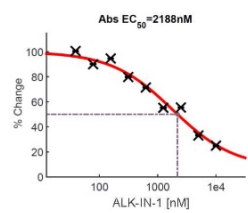
Supplementary Fig. S2



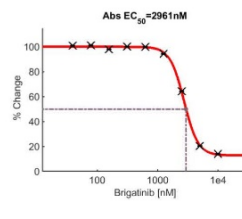
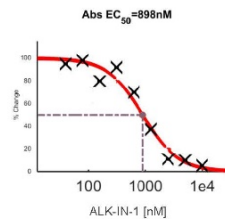
Supplementary Fig. S3

A ALK inhibitors: Single agent

Cell line: HS01



Cell line: MS02

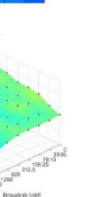
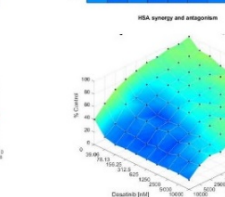
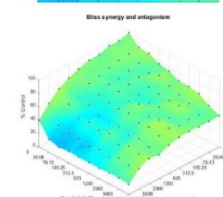
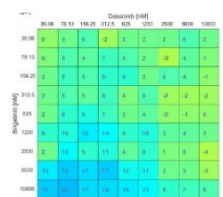
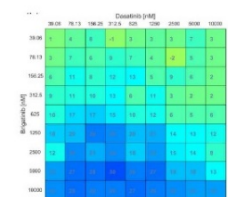
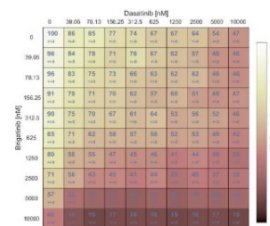


B

HS01

Combination dose-response data in matrix format

Brigatinib-Dasatinib
ALK- Bcr-Abl

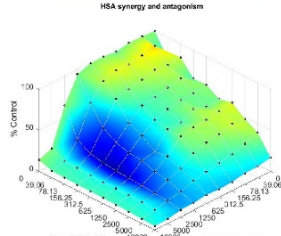
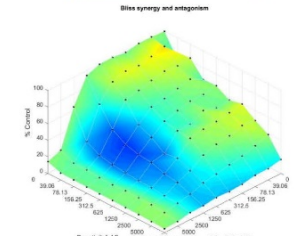
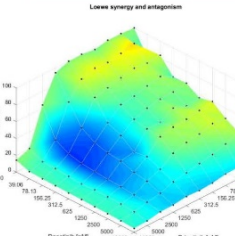
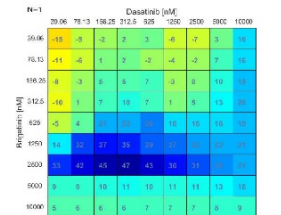
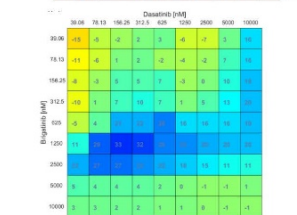
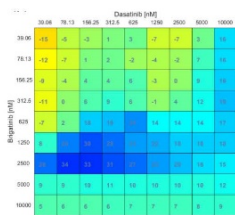
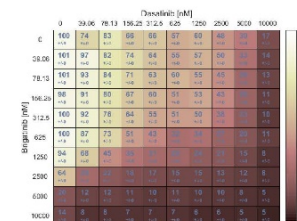


C

MS02

Combination dose-response data in matrix format

Brigatinib-Dasatinib
ALK- Bcr-Abl



Supplementary Fig. S5

A Number of Differentially Expressed Genes (DEG)

	Syn5	Syn1	Shared	Discrepant
Brigatinib				
Up	1281	242	180	0
Down	1324	318	276	0
MK-2206				
Up	0	0	0	0
Down	0	0	0	0
Brigatinib + MK-2206				
Up	1091	337	226	0
Down	1080	493	399	0

B

DEG in Untreated Syn5 vs Syn1

DEG in Syn5+Brigatinib vs Syn5 Untreated

	UP	DOWN
	(1281)	(1324)
UP (1034)	5	327
DOWN (1424)	653	3

DEG in Syn5+Brigatinib +MK-2206 vs Syn5 Untreated

	UP	DOWN
	(1091)	(1080)
UP (1034)	3	262
DOWN (1424)	567	0

C Number of Differentially Expressed Genes (DEG)

	HS01	HS11	Shared	Discrepant
Brigatinib				
Up	0	0	0	0
Down	0	1	0	0
Dasatinib				
Up	18	19	8	0
Down	7	21	2	0
Brigatinib + Dasatinib				
Up	731	451	324	0
Down	666	581	355	0
Simvastatin				
Up	35	16	12	0
Down	7	6	4	0
Dasatinib + Simvastatin				
Up	171	102	72	0
Down	174	283	108	0

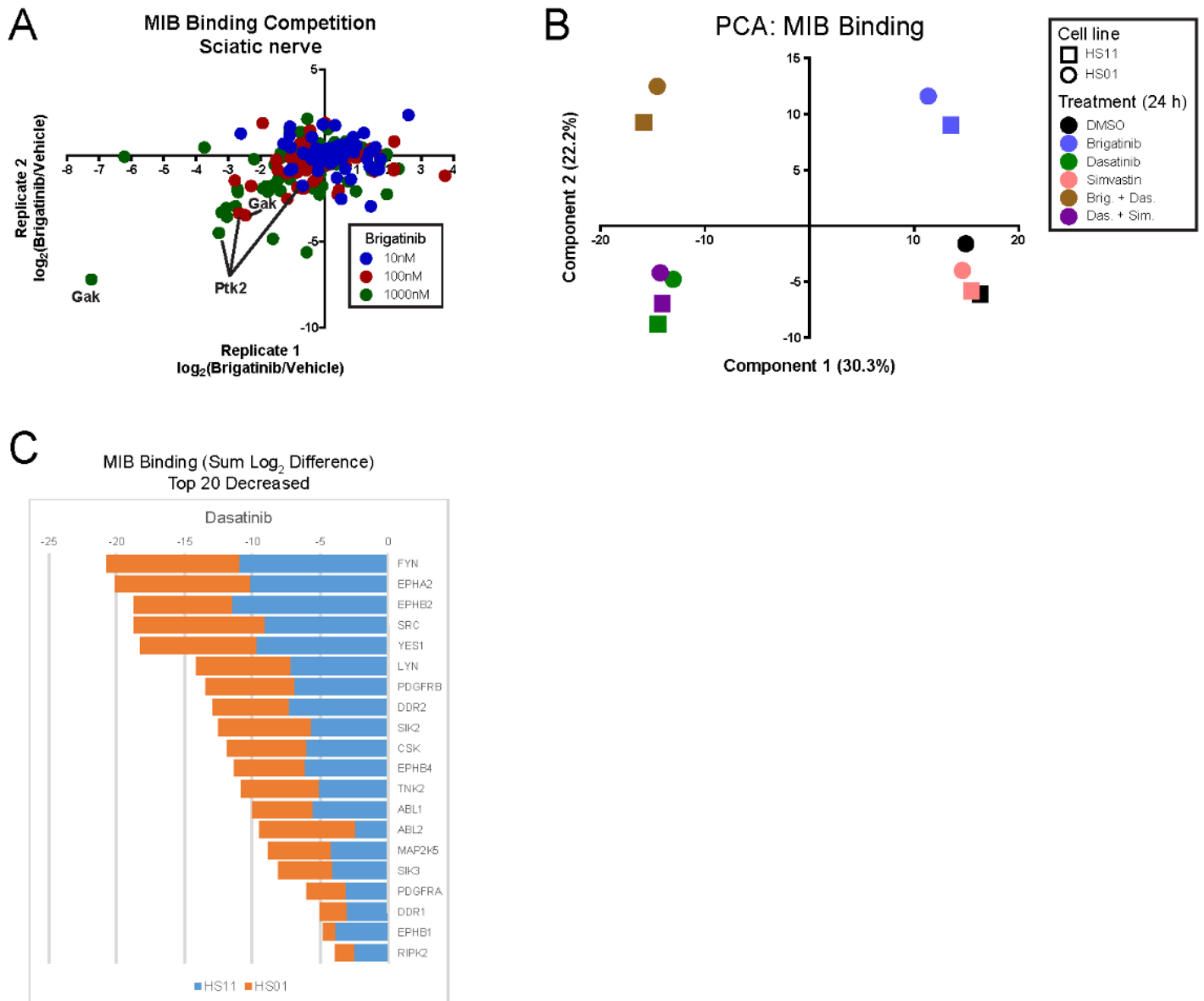
D

DEG in Untreated HS01 vs HS11

DEG in HS01+Brigatinib +Dasatinib vs HS01 Untreated

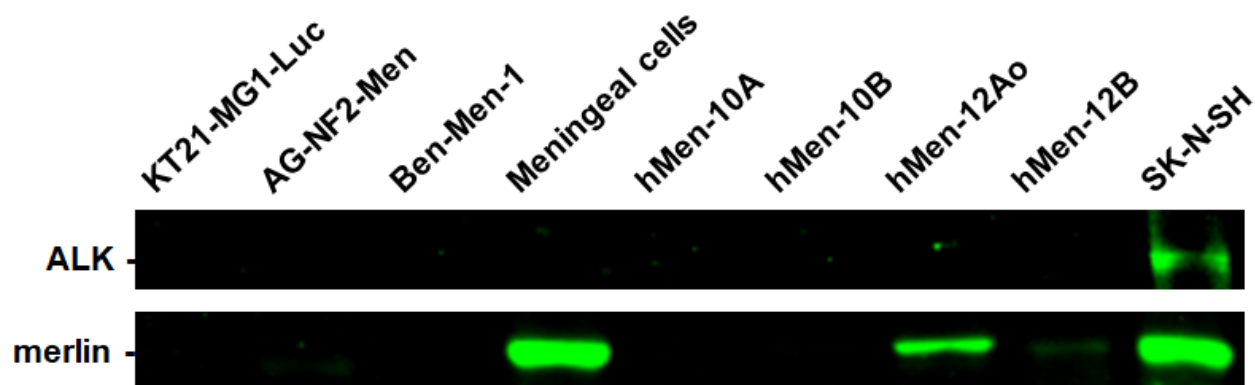
	UP	DOWN
	(731)	(666)
UP (40)	11	0
DOWN (15)	0	1

Supplementary Fig. S6



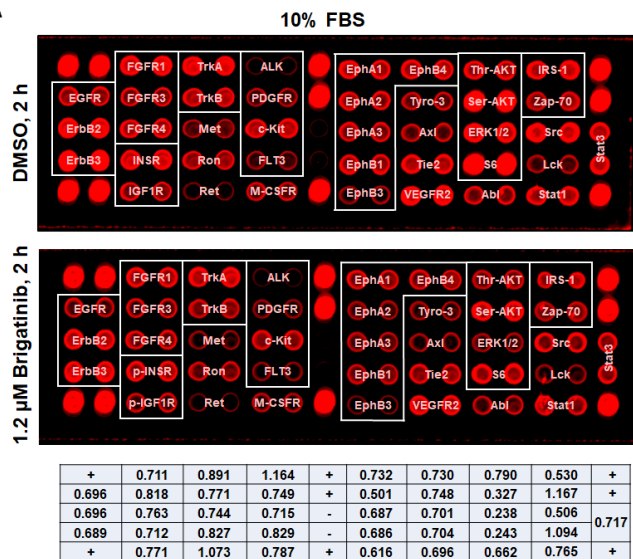
Supplementary Fig. S7

ALK was not detected in normal meningeal and *NF2*-deficient or expressing meningioma cells

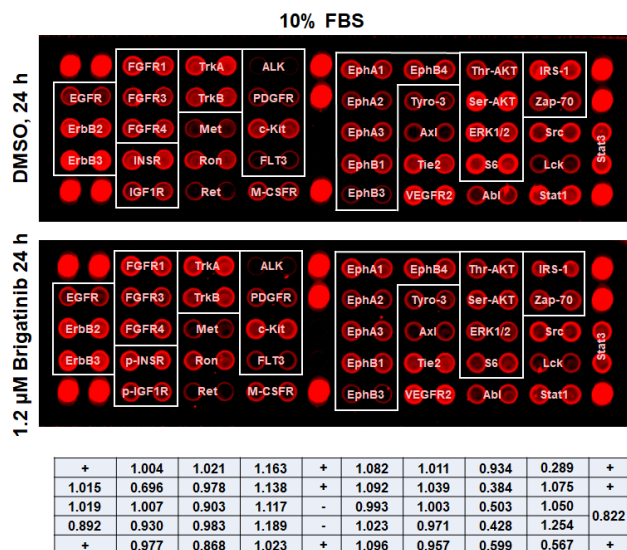


Supplementary Fig. S8

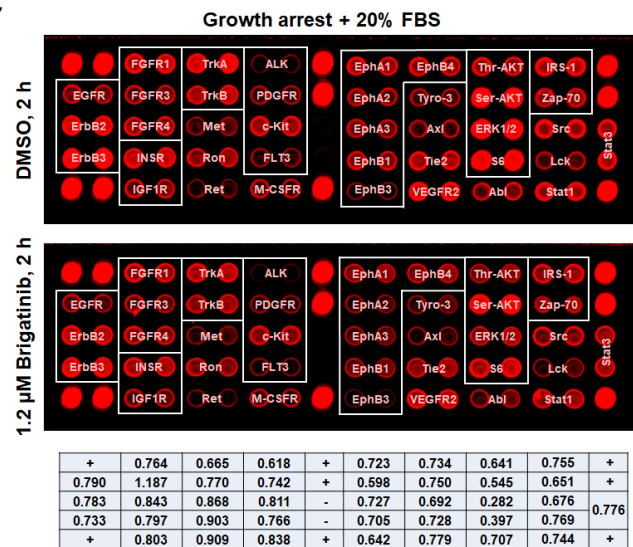
A



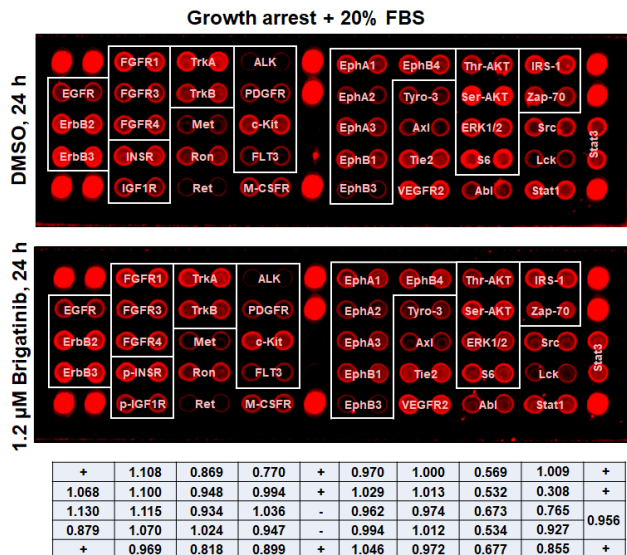
B



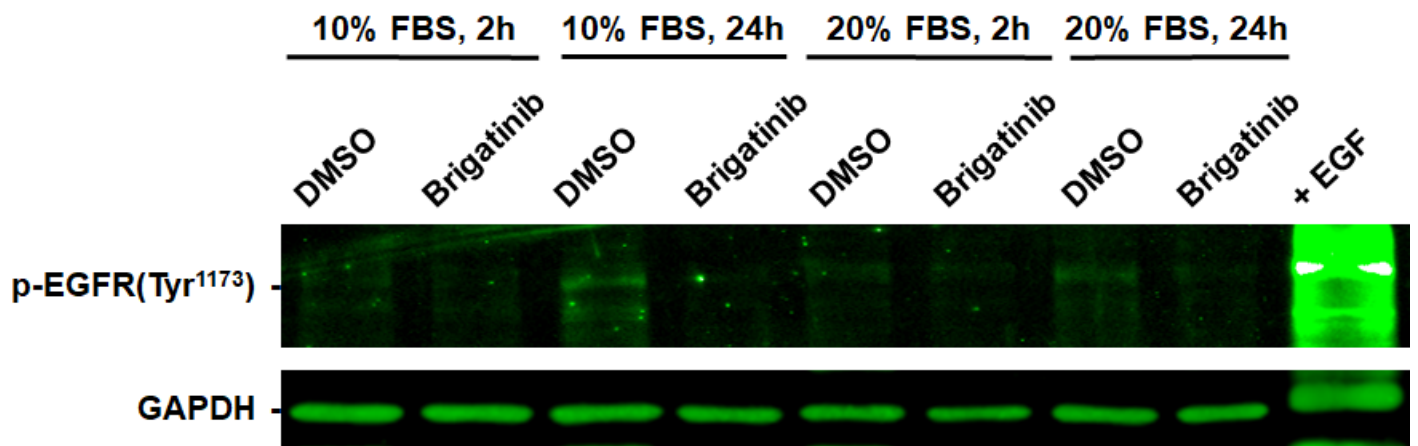
C



D

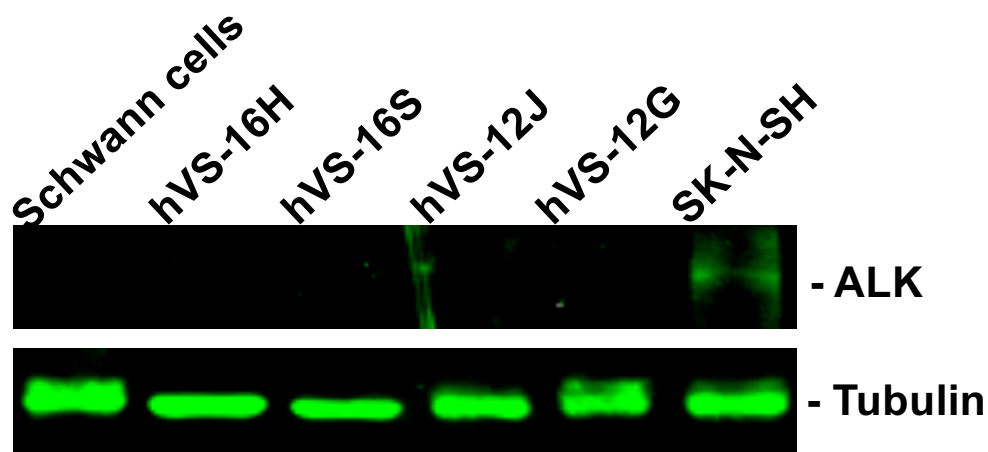


Supplementary Fig. S9

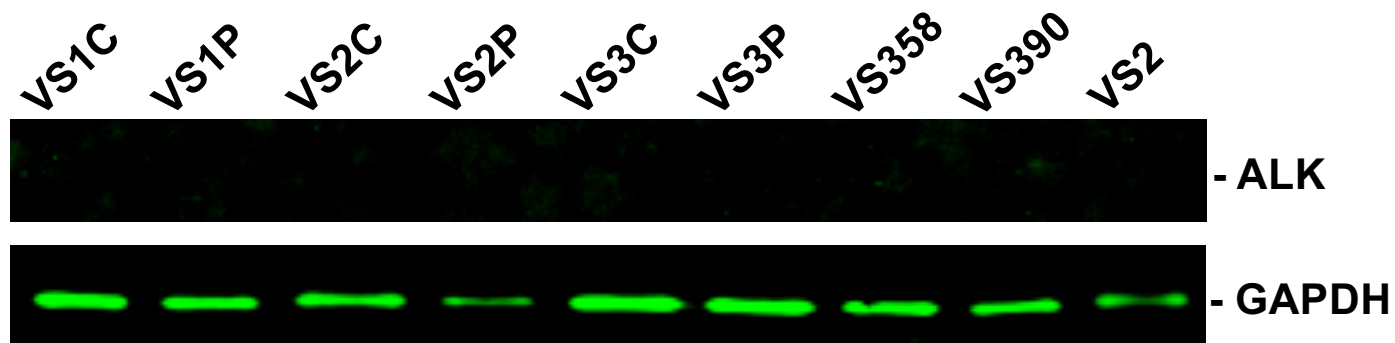


Supplementary Fig. S10

A



B



Supplementary Fig. S11

Mouse pharmacokinetic parameters following a single oral dose of brigatinib (50 mg/kg) or MK-2206 (120 mg/kg)

Drug	PK Parameters					
	T _{1/2} (h)	T _{max} (h)	C _{max} (ng/mL)	AUC _{0-∞} (h*ng/mL)	V/F (L/kg)	CL/F (L/h/kg)
Plasma						
Brigatinib	7.2	4	1311	18662	27.8	2.7
MK2206	5.6	1	2208	21286	45.3	5.6
Brain (Gross)						
	T _{1/2} (h)	T _{max} (h)	C _{max} (ng/g)	AUC _{0-∞} (h*ng/g)	V/F (kg/kg)	CL/F (kg/h/kg)
Brigatinib	6.2	4	170	2319	193.3	22.6
MK2206	6.0	4	406	5462	191.5	22.0

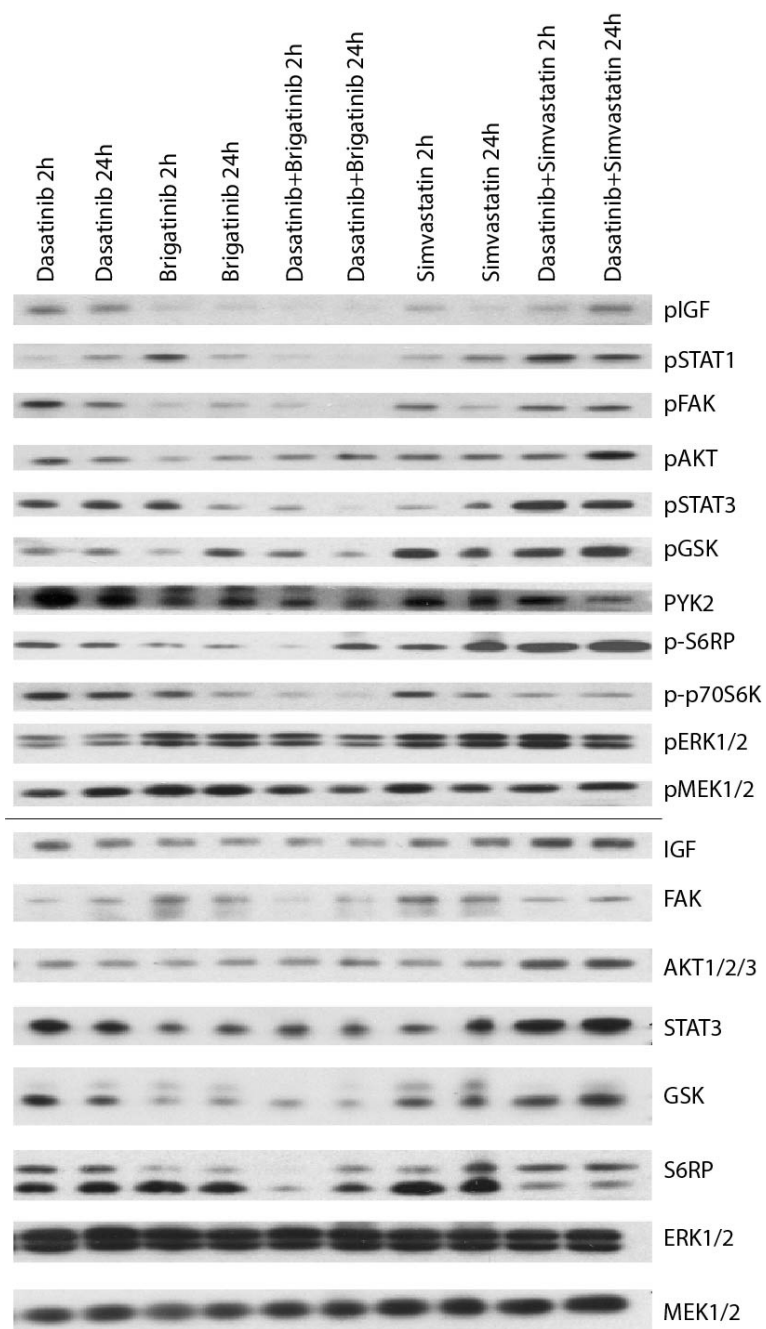
Supplementary Fig. S12

Relative tumor sizes in meningioma-bearing mice prior to or after treatment with MK-2206 and brigatinib, either alone or in combination

Week	Vehicle control	SD	MK-2206	SD	Brigatinib	SD	MK-2206 + Brigatinib	SD
0	1	0	1	0	1	0	1	0
2	2.00	0.77	1.31	0.58	1.02	0.44	0.35	0.20
4	2.88	1.33	1.68	0.54	0.79	0.44	0.28	0.18
6	4.29	2.13	2.24	1.01	1.02	0.37	0.31	0.18
8	4.85	2.62	2.52	1.05	0.54	0.14	0.34	0.21
10	5.39	2.63	3.35	1.31	0.75	0.23	0.39	0.20
12	6.69	2.85	4.43	1.86	0.62	0.20	0.37	0.18

The relative tumor size shown following drug treatment was normalized to the tumor size prior to treatment (week 0), which is designated as 1 (100%).

Supplementary Fig. S13



Supplementary Methods

Additional methods for MIPE screen

Brigatinib (ALUNBRIG®; CAS: 1197953-54-0), MK-2206 (CAS: 1032350-13-2), dasatinib (SPRYCEL®; CAS: 302962-49-8), and simvastatin (ZOCOR®; CAS: 79902-63-9) were synthesized by Proactive Molecular Research, Alachua, FL with purities of greater than 98-99% as determined by liquid chromatography-mass spectrometry (LC-MS) and nuclear magnetic resonance (NMR) spectroscopy. ALK-IN-1 (CAS: 1197958-12-5) was obtained from NCATS and Advanced ChemBlocks (Burlingame, CA) and dasatinib-d₈ (CAS: 1132093-70-9) was purchased from Cayman Chemical (Ann Arbor, MI). For *in vitro* study, all compounds were dissolved in DMSO as 10 mM stock solutions and diluted in medium prior to adding to cells with DMSO concentration kept constant at 0.1%.

Maximum tolerated dose (MTD) determination, and pharmacokinetic (PK) analysis in NSG mice

For animal dosing, MK-2206 was dissolved in 30% Captisol® and brigatinib was formulated in 90% polyethylene glycol 300 and 10% 1-methyl-2-pyrrolidinone. The MTD was determined as described (1). Eight-to-12 week-old NSG (NOD-SCID gamma or *NOD.Cg-Prkdc^{scid} Il2rg^{tm1Wjl}/SzJ*) mice (The Jackson Laboratory) were treated with various doses of MK-2206 every other day or brigatinib every day by oral gavage for two weeks (three mice per dose). The starting doses for MK-2206 and brigatinib were based on those used previously (2,3). Following MTD determination for each drug, a combination of MK-2206 and brigatinib at the MTD was also evaluated to ensure

tolerability.

For PK analysis, mice were fed a single oral dose of brigatinib, MK-2206, or their combination at the MTD. Prior to and at various times after dosing (n=3 per time point), whole blood was collected from the facial vein into EDTA-containing Microtainer[®] (Becton Dickinson). Plasma samples were obtained by centrifugation. Immediately after blood sampling, mice were euthanized for brain harvesting. Both the plasma and brain samples were frozen at -80 °C until analysis of compound concentrations using ultra-high pressure liquid chromatography tandem-mass spectrometry (UHPLC-MS/MS). Plasma and brain samples were deproteinized and were analyzed in the presence of the brigatinib analogue ALK-IN-1 and dasatinib-d₈ as the internal standards for brigatinib and MK-2206, respectively. Detailed UHPLC-MS/MS analysis is appended in Supplementary Methods.

Additional methods for Orthotopic Meningioma Model

The Institutional Animal Care and Use Committee at Nationwide Children's Hospital approved this animal study. The coordinates used were 1.5 mm anterior and 1.5 mm to the right of the bregma and 4.5 mm below the skull surface. The injected mice were monitored for tumor growth by bioluminescence imaging (BLI) every two weeks using a Xenogen IVIS[®] Spectrum imaging system (Perkin Elmer, Bradford, CT). Mice with successful tumor engraftment were randomized into four groups (n=10 each) and treated with MK-2206, brigatinib, MK-2206/brigatinib combination, or a mixture of the corresponding vehicles in which MK-2206 and brigatinib were formulated (1:1 ratio) by oral gavage. BLI was performed biweekly to assess the effects on tumor growth. Previously we showed that the BL signal detected in luciferase-expressing tumor

xenografts correlates with the tumor size (4). The luminescence detected in each mouse was normalized to its pretreatment signal and expressed as the mean normalized luminescence \pm standard deviation for each treatment group. After 14 weeks of treatment, treatment was halted in a subset of mice in the brigatinib alone and MK-2206/brigatinib combination cohorts and monitored possible tumor regrowth for 12 more weeks. Then, treatment was reinitiated to determine tumor response.

Meningioma Model Immunohistochemistry

The heads of drug- or vehicle-treated mice bearing meningiomas were decalcified, followed by paraffin embedding as described previously (4). Serial 5- μ m sections were cut and stained with hematoxylin and eosin to localize the tumor. Then, the sections containing tumors were processed for immunohistochemical staining using antibodies against Ki67 (RM-9106-S, Neomarkers), phospho-S6 (p-S6[Ser^{235/236}]; #4858, Cell Signaling), p-ERK1/2(Thr²⁰²/Tyr²⁰⁴) (#4370, Cell Signaling), and cleaved caspase 3 (CC3; #9664, Cell Signaling). Negative control slides were treated with the same procedures but without the primary antibody.

Additional methods for in vivo Schwannoma Model

Indiana University's Institutional Animal Care and Use Committee approved this study.

Postn-Cre; Nf2^{flox/flox} mice were divided into treatment groups and administered drug by oral gavage. The number of animals used in analysis for each treatment group is as follows: Dasatinib (n=14), Simvastatin (n=15), Brigatinib (n=10), Dasatinib/Simvastatin (n=14), Dasatinib/Brigatinib (n=14), Vehicle Controls (n=37). Drugs were formulated as

follows and administered by oral gavage: 50 mg/kg brigatinib dissolved in 90% PEG400 with 10% 1-methyl-2-pyrrolidinone; 20mg/kg dasatinib in pH3.0 citrate buffer; and 100 mg/kg simvastatin in 1% carboxymethylcellulose in water with 0.25% Tween80 and 0.05% antifoam 204 (Sigma). ABR testing, tissue processing, and DRG volume quantification methods were carried out as previously described (29). Dissected nerve trees were pre-embedded in 2% agar, processed in a Leica tissue processor through graded alcohols, xylenes, and finally in molten paraffin. Five-micron thick sections were cut on a Leica rotary microtome and mounted on charged slides, then stained with hematoxylin and eosin. Images were acquired with an Aperio CS2 slide scanner (Leica).

PK analysis of brigatinib and dasatinib in plasma samples of PostnCre; Nf2^{fox1/flox} mice

HPLC/MS was performed by the IU Simon Cancer Center's Clinical Pharmacology Analytical Core. Samples were acidified and extracted in hexane:ethyl acetate (50:50, v/v). After solvent evaporation, mobile phase (acetonitrile:5mM ammonium acetate; 70:30, v/v) was mixed with residual sample and injected into an Agilent 1290 HPLC system with an ESKigent Autosampler. Mass spectrometry was performed using an ABSciex 5500 Q-TRAP.

Phospho-receptor tyrosine kinase (RTK) array

Ben-Men-1 cells were plated in Dulbecco modified Eagle medium (DMEM) containing 10% fetal bovine serum (FBS). The following day, cells were growth-arrested in medium without serum for two days. Serum-starved cells were stimulated with 20% FBS-containing medium in the presence of 1x IC₅₀ concentration of brigatinib or DMSO

vehicle. Also, cells grown in 10% FBS were treated with 1x IC₅₀ concentration of brigatinib or DMSO in fresh 10% FBS-containing medium for 2 or 24 hours. Treated cells were lysed in 500 µL of 1x Cell Lysis buffer (#9803; Cell Signaling, Danvers, MA) with 1 mM freshly-added PMSF. Cell lysates were sonicated and their protein concentrations were assessed by microBCA assay (#23235; Thermo, Rockford, IL). 150 µg of total protein was added to each chamber of the PathScan RTK Antibody Array (#7949; Cell Signaling) according to the manufacturer's instructions. The fluorescent signal of the array was detected using an Odyssey CLx near-infrared scanner (LI-COR, Lincoln, NE), followed by quantitation using Image Studio software (LI-COR). Also, the remaining protein lysates from the above treated cells were analyzed by Western blotting to validate array findings.

Meningioma Cells Western blot analysis

Ben-Men-1 cells were growth-arrested in serum-free DMEM for two days and then pretreated for 2 hours with 1.5 µM of brigatinib or DMSO vehicle, followed by incubation for 10 minutes with 50 ng/mL each of the following ligands: epidermal growth factor (EGF) (#PHG0311; Thermo Fisher, Waltham, MA), heregulin (HRG) (#100-03; PeproTech, Rocky Hill, NJ), or insulin-like growth factor 1 (IGF1) (#1150-01; Gold Biotechnology, St. Louis, MO). Following ligand stimulation, cells were placed on ice, lysed in cold RIPA buffer containing protease/phosphatase inhibitor cocktail (#78440; Sigma-Aldrich, St. Louis, MO), and sonicated. Also, lysates were prepared from primary NF2-associated and sporadic meningioma, Ben-Men-1, normal human meningeal (ScienCell, Carlsbad, CA), and SK-N-SH neuroblastoma cells. Equal amounts of protein

lysates were used in Western blotting as previously described (4).

Drug concentrations used for Figure 2 (also used for Fig S2A-C).

For meningioma-related cells lines (Fig 2C), single drug dose response testing was carried out for MK-2206 or brigatinib at a concentration range of 0.0015 – 10 μ M (3-fold dilutions series, 9 dosage points) and DMSO (vehicle) control. For combination drug testing, cells were treated in a 10x10 dose matrix format using same concentrations listed above.

Additional methods for RNAseq and transcriptome analysis

RNAseq reads were aligned to human reference genome Ensembl GRCh37 (v.75) using STAR (v. 2.5.2a) (5) with parameters ‘–outSAMunmapped Within –outFilterMultimapNmax 1 –outFilterMismatchNoverLmax 0.1 –alignIntronMin 21 –alignIntronMax 0 –alignEndsType Local –quantMode GeneCounts –twopassMode Basic’. In this step, STAR also generated gene level counts for all libraries. Quality checking of alignments was assessed by a custom script utilizing Picard Tools (<http://broadinstitute.github.io/picard/>), RNASeQC (6), RSeQC (7) and samTools (8). These analyses identified two samples, Syn1_1, and Syn1_11 (Brigatinib), as outlier samples as they failed to pass the following thresholds: exonic rate ≥ 0.8 and intergenic rate ≤ 0.1 , and thus they were excluded from further analysis. Differentially expressed genes in pair-wise comparisons were identified by edgeR’s quasi-likelihood F test (v. 3.18.1) (9), which was run at the R platform (v. 3.4) on genes with greater than 10 counts across replicates per condition in pair-wise comparisons. Gene ontology (GO) enrichment analysis for each comparison was performed on differentially expressed

genes at Bonferroni adjusted p values < 0.05, where all the analyzed genes in a given comparison were used as a background list, using DAVID (v. 6.8) (10). GO terms with Benjamini Hochberg adjusted p values < 0.05 were reported as significantly enriched for a given gene list.

Western blot of drug-treated DRG tumor samples from Postn-Cre;Nf2^{flox/flox} mice

DRG tumor samples derived from mice shown in Figure 6 were collected at indicated time points after single dose oral gavage of indicated drugs. 9 DRGs for Dasatinib+Brigatinib treatment, 12 for all other conditions were collected in ice cold lysis buffer (1% IGEPAL; 0,1% DOC; 100 mM NaCl; 50 mM Tris pH 8.0) containing phosphatase and protease inhibitors (PhosSTOP, #04906837001 and cOmplete EDTA-free protease inhibitor cocktail, #4693132001, both from Roche). Lysis was performed in a Precellys 24 device (Bertin Technologies) at 2 x 5000 rpm for 30s with 5s break in-between. Cellular debris was removed twice by centrifugation at 12.000 rpm for 10 min and supernatant collected. Protein concentration was determined using a BCA protein assay kit (#23225; ThermoFisher). 10 µg each were separated by SDS-PAGE and transferred onto nitrocellulose membranes. Membranes were blocked in 5% milk/TBST and probed at 4°C overnight with the following primary antibodies in blocking buffer: p-AKT (Ser⁴⁷³) (#4060), ERK1/2 (#9102), p-ERK1/2 (Thr²⁰²/Tyr²⁰⁴) (#4696), p-FAK (Tyr³⁹⁷) (#8556), GSK (#9832), p-GSK (Ser⁹) (#8213), IGF1R-beta (#9750), p-IGF1R-beta (Tyr¹¹³⁵/Tyr¹¹³⁶) (#3024), MEK1/2 (#8727), p-MEK1/2 (Ser²¹⁷/Ser²²¹), p-p70S6K (Thr³⁸⁹) (#9234), S6RP (#2317), p-S6RP (Ser²³⁵/Ser²³⁶) (#4858), p-Stat1 (Tyr⁷⁰¹) (#7649), Stat3 (#9139), p-Stat3 (Tyr⁷⁰⁵) (#9145) [all from Cell Signaling], Pyk2 (#ab32571; Abcam),

AKT1/2/3 (#sc-8312), FAK (#sc-271126) (both from Santa Cruz Biotechnology).

Membranes were washed three times for 10 min each in TBST before probing with following secondary antibodies in blocking buffer for 1h at room temperature:

Chemiluminescent signals were generated using ECL (#32106) or ECL+ (#32132) (both ThermoFisher) following manufacturer's instructions and detected on Super RX-N films (#4141019289; Fuji).

Supplemental Methods References

1. Plowman J CR, Alley M, Sausville E, Schepartz S. US-NCI testing procedures. Relevance of Tumor Models for Anticancer Drug Development: Karger; 1999. p 121-35.
2. Hirai H, Sootome H, Nakatsuru Y, Miyama K, Taguchi S, Tsujioka K, *et al.* MK-2206, an allosteric Akt inhibitor, enhances antitumor efficacy by standard chemotherapeutic agents or molecular targeted drugs *in vitro* and *in vivo*. *Mol Cancer Ther* 2010;9:1956-67
3. Siaw JT, Wan H, Pfeifer K, Rivera VM, Guan J, Palmer RH, *et al.* Brigatinib, an anaplastic lymphoma kinase inhibitor, abrogates activity and growth in ALK-positive neuroblastoma cells, *Drosophila* and mice. *Oncotarget* 2016;7:29011-22
4. Burns SS, Akhmametyeva EM, Oblinger JL, Bush ML, Huang J, Senner V, *et al.* Histone deacetylase inhibitor AR-42 differentially affects cell-cycle transit in meningeal and meningioma cells, potently inhibiting NF2-deficient meningioma growth. *Cancer Res*; 2013; 73:792-803
5. Dobin, A., Davis, C.A., Schlesinger, F., Drenkow, J., Zaleski, C., Jha, S., Batut, P., Chaisson, M., and Gingeras, T.R. STAR: ultrafast universal RNA-seq aligner. *Bioinformatics*; 2013; 29, 15-21.
6. DeLuca, D.S., Levin, J.Z., Sivachenko, A., Fennell, T., Nazaire, M.D., Williams, C., Reich, M., Winckler, W., and Getz, G. RNA-SeQC: RNA-seq metrics for quality control and process optimization. *Bioinformatics*; 2012; 28, 1530-1532.
7. Li, H., Handsaker, B., Wysoker, A., Fennell, T., Ruan, J., Homer, N., Marth, G., Abecasis, G., Durbin, R., and Genome Project Data Processing, S. The Sequence Alignment/Map format and SAMtools. *Bioinformatics*; 2009; 25, 2078-2079.
8. Wang, L., Wang, S., and Li, W. RSeQC: quality control of RNA-seq experiments. *Bioinformatics*; 2012; 28, 2184-2185.
9. Robinson, M.D., McCarthy, D.J., and Smyth, G.K. edgeR: a Bioconductor package for differential expression analysis of digital gene expression data. *Bioinformatics*; 2010; 26, 139-140.
10. Huang da, W., Sherman, B.T., and Lempicki, R.A. Systematic and integrative analysis of large gene lists using DAVID bioinformatics resources. *Nat Protoc*; 2009; 4, 44-57.

Neurofibromatosis: Molecular Pathogenesis and Natural Compounds as Potential Treatments

Anusha Amaravathi^{1,2,¶}, Janet L. Oblinger^{1,¶}, D. Bradley Welling³, A. Douglas Kinghorn⁴, and Long-Sheng Chang^{1,5,6,*}

¹Center for Childhood Cancer and Blood Diseases, Abigail Wexner Research Institute at Nationwide Children's Hospital, Columbus, OH 43205,

²Department of Medicine, University of Rochester School of Medicine and Dentistry, Rochester, NY 14642,

³Department of Otolaryngology Head & Neck Surgery, Massachusetts Eye and Ear, Harvard University and Massachusetts General Hospital,

⁴Division of Medicinal Chemistry and Pharmacognosy, The Ohio State University College of Pharmacy, Columbus, OH 43210,

and

Departments of ⁵Pediatrics and ⁶Otolaryngology-Head & Neck Surgery, The Ohio State University College of Medicine, Columbus, OH 43210

Running title: Targeted and natural compounds for NF

Key words: Neurofibromatosis (NF), NF1, NF2, schwannomatosis, signaling pathway, targeted therapy, natural compound

¶These authors equally contributed to this work.

*Corresponding author: Long-Sheng Chang, Center for Childhood Cancer and Blood Diseases, Abigail Wexner Research Institute at Nationwide Children's Hospital, 700 Children's Drive, Columbus, OH 43205, USA; Phone: 614-355-2658; Fax: 614-722-5895; E-mail: Long-Sheng.Chang@nationwidechildrens.org

Abstract

The neurofibromatosis syndromes, including NF1, NF2, and schwannomatosis, are tumor suppressor syndromes characterized by multiple nervous system tumors, particularly Schwann cell neoplasms. NF-related tumors are mainly treated by surgery and often refractory to conventional chemotherapy. Recent advances in molecular genetics and genomics alongside the development of multiple animal models have provided a better understanding of NF tumor biology and facilitated target identification and therapeutic evaluation. Many targeted therapies have been evaluated in preclinical models and patients, including the MEK inhibitor selumetinib recently approved by the FDA for treating NF1-associated plexiform neurofibroma. Due to their anti-neoplastic, antioxidant, and anti-inflammatory properties, selected natural compounds could be useful as adjuvant therapy for patients with tumor predisposition syndromes as patients often take them as dietary supplements and for health enhancement purposes. Several natural compounds have been tested in NF models. Some have demonstrated potent anti-tumor effects and may become viable treatments in the future.

Neurofibromatosis (NF) comprises three distinct genetic disorders that cause tumors to grow along nerves but with limited treatment options.

As a group of slowly progressive autosomal-dominant syndromes, NF has been classified into neurofibromatosis type 1 (NF1), neurofibromatosis type 2 (NF2), and schwannomatosis¹. These syndromes typically present with neural tumors which manifest in different locations depending upon their genetic etiology. Although the tumors frequently remain benign, they incur severe patient morbidity and occasionally exhibit malignant progression.

NF1, previously known as von Recklinghausen disease, affects ~1 in 3,000 patients and is caused by inactivation of the *NF1* tumor suppressor gene on chromosome 17q11.2². Although *NF1* mutation can be inherited, the *de novo* mutation rate is relatively high, and ~42% of patients have new germline mutations. With 100% penetrance, NF1 patients are symptomatic, although there is highly variable expression. One of the earliest manifestations of NF1 are hyperpigmentation-like café-au-lait macules and freckling. The hallmark of NF1 is the development of neurofibromas, benign tumors composed of an admixture of dysplastic Schwann cells and stromal cells, including fibroblasts, mast cells, and perineural cells embedded in a collagenous extracellular matrix (ECM). These tumors are stratified based on their histology and anatomical location. Nearly all NF1 patients develop dermal neurofibromas (DNFs, or cutaneous neurofibroma), which arise along superficial nerves and are confined to the cutaneous tissues³. DNFs can cause itching and pain and be disfiguring if the tumor burden is high. Although the number of DNFs increases with age, they remain benign. About half of NF1 patients also develop more serious plexiform neurofibromas (PNFs)⁴. These tumors occur deeper within the body and are more extensive, surrounding multiple nerve roots and causing pain and disfigurement. PNFs can undergo malignant progression, and 8-13% of patients with PNFs will

develop highly aggressive soft-tissue sarcomas called malignant peripheral nerve sheath tumors (MPNSTs).

About 15-20% of NF1 patients develop optic pathway gliomas (OPGs or astrocytomas of the optic tract)⁵. OPGs often occur during the first four years of childhood. They tend to be slow-growing fusiform tumors that extend along the optic tract and can invade the subarachnoid space. Patients with OPGs may present with visual disturbances and progressive vision loss, although about two-thirds are spared these symptoms. Precocious puberty may also occur if the tumor compresses the hypothalamus. NF1 patients are also predisposed to other types of tumors, including gliomas, gastrointestinal stromal tumors (GIST), juvenile myelomonocytic leukemia, and glomus tumors². Although most NF1-related gliomas are classified as benign pilocytic astrocytomas (WHO grade I), adult NF1 patients are at ~50-fold increased risk of developing malignant glioblastomas (WHO grade IV).

For current NF1 treatment, surgical excision of café-au-lait spots and DNFs is performed³, but the recurrent nature of these lesions means that they can never be totally eradicated. Surgical removal of PNFs is more challenging than DNFs because they are more diffuse and involve multiple nerve roots. A recent exciting development is the FDA approval of the MEK inhibitor selumetinib (Koselugo™) for the treatment of children with symptomatic, inoperable PNF⁶. Children with OPGs are routinely monitored for clinical progression by neuroimaging and visual acuity tests⁷. Slow-growing gliomas causing minimal symptoms are usually not treated, but if the disease progresses, chemotherapy and occasionally, surgery are used to stabilize and reduce tumor burden. However, these treatments rarely improve visual acuity and may increase the risk of cognitive damage. Radiation is contraindicated in NF1 patients with benign tumors due to the heightened risk of secondary malignancies. Due to highly aggressive behavior, MPNSTs are

excised with wide margins to prevent recurrence⁴. Conventional chemotherapy is used to treat unresectable or metastatic MPNSTs. Despite these efforts, the local recurrence rate remains high (~32-65%)⁸. As it is difficult to remove PNFs and MPNSTs without transecting the affected nerves, complete surgical removal of these tumors may cause long-term neurological deficits. Therefore, identification of additional effective drugs could greatly improve the physical and mental development of patients afflicted by NF1.

NF2 has an incidence of ~1 in 30,000 and has nearly complete penetrance⁹. It is caused by mutations in the *NF2* tumor suppressor gene on chromosome 22q12.2. The hallmark of NF2 is bilateral vestibular schwannomas (VS; historically termed acoustic neuromas), so called for their occurrence on the vestibular branch of cranial nerve VIII. VS are the most common benign tumors of the cerebellopontine angle, and 95% of VS are unilateral and occur sporadically. Occasionally, unilateral tumors are found in NF2 patients, especially when they are mosaic for *NF2* loss. Like NF2-related VS, sporadic unilateral VS harbor *NF2* mutations. Compared to sporadic VS, NF2-associated tumors display more aggressive behavior, with a propensity towards multifocal, rapid growth. Due to their intracranial location and proximity to other cranial nerves, VS present with serious comorbidities, including hearing loss, tinnitus, balance dysfunction, facial weakness, seizures, blindness, and brainstem compression. NF2 is also associated with an increased incidence of cutaneous schwannomas, although they tend to be smaller and not as intrusive as NF1-related tumors.

Patients with NF2 are also often afflicted by meningiomas and less commonly spinal schwannomas, ependymomas, and astrocytomas^{1,9}. Meningiomas, which originate from the meningotheial cells of the arachnoid layer lining the brain, are the most common brain tumors¹⁰. About 80% of meningiomas are benign (WHO grade I), whereas the remaining are atypical

(grade II) and anaplastic (grade III). These tumors cause significant morbidity, including cranial nerve palsy, seizures, and brainstem compression, which may lead to paralysis, aspiration pneumonia, and death. Up to 60% of NF2 patients develop meningiomas, mostly benign, but often with multiple tumors. Additionally, meningiomas in NF2 patients are associated with disease severity and increased risk of mortality¹¹.

The current standard of care for treating NF2-related tumors is surgery. However, the recurrence rate is relatively high (~44%), and surgical excision of the tumors often damages nearby nerves and tissues^{1,9}. Alternatively, radiosurgery, such as stereotactic gamma-knife radiation, provides excellent short-term tumor control, especially in tumors that are unresectable. However, it must be weighed against the risk of causing malignant transformation of benign tumors and inducing second-site malignancies. Due to the benign nature and the risks inherent to surgical removal of schwannomas, physicians may monitor tumor growth and only resort to surgery if they become too large or symptomatic. Children with NF2 often develop multiple meningiomas. Surgery may not be possible if the tumor is located in a place where it is too difficult to operate or if there are too many tumors¹¹. Currently, an FDA-approved medical therapy is not available for NF2 patients.

Schwannomatosis manifests as multiple schwannomas on nerves throughout the body but without involvement of the vestibular nerves. Whereas NF2 patients nearly invariably develop bilateral VS, schwannomatosis-associated tumors tend to be non-intradermal and nonvestibular, with rare patients presenting with unilateral VS¹². Owing to the overlap in symptoms with NF2, the true incidence of schwannomatosis is unknown but is thought to be similar to NF2¹. Schwannomatosis usually occurs sporadically, although familial or mosaic cases occasionally occur. The most common familial mutations occur in either the *SNF5/SMARCB1/INI1*

(Switch/Sucrose Non-Fermentable chromatin remodeling complex subunit-5/SWI/SNF-related, Matrix-associated, Actin-dependent Regulator of Chromatin, subfamily-B, member-1/INtegrase Interactor 1) gene on chromosome 22q11.23 or the *LZTR1* (Leucine Zipper-like Transcriptional Regulator 1) gene on chromosome 22q11.21; both of which are located in proximity to the *NF2* locus¹³. Interestingly, schwannomas from schwannomatosis patients also exhibit inactivation of the *NF2* gene. It is currently thought that familial schwannomatosis is inherited through a “three-event, four-hit” process where inactivating mutations occur in the *NF2* gene located on the same chromosome as the germline-mutated *LZTR1* or *SMARCB1* allele. The loss of the remaining normal copy of chromosome 22q then results in biallelic loss-of-heterozygosity^{1,9}. However, some patients with schwannomatosis do not have *LZTR1* or *SNF5/SMARCB1/INI1* mutations, suggesting the presence of another tumor suppressor gene on chromosome 22q in schwannomatosis development.

Schwannomatosis is most often diagnosed in adults over the age of 30, in contrast to NF2 which is more likely to manifest in childhood. Where patients with NF2 are likely to have tumor-associated neurological problems, the most severe symptom in schwannomatosis patients is chronic debilitating pain. As an FDA-approved drug is also not available, surgery is considered for symptomatic patients. Schwannomatosis is also associated with an increased risk of meningioma, although its incidence is much less than that of NF2^{1,9}. Unlike NF2, schwannomatosis patients with germline loss of *SMARCB1* have an increased risk of developing MPNSTs.

Signaling pathways affected in NF-associated tumors

The *NF1* gene encodes neurofibromin, a member of the Ras-GAP (GTPase-activating

protein) family that stimulates the intrinsic GTPase activity of Ras-family members¹⁴. Ras proteins are anchored to the plasma membrane and closely situated to various membrane-associated signaling molecules, including receptor tyrosine kinases (RTKs) and non-RTKs. Activation of these signaling molecules leads to the generation of the active GTP-bound Ras. As a Ras-GAP, neurofibromin promotes the hydrolysis of GTP, forming inactive Ras-GDP. Therefore, *NF1*-deficient tumors consistently exhibit excessive levels of Ras-GTP and activation of downstream signaling¹⁵.

Functioning as a molecular master switch, Ras regulates at least 11 different effector pathways, including the Raf/MEK/ERK mitogen-activated protein kinase (MAPK) and phosphoinositide 3-kinase (PI3K)/AKT/mammalian target of rapamycin (mTOR) pathways^{14,15}. Active GTP-bound Ras recruits Raf serine-threonine kinases to the cell membrane, where they are activated. The only validated targets for Raf kinases are the dual-specificity kinases MAPK/ERK kinases 1 and 2 (MEK1/2). Phosphorylated and activated MEKs in turn stimulate the dual-specificity extracellular signal-regulated kinases ERK1 and ERK2, also by phosphorylation. Activated ERKs have several effectors, including cell-cycle proteins, transcription factors, components of the protein translation apparatus, and other kinases and phosphatases.

The second major signaling pathway activated by Ras is the PI3K/AKT/mTOR axis. PI3 kinases promote membrane recruitment, leading to phosphorylation and activation of the serine/threonine protein kinase AKT by the phosphoinositide-dependent kinase 1 (PDK1). Activated AKT signals multiple downstream targets, promoting cell proliferation, survival, and motility¹⁶. AKT directly phosphorylates and inactivates the cyclin-dependent kinase (CDK) inhibitors p21^{WAF1} and p27^{Kip1}, inducing cell-cycle progression. Through phosphorylation of

mTOR, AKT promotes protein translation to support rapid cell growth.

The mTOR protein is an atypical serine/threonine kinase that has significant homology to PI3K¹⁷. It functions as a component in two multi-protein complexes, mTORC1 and mTORC2. Despite some overlap in protein compositions, the cellular functions of these complexes are distinct. By integrating various extracellular and intracellular signals, including growth factor receptor signaling and the levels of ATP, oxygen, and nutrients, mTORC1 regulates ribosome biogenesis and protein translation and is responsible for the growth factor-mediated G₁-to-S phase transition. The immunosuppressive and antiproliferative effects of rapamycin and related analogs (rapalogs) are due to their indirect inhibition of mTORC1. The regulation and cellular function of mTORC2 is not as well-understood. The complex is insensitive to nutrient levels but is responsive to growth factor-mediated activation of PI3K. Paradoxically, mTORC1 can negatively regulate the activity of mTORC2. Acute inhibition of mTORC1 by rapalogs can cause feedback activation of mTORC2, which then phosphorylates AKT on serine-473 and facilitates the full activation of AKT by PDK1. This results in the restoration of PI3K/AKT signaling as the mTORC1 blockade is bypassed.

In addition to activation of the MAPK and PI3K/AKT/mTOR pathways, *NF1*-deficient tumor cells frequently exhibit deregulation of several RTKs and non-RTKs. Neurofibromas express several RTK ligands, including insulin-like growth factor-1 (IGF-1), hepatocyte growth factor (HGF), and neuregulin/heregulin¹⁸. Neurofibromin also associates several non-Ras proteins, including protein kinases A and C, tubulin, and caveolin, suggesting that NF1 may have functions beyond acting as a RasGAP.

Recent evidence indicates that NF1-related PNFs can progress from atypical neurofibromatous neoplasms of uncertain biological potential (ANNUBP), which arise within

PNFs. These tumors often have deletions of *CDKN2A/B*¹⁸. Malignant progression to MPNSTs occurs when ANNUBP contract further mutations. Inactivating mutations in *CDKN2A*, *TP53*, *SUZ12*, and *EED* have been identified during malignant progression of PNFs to MPNSTs. *CDKN2A* and *TP53* encode cell-cycle regulators, permitting inappropriate DNA synthesis. *SUZ12* and *EED* encode subunits of polycomb repressor complex-2 (PRC2), an important chromatin modifier, and its loss enhances Ras-driven gene transcription in *NFI*-deficient cells¹⁹. Also, MPNSTs overexpress various RTKs including HGF receptor (HGFR or MET), epidermal growth factor receptor (EGFR), platelet-derived growth factor receptor (PDGFR), and insulin-like growth factor-1 receptor (IGF-1R), potentially resulting in autocrine growth signaling. These aberrantly activated RTKs directly activate Ras, and also initiate Ras-independent survival signals through proteins, such as PI3K and the STAT (signal transducers and activators of transcription) transcription factor family.

The *NF2* gene encodes a protein named merlin for moesin, ezrin, and radixin-like protein or schwannomin, a word derived from schwannoma, the most prevalent tumor seen in NF2^{20,21}. Most, if not all, VS, including sporadic tumors, have biallelic loss of the *NF2* gene. Likewise, *NF2* mutations have also been found in ~50% of meningiomas, regardless of whether they are sporadic or NF2-related¹¹. The similarity to the protein 4.1, ezrin, radixin, and moesin (FERM) family of membrane-associated proteins that link cell-surface receptors to the actin cytoskeleton provides clues to the biological functions of merlin²². Loss of merlin in embryonic fibroblasts results in defective cell-cell adhesion through destabilization of adherens junctions. Merlin negatively regulates the ligand-induced internalization and recycling of multiple RTKs, such as EGFR and PDGFR²². Merlin-deficient cells also overexpress several other RTKs, including IGF-1R, MET, and the EGFR family members ErbB2 and ErbB3²³. In addition, the loss of adherens

junctions correlates with abnormal activation of the non-RTK focal adhesion kinase (FAK), a downstream target of ECM-binding integrins and the RTK MET²⁴. Merlin also regulates the PI3K enhancer (PIKE)/PI3K pathway, decreasing AKT activation and increasing cell death²⁵.

Other inhibitory targets of merlin include the small GTPase Rac and its effectors, the p21-activated kinases (PAKs)^{26,27}. Rac is a close relative of Ras and is regulated in a similar fashion, cycling between the Rac-GTP active and Rac-GDP inactive states. Rac signaling is terminated by the protein RhoGAP interacting with CIP4 homologues (Rich1), and the activity of Rich1 is inhibited by the angiomin (Amot) family²⁸. Merlin binds to Amot, resulting in the release of Rich1 and repression of Rac signaling. Downstream of Rac, the PAK family is comprised of six closely-related kinases that control cytoskeletal remodeling and cell motility. Phosphorylated PAK has been observed in merlin-deficient schwannoma cells and fibroblasts, and overexpressing merlin inhibits Rac and PAK activity in *NF2*-null mesothelioma cells and Schwann cells²⁹. The deregulation of PAK signaling may underlie the enhanced invasiveness seen in *NF2*-deficient cells.

Originally discovered in the fruit fly *Drosophila melanogaster*, merlin is a suppressor of the Hippo signaling pathway³⁰. The serine-threonine kinase Hippo and its downstream substrates large tumor suppressor kinases 1 and 2 (Lats1/2) restrain the growth-promoting activity of the transcriptional coactivator Yes-associated protein (YAP)³¹. In many cell types, the angiomin isoform Amot-p130 interacts with YAP and promotes YAP-dependent transcriptional activity²⁸. Merlin binding to Amot-p130 disrupts this complex, suppressing YAP nuclear translocation. Merlin may also regulate Lats1/2 by associating with the E3 ubiquitin ligase CRL4^{DCAF1} in the nucleus and inhibiting the proteasomal degradation of Lats1/2³². The loss of merlin is therefore associated with enhanced YAP-dependent gene transcription and cell proliferation. Interestingly,

in *NF2*-deficient cells, one of the YAP-regulated genes is cyclooxygenase-2, which synthesizes prostaglandin E₂³³. The PGE₂ receptor has been associated with transactivation of EGFR signaling, providing an alternate way in which merlin inhibits EGFR signaling.

Further, merlin regulates mTOR activity in meningeal cells³⁴. Genetic silencing of merlin expression in normal arachnoidal cells resulted in mTORC1 activation as determined by phosphorylation of the downstream target ribosomal protein S6. These merlin-depleted cells displayed an enlarged morphology that resembled that of *NF2*-associated meningioma cells, and treatment with the mTORC1 inhibitor rapamycin reversed this phenotype. Both meningiomas and VS exhibit elevated phospho-S6 staining, suggesting common mTORC1 activation in *NF2*-deficient tumors. Consistently, mesothelioma cells with *NF2* loss exhibit aberrant integrin and PAK signaling, with downstream activation of mTORC1³⁵. This results in enhanced protein synthesis via mTORC1-mediated inhibition of the eIF4E-binding proteins (4E-BPs), which repress cap-dependent mRNA translation. Also, *NF2* deficiency in normal meningeal and meningioma cells correlates with mTORC2 activation, and rapamycin treatment amplifies mTORC2-mediated AKT phosphorylation³⁶. These results indicate that successful treatment of *NF2*-related tumors may likely require dual inhibition of mTORC1 and 2 activity³⁷.

The molecular mechanisms by which inactivation of the *LZTR1* or *SMARCB1/INI1* genes causes schwannomatosis are not fully understood. Mutations in *LZTR1* also occur in several cancer types, including ~22% of glioblastomas³⁸. As a member of the BTB-kelch superfamily, the LZTR1 protein is localized to the Golgi apparatus and acts as an adaptor for cullin 3 (Cul3)-containing E3 ubiquitin ligases¹³. The ubiquitin-proteasome system is critical for the proteolytic removal of misfolded or damaged proteins as well as the degradation of proteins with short half-lives, such as cell-cycle proteins. In this context, LZTR1 facilitates the polyubiquitination and

degradation of Ras³⁹ and may also negatively affect Ras membrane localization⁴⁰. Cul3-containing ubiquitin ligases promote cell differentiation, and *LZTR1*-depleted human Schwann cells have a gene expression signature consistent with a demyelinated proliferative phenotype. In addition, introducing LZTR1 to *LZTR1*-mutated glioblastoma cells decreases the expression of cyclin A and polo-like kinase 1, indicating the importance of LZTR1 in cell cycle progression³⁸.

SMARCB1 is a component of the SWItch/Sucrose Non-Fermentable (SWI/SNF) chromatin remodeling complex, which affects the accessibility of genes to transcription factors and RNA polymerases⁴¹. Several schwannomatosis-associated mutations in *SMARCB1* occur in the winged helix DNA-binding domain responsible for targeting the SWI/SNF complex to chromatin. Loss of *SMARCB1* function is associated with deregulated Hedgehog/Gli and Wnt/ β -catenin signaling. Additionally, SWI/SNF antagonizes PRC function, and loss of SMARCB1 results in PRC placing repressive histone methylation marks on other tumor suppressor proteins, such as the p16^{INK4A} CDK inhibitor⁴².

Collectively, these deregulated signaling pathways due to tumor suppressor loss in NF-associated tumors provide several targets for therapeutic development. Notably, some of these pathways include protein kinases, which already have multiple drugs approved by the FDA for cancers and other diseases.

Unique challenges for developing medical therapies for NF

Neurofibromatoses are systemic, life-long diseases with diverse manifestations. Drug safety and high efficacy must be carefully considered for these patients. Due to their anatomical locations, routine biopsies of NF-associated tumors may not be possible. Determination of appropriate endpoints and identification of biomarkers for drug efficacy are of great importance.

Noninvasive biomarkers need to be identified to accurately predict which patients most likely respond to therapy and to monitor drug pharmacodynamics. Owing to their benign nature, NF-associated tumors exhibit variable growth patterns, characterized by slow increases in tumor volume interspersed with periods of fast growth. NF1-related PNFs tend to rapidly expand during childhood but develop a more indolent growth pattern in adults. NF2-associated VS frequently display variable growth rates. Therefore, the reduction in tumor volume may not be an ideal endpoint, and other metrics such as time to progression, pain, and hearing loss should be considered to assess drug efficacy⁴³. NF2 and schwannomatosis are rare diseases, and patients with these diseases may be difficult to recruit to clinical trials unless the drugs are effective and well tolerated. For most NF-associated tumors, it is thought that the medication may well have to be taken for the patients' lives. The dosing regimen should be as simple as possible to aid in patient compliance, with a daily oral tablet being ideal.

Since the development of imatinib (Gleevec[®]), the first tyrosine kinase inhibitor to receive FDA approval in 2001, targeted small molecules have been a mainstay of cancer therapy. The identification of targets deregulated in NF-related tumors using traditional and systems biology approaches and the development of animal models have allowed the evaluation of a number of these drugs. Several have advanced to clinical trials, culminating in April 2020 FDA approval of the MEK inhibitor selumetinib (Koselugo[™]) for the treatment of pediatric patients with symptomatic, inoperable PNF⁶. It is anticipated that additional targeted compounds in development will be successful. The preclinical and clinical evaluation of these targeted drugs have been focused in several recent reviews. Below, we summarize the current status of research on natural compounds as potential therapeutics for NF-associated tumors.

Natural compounds for preventative purposes and for the potential treatments of NF

Natural compounds from terrestrial microbes, higher plants, and marine organisms have been studied as cancer chemotherapeutic agents for many decades. Over the last 40 years, ~50% of FDA-approved drugs have been either natural products, natural product derivatives, or synthesized based on a pharmacophore originally identified in a natural product⁴⁴. For example, anti-neoplastic agents, such as anthracyclines, which intercalate DNA, are made by *Streptomyces* bacteria. Taxol[®] (paclitaxel), which suppresses microtubule dynamics, was originally isolated from the bark of the Pacific yew. Due to the slow-growing nature of this plant, taxol is manufactured semi-synthetically from a precursor and biosynthesized in *E. coli* and yeast. The topoisomerase I inhibitor camptothecin was obtained from the bark and stem of *Camptotheca acuminata* (happy tree). Several camptothecin analogs, including topotecan (Hycamtin[®]) and irinotecan (Camptosar[®]), have been synthesized. Trabectedin (Yondelis[®], ecteinascidin 743, ET-743), which interferes with transcription and related processes, was discovered from extracts of the sea squirt *Ecteinascidia turbinata* and later found to come from *Candidatus Endoecteinascidia frumentensis*, a γ -proteobacterium living in symbiosis with the sea squirt. Since natural compounds tend to have diverse structural complexity and may inhibit proteins previously thought to be untargetable, the U.S. National Cancer Institute has divisions focused on drug discovery within the natural product space that aim to identify compounds that inhibit difficult targets. Also, these compounds have served valuable roles as probes to delineate the signaling pathways responsible for driving tumor cell growth⁴⁵.

In addition to anti-neoplastic activity, natural compounds may possess antioxidant and anti-inflammatory effects and are a particularly attractive potential adjunct therapy for patients with tumor predisposition syndromes, such as NF. Due to limited treatment options, patients afflicted

by NF often take them in the form of dietary supplements and for health enhancement purposes. Although much research has been conducted to evaluate the anti-tumor activity of several natural products, most studies only report *in vitro* effects for a given compound. Sometimes extremely high doses were used, which may not be achievable or even desirable *in vivo*. At high concentrations, small molecules may result in off-target effects, unwanted redox activities, and anomalous plasma membrane permeability. Some natural products are sold as dietary supplements that are labeled to be safe and have health benefits but have not been validated for their claims. Many botanical dietary supplements are crude extracts, containing a mixture of compounds. The identities of the active components in the extracts are not known, and lot-to-lot variability could contribute to irreproducible results. Compound sourcing may affect the activity of natural products, especially when they are extracts or over-the-counter products. Also, some over-the-counter supplements may have dangerous contaminants, such as heavy metals, or may not contain the claimed ingredients. Therefore, botanical dietary supplements should be carefully verified for their overall chemical composition and safety⁴⁶. For purified single-chemical entity natural products that may be developed into new therapies for NF, it is important that their biological activities be carefully understood and that they be treated as tractable hits, which are defined as compounds with rational structure-activity relationships.

Phenolic compounds. Characterized by the presence of one or more phenol functional groups, these compounds include flavonoids, which are usually found in herbs, citrus fruits, and plants, and non-flavonoids, which are also found in plants and include the ellagitannins in strawberries and curcuminoids in turmeric⁴⁷. However, phenolic compounds may be difficult to develop into drugs as many nonspecifically perturb cell membranes and alter protein function.

The sections below summarize several phenolic compounds that have been evaluated, mostly *in vitro*, in NF-related tumor models.

(i) ***Curcumin and other curcuminoids.*** The diarylheptanoid curcumin is isolated from turmeric (*Curcuma longa*) and comprises 2-5% of the plant rhizome. Turmeric is commonly used in Indian cooking and is a component in Ayurvedic medicine for treating infections, inflammation, and other chronic conditions. Curcumin possesses anti-inflammatory properties through inhibition of the NF- κ B pathway, although the IC₅₀ (50% inhibitory concentration) value needed to observe these effects is relatively high ($\sim 20 \mu\text{M}$)⁴⁸. It also exhibits anti-inflammatory effects through suppression of phospho-Stat3 and interferes with the Warburg effect in cancer cells at similar doses⁴⁹. In contrast, curcumin can induce apoptosis by increasing pro-inflammatory oxidative damage⁵⁰, suggesting cell context dependence. Also, curcumin blocks p21-activated kinase 1 (PAK1)-dependent proliferation of gastric tumor cells.

In HEI-193, a human papillomavirus E6/7 oncogene-transformed cell line established from an NF2-associated vestibular schwannoma, curcumin dose-dependently inhibited colony formation by downregulating the ERK, AKT and NF- κ B pathways while increasing free radical-mediated apoptosis⁵⁰. However, the use of this cell line as an NF2-related cell model is of concern as viral oncogene transformation alters growth signaling and behavior of benign schwannoma cells. Also, the IC₅₀ value of curcumin in HEI-193 cells is relatively high (20 μM). In addition, curcumin enhanced the expression of heat shock protein 70 (HSP70), a molecular chaperone that is associated with drug resistance. Combining curcumin with the pan-HSP inhibitor KNK437 showed synergistic growth inhibition in HEI-193 cells, although the concentrations for both of these compounds used remained in the high micromolar range. Previously, we found that the IC₅₀ value of curcumin was $\sim 20 \mu\text{M}$ in primary VS cells⁵¹ and ~ 7

μM in *NF2*-deficient Ben-Men-1 benign meningioma cells (our unpublished data).

A dietary study in *NF1* patients with neurofibromas fed a Mediterranean diet supplemented with curcumin reported a 30-51% reduction in the number of neurofibromas⁵². However, a Western diet with the same supplement did not show any tumor inhibition, confounding the interpretation on the effects of curcumin. In addition, this was an unblinded study with only 2-3 patients per treatment group. Further studies with a large cohort of patients are needed to confirm these findings. A closely related curcuminoid, calebin-A, has also been tested in *NF1*-deficient MPNST cells. While this compound decreased the levels of phospho-AKT and survivin, the dose range was relatively high (12.5 to 25 μM)⁵³.

Curcumin has short half-life in aqueous solutions (<5 minutes), making makes it imperative that experiments be rigorously conducted with proper controls to ensure that the observed treatment effects are due to curcumin but not its degradation products⁵⁴. The instability of curcumin along with poor bioavailability may explain why many early clinical trials did not detect any significant clinical effects. To circumvent these issues, alternative delivery approaches have been explored. One approach used red blood cells coated with porous nanoparticles to deliver curcumin into tumor-bearing mice, resulting in ~72% reduced tumor volume of mouse hepatocellular carcinoma allografts. Other alternatives to increase the bioavailability of curcumin, including protein nanoparticles and liposomal formulations, may improve treatment outcomes.

(ii) *Propolis constituents*. Also called bee glue, propolis is found in beehives and has been used since the time of the ancient Egyptian civilization for its anti-inflammatory, anti-bacterial, and wound-healing properties. It comprises an admixture of different chemicals with wide variability in composition depending upon factors, such as the regional flora, climatic

conditions, and preparation method⁵⁵. Therefore, any studies using crude propolis extracts are highly liable to exhibit a lot-to-lot variability in their biological effects. Propolis contains a mixture of multiple compounds. A study of Chinese red propolis reported that it inhibited VEGF expression in breast adenocarcinoma cells, and high-performance liquid chromatography analysis revealed at least 12 components, including the phenolic ester, caffeic acid phenethyl ester (CAPE), and the flavonoid, kaempferol. Turkish propolis induces G₁ arrest and apoptosis in a variety of cancer cell lines and contains six major constituents, including caffeic acid and CAPE. Polish propolis inhibits S-phase entry and decrease cell viability of glioblastoma cells and contains multiple flavonoids. Bio 30 is a water-miscible extract of New Zealand propolis, which contains multiple phenolic compounds including CAPE, and suppresses the growth of HEI-193 schwannoma and *NFI*-deficient S462 MPNST cells and xenografts⁵⁶. Among these propolis specimens, a common constituent is CAPE, which possesses antiproliferative activity in multiple cancer cell lines. However, the IC₅₀ values in these cells are above 20 μM. We also found that CAPE has little growth-inhibitory activity in VS cells at doses up to 20 μM⁵¹ and modest activity in meningioma cells at doses up to 30 μM cells (our unpublished data). Propolis has been studied as a potential adjuvant to reduce the side effects and to improve efficacy of standard chemotherapy drugs⁵⁵.

(iii) **Honokiol**. As a biphenolic lignan from the bark of trees in the genus *Magnolia*, honokiol is commonly consumed as an ingredient of an herbal tea preparation in Asia that has been used for anxiety in traditional Chinese medicine. In HEI-193 schwannoma cells, honokiol inhibited cell proliferation and decreased phospho-AKT and ERK1/2 at a relatively high IC₅₀ of ~26 μM⁵⁷. It also reduces the growth of human breast carcinoma xenografts and induces apoptosis in chronic lymphoblastic leukemia and multiple myeloma cells. Although honokiol has

been reported to cross the BBB, its oral bioavailability and plasma half-life are quite low⁵⁸.

Several approaches have been attempted to solve these issues, including encapsulating honokiol in nanoparticles where the compound maintains activity against human ovarian and liver cancer cells.

(iv) *trans-Resveratrol*. This stilbenoid was isolated originally from white hellebore, but is found widely in various fruits and nuts, including red grapes, apples, and pistachios⁵⁹. It has beneficial metabolic effects in mouse models of diet-induced diabetes. It was originally thought to exert these effects by directly enhancing the catalytic activity of the nicotinamide-adenine dinucleotide (NAD⁺)-dependent protein deacetylase sirtuin 1 (SIRT1), but was later discovered that this mechanism was an experimental artifact due to resveratrol-mediated interaction with the fluorophore used in a fluorescent deacetylase assay. Resveratrol may indirectly activate SIRT1 or another potential molecular target adenosine monophosphate kinase (AMPK). Resveratrol also promotes autophagy and negatively modulates insulin and IGF-1 signaling. Low doses of resveratrol reduce the number of adenomas in a mouse model of colorectal carcinoma that receives a high-fat diet⁶⁰. Treated mice display activated AMPK and increased p21^{Waf1} expression in the intestinal mucosa. These results suggest that resveratrol may have chemopreventive effects. In clinical trials, resveratrol is well-tolerated and reaches a maximum plasma concentration of ~2.4 μM. However, due to the potential for adverse effects, the doses of resveratrol need to be reduced to significantly below the maximum tolerated dose⁶¹. Therefore, most of the effects observed in cell cultures typically require 5-100 μM, which are not safely achievable in humans. In VS cells and *NF2*-deficient Ben-Men-1 meningioma cells, resveratrol exhibits moderate antiproliferative activity at doses up to 20 μM⁵¹ and 30 μM (our unpublished data), respectively. In *NF2*-expressing HBL-52 benign meningioma cells, the IC₅₀ for resveratrol

was around 100 μM and the effective dose for inducing apoptosis was above 50 μM ⁶².

(v) **Quercetin.** As a pigmented pentahydroxylated flavone named after *quercetum* (Latin for oak forest), quercetin is widely found in oaks (genus *Quercus*) and many herbs, fruits, and vegetables. It induces apoptosis at a relative high dose and moderately reduces the growth of breast cancer xenografts and colorectal cancer allografts⁶³. Quercetin stabilizes the expression of the merlin protein with *NF2* missense mutations, although at fairly high doses of $>25 \mu\text{M}$ ⁶⁴. It is not known whether these concentrations can be achieved pharmacologically in humans. Additionally, quercetin is known to aggregate and promiscuously bind to proteins, making it less therapeutically effective.

(vi) **Uncharacterized constituents of Sichuan pepper extract.** The Sichuan peppercorns harvested from the seeds of the aromatic spiny shrub *Zanthoxylum piperitum* are used in East Asian cuisine as well as traditional Chinese medicine. These peppercorn extracts inhibit proliferation of *NF1*-deficient MDA-MB-231 breast cancer cells and MPNST cells by reducing PAK1 activation and cyclin D₁ levels⁶⁵. An extract also suppressed *NF1*-deficient MDA-MB-231 xenografts, but resistant cell populations rapidly developed during treatment, suggesting only transient benefits. Additionally, the active constituents in Sichuan pepper extract responsible for the antiproliferative effects have not been determined.

Isoprenoids. Terpenoids and steroids are both isoprene-derived, with terpenes being a type of naturally occurring hydrocarbons that were originally named for their occurrence in turpentine, a resin distilled from conifer sap. Isoprenoids are the largest group of natural products. Although they are mainly found in plants, some classes such as steroids are common in animals. In plants, terpenoids are often found as aromatic compounds that play important roles in

signal transduction and acts as a defense against herbivores⁶⁶. Terpenoids have great structural diversity and, as mentioned above, are made up of repeating units of the C₅-hydrocarbon, isoprene. They are broadly classified based on the number and structural organization of these isoprene units. For example, sesquiterpene lactones consist of three isoprenes linked to a lactone ring, and tetracyclic triterpenoids have six isoprene units arranged in four rings. Although the words terpenes and terpenoids are often used interchangeably, terpenoids more properly refer to modified terpenes that have additional oxygenated functional groups.

(i) **Cucurbitacin.** Originally isolated from the squash family (Cucurbitaceae), cucurbitacins are tetracyclic triterpenoids with a steroidal skeleton⁶⁷. These compounds are also found in a wide range of plant families and some mushroom genera. They often have glycosidic linkages and are classified into multiple variants according to their side chains. Cucurbitacins are contained in traditional preparations used to treat viral diseases and inflammatory conditions in Asia. Cucurbitacin B exhibits antiproliferative effects in breast cancer and glioblastoma cells by disrupting microtubule polymerization and the cytoskeleton. It also inhibits the growth of acute myelogenous leukemia cells by decreasing phospho-KIT and phospho-AKT. Cucurbitacin C suppresses the growth of multiple cancer cell lines at IC₅₀ concentrations of <200 nM. This compound also increases the levels of p21^{WAF1}, induces cell-cycle arrest at G₁ or G₂/M depending on the cell type, and promotes cell death. In gastric cancer cells, cucurbitacin E inhibits AKT phosphorylation, arrests cells at G₂/M, and modestly suppresses tumor xenograft growth. Also, this compound induces apoptosis in leukemia cells. Cucurbitacin I effectively inhibits proliferation of *NFI*-null MPNST cells and induces apoptosis by decreasing STAT3 signaling⁶⁸. We have also shown that cucurbitacin D has anti-proliferative activity against *Nf2*-null mouse schwannoma and *NF2*^{-/-} human meningioma cells⁶⁹. In both cell types, sub-

micromolar IC₅₀ concentrations of cucurbitacin D decreased the expression of cyclins and phospho-AKT and caused G₂/M arrest. Despite their anti-tumor activity, cucurbitacins exhibit nonspecific toxicity and a low therapeutic index, which hamper their further clinical development⁶⁷.

(ii) Celastrol. Originally isolated from *Tripterygium wilfordii* (colloquially known as thunder god vine), celastrol (tripterine) is a pentacyclic triterpenoid, which exhibits anti-obesity, antioxidant, anti-inflammatory, and anti-tumor effects⁷⁰. It inhibits NF-κB signaling and multiple other pathways. Celastrol reduces proliferation and invasion of ovarian cancer cells with an IC₅₀ of ~2 μM. At lower concentrations (800 nM), celastrol impeded the degradation of the merlin protein in malignant meningioma cells carrying a missense mutation in the *NF2* gene⁶⁴. However, celastrol has a problematic *ortho*-quinone methide functional group that possesses redox activity and is reactive promiscuously with the sulfur nucleophiles found in the active sites of several enzymes, including metabolic coenzymes, needed by normal cells. These features may explain the serious adverse effects that have been reported after consuming *T. wilfordii* supplements⁷¹.

(iii) Goyazensolide. Isolated from *Eremanthus goyazensis* (commonly called velvetshrub), a member of the sunflower family (*Asteraceae*), goyazensolide is a sesquiterpene lactone. It was identified initially as an anti-schistosomal agent and also has antiproliferative activity against colorectal carcinoma cells by inhibiting NF-κB expression and inducing apoptosis⁷². We found that goyazensolide suppresses proliferation of *Nf2*-deficient mouse schwannoma cells and human *NF2*^{-/-} meningioma cells at IC₅₀ doses of ~1 μM⁶⁹. These growth-suppressive effects appear to be due to the decreased expression of AKT and cyclins E, A, and B, followed by prominent G₂/M arrest. Unfortunately, goyazensolide was too toxic in mice at

therapeutic doses for further development (our unpublished observation).

(iv) DAW22. This compound is a sesquiterpene coumarin isolated from the roots of *Ferula ferulaeoides*, a member of the carrot family (Apiaceae). It is antiproliferative and proapoptotic but at relatively high IC₅₀ doses, ranging from 30-47 μ M in five sporadic and NF1-associated MPNST cell lines⁷³. Also, it modestly suppresses tumor growth in a mouse xenograft model of sporadic MPNST. For these reasons, DAW22 has not been further evaluated as a potential MPNST treatment.

Sulforaphane. Frequently found as a glycosidic precursor form in cruciferous vegetables of the mustard family (Brassicaceae), sulforaphane is a sulfur-containing compound and a member of the isothiocyanate compound class⁷⁴. It has anti-inflammatory and anti-neoplastic activities in several types of cancer cells, possibly acting via inhibition of NF- κ B. In HEI-193 schwannoma cells, sulforaphane has growth-inhibitory effects; however, the IC₅₀ value was relatively high (>10 μ M)⁷⁵. We also found that sulforaphane inhibited the growth of primary VS cells at an IC₅₀ of >20 μ M⁵¹ and NF2-deficient meningioma cell growth at an IC₅₀ of ~30 μ M (our unpublished data). These results indicate that sulforaphane is not very effective against NF2-related tumor cells.

Cannabinoids. These compounds are the characteristic constituents of *Cannabis sativa*, commonly known as marijuana or hemp. This plant is used in traditional Chinese and Ayurvedic medicine, but in the West is more well-known as a recreational drug. Cannabis extracts as well as individual cannabinoids have been increasingly used medicinally, including by patients suffering from glaucoma, neuropathic pain, and cancer⁷⁶. Although *Cannabis sativa* varieties

synthesize about 100 different cannabinoid metabolites, two compounds have been primarily studied for their clinical effects, Δ^9 -tetrahydrocannabinol (THC) and cannabidiol (CBD). THC is best known for its appetite stimulation and psychoactive properties and is a Schedule 1 controlled substance. Dronabinol (Marinol[®], Syndros[™]) is a synthetic analog of THC that is FDA-approved for the treatment of HIV-induced loss of appetite and chemotherapy-related nausea and vomiting. CBD is thought to have analgesic and anxiolytic effects and is considered to have a low potential for abuse. Although plant-derived CBD is a Schedule 1 substance, chemically-synthesized CBD is sold legally as an over-the-counter supplement in the U.S. The FDA recently approved a purified CBD extractive (Epidiolex) to treat Lennox-Gastaut syndrome and Dravet syndrome, two rare forms of severe epilepsy. Cannabinoids are thought to have anti-tumor activity through their effects on the CB₁ and CB₂ endocannabinoid receptors⁷⁷. The aminoalkylindole, WIN-55212-2, a synthetic cannabinoid, is an agonist of the endocannabinoid receptors and inhibits prostate carcinoma cell proliferation by inducing G₁ cell cycle arrest⁷⁸. However, in some contexts, cannabinoids may be pro-tumorigenic. For example, glioblastoma and lung cancer cells treated with 100-300 nM of THC or synthetic cannabinoids show accelerated proliferation via transactivation of EGFR⁷⁹.

Cannabinoids could play a role in controlling NF1-associated neuropathic pain and mood disorders as a case report of CBD in an NF1 patient indicated success in pain relief and mood control⁸⁰; however, a systematic study has not been conducted. A meta-analysis of various cannabinoids indicated that oral administration of cannabinoids did not yield statistical significance in pain relief, but intramuscular delivery of the synthetic THC analog levonantradol (CP50,556-1) produced significant analgesic effects, compared to placebo⁸¹. Studies with a larger number of patients are needed to confirm these findings. Overall, the pain relief qualities

of cannabinoids require more rigorous clinical examination to validate analgesic qualities.

Ivermectin. The anti-parasitic avermectins were originally isolated from the soil bacterium, *Streptomyces avermitilis*. Subsequently, a semi-synthetic derivative of avermectin B₁, ivermectin, was developed and has been used routinely in veterinary medicine to treat parasite infestations, including worms, ticks, and mites. Ivermectin has also been approved by the FDA to treat river blindness and other nematode infections in humans. Two of the discoverers of ivermectin, William C. Campbell and Satoshi Ōmura, were awarded the 2015 Nobel Prize in Physiology or Medicine. Ivermectin has anti-tumor activity in various types of cancer. It inhibits proliferation of several ovarian cancer cell lines and HEI-193 schwannoma cells at IC₅₀ values of 10-20 μM and 5 μM, respectively, by blocking PAK1 and decreasing phospho-Raf⁸². However, the FDA-approved therapeutic dose of ivermectin in humans could only reach plasma concentrations of <100 nM⁸³. Ivermectin is a substrate for the multidrug receptor 1 (MDR1) transporter, which prevents the drug from reaching high concentrations in the brain. Thus, this drug is not likely to be effective against VS and meningiomas.

Silvestrol, rocaglamide, and didesmethylrocaglamide. Rocaglates, also called flavaglines, are a large family of cyclopenta[*b*]benzofurans that are synthesized by tropical trees of the *Aglaia* genus in the mahogany family Meliaceae⁸⁴. Among this family of natural compounds, rocaglamide (also known as rocaglamide A or RocA) was the first to be isolated and found to possess antileukemic activity⁸⁵. Due to its scarcity, this compound was not further investigated for human use. Subsequently, a few other rocaglates, including silvestrol, were identified. Originally discovered in *Aglaia foveolata*, silvestrol was the first flavagline with an unusual

sugar-like dioxanyl ring⁸⁶. Silvestrol has potent anti-proliferative activity at low nanomolar concentrations similar to camptothecin and paclitaxel in a variety of cancer cell lines⁸⁴. It acts as an inhibitor of the eukaryotic translation initiation factor 4A (eIF4A), an RNA helicase important for protein translation initiation⁸⁷. Silvestrol binds eIF4A and locks it onto purine-rich sequences in the 5'-untranslated region (UTR) of certain mRNAs, leading to translation inhibition⁸⁸. As the transcripts for many oncogenic proteins contain G-rich 5'-UTRs that form complex secondary structures, silvestrol treatment diminishes translation of these proteins. Rocaglamide and some synthetic rocaglates have also been found to operate in a similar fashion⁸⁹.

We have shown that benign and malignant schwannomas (VS and MPNSTs) as well as meningiomas frequently overexpress the eIF4F components, including eIF4A^{51,90}. Genetic depletion of eIF4A using short hairpin RNAs and pharmacological inhibition by silvestrol effectively suppress proliferation of these tumor cells. As an eIF4A inhibitor, silvestrol reduces the protein levels of multiple cyclins and oncogenic kinases, including AKT, ERK, and FAK, leading to G₂/M arrest and apoptosis. When delivered by intraperitoneal injection, silvestrol profoundly suppresses tumor growth of *Nf2*^{-/-} schwannomas and *NF1*^{-/-} MPNSTs. However, a toxicology study in dogs revealed that it caused lung damage

https://dtp.cancer.gov/publications/silvestrol_rocaglamide_studies.pdf), and its further clinical development was suspended. By side-by-side comparing 10 silvestrol-related rocaglates⁹¹, we identified rocaglamide and didesmethylrocaglamide (also called RocB) with growth-inhibitory activity comparable to silvestrol in MPNST, schwannoma, and meningioma cells⁹². Treatment with these compounds reduced expression of multiple oncogenic kinases IGF-1R, AKT, and ERKs while simultaneously inducing DNA damage response, caspase cleavage, and cell death. Also, we showed that rocaglamide exhibited 50% oral bioavailability and was not susceptible to

multi-drug resistance 1 (MDR1) efflux. When delivered by oral gavage or intraperitoneal injection, rocaglamide potently suppressed tumor growth in an MPNST xenograft mouse model. Most importantly, rocaglamide was well tolerated in mice and did not induce the pulmonary toxicity found with silvestrol in dogs, even when administered at higher doses. Furthermore, we have also found that rocaglamide and didesmethylrocaglamide exhibited strong anti-tumor effects against other types of sarcomas, including osteosarcoma, Ewing sarcoma, and rhabdomyosarcoma. These results suggest that a clinical trial is warranted to evaluate these rocaglamides in patients with sarcomas and those afflicted by NF in the future. It should also be mentioned that the synthetic rocaglate (-)-CR-1-31B prolongs survival of mice bearing pancreatic ductal adenocarcinoma allografts⁹³. Another synthetic rocaglate-like compound, eFT226 (zotatifin), has anti-tumor activity against several fibroblast growth factor receptor- and ErbB2-driven cancers⁹⁴ and has recently entered a phase 1/2 clinical trial in patients with K-Ras- or RTK-driven advanced solid tumors (ClinicalTrials.gov Identifier: NCT04092673).

Annonacin. Also called guyabano or graviola, soursop is the fruit of *Annona muricata*, a member of the custard apple family (Annonaceae). With its pleasant aroma, soursop fruits have been used to make juices and as a flavoring agent. A tea can be made from steeping the leaves. Extracts from fruits and leaves of soursop are reported to have anti-tumor activity, including anecdotally shrinking NF2-associated vestibular schwannomas⁹⁵. One active principle in soursop is annonacin, an acetogenin with potent anti-proliferative activity against estrogen-receptor positive breast cancer cells and xenografts; however, this compound inhibits mitochondrial complex I and can have severe neurotoxic effects, potentially causing atypical Parkinson's disease⁹⁶. This serious adverse effect prevents it from further development as an anti-tumor

compound.

Additionally, there are several natural compounds that may be of interest to NF patients. Silibinin, the main active flavonolignan component of the extract of the seeds of milk thistle (*Silybum marianum*), a plant used in folk medicine to treat liver toxicity caused by poisoning from the death cap mushroom *Amanita phalloides*, inhibits lung cancer cell proliferation by suppressing AKT and ERK activation and reducing matrix metalloproteinase expression⁹⁷. Gingerol, an alkylphenol found in ginger, decreases the growth of breast cancer cells by lowering the expression of EGFR and β 1-integrin⁹⁸. Shikonin, a naphthoquinone pigment found in the root of *Lithospermum erythrorhizon* in the borage family (Boraginaceae), has been used in traditional Chinese medicine for the treatment of inflammatory diseases. It inhibits the growth of several acute lymphocytic leukemia and histiocytic leukemia cell lines and decreases phosphorylated AKT and ERKs⁹⁹. *Angelica sinensis*, commonly known as dong quai (danggui or dang'ui) is an herb in the carrot family (Apiaceae) that is used in traditional Asian medicine for reproductive disorders. One of the active components in dong quai is the γ -lactone *N*-butylidenephthalide (BP), which suppresses proliferation of gastric carcinoma cells by increasing the levels of REDD1 (regulated in development and DNA damage responses 1), a negative regulator of the mTOR pathway¹⁰⁰. Genistein is an isoflavone found in soy-based foods, such as soymilk. It induces apoptosis and reduces tumor vascularity in stomach and colon cancers and suppresses prostate cancer metastasis by inhibiting cyclins and AKT activation¹⁰¹. Epigallocatechin gallate (EGCG) is the most abundant catechin ester found in green tea (*Camellia sinensis*). It decreases phosphorylation of PI3K and AKT and reduces IGF-1R protein levels in some cancer cells¹⁰². Since these natural compounds inhibit the signaling pathways that are frequently activated in

NF-associated tumors, it will be interesting to see whether they have any effects in NF-related cell culture and animal models.

Conclusion

NF are characterized by multiple nervous system tumors and other non-tumoral manifestations. The recent approval of the MEK inhibitor selumetinib (Koselugo[®]) for the treatment of NF1-associated plexiform neurofibroma suggests that medications targeting specific NF signaling pathways can be successful. However, additional drugs and drug combinations that block multiple signaling pathways may be required to eradicate the disease. Several other targeted compounds are being clinically evaluated to treat various NF-associated tumors. It is anticipated that some of them will prove to be efficacious. Also, natural compounds have been investigated as potential cancer therapies for many decades, and several of them are on the World Health Organization's List of Essential Medicines. Of the natural compounds that have been evaluated, the novel eIF4A inhibitors rocaglamide and didesmethylrocaglamide have demonstrated promising preclinical data with good bioavailability and anti-tumor efficacy and are expected to enter clinical trials in the near future.

Acknowledgments

This study was supported by grants from the Department of Defense W81XWH-14-1-0167 to DBW, National Cancer Institute P01CA125066 to ADK, and the Galloway Family, Advocure NF2, CancerFree KIDS, Sunbeam Foundation, and Department of Defense W81XWH-18-1-0547 to LSC.

References:

1. Plotkin SR, Wick A. Neurofibromatosis and schwannomatosis. *Semin Neurol*. 2018;38(1):73-85.
2. Evans DGR, Salvador H, Chang VY, et al. Cancer and central nervous system tumor surveillance in pediatric neurofibromatosis 1. *Clin Cancer Res*. 2017;23(12):e46-e53.
3. Chamseddin BH, Le LQ. Management of cutaneous neurofibroma: current therapy and future directions. *Neurooncol Adv*. 2019;2(Suppl 1):i107-i116.
4. Kim A, Stewart DR, Reilly KM, Viskochil D, Miettinen MM, Widemann BC. Malignant peripheral nerve sheath tumors state of the science: leveraging clinical and biological insights into effective therapies. *Sarcoma*. 2017;2017:7429697.
5. Costa ADA, Gutmann DH. Brain tumors in neurofibromatosis type 1. *Neurooncol Adv*. 2020;2(Supplement 1):i85-i97.
6. Gross AM, Wolters PL, Dombi E, et al. Selumetinib in children with inoperable plexiform neurofibromas. *N Engl J Med*. 2020;382(15):1430-1442.
7. de Blank PMK, Fisher MJ, Liu GT, et al. Optic pathway gliomas in neurofibromatosis type 1: an update: surveillance, treatment indications, and biomarkers of vision. *J Neuroophthalmol*. 2017;37(Suppl 1):S23-S32.
8. Wu LMN, Lu QR. Therapeutic targets for malignant peripheral nerve sheath tumors. *Future Neurol*. 2019;14(1):FNL7.
9. Evans DGR, Salvador H, Chang VY, et al. Cancer and central nervous system tumor surveillance in pediatric neurofibromatosis 2 and related disorders. *Clin Cancer Res*. 2017;23(12):e54-e61.

10. Kruchko C, Ostrom QT, Gittleman H, Barnholtz-Sloan JS. The CBTRUS story: providing accurate population-based statistics on brain and other central nervous system tumors for everyone. *Neuro Oncol.* 2018;20(3):295-298.
11. Goutagny S, Kalamarides M. Meningiomas and neurofibromatosis. *J Neuro-Oncol.* 2010;99(3):341-347.
12. Smith MJ, Isidor B, Beetz C, et al. Mutations in LZTR1 add to the complex heterogeneity of schwannomatosis. *Neurology.* 2015;84(2):141-147.
13. Kehrer-Sawatzki H, Farschtschi S, Mautner V-F, Cooper DN. The molecular pathogenesis of schwannomatosis, a paradigm for the co-involvement of multiple tumour suppressor genes in tumorigenesis. *Hum Genet.* 2017;136(2):129-148.
14. Karnoub AE, Weinberg RA. Ras oncogenes: split personalities. *Nat Rev Mol Cell Biol.* 2008;9(7):517-531.
15. Zhou B, Der CJ, Cox AD. The role of wild type RAS isoforms in cancer. *Semin Cell Dev Biol.* 2016;58:60-69.
16. Goncalves MD, Hopkins BD, Cantley LC. Phosphatidylinositol 3-kinase, growth disorders, and cancer. *N Engl J Med.* 2018;379(21):2052-2062.
17. Laplante M, Sabatini DM. mTOR signaling in growth control and disease. *Cell.* 2012;149(2):274-293.
18. Lemberg KM, Wang J, Pratilas CA. From genes to -omics: the evolving molecular landscape of malignant peripheral nerve sheath tumor. *Genes.* 2020;11(6):691.
19. De Raedt T, Beert E, Pasmant E, et al. PRC2 loss amplifies Ras-driven transcription and confers sensitivity to BRD4-based therapies. *Nature.* 2014;514(7521):247-251.

20. Rouleau GA, Merel P, Lutchman M, et al. Alteration in a new gene encoding a putative membrane-organizing protein causes neuro-fibromatosis type 2. *Nature*. 1993;363(6429):515-521.
21. Trofatter JA, MacCollin MM, Rutter JL, et al. A novel moesin-, ezrin-, radixin-like gene is a candidate for the neurofibromatosis 2 tumor suppressor. *Cell*. 1993;72(5):791-800.
22. Casaletto JB, McClatchey AI. Spatial regulation of receptor tyrosine kinases in development and cancer. *Nat Rev Cancer*. 2012;12(6):387-400.
23. Lallemand D, Manent J, Couvelard A, et al. Merlin regulates transmembrane receptor accumulation and signaling at the plasma membrane in primary mouse Schwann cells and in human schwannomas. *Oncogene*. 2009;28(6):854-865.
24. Fernandez-Valle C, Tang Y, Ricard J, et al. Paxillin binds schwannomin and regulates its density-dependent localization and effect on cell morphology. *Nat Genet*. 2002;31(4):354-362.
25. Rong R, Tang X, Gutmann DH, Ye K. Neurofibromatosis 2 (NF2) tumor suppressor merlin inhibits phosphatidylinositol 3-kinase through binding to PIKE-L. *Proc Natl Acad Sci USA*. 2004;101(52):18200-18205.
26. Kissil JL, Wilker EW, Johnson KC, Eckman MS, Yaffe MB, Jacks T. Merlin, the product of the Nf2 tumor suppressor gene, is an inhibitor of the p21-activated kinase, Pak1. *Mol Cell*. 2003;12(4):841-849.
27. Morrison H, Sperka T, Manent J, Giovannini M, Ponta H, Herrlich P. Merlin/neurofibromatosis type 2 suppresses growth by inhibiting the activation of Ras and Rac. *Cancer Res*. 2007;67(2):520-527.

28. Yi C, Troutman S, Fera D, et al. A tight junction-associated merlin-angiomin complex mediates merlin's regulation of mitogenic signaling and tumor suppressive functions. *Cancer Cell*. 2011;19(4):527-540.
29. Zhou L, Hanemann CO. Merlin, a multi-suppressor from cell membrane to the nucleus. *FEBS Letters*. 2012;586(10):1403-1408.
30. Hamaratoglu F, Willecke M, Kango-Singh M, et al. The tumour-suppressor genes NF2/Merlin and Expanded act through Hippo signalling to regulate cell proliferation and apoptosis. *Nat Cell Biol*. 2006;8(1):27-36.
31. Zhao B, Li L, Lei Q, Guan K-L. The Hippo–YAP pathway in organ size control and tumorigenesis: an updated version. *Genes Dev*. 2010;24(9):862-874.
32. Li W, You L, Cooper J, et al. Merlin/NF2 suppresses tumorigenesis by inhibiting the E3 ubiquitin ligase CRL4(DCAF1) in the nucleus. *Cell*. 2010;140(4):477-490.
33. Guarrant W, Kota S, Troutman S, et al. YAP mediates tumorigenesis in neurofibromatosis type 2 by promoting cell survival and proliferation through a COX-2–EGFR signaling axis. *Cancer Res*. 2016;76(12):3507-3519.
34. James MF, Han S, Polizzano C, et al. NF2/merlin is a novel negative regulator of mTOR complex 1, and activation of mTORC1 is associated with meningioma and schwannoma growth. *Mol Cell Biol*. 2009;29(15):4250-4261.
35. López-Lago MA, Okada T, Murillo MM, Socci N, Giancotti FG. Loss of the tumor suppressor gene NF2, encoding merlin, constitutively activates integrin-dependent mTORC1 signaling. *Mol Cell Biol*. 2009;29(15):4235-4249.

36. Beauchamp RL, James MF, DeSouza PA, et al. A high-throughput kinome screen reveals serum/glucocorticoid-regulated kinase 1 as a therapeutic target for NF2-deficient meningiomas. *Oncotarget*. 2015;6(19):16981-16997.
37. Angus SP, Oblinger JL, Stuhlmiller TJ, et al. EPH receptor signaling as a novel therapeutic target in NF2-deficient meningioma. *Neuro Oncol*. 2018;20(9):1185-1196.
38. Frattini V, Trifonov V, Chan JM, et al. The integrated landscape of driver genomic alterations in glioblastoma. *Nat Genet*. 2013;45(10):1141-1149.
39. Abe T, Umeki I, Kanno S, Inoue S, Niihori T, Aoki Y. LZTR1 facilitates polyubiquitination and degradation of RAS-GTPases. *Cell Death Differ*. 2020;27(3):1023-1035.
40. Steklov M, Pandolfi S, Baietti MF, et al. Mutations in LZTR1 drive human disease by dysregulating RAS ubiquitination. *Science*. 2018;362(6419):1177-1182.
41. Hodges C, Kirkland JG, Crabtree GR. The many roles of BAF (mSWI/SNF) and PBAF complexes in cancer. *Cold Spring Harb Perspect Med*. 2016;6(8):a026930.
42. Mittal P, Roberts CWM. The SWI/SNF complex in cancer - biology, biomarkers and therapy. *Nat Rev Clin Oncol*. 2020;17(7):435-448.
43. Widemann BC, Dombi E, Gillespie A, et al. Phase 2 randomized, flexible crossover, double-blinded, placebo-controlled trial of the farnesyltransferase inhibitor tipifarnib in children and young adults with neurofibromatosis type 1 and progressive plexiform neurofibromas. *Neuro Oncol*. 2014;16(5):707-718.
44. Newman DJ, Cragg GM. Natural products as sources of new drugs over the nearly four decades from 01/1981 to 09/2019. *J Nat Prod*. 2020;83(3):770-803.

45. Kinghorn AD, DE Blanco EJC, Lucas DM, et al. Discovery of anticancer agents of diverse natural origin. *Anticancer Res.* 2016;36(11):5623-5637.
46. Shipkowski KA, Betz JM, Birnbaum LS, et al. Naturally complex: perspectives and challenges associated with botanical dietary supplement safety assessment. *Food Chem Toxicol.* 2018;118:963-971.
47. Perrone L, Sampaolo S, Melone MAB. Bioactive phenolic compounds in the modulation of central and peripheral nervous system cancers: facts and misdeeds. *Cancers.* 2020;12(2).
48. Peng Y, Zheng J, Zhou Y, Li J. Characterization of a novel curcumin analog P1 as potent inhibitor of the NF- κ B signaling pathway with distinct mechanisms. *Acta Pharmacol Sin.* 2013;34(7):939-950.
49. Siddiqui FA, Prakasam G, Chattopadhyay S, et al. Curcumin decreases Warburg effect in cancer cells by down-regulating pyruvate kinase M2 via mTOR-HIF1 α inhibition. *Sci Rep.* 2018;8(1):1-9.
50. Angelo LS, Wu JY, Meng F, et al. Combining curcumin (diferuloylmethane) and heat shock protein inhibition for neurofibromatosis 2 treatment: analysis of response and resistance pathways. *Mol Cancer Ther.* 2011;10(11):2094-2103.
51. Oblinger JL, Burns SS, Akhmametyeva EM, et al. Components of the eIF4F complex are potential therapeutic targets for malignant peripheral nerve sheath tumors and vestibular schwannomas. *Neuro Oncol.* 2016;18(9):1265-1277.
52. Esposito T, Schettino C, Polverino P, et al. Synergistic interplay between curcumin and polyphenol-rich foods in the Mediterranean diet: therapeutic prospects for neurofibromatosis 1 patients. *Nutrients.* 2017;9(7).

53. Lee M-J, Tsai Y-J, Lin M-Y, et al. Calebin-A induced death of malignant peripheral nerve sheath tumor cells by activation of histone acetyltransferase. *Phytomedicine*. 2019;57:377-384.
54. Nelson KM, Dahlin JL, Bisson J, Graham J, Pauli GF, Walters MA. The essential medicinal chemistry of curcumin. *J Med Chem*. 2017;60(5):1620-1637.
55. Tran TD, Ogbourne SM, Brooks PR, Sánchez-Cruz N, Medina-Franco JL, Quinn RJ. Lessons from exploring chemical space and chemical diversity of propolis components. *Int J Mol Sci*. 2020;21(14).
56. Demestre M, Messerli SM, Celli N, et al. CAPE (caffeic acid phenethyl ester)-based propolis extract (Bio 30) suppresses the growth of human neurofibromatosis (NF) tumor xenografts in mice. *Phytother Res*. 2009;23(2):226-230.
57. Lee JD, Lee JY, Baek BJ, et al. The inhibitory effect of honokiol, a natural plant product, on vestibular schwannoma cells. *Laryngoscope*. 2012;122(1):162-166.
58. Ong CP, Lee WL, Tang YQ, Yap WH. Honokiol: a review of its anticancer potential and mechanisms. *Cancers*. 2020;12(1):48.
59. Berretta M, Bignucolo A, Di Francia R, et al. Resveratrol in cancer patients: from bench to bedside. *Int J Mol Sci*. 2020;21(8):2945.
60. Cai H, Scott E, Kholghi A, et al. Cancer chemoprevention: evidence of a nonlinear dose response for the protective effects of resveratrol in humans and mice. *Sci Transl Med*. 2015;7(298):298ra117-298ra117.
61. Patel KR, Scott E, Brown VA, Gescher AJ, Steward WP, Brown K. Clinical trials of resveratrol. *Ann N Y Acad Sci*. 2011;1215(1):161-169.

62. Hu S, Wei W, Yuan J, Cheng J. Resveratrol inhibits proliferation in HBL-52 meningioma cells. *Onco Targets Ther.* 2019;12:11579-11586.
63. Hashemzaei M, Delarami Far A, Yari A, et al. Anticancer and apoptosis-inducing effects of quercetin in vitro and in vivo. *Oncol Rep.* 2017;38(2):819-828.
64. Yang C, Asthagiri AR, Iyer RR, et al. Missense mutations in the NF2 gene result in the quantitative loss of merlin protein and minimally affect protein intrinsic function. *Proc Natl Acad Sci USA.* 2011;108(12):4980-4985.
65. Hirokawa Y, Nheu T, Grimm K, et al. Sichuan pepper extracts block the PAK1/Cyclin D1 pathway and the growth of NF1-deficient cancer xenograft in mice. *Cancer Biol Ther.* 2006;5(3):305-309.
66. Pichersky E, Raguso RA. Why do plants produce so many terpenoid compounds? *New Phytol.* 2018;220(3):692-702.
67. Jing S, Zou H, Wu Z, et al. Cucurbitacins: bioactivities and synergistic effect with small-molecule drugs. *J Func Foods.* 2020;72:104042.
68. Banerjee S, Byrd JN, Gianino SM, et al. The neurofibromatosis type 1 tumor suppressor controls cell growth by regulating signal transducer and activator of transcription-3 activity in vitro and in vivo. *Cancer Res.* 2010;70(4):1356-1366.
69. Spear SA, Burns SS, Oblinger JL, et al. Natural compounds as potential treatments of NF2-deficient schwannoma and meningioma: cucurbitacin D and goyazensolide. *Otol Neurotol.* 2013;34(8):1519-1527.
70. Hou W, Liu B, Xu H. Celastrol: progresses in structure-modifications, structure-activity relationships, pharmacology and toxicology. *Eur J Med Chem.* 2020;189:112081.

71. Du X, Nyagblordzro M, An L, et al. Pharmacokinetic and toxicological characteristics of Tripterigium glycosides and their derivatives. *Curr Drug Metab.* 2018;19(7):605-627.
72. Muñoz-Acuña U, Shen Q, Ren Y, et al. Goyazensolide induces apoptosis in cancer cells in vitro and in vivo. *Int J Cancer Res.* 2013;9(2):36-53.
73. Li X-X, Zhang S-J, Chiu AP, et al. Targeting of AKT/ERK/CTNNB1 by DAW22 as a potential therapeutic compound for malignant peripheral nerve sheath tumor. *Cancer Med.* 2018;7(9):4791-4800.
74. Kamal MM, Akter S, Lin C-N, Nazzal S. Sulforaphane as an anticancer molecule: mechanisms of action, synergistic effects, enhancement of drug safety, and delivery systems. *Arch Pharm Res.* 2020;43(4):371-384.
75. Kim BG, Fujita T, Stankovic KM, et al. Sulforaphane, a natural component of broccoli, inhibits vestibular schwannoma growth in vitro and in vivo. *Sci Rep.* 2016;6.
76. Montero-Oleas N, Arevalo-Rodríguez I, Nuñez-González S, Viteri-García A, Simancas-Racines D. Therapeutic use of cannabis and cannabinoids: an evidence mapping and appraisal of systematic reviews. *BMC Complement Med Ther.* 2020;20.
77. Kovalchuk O, Kovalchuk I. Cannabinoids as anticancer therapeutic agents. *Cell Cycle.* 2020;19(9):961-989.
78. Sarfaraz S, Afaq F, Adhami VM, Malik A, Mukhtar H. Cannabinoid receptor agonist-induced apoptosis of human prostate cancer cells LNCaP proceeds through sustained activation of ERK1/2 leading to G1 cell cycle arrest. *J Biol Chem.* 2006;281(51):39480-39491.

79. Hart S, Fischer OM, Ullrich A. Cannabinoids induce cancer cell proliferation via tumor necrosis factor α -converting enzyme (TACE/ADAM17)-mediated transactivation of the epidermal growth factor receptor. *Cancer Res.* 2004;64(6):1943-1950.
80. Hegazy O, Platnick H. Cannabidiol (CBD) for treatment of neurofibromatosis-related pain and concomitant mood disorder: a case report. *Cureus.* 2019;11(12):e6312.
81. Gazendam A, Nucci N, Gouveia K, Abdel Khalik H, Rubinger L, Johal H. Cannabinoids in the management of acute pain: a systematic review and meta-analysis. *Cannabis Cannabinoid Res.* Published online March 9, 2020.
82. Hashimoto H, Messerli SM, Sudo T, Maruta H. Ivermectin inactivates the kinase PAK1 and blocks the PAK1-dependent growth of human ovarian cancer and NF2 tumor cell lines. *Drug Discov Ther.* 2009;3(6):243-246.
83. González Canga A, Sahagún Prieto AM, Díez Liébana MJ, Fernández Martínez N, Sierra Vega M, García Vieitez JJ. The pharmacokinetics and interactions of ivermectin in humans—a mini-review. *AAPS J.* 2008;10(1):42-46.
84. Pan L, Woodard JL, Lucas DM, Fuchs JR, Kinghorn AD. Rocaglamide, silvestrol and structurally related bioactive compounds from *Aglaia* species. *Nat Prod Rep.* 2014;31(7):924-939.
85. King ML, Chiang C-C, Ling H-C, Fujita E, Ochiai M, McPhail AT. X-Ray crystal structure of rocaglamide, a novel antileukemic 1H-cyclopenta[b]benzofuran from *Aglaia elliptifolia*. *J Chem Soc, Chem Commun.* 1982;(20):1150-1151.
86. Hwang BY, Su B-N, Chai H, et al. Silvestrol and episilvestrol, potential anticancer rocaglate derivatives from *Aglaia silvestris*. *J Org Chem.* 2004;69(10):3350-3358.

87. Sadlish H, Galicia-Vazquez G, Paris CG, et al. Evidence for a functionally relevant rocaglamide binding site on the eIF4A-RNA complex. *ACS Chem Biol.* 2013;8(7):1519-1527.
88. Wolfe AL, Singh K, Zhong Y, et al. RNA G-quadruplexes cause eIF4A-dependent oncogene translation in cancer. *Nature.* 2014;513(7516):65-70.
89. Iwasaki S, Iwasaki W, Takahashi M, et al. The translation inhibitor rocaglamide targets a bimolecular cavity between eIF4A and polypurine RNA. *Mol Cell.* 2019;73(4):738-748.e9.
90. Oblinger JL, Burns SS, Huang J, et al. Overexpression of eIF4F components in meningiomas and suppression of meningioma cell growth by inhibiting translation initiation. *Exp Neurol.* 2018;299(Pt B):299-307.
91. Pan L, Acuña UM, Li J, et al. Bioactive flavaglines and other constituents isolated from *Aglaia perviridis*. *J Nat Prod.* 2013;76(3):394-404.
92. Chang L-S, Oblinger JL, Burns SS, et al. Targeting protein translation by rocaglamide and didesmethylrocaglamide to treat MPNST and other sarcomas. *Mol Cancer Ther.* 2020;19(3):731-741.
93. Chan K, Robert F, Oertlin C, et al. eIF4A supports an oncogenic translation program in pancreatic ductal adenocarcinoma. *Nat Commun.* 2019;10(1):5151.
94. Ernst JT, Thompson PA, Nilewski C, et al. Design of development candidate eFT226, a first in class inhibitor of eukaryotic initiation factor 4A RNA helicase. *J Med Chem.* 2020;63(11):5879-5955.
95. Ecosystems Research and Development Bureau. *Guyabano (Annona Muricata L. Innaeus)*. Department of Environment and Natural Resources; 2014:1-13.

96. Lannuzel A, Höglinger GU, Champy P, Michel PP, Hirsch EC, Ruberg M. Is atypical parkinsonism in the Caribbean caused by the consumption of Annonaceae? *J Neural Transm Suppl.* 2006;(70):153-157.
97. Chen P-N, Hsieh Y-S, Chiou H-L, Chu S-C. Silibinin inhibits cell invasion through inactivation of both PI3K-Akt and MAPK signaling pathways. *Chem Biol Interact.* 2005;156(2-3):141-150.
98. Martin ACBM, Fuzer AM, Becceneri AB, et al. [10]-gingerol induces apoptosis and inhibits metastatic dissemination of triple negative breast cancer in vivo. *Oncotarget.* 2017;8(42):72260-72271.
99. Zhao Q, Assimopoulou AN, Klauck SM, et al. Inhibition of c-MYC with involvement of ERK/JNK/MAPK and AKT pathways as a novel mechanism for shikonin and its derivatives in killing leukemia cells. *Oncotarget.* 2015;6(36):38934-38951.
100. Liao K-F, Chiu T-L, Huang S-Y, et al. Anti-cancer effects of radix *Angelica sinensis* (danggui) and N-butylenephthalide on gastric cancer: implications for REDD1 activation and mTOR inhibition. *CPB.* 2018;48(6):2231-2246.
101. Spagnuolo C, Russo GL, Orhan IE, et al. Genistein and cancer: current status, challenges, and future directions. *Adv Nutr.* 2015;6(4):408-419.
102. Luo K-W, Lung W-Y, Chun-Xie, Luo X-L, Huang W-R. EGCG inhibited bladder cancer T24 and 5637 cell proliferation and migration via PI3K/AKT pathway. *Oncotarget.* 2018;9(15):12261-12272.

Abstract Submission

Basic and translational research

NF2/Schwannomatosis

NF2018/ABS-184

Novel drug discovery for NF2-deficient meningiomas: Brigatinib causes tumor shrinkage in NF2-deficient meningiomas

Long-Sheng Chang¹, Sarah S Burns¹, Janet L Oblinger¹, Marc Ferrer², Jie Huang¹, Ming Poi³, Vijaya Ramesh⁴, On behalf of the Synodos for NF2 Consortium⁵ and Full list of Investigators of the Children's Tumor Foundation (CTF)-supported Synodos for NF2 Consortium: <https://www.synapse.org/#!Synapse:syn2343195/wiki/62126>

¹Center for Childhood Cancer & Blood Diseases/Department of Pediatrics, The Res Inst at Nationwide Children's Hosp/The Ohio State Univ College of Medicine, Columbus, OH, ²National Center for Advancing Translational Sciences, NIH, Bethesda, MD, ³Division of Pharmacy Practice & Science, The Ohio State Univ College of Pharmacy, Columbus, OH, ⁴Center for Genomic Medicine and Department of Neurology, Massachusetts General Hospital, Boston, MA, ⁵The CTF-supported Synodos for NF2 Consortium, NY, United States

Select your preferred type of presentation: Platform presentation

Background: Originating from meningotheial cells of the arachnoid layer lining the brain, meningiomas cause significant morbidities by compressing adjacent brain tissues, cranial nerves, and blood vessels. Meningiomas can occur spontaneously or are frequently found in NF2 patients carrying *NF2* mutations. As an FDA-approved drug is presently not available for *NF2*-deficient meningioma, we aimed to identify novel targeted drugs that delay tumor progression or cause tumor shrinkage.

Methods: A panel of isogenic *NF2* and *NF2*⁺ arachnoidal cells and *NF2* meningioma cells was used to screen ~2000 compounds of diverse mechanisms of action. The anti-tumor activity of the selected drug combination, pharmacokinetic (PK) analysis, PathScan RTK Signaling Antibody Arrays, and Western blots were performed.

Results: From the single agent screen, 45 potent compounds were selected for further combination screening, and 33 drug combinations, including the combination of brigatinib, an inhibitor of multi-RTKs including ALK, and MK2206, an AKT inhibitor, were identified that exhibited a greater synergistic growth inhibition in *NF2* cells versus *NF2*⁺ cells. As a single agent, brigatinib effectively blocked tumor growth and reduced tumor size in the intracranial *NF2*-deficient Ben-Men-1-LucB meningioma model, while MK2206 only modestly suppressed tumor growth. Combined treatment with brigatinib and MK2206 further reduced tumor size. Upon cessation of treatment, the tumors treated with brigatinib or the brigatinib/MK2206 combination regrew. Importantly, these regrown tumors were responsive to these drugs when retreated again. PK analysis revealed that both brigatinib and MK2206 crossed the blood-brain barrier and accumulated in tumor-containing brain tissues. Intriguingly, Ben-Men-1 cells did not express ALK but expressed several phospho-RTKs (p-RTKs) with strong expression of p-ErbB2, ErbB3, FGFR1, TrkA, and VEGFR2. Brigatinib treatment reduced the levels of most of these p-RTKs with the most significant reduction in EGFR, ErbB2, ErbB3, VEGFR2, several Eph receptor members, as well as FAK. In addition, brigatinib treatment attenuated the downstream signals of these kinases, including p-AKT and p-ERKs.

Conclusions: The anti-tumor effects of brigatinib in *NF2*-deficient meningiomas are mediated through inhibition of multiple growth-promoting RTKs but not ALK. Brigatinib and its combination with an AKT inhibitor should be further evaluated in patients with *NF2*-deficient meningiomas (Support: the CTF and US Department of Defense)

Disclosure of Interest: None Declared

Keywords: None

Abstract Submission

Basic and translational research

NF1

NF2018/ABS-185

Identification of silvestrol-related rocaglates with better bioavailability and high potency against malignant peripheral nerve sheath tumors

Long-Sheng Chang¹, Janet L Oblinger¹, Sarah S Burns¹, Jie Huang¹, Larry Anderson², Rulong Shen³, Li Pan⁴, Yulin Ren⁴, Barry R O'Keefe⁵, A Douglas Kinghorn⁴, Jerry M Collins²

¹Center for Childhood Cancer & Blood Diseases/Department of Pediatrics, The Research Institute at Nationwide Children's Hospital/The Ohio State University College of Medicine, Columbus, OH, ²Division of Cancer Treatment and Diagnosis, National Cancer Institute, NIH, Bethesda, MD, ³Department of Pathology, The Ohio State University College of Medicine, ⁴Division of Medicinal Chemistry and Pharmacognosy, The Ohio State University College of Pharmacy, Columbus, OH, ⁵Division of Cancer Treatment and Diagnosis and Molecular Targets Program, Center for Cancer Research, National Cancer Institute, NIH, Bethesda, MD, United States

Select your preferred type of presentation: Platform presentation

Background: Malignant peripheral nerve sheath tumors (MPNSTs) frequently overexpress eIF4F components, and the eIF4A inhibitor silvestrol effectively suppresses MPNST growth. However, silvestrol has suboptimal drug-like properties, including a bulky structure and poor oral bioavailability. Our objectives are to identify potent silvestrol-related rocaglates and to determine their bioavailability, anti-tumor effects, and mechanisms of action.

Methods: *NF1*^{+/+} STS26T and *NF1*^{-/-} ST8814 MPNST and 697 and silvestrol-resistant 697-R leukemic cells were treated with various concentrations of each rocaglate. Cell proliferation assays, flow cytometry, Western blots, and pharmacokinetic (PK) analysis were performed. A quantifiable, orthotopic *NF1*-deficient MPNST mouse model and immunohistochemistry were conducted to assess antitumor effects.

Results: Among 10 silvestrol-related rocaglates lacking the dioxanyl ring examined, didesmethylrocaglamide (DDR) and rocaglamide (ROC) had potent growth-inhibitory activity comparable to silvestrol in MPNST cells. Structure-activity relationship analysis revealed that the dioxanyl ring in silvestrol was dispensable while the C-8b hydroxyl group was essential for cytotoxicity. DDR and ROC arrested MPNST cells at G₂/M and significantly increased the sub-G₁ fraction. Accordingly, these rocaglamides induced cleavage of caspases 3 and 7 and poly(ADP-ribose) polymerase, while decreasing total protein levels of these apoptotic markers, consistent with translation inhibition. Additionally, DDR and ROC reduced the levels of mitogenic kinases AKT and ERK1/2. Unlike silvestrol, DDR and ROC inhibited proliferation of silvestrol-resistant 697-R leukemic cells, which over-express the MDR1 multidrug transporter, at IC₅₀ values similar to silvestrol-sensitive 697 cells, suggesting that these rocaglamides may be more bioavailable. PK analysis confirmed that ROC had 50% oral bioavailability. Importantly, ROC, when administered intraperitoneally or orally, potently suppressed the growth of luciferase-expressing *NF1*^{-/-} ST8814-Luc MPNST xenografts with no overt toxicity. Treated tumors had abundant phospho-histone H3 labeling and more cleaved caspase 3-positive cells, consistent with G₂/M arrest and indicative of increased apoptosis, respectively.

Conclusions: The more favorable drug-like properties and potent anti-tumor effects suggest that ROC and DDR have potential to become viable MPNST treatments. (Support: CancerFree Kids, the US Department of Defense, and National Cancer Institute, NIH)

Disclosure of Interest: None Declared

Keywords: None

Abstract Submission

Basic and translational research

NF2/Schwannomatosis

NF2018/ABS-151

Preclinical Assessment of MEK1/2 Inhibitors for Neurofibromatosis Type 2-Associated Schwannomas Reveals Differences in Efficacy and Drug Resistance Development.

Cristina Fernandez-Valle*¹, Marisa Fuse¹, Christine Dinh², Jeremie Vitte³, Joanna Kirkpatrick⁴, Thomas Mindos⁴, Stephani Champion⁵, Konstantin Brnjos¹, Maria Clara Franco⁶, Jie Huang⁷, Juan Young², Alejandra Petrilli¹, Denise Yan², Rahul Mittal², Rulong Shen⁸, Fred Telischi², Long-Sheng Chang⁷, Helen Morrison⁴, Marco Giovannini³, Xue-Zhong Liu²

¹University of Central Florida, Orlando, ²University of Miami Miller School of Medicine, Miami, ³David Geffen School of Medicine, UCLA, Los Angeles, United States, ⁴Leibniz Institute on Aging, Jena, Germany, ⁵Orlando Health, Orlando, ⁶Oregon State University, Corvallis, ⁷Nationwide Children's Hospital, ⁸Ohio State University, Columbus, United States

Select your preferred type of presentation: Platform presentation

Background: Neurofibromatosis type 2 (NF2) is a genetic tumor disorder caused by loss of function of the *NF2*/merlin tumor suppressor gene. A hallmark of NF2 is formation of bilateral vestibular schwannomas (VS) for which no FDA-approved drug is presently available. Because merlin modulates activity of the Ras/Raf/MEK/ERK pathway, we investigated repurposing drugs targeting MEK1/2 to treat NF2-associated schwannomas.

Methods: Mouse and human merlin-deficient Schwann cell (MD-MSCHSC) lines were screened against six MEK1/2 inhibitors. Efficacious drugs were tested in orthotopic allograft and *NF2* transgenic mouse models. Proteome and pathway analyses were conducted. Drug efficacy was examined in primary human VS cells with *NF2* mutations and correlated with differential DNA methylation patterns.

Results: Trametinib, PD0325901, and cobimetinib were the most potent in reducing MD-MSCHSC viability. Each decreased pERK1/2 and cyclin D₁, increased p27, and induced caspase 3 cleavage in MD-MSCHSCs. Proteome analysis was consistent with cell cycle arrest and activation of pro-apoptotic pathways in trametinib-treated MD-MSCHSCs. The three inhibitors slowed the growth of MD-MSCHSC allografts compared to controls. However, decreased pERK1/2, cyclin D₁, and Ki67 levels were observed in PD0325901 and cobimetinib, but not trametinib treated grafts. Eight weeks of trametinib treatment reduced tumor burden and average tumor size compared to controls in the *NF2* transgenic mouse model; tumors did not exhibit reduced pERK1/2 staining compared to control. Both trametinib and PD0325901 modestly reduced viability of several primary human VS cells with *NF2* mutations. DNA methylation analysis of PD0325901-resistant versus -susceptible VS identified differentially methylated regions in genes that could contribute to drug-resistance.

Conclusions: This comprehensive pre-clinical study demonstrates efficacy differences and possible emergence of drug resistance among MEK inhibitors in schwannoma models and supports further investigation of MEK inhibitors alone and in combination with other targeted drugs as treatments for NF2-associated schwannomas.

Disclosure of Interest: None Declared

Keywords: None

Abstract Submission

Clinical research

NF2/Schwannomatosis

NF2018/ABS-215

Phase 1 and Phase 0 studies of AR-42, a pan histone deacetylase inhibitor, in subjects with neurofibromatosis type 2 (NF2)-associated vestibular schwannomas and meningiomas

D. Bradley **Welling***¹, Sarah **Burns**², Janet **Oblinger**³, Beth **Miles-Markley**⁴, Amir **Mortazavi**⁵, Amy **Quinkert**⁶, Jaishri **Blakeley**⁷, S. Alireza **Monsouri**⁸, Brian **Neff**⁹, Robert **Jackler**¹⁰, Long-Sheng **Chang**^{2,3,4}

¹Otolaryngology, Harvard Medical School, Massachusetts Eye and Ear, Massachusetts General Hospital, Boston, ²

Departments of Pediatrics, ³Center for Childhood Cancer, Nationwide Children's Hospital, ⁴Otolaryngology Head & Neck Surgery, ⁵Internal Medicine, The Ohio State University, Columbus, ⁶Otolaryngology, Harvard University/MEEI, Boston,

⁷Departments of Neurology,

Neurosurgery and Oncology, ⁸Neurosurgery, Johns Hopkins University, Baltimore, ⁹Department of Otolaryngology, Mayo Clinic, Rochester, ¹⁰Department of Otolaryngology, Stanford University, Palo Alto, United States

Select your preferred type of presentation: Platform presentation

Background: Patients with NF2 frequently develop bilateral vestibular schwannomas (VS) and multiple meningiomas.

Presently, an FDA-approved medical therapy is not available. The histone deacetylase inhibitor AR-42 suppresses schwannoma growth and causes tumor shrinkage in meningiomas in preclinical models.

Methods: As part of a phase I trial of AR-42 in patients with advanced or recurrent solid tumors for which no standard therapy is available or patients who decline available standard treatment options, patients with NF2-associated VS and meningiomas were enrolled and received AR-42 treatment 3 times weekly for 3 weeks followed by 1-week break. Subsequently, a phase 0 exploratory evaluation of AR-42 for intratumoral pharmacodynamics and pharmacokinetics in VS and meningiomas was performed.

Results: In the phase I trial, 5 NF2 patients were recruited. AR-42 was overall well-tolerated, and the maximum tolerated dose (MTD) was defined at 60 mg. AR-42 demonstrated anti-tumor activity mostly in the form of tumor stability. In one NF2 patient treated for 10 months, AR-42 significantly reduced tumor size in meningiomas and slowed VS growth rates. After cessation of treatment, meningiomas remained small, but VS quickly resumed growth. Tissue samples including bilateral right and left VS, a skull base meningioma, and an optic meningioma from this patient as well as a VS from a second person with NF2 were collected. These 5 tumors underwent comprehensive genomic profiling via FoundationOne. Mutations in *NF2* and *NUP98* were found. A phase 0 study with the primary objective to estimate p-AKT and p16^{INK4A} levels after 3 weeks of oral AR-42 at 40 mg every other day, 3 times a week for 3 weeks preceding surgery, in NF2-related and sporadic VS and meningiomas, as well as control tumor samples from a tissue bank is ongoing. The secondary objectives include assessment of audiometric changes and volumetric tumor reduction and determination of plasma and intra-tumoral AR-42 concentrations. So far, 5 patients were studied. AR-42 concentrations in the plasma and VS of treated patients reached levels around the IC₅₀ value determined *in vitro* and was more preferentially concentrated in the tumors. AR-42 decreased the levels of p-AKT, pERK1/2, p-PRAS40, and p-S6 in treated VS.

Conclusions: **Conclusions:**AR-42 achieves therapeutic concentrations in the tumors and hits its targets. Further investigation of AR-42 as an NF2 treatment is ongoing.

(Funding: The US Department of Defense, The Galloway Family, and Advocure NF2)

Disclosure of Interest: None Declared

Keywords: None

revealed by flow cytometry analysis. Overall, we demonstrated that gp120 triggers activation of ERK and Akt signaling in glioma cells, resulting in increased protein synthesis and cell growth. This research was made possible by NIH grant number 1SC1GM122691 and Puerto Rico Science, Technology, and Research Trust grant 2016-00157.

CSIG-40. HETEROZYGOUS *IDH1*^{R132H/WT} CREATED BY “SINGLE BASE EDITING” INHIBITS HUMAN ASTROGLIAL CELL GROWTH AND PROMOTES CELL MIGRATION

Shuang Wei¹, Jie Wang², Olurobi Oyinlade¹, Ding Ma¹, Shuyan Wang¹, Jiang Qian² and Shuli Xia¹; ¹Kennedy Krieger Institute, Baltimore, MD, USA, ²Johns Hopkins University, Baltimore, MD, USA

Mutations in the isocitrate dehydrogenase 1 (*IDH1*) gene have been identified in a number of cancer types, including brain cancer. The Cancer Genome Atlas project has revealed that *IDH1* mutations occur in 70–80% of grade II and grade III gliomas. Until recently, most of the functional studies of *IDH1* mutations in cellular models have been conducted in over-expression systems with the *IDH1* wild type background. In this study, we employed a modified CRISPR/Cas9 genome editing technique called “single base editing”, and efficiently introduced heterozygous *IDH1* R132H mutation (*IDH1*^{R132H/WT}) in human astroglial cells. Global DNA methylation profiling revealed hypermethylation as well as hypomethylation induced by *IDH1*^{R132H/WT}. Global gene expression analysis identified molecular targets and pathways altered by *IDH1*^{R132H/WT}, including cell proliferation, extracellular matrix, and cell migration. Our phenotype analysis indicated that compared with *IDH1* wild type cells, *IDH1*^{R132H/WT} promoted cell migration by up-regulating integrin b4 (ITGB4), and significantly inhibited cell proliferation. All these genotype and phenotype changes were reversed by mutant *IDH1* inhibitor AGI-5198. Using our mutated *IDH1* models generated by genome editing, we identified novel molecular targets of *IDH1*^{R132H/WT}, namely Yes-associated protein (YAP) and its downstream signaling pathway Notch, to mediate the cell growth-inhibiting effect of *IDH1*^{R132H/WT}. In summary, the “single base editing” strategy has successfully created heterozygous *IDH1* R132H mutation that recapitulates the naturally occurring *IDH1* mutation. Our isogenic cellular systems that differ in a single nucleotide in one allele of the *IDH1* gene provide a valuable model for novel discoveries of *IDH1*^{R132H/WT}-driven biological events.

CSIG-41. ONCOGENE ADDICTION SWITCH FROM NOTCH TO PI3K REQUIRE SIMULTANEOUS TARGETING OF DUAL PATHWAY INHIBITION IN GLIOBLASTOMA

Norihiko Saito, Kazuya Aoki, Nozomi Hirai, Ryo Suzuki, Satoshi Fujita, Haruo Nakayama, Morito Hayashi, Takatoshi Sakurai and Satoshi Iwabuchi; Toho University Ohashi Medical Center, Tokyo, Japan

Notch signaling pathway regulates normal stem cells in the brain and glioma stem cells (GSCs). However, blocking the proteolytic activation of NOTCH with γ -secretase inhibitors (GSI) fails to alter the growth of some GSCs as GSIs seem to be active in only a fraction of GSCs lines with constitutive NOTCH activity. Here we report loss of PTEN as a critical event leading to resistance to NOTCH inhibition, which causes the transfer of “oncogene addiction” from the NOTCH to the phosphoinositol-3 kinase (PI3K) pathway. We investigated the effects of Notch inhibition in GSC using GSI. Drug cytotoxicity test on 16 GSCs show differential growth response to GSI stratifying GSCs into two groups: responders vs non-responders. Active Notch signaling seems to be important features for the GSC as Notch inhibition only affected GSCs defined as having increased Notch activity. However in the responder group GSCs with the PTEN mutation seems to be less sensitive to GSI treatment. Here we show that NOTCH regulates the expression of PTEN and the activity of the PI3K signaling pathway in GSCs since treatment with GSI attenuated Notch signaling and increases PTEN expression. NOTCH regulates PTEN expression via Hes-1 as knockdown of either Notch or Hes1 led to increase expression of PTEN. This novel observation suggests the need to simultaneous inhibition of both pathways as a means to improve therapeutic efficacy in human glioblastoma.

CSIG-42. HIGH THROUGHPUT KINOME AND TRANSCRIPTOME ANALYSES REVEAL NOVEL THERAPEUTIC TARGETS IN NF2-DEFICIENT MENINGIOMA

Roberta Beauchamp¹, Serkan Erdin¹, Steven Angus², Timothy Stuhlmiller², Janet Oblinger³, Justin Jordan⁴, Stephen J. Haggarty¹, Scott R. Plotkin⁴, Long-Sheng Chang³, Gary L. Johnson², James F. Gusella¹ and Vijaya Ramesh¹; ¹Massachusetts General Hospital, Center for Genomic Medicine, Boston, MA, USA, ²University of North Carolina School of Medicine, Department of Pharmacology, Chapel Hill, NC, USA, ³The Ohio State University College of Medicine, Center for Childhood Cancer and

Blood Diseases, Columbus, OH, USA, ⁴Massachusetts General Hospital, Department of Neurology, Boston, MA, USA

Meningiomas (MN), the most common adult primary intracranial tumor, arise from the arachnoid/meninges and are non-responsive to chemotherapies with a high recurrence rate despite surgery, necessitating effective non-invasive therapies. Our previous work showed that *NF2* loss activates mechanistic target of rapamycin complex 1 (mTORC1) and mTORC2 signaling, which led to past *NF2* clinical trials using rapalogs (RAD001/everolimus), and current meningioma clinical trials with dual mTORC1/mTORC2 inhibitor (mTORi) AZD2014. To understand additional dysregulated, potentially druggable pathways, we undertook an ‘omics approach of large-scale kinomics and RNA-sequencing employing CRISPR-modified human arachnoidal cells (ACs), *NF2*-expressing vs *NF2*-null. In *NF2*-null ACs, several kinases were elevated including erythropoietin-producing hepatocellular (EPH)-receptor tyrosine kinase (RTK) family members, Src family kinase (SFK) members, and c-KIT, all targets of dasatinib. *In vitro* treatment of MN cells using mTORi (AZD2014 or INK128) and dasatinib enhanced growth inhibition upon combination mTORi+dasatinib. *In vivo* treatment of an orthotopic mouse MN model showed moderate response to dasatinib with stronger response using INK128 or INK128+dasatinib (e-published in Neuro-Oncology). Our transcriptomic data also revealed increased expression of several ligands/growth factors, particularly NRG1/neuregulin. Expanding these results, we have confirmed increased expression of NRG1 in human *NF2*-null ACs. We also find *NF2*-null ACs secrete NRG1, and in conditioned-media experiments we observe stimulation of ErbB3, EPHA2 and mTOR pathways, suggesting an autocrine signaling mechanism. *NF2*-null AC or MN cells, when stimulated with exogenous NRG1, show enhanced activation of mTOR and EPH pathways besides ErbB3 signaling. Further, lapatinib (multi-ErbB inhibitor) but not erlotinib (EGFR inhibitor) attenuates the NRG1-stimulated activation of ErbB3, EPHA2 and mTOR, suggesting that NRG1-induced activation is EGFR-independent. Taken together, our results support a mechanistic link where *NF2* loss increases NRG1/ErbB signaling to EPH/SFK and mTOR pathways, which may be a critical driver of tumorigenesis, thus providing a therapeutic opportunity to co-target these pathways in *NF2*-deficient meningiomas.

CSIG-43. THE TYROSINE PHOSPHATASE PTPN12/PTP-PEST REGULATES PHOSPHORYLATION-DEPENDENT UBIQUITINATION AND STABILITY OF FOCAL ADHESION SUBSTRATES IN INVASIVE GLIOBLASTOMA CELLS

Joseph McCarty, John Morales, Paola Guerrero and Zhihua Chen; MD Anderson Cancer Center, Houston, TX, USA

Glioblastoma (GBM) is an invasive brain cancer with tumor cells that disperse from the primary mass escaping surgical resection, displaying resistance to chemotherapy and radiation, and invariably giving rise to lethal recurrent lesions. Targeted therapies such as the anti-vascular endothelial growth factor (VEGF) blocking antibody bevacizumab have yielded disappointing results in GBM clinical trials, with no improvements in overall patient survival. Many patients treated with bevacizumab develop acquired resistance leading to lethal recurrent lesions associated with robust tumor cell invasion. While a great deal is known about genes and pathways that promote GBM proliferation and neovascularization, relatively little is understood about mechanisms that drive GBM cell invasion during progression or following anti-angiogenic therapy. Here, we report that PTP-PEST, a cytoplasmic protein tyrosine phosphatase encoded by the PTPN12 gene, controls GBM cell invasion by physically bridging the focal adhesion protein Crk-associated substrate (Cas) to valosin containing protein (Vcp), an ATP-dependent protein segregase that selectively extracts ubiquitinated proteins from multiprotein complexes and targets them for degradation via the ubiquitin proteasome system. Both Cas and Vcp are substrates for PTP-PEST, with the phosphorylation status of tyrosine 805 (Y805) in Vcp impacting affinity for Cas in focal adhesions and controlling ubiquitination levels and protein stability. Perturbing PTP-PEST-mediated phosphorylation of Cas and Vcp led to alterations in GBM cell invasive growth *in vitro* and in pre-clinical mouse models generated with GBM stem cells. Furthermore, acquired resistance to bevacizumab correlates with reduced expression of PTP-PEST in invasive GBM cells. Collectively, these data reveal a novel regulatory mechanism involving PTP-PEST, Vcp, and Cas that dynamically balances phosphorylation-dependent ubiquitination of key focal proteins involved in GBM cell invasion.

CSIG-44. TREATMENT WITH THE CASEIN KINASE 2 INHIBITOR, CX-4945, SENSITIZES MEDULLOBLASTOMA TO TEMOZOLOMIDE

Ryan Nitta¹ and Gordon Li²; ¹Stanford University, Stanford, CA, USA, ²Stanford University, Palo Alto, CA, USA

Medulloblastoma (MB) is the most common malignant pediatric brain tumor, accounting for ~20% of all cases. While current treatments result in

Abstract presented at the 2019 NF Conference, San Francisco, CA. (Sept. 2019)

Brigatinib as a potential therapy for malignant peripheral nerve sheath tumors

Janet Oblinger, Ph.D.

Nationwide Children's Hospital & The Ohio State University

MPNSTs are highly aggressive soft-tissue sarcomas that have a high risk of recurrence and metastasis and are refractory to current treatment. These tumors can arise spontaneously or from pre-existing plexiform neurofibromas in patients with neurofibromatosis type 1 (NF1), a tumor predisposition syndrome caused by inactivating mutations in the *NF1* tumor suppressor gene which encodes a Ras-GTPase-activating protein. Importantly, even sporadic tumors often incur mutations in the *NF1* gene or the Ras pathway. As a consequence, MPNSTs exhibit upregulation of Ras downstream kinase signaling, including the phosphatidylinositol 3-kinase (PI3K)-AKT-mammalian target of rapamycin (mTOR) and Raf-MEK-ERK mitogen-activated protein kinases. MPNSTs also harbor other genetic alterations, such as aberrant activation of epidermal growth factor receptor (EGFR) and insulin-like growth factor-1 receptor (IGF-1R), suggesting that these receptor tyrosine kinases (RTKs) may be therapeutic targets. Previously we showed that the FDA-approved ALK inhibitor brigatinib (ALUNBRIG™) suppresses multiple RTKs and non-RTKs, including focal adhesion kinase (FAK). Here we demonstrate that brigatinib exhibited growth-inhibitory activity in *NF1*-deficient ST8814 and *NF1*-expressing STS26T MPNST cells. Combination of brigatinib with the dual mTORC1/2 inhibitor INK128 (sapanisertib) yielded enhanced anti-proliferative effects. Treatment of ST8814 cells with brigatinib decreased p-EGFR and p-IGF-1R and their downstream p-AKT and p-S6. Treatment with INK128 also profoundly inhibited p-AKT and p-S6. Interestingly, combination of brigatinib and INK128 further reduced the phosphorylation of these signaling mediators and p-FAK compared to either monotherapy, suggesting cooperation in suppressing the AKT-mTOR pathway. However, we did not detect ALK expression in ST8814 and STS26T cells, indicating that brigatinib mediates growth inhibition via targeting of other tyrosine kinases. Experiments are in progress to investigate the anti-tumor activity of brigatinib in patient-derived xenograft (PDX) models for MPNST. Collectively, our data suggest that brigatinib should be further evaluated as a potential treatment for MPNST.

Full List Authors: Janet Oblinger^{1,2} and Long-Sheng Chang^{1,2,3}

¹*Center for Childhood Cancer and Blood Diseases, Abigail Wexner Research Institute at Nationwide Children's Hospital and Depts of* ²*Pediatrics &* ³*Otolaryngology-Head & Neck Surgery, The Ohio State University*

Funding: CancerFree KIDS, Department of Defense

Abstract presented at the 2019 NF Conference, San Francisco, CA. (Sept. 2019)

Targeting protein translation with rocaglamide and didesmethylrocaglamide to treat NF1 and NF2 tumors

Long-Sheng Chang

Nationwide Children's Hospital & The Ohio State University

To sustain uncontrolled growth, cancer cells exhibit enhanced protein synthesis by upregulation of the protein translation machinery. Previously we reported that NF1-associated malignant peripheral nerve sheath tumors (MPNSTs) and NF2-related vestibular schwannomas and meningiomas exhibit elevated expression of eIF4A, eIF4E, and eIF4G, components of the eIF4F translation initiation complex, and that the eIF4A inhibitor silvestrol potently suppresses the growth of these tumor cells. Studies by others also show strong anti-tumor activity of silvestrol in several other cancer models, suggesting that it may be a potential cancer treatment. However, silvestrol has suboptimal drug-like properties, including a bulky structure, sensitivity to inhibition by the MDR1 multidrug-resistant transporter, and poor oral bioavailability. By screening 10 silvestrol-related rocaglates lacking the dioxanyl ring, we identified rocaglamide (Roc) and didesmethylrocaglamide (DDR) with potent growth-inhibitory activity comparable to silvestrol in MPNST cells. Structure-activity relationship analysis revealed that the dioxanyl ring present in silvestrol was dispensable for, but may enhance, cytotoxicity. Both Roc and DDR arrested MPNST cells at G₂/M, significantly increased the sub-G₁ fraction, and induced cleavage of caspases 3 and 7 and poly(ADP-ribose) polymerase, while decreasing total protein levels of these apoptotic markers and mitogenic kinases AKT and ERK1/2, consistent with translation inhibition. Additionally, these rocaglamides elevated the levels of γH2AX, a marker of the DNA damage response. Unlike silvestrol, Roc and DDR were not sensitive to MDR1 inhibition. Pharmacokinetic analysis confirmed that Roc had 50% oral bioavailability. Importantly, Roc, when administered intraperitoneally or orally, potently suppressed the growth of orthotopic *NF1*-deficient MPNST xenografts with no overt toxicity. Treated MPNSTs had abundant phospho-histone H3 labeling and more cleaved caspase 3-positive cells, consistent with G₂/M arrest and indicative of increased apoptosis, respectively. In addition, Roc exhibited anti-tumor effects in patient-derived xenograft models for several types of sarcomas, including Ewing sarcoma, osteosarcoma, and rhabdomyosarcoma. Western blot analysis revealed that Roc and DDR decreased multiple oncogenic kinases, including IGF-1R, in sarcoma cells. Further, these rocaglamides potently inhibited proliferation of *NF2*-deficient schwannoma and meningioma cells. The more favorable drug-like properties and potent anti-tumor effects of Roc and DDR suggest that these rocaglamides have potential to become viable treatments for NF1- and NF2-associated tumors, including MPNST, as well as other sarcomas.

Full List Authors: Long-Sheng Chang¹, Janet L Oblinger¹, Sarah S Burns¹, Jie Huang¹, Larry Anderson², Rulong Shen³, Li Pan⁴, Yulin Ren⁴, Ryan Roberts¹, Barry R O'Keefe⁵, A Douglas Kinghorn⁴, Jerry M Collins²

¹*Ctr for Childhood Cancer & Blood Diseases, Nationwide Children's Hospital/Dept of Pediatrics, The Ohio State Univ*, ²*Div of Cancer Treatment and Diagnosis, National Cancer Institute, NIH*, ³*Dept of Pathology, The Ohio State Univ*, ⁴*Div of Medicinal Chemistry and Pharmacognosy, The Ohio State Univ Coll of Pharmacy*, ⁵*Div of Cancer Treatment and Diagnosis and Molecular Targets Program, Ctr for Cancer Research, National Cancer Institute, NIH*

Funding: CancerFree KIDS, Sunbeam Foundation, Department of Defense

November 9th, 2019

Saturday, 8:00 am to 4:30 pm; Northern Illinois Building, Hoffman Estates, IL

Neurofibromatosis Symposium & iNFo Fair!

Presented by NF Midwest

*You don't want to miss
this opportunity!*

Join us for a day of learning and sharing at our 2019 NF Symposium and iNFo Fair. There will be plenty of opportunities to meet others. Plus, we will have special tables for extra iNFo and questions.

TOPICS AND AGENDA*

8:00 – 9:00 am Registration, Continental Breakfast, and Socializing
CART (Captioning will be provided for MOST sessions. Email us for more info at info@nfmidwest.org.
Speakers may be added or changed. Look for updated information at www.nfmidwest.org/symposium.

SCHEDULED PRESENTATIONS

(Topics are NOT in order of the actual schedule or in any order of importance and may be subject to change)

- **New NF1, NF2, and Schwannomatosis New Diagnostic Criteria**
- **Regional Clinic Info and Trial Updates**
- **Encouraging Social Connections and Adaptive Behaviors. How Parents Can Help!**—Sandra Cushner-Weinstein LICSW, Children's National Medical Center in Washington, DC; Director of Brainy Camps and Camp New Friends
- **Gene Therapy/Gene Editing**—Robert Kesterson, PhD, University of Alabama, Department of Genetics

NF Type 1 Topics

- **Surgical Management of Cutaneous Neurofibroma: Current Therapy and Future Directions** – Lu Le, MD PhD, University of Texas Southwestern Medical Center
- **Drug Treatment of Cutaneous Neurofibromas: Past, Present, and Future**—Ashley Cannon, MS, CGC, PhD, University of Alabama
- **Translational Research Update on Cutaneous Neurofibromas**—Matt Steensma, MD, Spectrum Health, Francis S Collins Scholar
- **Research Update: Photodynamic Therapy on Cutaneous Neurofibromas**—Medical College of Wisconsin
- **Optic Gliomas/Research and Treatment Update**—Robert Listernick, MD, Lurie Children's Hospital and NF Clinic, Chicago, IL

NF Type 2 Topics

- **Hearing Rehabilitation in NF2: Auditory Brainstem and Cochlear Implantation**—Kevin Peng, MD, Otologist/Neurotologist, House Clinic. Los Angeles, CA
- **Discoveries from Synodos for NF2**—Long-Sheng Chang, PhD, Nationwide Children's Hospital and The Ohio State University College of Medicine
- **NF2 BioSolutions: Accelerating Gene Therapy Research for Neurofibromatosis Type 2**—John Manth, NF2 BioSolutions Board Member

INFORMATION TABLES

We will have tables of various iNformation on topics related to NF, plus opportunities to visit with our presenters to ask more questions. We will be bringing virtually all the material we have available, with copies for you to take. Examples of iNformation provided includes (there will be much more!)...

- NF Clinics and their clinical trials
- New Health Supervision Guidelines for Children with NF1
- Care Guideline for Adults with NF1
- Participating in Research
- Learning Disabilities and School Issues
- Medical Imaging for NF1: Radiation Exposure
- Autism Spectrum Disorder Symptomatology in Children with NF1
- Insurance Coverage for Neurofibroma Removal by NF Midwest
- Procedure Codes for Removing a High Quantity of Neurofibromas
- Info on Various Complications in NF1 including...
 - Optic gliomas, seizures, scoliosis, pain, vascular disease, brainstem tumors
- Making a Difference—Raising Funds and Awareness

KIDS GROUPS

CHILDRENS GROUP (Ages 5-12) A fun day is provided for children ages 5-11. This childcare will be provided FREE of charge, but you MUST make a reservation.

TEEN GROUP (Ages 13-18) Bring the older kids for a day of fun, games, and just hanging out. This is a great chance for your kids to meet others with NF. Siblings are also welcome! We ask that you donate \$10 per child, if possible. Reservations required.

The kids will be served pizza for lunch.

Please let us know if your children have any special needs so that we can accommodate them better.



SPECIAL NEEDS

- The NF Midwest Symposium will have CART services for the hearing impaired that **will follow the shared and NF2 sessions only**. If you need CART services for the NF1 sessions, please let us know.
- Financial assistance is available from NF Midwest for people from our region who are in need and we waive the registration fee for people traveling more than 90 miles. Our region includes Illinois, Wisconsin, Indiana, Iowa, Kentucky and the eastern half of Missouri. If you are not from our area, you will have to contact your local NF organization or another institution that may be able to assist you. Please, call us if you need assistance from us or in reaching another organization.
- If you have any other special needs, please let us know as soon as possible.

ACCOMMODATIONS AND TRANSPORTATION

HOTELS A block of rooms is available at the Chicago Marriott Northwest/Hoffman Estates for \$89 a night. A shuttle can take you to and from the venue if needed. Make a reservation at www.nfmidwest.org/hotel or call (847) 645-9500 and ask for the NF Midwest group rate. There are also many other hotels in the area.

TRAVEL BY CAR See map in this brochure for directions.

TRAVEL BY AIR NIU is 20 miles from O'Hare International Airport; 40 miles from Midway Airport.

TRAVEL FROM CHICAGO We would like to try to help people who may not have cars travel to the symposium from the city. If you are traveling from the city and need help please contact us so we can see if special arrangements can be made.

TRAVELING MORE THAN 90 MILES If you are traveling more than 90 miles and are in our region, or NF Upper Midwest's region, (this includes Illinois, Indiana, Iowa, Kentucky, Minnesota, Missouri, North Dakota, South Dakota, or Wisconsin) as a service to both of our communities we will waive your fees. Use the coupon code "90miles".

ADDRESS AND DIRECTIONS

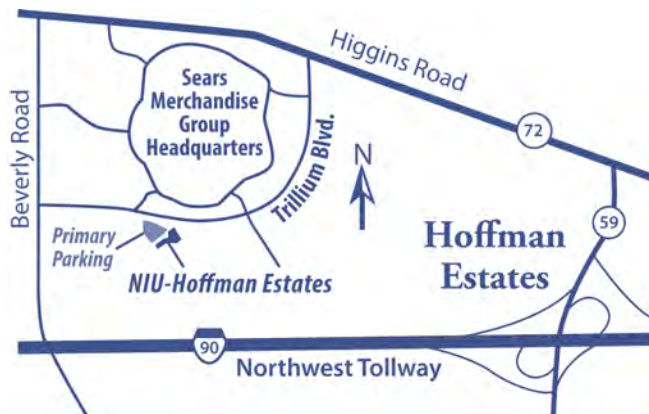
Northern Illinois University (NIU)—Hoffman Estates
5555 Trillium Blvd.
Hoffman Estates, IL 60192
Phone: (847) 645-3000

From I-90 Eastbound

Exit Route 59 north (left) to Higgins Road (IL Rt. 72). Turn west (left) onto Higgins Road. Turn south (left) onto Beverly Road. Turn east (left) onto Trillium Boulevard. The NIU Hoffman-Estates is on the right, across from the Sears Merchandising Group Headquarters.

From I-90 Westbound

Exit Beverly Road north (right) to Trillium Boulevard. Turn east (right) onto Trillium Boulevard. The NIU Hoffman-Estates is on the right, across from the Sears Merchandising Group Headquarters.



Note: You cannot turn left into the NIU lot from Trillium Blvd. You will have to make a U-turn or come in from Beverly Road.

FRIDAY NIGHT GATHERING!

**This year we are holding a special social event
on Friday night before the symposium!**

Details are still in the works, but the event will be free and probably at the hotel.
Please, mark during registration whether or no you are interested in attending.

REGISTER ONLINE!

Please register online at
www.nfmidwest.org/symposium
or
call the office at **630-945-3562**.

Registration deadline is November 6, 2018

Please register as early as possible!

Symposium Registration Fees include Continental Breakfast, Lunch, & Snack

\$25.00—per adult over 18

\$10—Teens ages 13-18

FREE—Children ages 5-12

Bowling—\$15

Children under 5 are not allowed, though we MAY make an exception for 4 year olds (please call).

Note: The cost for the symposium and bowling are well below our actual costs. We do all we can to make this event affordable for the NF Midwest community. If you'd like to help defray the costs, please make a donation at www.nfmidwest.org/donate.

Help NF Education by donating at www.nfmidwest.org/donate



Neurofibromatosis Midwest

473 Dunham Road, Suite 3
St. Charles, IL 60174

630-945-3562

info@nfmidwest.org

www.nfmidwest.org

Register Now!

...Or donate to support the
symposium and future
educational events for NF!



Neurofibromatosis Symposium & iNFo Fair!

Presented by NF Midwest

November 9th

Saturday, 8:00 am to 4:30 pm

Northern Illinois Building

Hoffman Estates, IL

***Plus Friday Night
Gathering!***

Socialize, strengthen and learn from
Leading experts and each other.

Don't miss it!



Drug Discoveries from Synodos for NF2 and Identification of Natural Compounds to Treat NF1 and NF2 Tumors

Long-Sheng Chang

*OSU Dept of Pediatrics, Biol Chem & Pharmacol,
Otolaryngology-Head & Neck Surgery, and Pathology and
Ctr for Childhood Cancer & Blood Diseases, Abigail Wexner
Res Inst at Nationwide Children's Hosp*



Long-Sheng.Chang@nationwidechildrens.org

NF Midwest – Neurofibromatosis Symposium & iNFo Fair 2019

Targeting protein translation via eIF4A inhibition with didesmethylrocaglamide (DDR) and rocaglamide (Roc) to treat pediatric osteosarcoma

Long-Sheng Chang

Long-Sheng.Chang@nationwidechildrens.org

*Ctr for Childhood Cancer & Blood Diseases, Nationwide Children's Hosp
& Dept of Pediatrics, The Ohio State Univ College of Medicine*



Kids Beating Cancer – Science Is the Cure Symposium 2020



[Print this Page for Your Records](#)

[Close Window](#)

Control/Tracking Number: 20-A-7875-AACR

Activity: Abstract Submission

Current Date/Time: 12/5/2019 9:00:29 PM

The eIF4A inhibitors didesmethylrocamamide and rocamamide as effective treatments for pediatric bone and soft-tissue sarcomas

Short Title:

Rocaglamides to treat bone sarcomas

Author Block: Long-Sheng Chang¹, Janet L. Oblinger¹, Garima Agarwal², Tyler A. Wilson², Ryan Roberts¹, James Fuchs², Barry R. O'Keefe³, A. Douglas Kinghorn², Jerry M. Collins³. ¹Nationwide Children's Hospital and The Ohio State University Wexner Medical Center, Columbus, OH; ²The Ohio State University College of Pharmacy, Columbus, OH; ³Center for Cancer Research, National Cancer Institute, NIH, Frederick, MD

Abstract:

Background: Development of an effective medical therapy for osteosarcoma and Ewing sarcoma, the two most common aggressive forms of pediatric bone and soft-tissue sarcomas, is urgently needed as current treatments are inadequate particularly for those with recurrent or metastatic diseases. To achieve this goal, we have identified two natural eIF4A inhibitors, rocamamide (Roc) and didesmethylrocamamide (DDR), which potently inhibit proliferation of a series of commonly-used osteosarcoma and Ewing sarcoma cell lines. We also demonstrated that Roc effectively suppresses tumor growth in patient-derived xenograft (PDX) models of osteosarcoma and Ewing sarcoma. Both Roc- and DDR-treated sarcoma cells show decreased levels of multiple oncogenic kinases, including insulin-like growth factor-1 receptor (IGF-1R). Importantly, these rocamlamides are not sensitive to multidrug resistance 1 (MDR1) efflux. In addition, Roc exhibits 50% oral bioavailability, is well-tolerated in mice, and does not induce pulmonary toxicity in dogs as found with another eIF4A inhibitor silvestrol (Chang et al. Mol Cancer Ther. 2019; In Revision). **Methods:** Various osteosarcoma and Ewing sarcoma cell lines were treated with DDR and Roc, followed by cell proliferation assay, flow cytometry, and immunoblotting. Mesenchymal stem cells (MSCs) were used as a control for comparing the expression levels of the eIF4F components important for translation initiation. RNA interference (RNAi) and CRISPR/Cas9 techniques were used to verify eIF4A dependency. An orthotopic cell line-derived xenograft (CDX), a metastatic xenograft, and a PDX models for osteosarcoma and immunohistochemistry were used to assess antitumor efficacy. **Results:** We hypothesize that osteosarcoma and Ewing sarcoma cells are highly addicted to active protein synthesis and that Roc and DDR, by acting as potent eIF4A inhibitors with an ability to induce apoptosis and the DNA damage response, effectively eliminate these malignant sarcomas. We found that various osteosarcoma and Ewing sarcoma cell lines expressed higher levels of eIF4A2, but not eIF4A1, eIF4E, and eIF4G, than MSCs, suggesting a role of eIF4A2 in enhancing protein translation in these sarcoma cells. RNAi knockdown and CRISPR/Cas9 knockout experiments are being evaluated to verify this finding. Both DDR and Roc effectively blocked tumor growth in an orthotopic CDX model. As found with Roc previously, DDR also potently inhibited the growth of an osteosarcoma PDX model. Both rocamlamides were well tolerated at 3 mg/kg by IP every other day and did not cause any significant changes in body weight, compared with vehicle-treated controls. We are presently determining the effects of Roc and DDR on osteosarcoma metastasis. **Conclusions:** The potent anti-tumor activity and favorable toxicity profile of Roc and DDR suggest that these rocamlamides should be further evaluated as potential treatments for osteosarcomas and Ewing sarcomas.

Author Disclosure Information:

L. Chang: None. **J.L. Oblinger:** None. **G. Agarwal:** None. **T.A. Wilson:** None. **R. Roberts:** None. **J. Fuchs:** None. **B.R. O'Keefe:** None. **A.D. Kinghorn:** None. **J.M. Collins:** None.

Sponsor (Complete):

Category and Subclass (Complete): ET06-04 Novel antitumor agents

Research Type (Complete): Translational research

Organ Site/Structures (Complete):

***Primary Organ Site:** Pediatric cancers

***Choose Chemical Structure Disclosure Option:**

YES, and I WILL DISCLOSE. Compounds with defined structures were used, and I WILL DISCLOSE them in my presentation.

***Please explain reason for not disclosing (maximum 250 characters with spaces):** : NA

***Reference or patent application number :** NA

Manuscript Publication (Complete):

Manuscript Publication Options: YES, I INTEND to submit a manuscript to be peer-reviewed for AACR journal publication simultaneously with presentation of the abstract (if selected).

Journal Preference : Mol Cancer Ther

Is this study/trial supported in whole or in part by an AACR grant?: No

Is this study/trial sponsored in whole or in part by the pharmaceutical industry?: No

Submission Fee (Complete): Your credit card order has been processed on Thursday 5 December 2019 at 8:57 PM.

Status: Complete

***To log out, simply close your browser window. All information will be saved if you hit the Continue button after each step.

For all log-in problems or technical questions, please contact the [OASIS Helpdesk](#) or call (217) 398-1792.

If you have any policy questions related to the AACR Annual Meeting 2020,

please contact the AACR [E-mail: abstract@aacr.org; Phone: (215) 440-9300 or (866) 423-3965].

Powered by [cOASIS](#), The Online Abstract Submission and Invitation System SM
© 1996 - 2019 [CTI Meeting Technology](#). All rights reserved. [Privacy Policy](#).